

Modelling the impact of air pollution on the terrestrial  
carbon and nitrogen cycling

Zur Erlangung des akademischen Grades einer  
DOKTORIN DER NATURWISSENSCHAFTEN  
von der KIT-Fakultät für  
Bauingenieur-, Geo- und Umweltwissenschaften

des Karlsruher Instituts für Technologie (KIT)

genehmigte

DISSERTATION

von

Dipl.-Bio. Martina Franz

aus Jena

Tag der mündlichen Prüfung: 18.12.2019

Referentin: Prof. Dr. Almut Arneth  
Korreferentin: Prof. Dr. Julia Pongratz  
Korreferent: Dr. Ir. Laurens Ganzeveld

Karlsruhe 2019



## Abstract

Ozone ( $O_3$ ) is a toxic air pollutant that can injure plant leaves and substantially affect plant growth and health. Tropospheric  $O_3$  concentrations multiplied from pre-industrial values until the end of the 20th century in polluted areas, accompanied by an increase of  $O_3$  precursors like nitrogen oxides ( $NO_x$ ). Reactive forms of nitrogen like  $NO_x$  are a limited nutrient for plants and are assumed to constrain net primary production in large parts of the world. Part of the  $NO_x$  in the atmosphere is deposited back on land and stimulates plant growth in nutrient limited regions. Despite the role of  $NO_x$  as a ozone precursor, previous studies focused on the growth stimulating effect of nitrogen deposition and omitted the detrimental effects of ozone.

To assess the past and future capacity of the terrestrial biosphere as a carbon sink, a realistic estimate of the effects of tropospheric  $O_3$  on gross primary production (GPP) might be important. The combined implementation of the growth stimulating effect of nitrogen deposition and the detrimental effects of  $O_3$  on plant growth and carbon storage might yield a more realistic estimate of past and future terrestrial carbon uptake.

To better understand the impact of ozone damage on the terrestrial carbon cycle, a module to estimate  $O_3$  uptake and damage of plants was developed for O-CN, a state-of-the-art global terrestrial biosphere model. A comparison to literature values demonstrates that the new model version produces realistic key characteristics of ozone deposition. The use of this comparatively detailed ozone deposition scheme, which accounts for non-stomatal as well as stomatal deposition when calculating surface  $O_3$  concentrations, substantially affects plant  $O_3$  uptake in O-CN. The application of the updated model in a Europe-wide simulation of present day ozone damage to GPP and transpiration indicates that the regional carbon and water cycling is less impacted than expected from previous studies. Previously published simulated ozone induced reductions on GPP vary substantially between models and model versions. A possible reason for this is the use of different injury functions which relate ozone uptake to plant damage.

The role that different injury functions play in determining the variability of the estimated ozone impacts was investigated by including four previously published injury functions into a standardised modelling framework, the O-CN model. Model versions including different injury functions are evaluated in terms of their ability to simulated whole-tree biomass responses observed in 23 ozone filtration/fumigation experiments conducted with young trees from European tree species at sites across Europe with a range of climatic conditions. The results show that none of these previously published injury functions lead to simulated whole-tree biomass reductions in agreement with the observed dose–response relationships derived from these field experiments and instead lead to significant over- or underestimations of the ozone effect. By re-parameterising these injury functions, I developed linear, plant-functional-type-specific dose–response relationships, which provide accurate simulations of the observed whole-tree biomass response across these 23 experiments.

The updated model including the ozone deposition scheme and two re-parameterised injury functions was applied to simulate past and future impacts of air pollution (ozone and nitrogen deposition) on the terrestrial carbon uptake and storage in the temperate and boreal Northern Hemisphere. Two scenarios of future air pollution are simulated in a factorial design to understand the effect of present and future changes in nitrogen

deposition, and  $O_3$  concentrations against a background of changes in climate and carbon dioxide concentrations ( $CO_2$ ) for the most optimistic and most pessimistic representative concentration pathway scenario (RCP2.6 and RCP8.5 respectively). The simulations showed that  $O_3$  damage considerably reduced northern hemispheric gross carbon uptake (GPP) and long-term carbon storage in the past. The ozone effect on GPP and total carbon storage peaked around the end of the 20th century with reductions of 4% and 9%, respectively. The  $CO_2$  fertilisation effect and its impact on stomatal conductance restricts peak values of ozone uptake during the the 21st century and cause a decline in ozone induced damage. By the end of the 21st century mean regional reductions of 0-1% for GPP and 4-5% for total carbon biomass are simulated for both RCPs compared to pre-industrial values. However, in hotspot regions like Eastern Asia a sustained decline in GPP of more than 8% is simulated at the end of the 21st century and carbon storage remains reduced by up to 15% in parts of Europe, the US and Eastern Asia.

The comparison of the effect of air pollution from  $O_3$  to that of nitrogen deposition showed that ozone damage offsets the growth stimulating effect induced by nitrogen deposition during a large fraction of the simulation period. The detrimental effect of  $O_3$  on GPP outweighs the stimulating effect of nitrogen deposition until the first half of the 21st century, after which nitrogen deposition starts to outweigh the effects of  $O_3$ . The detrimental effect of  $O_3$  on carbon biomass outweighs the stimulating effect of nitrogen deposition during the entire simulation period.

In conclusion, the implementation of a relative detailed ozone deposition scheme considerably impacts the estimates of ozone uptake in then O-CN model and thus has the potential to strongly impact ozone induced damage estimates. The use of evaluated ozone injury functions in models can help to prevent considerable over- or underestimations of damage. The application of the updated model indicates that  $O_3$  damage considerably slowed the increase of carbon uptake and storage in the past. However, past and future estimates of ozone induced damage are lower than expected from previous studies. Accounting for the stimulating effects of nitrogen deposition but omitting the detrimental effect of  $O_3$  might lead to an over estimation of carbon uptake and storage.

## Zusammenfassung (German)

Ozon ( $O_3$ ) ist ein Luftschadstoff, welcher die Blätter von Pflanzen schädigen und deren Bruttoprimärproduktion (GPP) senken kann. In verschmutzten Regionen haben sich die Ozonkonzentrationen in der Troposphäre seit der Vorindustriellenzeit bis zum Ende des 20. Jahrhunderts vervielfacht, begleitet von einem Anstieg in Vorläuferstoffen wie Stickoxide. Reaktive Stickstoffverbindungen, wie zum Beispiel Stickoxide ( $NO_x$ ), sind ein begrenzter Pflanzennährstoff. Es wird angenommen, dass deren Verfügbarkeit die GPP in weiten Teilen der Welt begrenzt. Ein Teil des in die Atmosphäre eingebrachten  $NO_x$  wird zurück auf das Land abgeschieden, wo es das Pflanzenwachstum stimulieren kann. Obwohl  $NO_x$  Vorläuferstoffe für  $O_3$  darstellen, haben sich bisherige Studien auf den wachstumsstimulierenden Effekt von Stickstoffabscheidung konzentriert ohne gleichzeitig den schädlichen Einfluss von  $O_3$  zu beachten.

Zur Schätzung der Kapazität der terrestrischen Biosphäre als Kohlenstoffsенke, könnte eine realistische Abschätzung der Einflüsse von Ozon auf die GPP eine wichtige Rolle spielen. Die gemeinsame Implementierung der wachstumsstimulierenden Effekte der Abscheidung von reaktiven Stickstoffverbindungen und der schädlichen Effekte von Ozon auf Pflanzenwachstum und Kohlenstoffspeicherung könnte eine realistischere Abschätzung vergangener und zukünftiger terrestrischer Kohlenstoffspeicherung ermöglichen.

Um den Einfluss von Ozon auf den terrestrischen Kohlenstoffkreislauf besser zu verstehen, wurde ein Ozonabscheidungsschema in das Biosphärenmodell O-CN eingebaut, welches Ozonaufnahme und -pflanzenschaden schätzt. Ein Vergleich mit veröffentlichten Werten zeigt, dass dieses neue Modul realistische Werte für Schlüsselwerte der Ozonabscheidung produziert. Die Verwendung eines detaillierten Schemas welches bei der Berechnung der bodennahen Ozonkonzentration die Abscheidung von Ozon in die Spaltöffnungen der Blätter und außerhalb dieser berücksichtigt, hat einen substantiellen Einfluss auf die pflanzliche Ozonaufnahme in O-CN. Die Anwendung des aktualisierten Modells im Rahmen einer europaweiten Simulation von gegenwärtigen Ozonschäden auf GPP und Transpiration deutet an, dass der regionale Kohlenstoff- und Wasserkreislauf geringer beeinflusst wird als auf Grund von bereits publizierten Studien zu erwarten wäre. Verschiedene Modelle und Modellversionen unterscheiden sich jedoch erheblich in ihren Abschätzungen des durch Ozon verursachten Schadens von GPP. Ein möglicher Grund dafür ist die Verwendung verschiedener Schadensfunktionen, welche die Ozonaufnahme in Relation setzen zu Pflanzenschaden.

Die Auswirkung verschiedener Schadensfunktionen auf die Schwankung der geschätzten Ozoneffekte wird untersucht in dem vier bereits veröffentlichte Schadensfunktionen in ein standardisiertes Modellgerüst eingebaut werden, das O-CN Modell. Verschiedene Modellversionen werden untersucht hinsichtlich ihrer Fähigkeit die beobachteten Gesamtbiomassereaktionen in 23 Ozon-Filtrierungs-Begasungsexperimenten mit jungen Bäumen europäischer Baumarten an zehn Orten quer durch Europa zu simulieren. Die Ergebnisse zeigen, dass keine vorab veröffentlichte Schadensfunktion zu einer Gesamtbiomassereaktionen führt, welche vereinbar ist mit den beobachteten Zusammenhängen in den Experimenten. Anstatt dessen wird eine erhebliche Überschätzung oder Unterschätzung der Ozoneffekte simuliert. Durch eine Reparameterisierung dieser Schadensfunktionen habe ich lineare, pflanzentypspezifische Schadenszusammenhänge entwickelt, welche eine akkurate Simulation der beobachteten Gesamtbiomassereaktionen in den 23 Experi-

menten ermöglicht.

Das aktualisierte Modell, welches das Ozonabscheidungsschema und zwei reparameterisierte Schadensfunktionen enthält, wurde genutzt um vergangene und zukünftige Einflüsse von Luftverschmutzung, durch Ozon und Stickstoffabscheidung, auf die terrestrische Kohlenstoffaufnahme und -speicherung in temperaten und borealen Regionen der Nordhalbkugel zu simulieren. In einem faktoriellen Versuchsplan werden zwei zukünftige Szenarien der Luftverschmutzung simuliert um den Einfluss gegenwärtigen und zukünftigen Änderungen in Stickstoffabscheidung und O<sub>3</sub> Konzentrationen zu untersuchen bei einem gleichzeitigem Wandel des Klimas und der Kohlendioxid (CO<sub>2</sub>) Konzentrationen. Diese Simulationen werden jeweils für das optimistischste und pessimistischste Repräsentative Konzentrationspfad-Szenario (RCP2.6 und RCP8.8) durchgeführt.

Die Simulationsergebnisse zeigen, dass in der Vergangenheit Ozonschäden die mittlere regionale Kohlenstoffaufnahme (GPP) und -speicherung (Gesamtkohlenstoffbiomasse) in der simulierten Region deutlich reduziert haben. Die maximale Reduktion tritt um das Ende des 20. Jahrhunderts herum auf und beträgt ungefähr 4% für GPP und 9% für Gesamtkohlenstoffbiomasse. Die durch den CO<sub>2</sub> Düngeeffekt reduzierte Spaltöffnungsbewegung von Pflanzen begrenzt die Aufnahme von Ozonspitzenwerten und verursacht eine Reduktion von Ozonschäden während des 21. Jahrhunderts. Für beide Verschmutzungsszenarien werden am Ende des 21. Jahrhunderts im regionalen Mittel Reduktionen von 0-1% für GPP 4-5% für Gesamtbiomasse simuliert im Vergleich zu vorindustriellen Werten. In Schadensbrennpunkten werden am Ende des 21. Jahrhunderts Reduktionen von mehr als 8% für GPP (Ostasien) und bis zu 15% für Gesamtkohlenstoffbiomasse (in Teilen von Europa, dem Osten und Westen der USA und Ostasien) simuliert.

Ein Vergleich der Auswirkung von Luftverschmutzung durch Ozon zu dem von Stickstoffabscheidung zeigte, dass Ozonschäden den wachstumsstimulierenden Effekt von Stickstoffabscheidung während eines Großteils des simulierten Zeitraums ausgleicht. Die schädliche Wirkung von Ozon wiegt den stimulierenden Einfluss von Stickstoffabscheidung auf GPP bis zur ersten Hälfte des 21. Jahrhunderts auf. Danach beginnt die stimulierende Wirkung von Stickstoffabscheidung auf GPP zu dominieren. Die schädliche Wirkung von Ozon auf die Gesamtkohlenstoffbiomasse überwiegt dem stimulierenden Effekt von Stickstoffabscheidung während des gesamten Simulationszeitraums.

Zusammenfassend ist zu sagen, dass die Implementierung eines relativ detaillierten Ozonabscheidungsschemas die Schätzung der Ozonaufnahme in O-CN deutlich beeinflusst und somit potentiell auch Schadensschätzungen. Die Verwendung von evaluierten Schadensfunktionen in Modellen kann helfen eine erhebliche Über- oder Unterschätzung des Schadens zu verhindern. Die Anwendung des aktualisierten Modells zeigt, dass Ozonschäden den Anstieg von Kohlenstoffaufnahme und -speicherung in der Vergangenheit deutlich reduziert haben. Hier präsentierte Schätzungen von gegenwärtigen und zukünftigen Ozonschäden sind geringer als auf Grund vorheriger Studien zu erwarten wäre. Der Einbezug des stimulierenden Effekts von Stickstoffabscheidung in die Schätzung von Kohlenstoffaufnahme und -speicherung ohne die schädlichen Einflüsse von Ozon zu beachten kann zu einer Überschätzung dieser führen.

**Eidesstattliche Versicherung gemäß § 6 Abs. 1 Ziff. 4 der Promotionsordnung des Karlsruher Instituts für Technologie für die Fakultät für Bauingenieur-, Geo- und Umweltwissenschaften.**

1. Bei der eingereichten Dissertation zu dem Thema "Modelling the impact of air pollution on the terrestrial carbon and nitrogen cycling" handelt es sich um meine eigenständig erbrachte Leistung.
2. Ich habe nur die angegebenen Quellen und Hilfsmittel benutzt und mich keiner unzulässigen Hilfe Dritter bedient. Insbesondere habe ich wörtlich oder sinngemäß aus anderen Werken übernommene Inhalte als solche kenntlich gemacht.
3. Die Arbeit oder Teile davon habe ich bislang nicht an einer Hochschule des In- oder Auslands als Bestandteil einer Prüfungs- oder Qualifikationsleistung vorgelegt.
4. Die Richtigkeit der vorstehenden Erklärungen bestätige ich.
5. Die Bedeutung der eidesstattlichen Versicherung und die strafrechtlichen Folgen einer unrichtigen oder unvollständigen eidesstattlichen Versicherung sind mir bekannt.

Ich versichere an Eides statt, dass ich nach bestem Wissen die reine Wahrheit erklärt und nichts verschwiegen habe.

Auckland, 04.02.2020

Unterschrift

This thesis is submitted as a monograph and contains three results chapters (chapters 2-4). Chapter 2 and 3 are slightly adapted versions of previously published articles in peer-reviewed journals.

**Chapter 2: Development and evaluation of an ozone deposition scheme for coupling to a terrestrial biosphere model**, is based on the paper: Franz, M., Simpson, D., Arneth, A., and Zaehle, S.: Development and evaluation of an ozone deposition scheme for coupling to a terrestrial biosphere model, *Biogeosciences*, 14, 45–71, <https://doi.org/10.5194/bg-14-45-2017>, <http://www.biogeosciences.net/14/45/2017/>, 2017.

**Chapter 3: Evaluation of simulated ozone effects in forest ecosystems against biomass damage estimates from fumigation experiments**, is based on the paper: Franz, M., Alonso, R., Arneth, A., Büker, P., Elvira, S., Gerosa, G., Emberson, L., Feng, Z., Le Thiec, D., Marzuoli, R., Oksanen, E., Uddling, J., Wilkinson, M., and Zaehle, S.: Evaluation of simulated ozone effects in forest ecosystems against biomass damage estimates from fumigation experiments, *Biogeosciences*, 15, 6941-6957, <https://doi.org/10.5194/bg-15-6941-2018>, 2018.

These published papers involve the work of co-authors. My contribution to both papers is as follows: I contributed to the experiment design, extended the model O-CN model, performed the simulations and analyses, and led the writing of both papers.

# Contents

<b>Abstract</b>	<b>i</b>
<b>Zusammenfassung (German)</b>	<b>iii</b>
<b>Contents</b>	<b>vii</b>
<b>List of Figures</b>	<b>xi</b>
<b>List of Tables</b>	<b>xv</b>
<b>Abbreviations, symbols and units</b>	<b>xvii</b>
<b>1 General introduction</b>	<b>1</b>
1.1 The global carbon and nitrogen cycle . . . . .	1
1.1.1 Carbon emissions and sinks . . . . .	1
1.1.2 The net land sink . . . . .	2
1.1.3 The terrestrial biosphere . . . . .	2
1.1.4 Climate effects on the global carbon cycle . . . . .	3
1.1.5 The nitrogen cycle and the nitrogen fertilisation effect . . . . .	3
1.2 Tropospheric ozone concentrations and their impact on plants . . . . .	5
1.2.1 Ozone formation and cycling . . . . .	5
1.2.2 Background concentrations . . . . .	6
1.2.3 Trends . . . . .	7
1.3 Ozone effects on plants . . . . .	8
1.3.1 Overview of types of effects . . . . .	8
1.3.2 Detoxification, respiration, repair . . . . .	9
1.3.3 Injury . . . . .	10
1.3.4 Impacts on stomatal conductance . . . . .	11
1.3.5 Exposure indices . . . . .	12
1.4 Impacts of elevated CO <sub>2</sub> concentrations on plants . . . . .	13
1.4.1 Coupled effects of elevated CO <sub>2</sub> and O <sub>3</sub> . . . . .	14
1.4.2 Coupled effects of elevated CO <sub>2</sub> , O <sub>3</sub> and N availability . . . . .	15
1.5 Future projections of climate change . . . . .	15
1.5.1 Representative concentration pathways (RCPs) . . . . .	16

1.5.2	Simulated changes during the 21st century . . . . .	16
1.6	Global terrestrial biosphere models . . . . .	17
1.6.1	The O-CN model . . . . .	17
1.6.2	Modelling air pollution impacts in O-CN . . . . .	18
1.7	Thesis structure and objectives . . . . .	19
<b>2</b>	<b>Development and evaluation of an ozone deposition scheme for coupling to a terrestrial biosphere model</b>	<b>21</b>
2.1	Introduction . . . . .	21
2.2	Methods . . . . .	22
2.2.1	Ozone module . . . . .	23
2.2.2	Relating stomatal uptake to leaf injury . . . . .	26
2.2.3	Sensitivity analysis . . . . .	27
2.2.4	Modelling protocol and data for site-level simulations . . . . .	27
2.2.5	Modelling protocol and data for regional simulations . . . . .	30
2.2.6	Emissions inventory . . . . .	30
2.2.7	Impacts of using the ozone deposition scheme . . . . .	31
2.3	Results . . . . .	31
2.3.1	Evaluation against daily eddy-covariance data . . . . .	31
2.3.2	Mean diurnal cycles of key O <sub>3</sub> parameters. . . . .	33
2.3.3	Sensitivity analysis . . . . .	38
2.3.4	Regional simulations . . . . .	41
2.3.5	Impacts of using the ozone deposition scheme . . . . .	44
2.4	Discussion . . . . .	45
2.4.1	Atmosphere-leaf transport of ozone . . . . .	46
2.4.2	Estimating vegetation damage from ozone uptake . . . . .	48
2.5	Conclusion . . . . .	49
<b>3</b>	<b>Evaluation of simulated ozone effects in forest ecosystems against biomass damage estimates from fumigation experiments</b>	<b>51</b>
3.1	Introduction . . . . .	51
3.2	Methods . . . . .	53
3.2.1	Ozone injury calculation in O-CN . . . . .	53
3.2.2	Model set-up . . . . .	55
3.2.3	Model and protocol for young trees . . . . .	57
3.2.4	Modelling protocol for mature trees . . . . .	59
3.2.5	Calculation of the biomass damage relationships . . . . .	60
3.3	Results . . . . .	61
3.3.1	Testing published injury functions . . . . .	61
3.3.2	Tuned injury relationships . . . . .	64
3.3.3	Ozone injury to mature trees . . . . .	65
3.4	Discussion . . . . .	67
3.5	Conclusion . . . . .	73

<b>4</b>	<b>Simulated air pollution impacts from 1850-2099</b>	<b>75</b>
4.1	Introduction . . . . .	75
4.2	Methods . . . . .	79
4.2.1	Modelling protocol . . . . .	79
4.2.2	Factorial simulation runs . . . . .	80
4.2.3	Factorial analysis . . . . .	80
4.3	Results . . . . .	81
4.3.1	Regional means and sums of air pollution impacts . . . . .	81
4.3.1.1	Ozone uptake and accumulation . . . . .	82
4.3.1.2	Carbon fixation and biomass production . . . . .	84
4.3.1.3	Magnitude of impact and differences between the RCPs . . . . .	84
4.3.1.4	Impact of the ozone deposition scheme . . . . .	90
4.3.2	Simulated spatial differences of air pollution impacts . . . . .	92
4.4	Discussion . . . . .	96
4.4.1	Air pollution impacts on GPP and total carbon biomass . . . . .	96
4.4.2	Limitations of comparisons between publications . . . . .	100
4.4.3	Potential impacts of vegetation dynamics . . . . .	101
4.4.4	Impact of the ozone deposition scheme . . . . .	102
4.5	Conclusion . . . . .	102
<b>5</b>	<b>General conclusion and outlook</b>	<b>103</b>
5.1	Answers to the underlying research questions . . . . .	104
5.2	Limitations . . . . .	108
5.3	Outlook . . . . .	109
5.4	Final remarks . . . . .	111
	<b>Acknowledgements</b>	<b>113</b>
	<b>Bibliography</b>	<b>115</b>
	<b>Appendix</b>	<b>141</b>



# List of Figures

2.1	Comparison of measured a) GPP, b) canopy conductance ( $G_c$ ), c) latent heat flux (LE), and d) LAI at 26 European FLUXNET sites and simulations by O-CN. . . . .	32
2.2	Comparison of measured (a) GPP, (b) $G_c$ , (c) latent heat flux (LE), and (d) LAI at 26 European FLUXNET sites (red) and simulations by O-CN (blue). . . . .	34
2.3	Simulated and observed hourly means over all days of the months of July of 2002-2006 for CH-Oe1 and IT-Ro1, as well as for 2001-2006 for FI-Hyy. . . . .	35
2.4	Simulated monthly mean values of $O_3$ uptake ( $F_{stC}$ ), $O_3$ deposition velocity ( $V_g$ ), $O_3$ surface resistance ( $R_c$ ), and the flux ratio ( $F_R$ ) for sites dominated by broadleaved trees (left column), needle-leaved trees (central column) and $C_3$ grasses (right column). . . . .	37
2.5	a) Mean partial correlation coefficients and b) strength of the correlation in % per %. . . . .	39
2.6	Ensemble range of key $O_3$ uptake/deposition variables resulting from the perturbation of $R_a$ , $b$ , $r_{ext}$ , $\hat{R}_{gs}$ and $G_c$ within $\pm 20\%$ of their central estimate. . . . .	40
2.7	Europe-wide simulated GPP and difference between modelled GPP by O-CN and a GPP estimate by a FLUXNET-MTE product. . . . .	41
2.8	Mean decadal (a) $O_3$ concentration [ppb], (b) canopy-integrated $O_3$ uptake into the leaves [ $\text{nmol m}^{-2} \text{s}^{-1}$ ], (c) canopy-integrated cumulative uptake of $O_3$ (CUO) [ $\text{mmol m}^{-2}$ ], and (d) AOT40 [ $\text{ppm yr}^{-1}$ ], for Europe of the years 2001-2010. . . . .	42
2.9	Mean decadal (a) reduction in GPP [ $\text{g C m}^{-2} \text{yr}^{-1}$ ], (b) percent reduction in GPP, (c) reduction in transpiration [ $\text{mm yr}^{-1}$ ] and (d) percent reduction in transpiration due to ozone damage averaged for the years 2001-2010. . . . .	43
2.10	Mean daily values of the (a) $O_3$ surface concentration, (b) canopy-integrated $O_3$ uptake into the leaves, and (c) canopy-integrated cumulative uptake of $O_3$ (CUO) at the FLUXNET site FI-Hyy. . . . .	44
2.11	Differences in mean daily values of the (a) $O_3$ surface concentration, (b) canopy-integrated $O_3$ uptake into the leaves, and (c) canopy integrated cumulative uptake of $O_3$ (CUO) for the three FLUXNET sites CH-Oe1, FI-Hyy and IT-Ro1. . . . .	45

2.12	Mean decadal canopy-integrated cumulative uptake of O <sub>3</sub> (CUO) for Europe of the years 2001–2010. (a) Canopy O <sub>3</sub> concentration is equal to the atmospheric concentration (ATM) and (b) O <sub>3</sub> surface resistance is only determined by stomatal resistance (D-STO).	46
3.1	Biomass dose-response relationships for simulations based on published injury relationships, separate for a) broadleaved species and b) needleleaf species.	62
3.2	Simulated cumulative ozone uptake above a threshold of 0.8 nmol m <sup>-2</sup> s <sup>-1</sup> (CUOY), canopy-integrated net photosynthesis ( $A_n^{can}$ ), leaf carbon content ( <i>Leaf C</i> ), total carbon in biomass ( <i>biomass C</i> ) and relative biomass ( <i>RB</i> ) of <i>Pinus halepensis</i> at the Ebro Delta fumigated with the NF+ ozone treatment.	63
3.3	Biomass dose-response relationships for simulations based on tuned injury functions (see Tab. 3.1 for abbreviations), separate for a) broadleaved species, and b) needleleaf species.	64
3.4	Biomass ( <i>RB</i> ) and NPP ( <i>RN</i> ) dose-response relationships of simulations with young ( $tun_{VC}^{young}$ ) and mature trees ( $tun_{VC}^{mature}$ ) separately for a,c) broadleaf species and b,d) needleleaf species.	66
4.1	Mean nitrogen deposition rates for the temperate and boreal Northern Hemisphere ( $\geq 30^\circ N$ ) in the decades of the years of 1850, 1990, 2050 and 2090, each according to the RCP2.6 and RCP8.5 pollution scenario.	76
4.2	Projected mean canopy level O <sub>3</sub> concentration for the temperate and boreal Northern Hemisphere ( $\geq 30^\circ N$ ) in the decades of the years of 1850, 1990, 2050 and 2090, each according to the RCP2.6 and RCP8.5 pollution scenario.	77
4.3	Time series of the regional mean (temperate and boreal Northern Hemisphere ( $\geq 30^\circ N$ )) ozone concentration and summed nitrogen deposition according to the RCP2.6 and RCP8.5 pollution scenario.	78
4.4	Simulated regional mean ozone uptake ( $F_{st}$ ) and regional mean cumulative canopy O <sub>3</sub> uptake above a flux threshold of 1 nmol m <sup>-2</sup> s <sup>-1</sup> (CUO1) of the simulations based on RCP8.5.	82
4.5	Simulated canopy O <sub>3</sub> concentration, ozone uptake ( $F_{st}$ ), cumulative O <sub>3</sub> uptake without a flux threshold (CUO0) and cumulative O <sub>3</sub> uptake above a flux threshold of 1 nmol m <sup>-2</sup> s <sup>-1</sup> (CUO1) of the factorial run S5 (all forcing variables are simulated transient) based on RCP8.5.	83
4.6	The amount of simulated regional summed GPP, regional summed stocks of total carbon biomass ( <i>C-biomass</i> ) and soil organic matter carbon ( <i>SOM C</i> ) of the simulations based on RCP8.5.	85

4.7	Ozone induced %-change of regional mean ozone uptake ( $F_{st}$ ), mean cumulative O <sub>3</sub> uptake above a flux threshold of 1 nmol m <sup>-2</sup> s <sup>-1</sup> (CUO1), summed GPP, summed carbon biomass (C-biomass) and summed carbon soil organic matter (SOM C) compared to pre-industrial values in the simulation region. . . . .	87
4.8	Ozone induced absolute change of regional mean ozone uptake ( $F_{st}$ ) and mean cumulative O <sub>3</sub> uptake above a flux threshold of 1 nmol m <sup>-2</sup> s <sup>-1</sup> (CUO1) compared to pre-industrial values in the simulation region. . . . .	88
4.9	Nitrogen deposition induced %-change of regional mean ozone uptake ( $F_{st}$ ), mean cumulative O <sub>3</sub> uptake above a flux threshold of 1 nmol m <sup>-2</sup> s <sup>-1</sup> (CUO1), summed GPP, summed carbon biomass (C-biomass), and summed carbon soil organic matter (SOM C) compared to pre-industrial values in the simulation region. . . . .	89
4.10	Ozone impacts on the regional mean ozone uptake ( $F_{st}$ ), mean cumulative O <sub>3</sub> uptake above a flux threshold of 1 nmol m <sup>-2</sup> s <sup>-1</sup> (CUO1), summed GPP, summed carbon biomass (C-biomass), and summed carbon soil organic matter (SOM C) compared to pre-industrial values in the simulation region. . . . .	91
4.11	Absolute change in CUO1 compared to pre-industrial values induced by ozone, calculated according to approach 2. . . . .	93
4.12	Absolute change in GPP compared to pre-industrial values induced by nitrogen deposition (left column) and ozone calculated according to approach 2 (right column). . . . .	94
4.13	Relative change in GPP compared to pre-industrial values induced by nitrogen deposition (left column) and ozone calculated according to approach 2 (right column). . . . .	95
4.14	Absolute change in C-biomass compared to pre-industrial values induced by nitrogen deposition (left column) and ozone calculated according to approach 2 (right column). . . . .	97
4.15	Relative change in C-biomass compared to pre-industrial values induced by nitrogen deposition (left column) and ozone calculated according to approach 2 (right column). . . . .	98



# List of Tables

2.1	Characteristics of the FLUXNET sites used in this study. . . . .	29
2.2	Coefficient of determination ( $R^2$ ) and root mean square error (RMSE) for $GPP$ , canopy conductance ( $G_c$ ), and latent heat flux ( $LE$ ) for all sites and for sites dominated by broadleaved trees, needle-leaved trees, $C_3$ grass, and $C_3$ grass excluding the AT-Neu site (outlier). . . . .	33
3.1	Slopes and intercepts, partly PFT specific, of all four published (W07 $_{PS}$ , L12 $_{PS}$ , L12 $_{VC}$ , L13 $_{PS}$ ) and two tuned (tun $_{PS}$ , tun $_{VC}$ ) injury functions included in O-CN. . . . .	56
3.2	List of fumigation experiments used by Büker et al. (2015) and simulated here. . . . .	58
3.3	Original and adapted values of the nitrogen-specific photosynthetic capacity of a leaf (npl) for three out of four different O-CN versions (ID) including published injury functions. . . . .	59
3.4	Slopes and intercepts of biomass dose-response relationships for broadleaf and needleleaf species simulated by O-CN versions based on published injury functions to net photosynthesis or $V_{cmax}$ (see Tab. 3.1). . . . .	62
3.5	Slopes and intercepts of biomass dose-response relationships for broadleaf and needleleaf species simulated by O-CN versions based on tuned injury functions to net photosynthesis or $V_{cmax}$ (see Tab. 3.1). . . . .	65
3.6	Slopes and intercepts of biomass (RB) and NPP (RN) dose-response relationships (DRRs) for broadleaf and needleleaf species simulated by the tun $_{VC}$ model version (see Tab. 3.1). . . . .	67
4.1	Forcing setting of the factorial runs. . . . .	80
4.2	Calculation of the single driver effects ( $CO_2$ , climate, nitrogen deposition, $O_3$ ) from the conducted simulations. . . . .	81
4.3	Absolute and relative change in GPP, total carbon biomass (C-biomass) and soil organic matter carbon (SOM C) induced by changing atmospheric $CO_2$ concentrations, climate, nitrogen deposition (Ndep), and $O_3$ concentrations. . . . .	86

4.4	Mean percent change in GPP and C-biomass induced by ozone during the decades of 1990 (1990-1999), 2050 (2050-2059) and 2090 (2090-2099) compared to pre-industrial values for the Northern Hemisphere north of 30°N (NH <sub>30</sub> ), Europe, USA and China. . . . .	90
4.5	Mean percent change in GPP and C-biomass induced by nitrogen deposition during the decades of 1990 (1990-1999), 2050 (2050-2059) and 2090 (2090-2099) compared to pre-industrial values for the Northern Hemisphere north of 30°N (NH <sub>30</sub> ), Europe, USA and China. . . . .	90

# Abbreviations, symbols and units

$J_{max}$	Electron transport capacity (leaf photosynthetic trait)
$V_{cmax}$	Maximum carboxylation capacity of the leaf
CH <sub>4</sub>	Methane
CO <sub>2</sub>	Carbon dioxide
CO	Carbon monoxide
C	Carbon
NH <sub>3</sub>	Ammonia
NO <sub>2</sub>	Nitrogen dioxide
NO <sub>x</sub>	Nitrogen oxides
NO	Nitric oxide
N <sub>2</sub>	Unreactive diatomic nitrogen
N	Nitrogen
O <sub>3</sub>	Ozone
eCO <sub>2</sub>	Elevated atmospheric CO <sub>2</sub> concentration
eO <sub>3</sub>	Elevated atmospheric O <sub>3</sub> concentration
GtC	Giga-tons of carbon
PgC	Peta-grams of carbon
TgN	Tera-grams of nitrogen
ppb	Parts per billion
ppm	Parts per million
AOTX	Accumulated O <sub>3</sub> concentration over a threshold of $X$ ppb)
BNF	biological nitrogen fixation
CLM	Community Land Model
CRU-NCEP	An atmospheric forcing dataset used to force land surface models
CTM	Chemical transport model
CUOY	Cumulative canopy O <sub>3</sub> uptake above a flux threshold of $Y$ $nmol m^{-2} s^{-1}$

DDR	Dose-response relationship
ECHAM5	The atmospheric general circulation model, developed at the Max Planck Institute for Meteorology, version number 5
EMEP	European Monitoring and Evaluation Programme
EU	European union
EU directive 2008/50/EC	Directive of the European Parliament and of the Council of 21 May 2008 on ambient air quality and cleaner air for Europe
FACE	Free-Air Carbon dioxide Enrichment
FLUXNET	global network of micrometeorological tower sites to measure the exchanges of carbon dioxide, water vapor, and energy between terrestrial biosphere and the atmosphere by application of eddy covariance methods
GPP	Gross Primary Production
IIASA	International Institute for Applied Systems Analysis
IPCC	Intergovernmental Panel on Climate Change
IPCC SRES	IPCC Special Report on Emissions Scenarios
JULES	Joint UK Land Environment Simulator
LAI	Leaf area index
LE	Latent heat flux
LRTAP	The Convention on Long-range Transboundary Air Pollution
LSCE	Le Laboratoire des Sciences du Climat et de l'Environnement
MACC-2	Monitoring Atmospheric Composition and Climate - Interim Implementation
MTE	Model tree ensembles
NPP	Net primary productivity
O-CN	A further development of the land-surface-scheme ORCHIDEE

ORCHIDEE	ORganizing Carbon and Hydrology In Dynamic EcosystEms model
PCC	Partial correlation coefficient
PFT	Plant functional type
POD <sub>y</sub>	Phytotoxic Ozone Dose [ $\text{nmol m}^{-2} \text{s}^{-1}$ ], refers to the accumulated ozone uptake above a flux threshold of $y \text{ nmol m}^{-2} \text{s}^{-1}$ by the leaves representative of the upper-canopy leaves of the plant
RCA3	Rosby Centre Regional Climate model
RCP	Representative concentration pathway
ROS	Reactive oxygen species
RuBisCO	Ribulose-1,5-bisphosphate carboxylase/oxygenase
SOM	Soil organic matter
TNO	Netherlands Organisation for Applied Scientific Research
UNECE	United Nations Economic Commission for Europe
VOC	Volatile organic compound
VPD	Vapour pressure deficit
WUE	Water use efficiency

# Chapter 1

## General introduction

### 1.1 The global carbon and nitrogen cycle

The global carbon cycle describes the reservoirs of carbon and the fluxes amongst them (Schimel, 1995; Ciais et al., 2013). Carbon dioxide ( $\text{CO}_2$ ) emitted to the atmosphere is at first rapidly (within years) distributed between the atmosphere, the upper ocean and the vegetation; on longer time scales (within decades to millennia) it is moved to other reservoirs like soils, the deep ocean and rocks (Ciais et al., 2013). The global carbon cycle plays a key role in understanding climate change since about 60% of the observed global warming can be attributable to the increase in carbon dioxide concentration from pre-industrial to present day mixing ratios (Grace, 2004).

#### 1.1.1 Carbon emissions and sinks

Since the beginning of the Industrial Era the atmospheric  $\text{CO}_2$  concentration has increased from approximately 277 parts per million (ppm) in 1750 (Joos and Spahni, 2008; Le Quéré et al., 2016) to 399.4 ppm in 2015 (Dlugokencky and Tans, 2016; Le Quéré et al., 2016). Between 2002-2011 the atmospheric  $\text{CO}_2$  concentration increased by about  $2 \text{ ppm yr}^{-1}$  (Ciais et al., 2013). In 2015 9.9 GtC from fossil fuel emissions and industry and 1.3 GtC from land-use change (mainly deforestation) were emitted to the atmosphere (Le Quéré et al., 2016). The total cumulative emissions of fossil carbon and from land-use change between 1870-2015 is estimated to  $555 \pm 55 \text{ GtC}$  (Le Quéré et al., 2016). The atmosphere retained less than half of the emissions ( $235 \pm 5 \text{ GtC}$ ), the rest was absorbed by the ocean ( $160 \pm 20 \text{ GtC}$ ) and the land ( $160 \pm 60 \text{ GtC}$ ) (Le Quéré et al., 2016). Atmospheric  $\text{CO}_2$  rapidly exchanges with the  $\text{CO}_2$  dissolved in the surface layer of the ocean and the terrestrial biosphere (Falkowski et al., 2000). About  $90 \text{ GtC yr}^{-1}$  are exchanged between the atmosphere and the surface ocean and cause a rapid equilibration between both reservoirs (Falkowski et al., 2000). Rising atmospheric  $\text{CO}_2$  concentrations cause a disequilibrium in the fluxes between the atmosphere, ocean and terrestrial biosphere. This disequilibrium causes a net flux of  $\text{CO}_2$  into the ocean and on land has the potential to stimulate photosynthesis (Ciais et al., 2013)

### 1.1.2 The net land sink

The atmospheric CO<sub>2</sub> growth rate increased from 1.7 GtCyr<sup>-1</sup> in the 1960s to 4.5 GtCyr<sup>-1</sup> during 2006-2015 (Le Quéré et al., 2016). The increase in atmospheric CO<sub>2</sub> levels was paralleled by a similar increase in ocean and land uptake of CO<sub>2</sub> (Le Quéré et al., 2016). Between 2006-2015 44% of the total emissions remained in the atmosphere, 26% were taken up by the ocean, and 30% by the terrestrial biosphere (Le Quéré et al., 2016). Terrestrial Gross Primary Production (GPP) removes about 120 PgCyr<sup>-1</sup> from the atmosphere (Beer et al., 2010). The terrestrial biosphere takes up carbon if net primary productivity (NPP) exceeds carbon losses from heterotrophic decomposition processes in soils and disturbances (Arneeth et al., 2010). This so called 'net land sink' is maintained through several processes for example stimulated photosynthesis by increasing levels of atmospheric CO<sub>2</sub>, lengthening of the growing season in northern temperate and boreal areas, nitrogen deposition and regional reforestation (Arneeth et al., 2010; Friedlingstein et al., 2006; Le Quéré et al., 2016). The net land sink is lowered by processes/ factors that restrict CO<sub>2</sub> uptake like deforestation and air pollution, for example by ozone (Le Quéré et al., 2016; Oliver et al., 2018; Sitch et al., 2007; Simpson et al., 2014a). The relative contribution of them to the net land sink is uncertain. The magnitude of the land sink is commonly estimated by subtracting the increase in atmospheric CO<sub>2</sub> concentrations and the ocean CO<sub>2</sub> uptake of the fossil fuel emissions and emissions via land-use change (Le Quéré et al., 2016). The land sink is generally estimated to amount approximately 2 PgCyr<sup>-1</sup> (Luyssaert et al., 2007; Le Quéré et al., 2016). However, for the period of 2006-2015 the land sink is estimated to about 3.1 GtCyr<sup>-1</sup> (Le Quéré et al., 2016).

### 1.1.3 The terrestrial biosphere

The terrestrial biosphere rapidly exchanges CO<sub>2</sub> with the atmosphere (Falkowski et al., 2000). Via photosynthesis carbon is taken up from the atmosphere and partly bound in organic matter for example plant tissue and soil organic matter (Falkowski et al., 2000; Ciais et al., 2013). Carbon is released back to the atmosphere through autotrophic respiration by the plants, heterotrophic respiration by soil organisms and disturbances like fire (Falkowski et al., 2000; Ciais et al., 2013). The terrestrial biosphere constitutes a carbon sink if the CO<sub>2</sub> uptake from the atmosphere exceeds the release to it. The land sink is subject to considerable inter-annual variability and believed to be the main driver of the inter-annual variability of the atmospheric CO<sub>2</sub> growth rate (Gurney et al., 2008; Jung et al., 2017). Causes for the existence of a land sink are likely increased rates of photosynthesis at higher atmospheric CO<sub>2</sub> concentrations, nitrogen deposition and changes in climate that favour carbon sinks, for example longer growing seasons (Stocker, 2014).

Forests cover about 30% of the land surface, sequester large amounts of carbon annually and thus play an important role in the terrestrial carbon cycle (Luyssaert et al., 2007; Bonan, 2008). The impact of forests and the entire terrestrial biosphere on the global climate is difficult to investigate through observations and often origins from

computer models (Bonan, 2008). Current generation models for example simulate the carbon cycle, vegetation dynamics and a reciprocal impact of the atmosphere and land biosphere (Bonan, 2008). However, processes that are not yet or poorly included might induce unforeseen feedback loops (Bonan, 2008).

#### 1.1.4 Climate effects on the global carbon cycle

Besides the biological processes that impact the carbon storage (for example photosynthesis and decomposition) the global climate is furthermore impacted by biophysical processes (Bonan, 2008). Plant evapotranspiration has a cooling effect and a drier climate has the potential to reduce evapotranspiration and thereby amplify surface warming (Bonan, 2008). The surface cover can have a cooling or warming effect through its impacts on the albedo and hence the amount of energy that is retained at the surface. Forest growth in boreal tundra regions increases local carbon uptake and induces evaporative cooling, however it also decreases the albedo which has a warming effect (Bonan, 2008). Elevated atmospheric CO<sub>2</sub> concentrations have the potential to stimulate photosynthesis and increase carbon uptake, but on the other hand decreases stomatal conductance and transpirative cooling (Bonan, 2008). The net effect of all these and other factor is unknown (Bonan, 2008).

The atmospheric CO<sub>2</sub> concentration impacts the global temperature and hence climate via its impact on heat retention of the incoming solar radiation. The atmospheric CO<sub>2</sub> concentration and the carbon cycle are connected in a feedback loop since increases in the atmospheric CO<sub>2</sub> concentration induce climate change and climate change impacts the atmospheric CO<sub>2</sub> concentration (Friedlingstein et al., 2006). Climate change induces a multitude of changes that impact both carbon uptake (photosynthesis) and carbon loss (respiration). Soil warming leads to a stimulation of heterotrophic respiration and an increased carbon release as well as to an increase in mineralisation of soil organic matter which releases nutrients and can enhance carbon storage and compensate for the carbon losses and possibly exceed them (Melillo et al., 2002, 2011). Another example is the stimulation of plant photosynthesis and productivity in the high northern latitudes by climate change and an associated change in vegetation cover and a replacement of herbaceous plants with forests, which increases carbon uptake in these regions (Forkel et al., 2016).

#### 1.1.5 The nitrogen cycle and the nitrogen fertilisation effect

A large fraction of the atmosphere (78%) consists of very unreactive nitrogen (N<sub>2</sub>). Reactive forms of nitrogen are comparatively rare but are a limited nutrient for plants. The availability of reactive nitrogen constrains net primary production in large parts of the world (LeBauer and Treseder, 2008). The dependence of plant and soil microorganisms on reactive nitrogen as a nutrient is an important point where the global carbon and nitrogen cycle interlink. Reactive nitrogen is produced by natural processes in the ocean (biological nitrogen fixation) and by natural (biological nitrogen fixation and lightning) and anthropogenic (combustion, fertiliser production and agricultural biological nitrogen

fixation) processes on land and in the atmosphere (Fowler et al., 2013). Reactive nitrogen comprises oxidised ( $\text{NO}_y$ ) and reduced ( $\text{NH}_x$ ) nitrogen compounds (Simpson et al., 2014b). Major  $\text{NO}_y$  compounds are nitric oxide (NO) and nitrogen dioxide ( $\text{NO}_2$ ), which are together referred to as nitrogen oxides ( $\text{NO}_x = \text{NO} + \text{NO}_2$ ) (Simpson et al., 2014b). Important  $\text{NH}_x$  compounds are ammonia ( $\text{NH}_3$ ) and particulate ammonium (Simpson et al., 2014b). Part of the reactive nitrogen produced in or emitted to the atmosphere is deposited back on land where it might be taken up by plants or soil organisms or leached to the ocean. Denitrification by soil organism produces  $\text{N}_2$  which is emitted back to the atmosphere (see Fig. 2 in Fowler et al. (2013) for an overview of these processes).

Main natural sources of reactive nitrogen are lightening ( $5 \text{ TgN yr}^{-1}$ ) and biological nitrogen fixation (BNF) by bacteria, which amounts  $58 \text{ TgN yr}^{-1}$  on land and  $140 \text{ TgN yr}^{-1}$  in the ocean (Fowler et al., 2013). Anthropogenic activities produce further reactive nitrogen for example by combustion processes ( $30 \text{ TgN yr}^{-1}$ ), fertiliser production ( $120 \text{ TgN yr}^{-1}$ ) and the cultivation of crops and legumes which enhance biological nitrogen fixation (agricultural BNF  $60 \text{ TgN yr}^{-1}$ ) (Fowler et al., 2013). In the three major industrialised regions of the world (North America, Western Europe, eastern Asia) nitrogen oxides ( $\text{NO}_x$ ) emissions strongly increased between 1950 and 1970. Air cleansing regulations slowed the rate of increase or decreased  $\text{NO}_x$  emissions in the following decades in Europe and North America whereas emissions kept on increasing in Asia (Fusco and Logan, 2003). It is estimated that in 2010 the nitrogen cycling was doubled compared to pre-industrial values by the creation of  $203 \text{ TgN yr}^{-1}$  anthropogenic reactive nitrogen compared to  $210 \text{ TgN yr}^{-1}$  of natural fixed nitrogen (Fowler et al., 2013). Of the  $\approx 280 \text{ TgN yr}^{-1}$  of terrestrial origin 60% is stored in the land biosphere, transported by rivers or the atmosphere, deposited to the ocean or emitted as nitrous oxide,  $\text{N}_2\text{O}$  (Ciais et al., 2013). The smaller fraction of  $\approx 40\%$  ( $110 \text{ TgN yr}^{-1}$ ) is converted to  $\text{N}_2$  by denitrification of microorganisms and released back to the atmosphere (Ciais et al., 2013; Bouwman et al., 2013).

Nitrogen compounds emitted to the atmosphere reside there hours to days before they are deposited back on land or into the ocean (Galloway et al., 1995). Estimates suggest that of the  $\approx 98 \text{ TgN yr}^{-1}$  of  $\text{NO}_x$  and  $\text{NH}_3$  that are emitted to the atmosphere about  $\approx 65 \text{ TgN yr}^{-1}$  are deposited back to the continents (Galloway et al., 2004). Applying the assumption that in large parts of the world plant net primary production is restrained by the availability of nitrogen (LeBauer and Treseder, 2008), the deposition of reactive nitrogen from anthropogenic sources can be assumed to have increased plant growth and carbon sequestration from the atmosphere, thereby slowing down climate change (Norby, 1998). However, reactive nitrogen species ( $\text{NO}_x$ ) are also precursors for ozone formation (Derwent et al., 2002). Ozone is a toxic substance that can damage plants and reduce carbon uptake and storage (see Wittig et al. (2007, 2009); Sitch et al. (2007); Franz et al. (2017) and section 1.3 for more details). The role of  $\text{NO}_x$  as precursors for ozone formation might significantly reduce the mitigating effect of anthropogenic nitrogen depositions on climate change due to decreases in terrestrial net primary production caused by ozone damage to plants (Zaehle et al., 2011). The extend of this effect is so far unconstrained and needs to be investigated.

## 1.2 Tropospheric ozone concentrations and their impact on plants

### 1.2.1 Ozone formation and cycling

In the 19th century, ozone was discovered by C.F. Schönbein (Professor for chemistry in Basel, Switzerland) who developed a technique to measure the abundance of it in the atmosphere (Cooper et al., 2014). Tropospheric ozone is highly toxic to plants and animals because of its power as an oxidising agent (see subsection 1.3). It is formed in a photochemical process by the oxidation of CO, CH<sub>4</sub> or some volatile organic compounds (VOCs) catalysed by nitrogen oxides (NO<sub>x</sub> = NO, NO<sub>2</sub>) (Derwent et al., 2002). At high NO<sub>x</sub> levels, for example at polluted sites, O<sub>3</sub> is destroyed through its reaction with nitric oxide (NO), whereas at low NO<sub>x</sub> levels O<sub>3</sub> is formed (Parrish et al., 2012). The destruction of ozone mainly occurs in its reactions with water vapour and with hydrogen peroxy and hydroxyl radicals (Stevenson et al., 2006). Ozone impacts the lifetime of trace gases subject to oxidation by being the primary source of the hydroxyl radical (OH) in the troposphere (Cooper et al., 2014). Hydroxyl radicals are the primary oxidant for CH<sub>4</sub>, CO and VOCs in the troposphere (Parrish et al., 2012), which themselves are precursors for ozone formation.

Tropospheric ozone is either photochemically formed in the troposphere from natural and anthropogenic precursors or transported downwards from the stratosphere via the Brewer-Dobson circulation, primarily at the mid-latitudes (Collins et al., 2003; Cooper et al., 2014). The formation of ozone shows a pronounced diurnal and seasonal cycle, an increase from the poles towards the equator, as well as an increase with altitude, because higher temperatures and higher solar radiation intensify the photochemical processes (Sanz et al., 2007). Increasing emissions of volatile hydrocarbons with increasing temperature including emissions from the vegetation further amplify ozone formation (Sanz et al., 2007).

The impact of stratospheric influx of ozone on tropospheric ozone concentrations is still uncertain. The GEOS-CHEM model predicts that stratospheric influx in the troposphere accounts for 15-20% of the ozone concentrations in winter and less than 5% in summer at the northern mid-latitudes (Fusco and Logan, 2003). However, the ozone influx from the stratosphere into the troposphere may have decreased by up to 30% due to decreased stratospheric ozone concentrations in recent years (Fusco and Logan, 2003).

Continuous (day and night) anthropogenic emissions of NO<sub>x</sub> and VOCs can amplify the diurnal cycle due to the increase of ozone formation at daytime and the enhanced removal of ozone during nighttime caused by the continuing NO emissions (Zhang et al., 2004). A typical 19th century seasonal pattern of ozone cycling at rural sites in the Northern Hemisphere is characterised by a spring maximum of the concentrations which is likely caused by enhanced photochemistry and/or downward transport from the stratosphere related to tropopause foldings at the end of winter or beginning of spring (Cooper et al., 2014; Marenco et al., 1994; Vingarzan, 2004). At the end of the 20th century peak ozone concentrations shifted to summer in polluted regions (Cooper et al., 2014). Inter-annual variability of ozone concentrations is strongly dependent on meteorological

variables like temperature, radiation, and cloudiness (Sanz et al., 2007).

Worldwide changes in the release of ozone precursors affect the formation of ozone. The anthropogenic increase in  $\text{NO}_x$  emissions primarily from combustion sources has been identified as the major cause for the increasing near-surface ozone concentrations between 1970-1995 in the mid-latitudes of the Northern Hemisphere (Fusco and Logan, 2003). Future climate conditions with increasing temperatures and reduced cloudiness and precipitation will tend to increase ozone formation with increasing daily ozone peaks and average concentrations in summer (Meleux et al., 2007).

The distance a pollutant is transported is determined by the geographic location of its creation, the atmospheric circulation, and strongly depends on the lifetime of the pollutant in the free atmosphere. A compound needs to have an atmospheric lifetime of at least a week to be transported to another continent and thus become a global issue (Akimoto, 2003). The lifetime of ozone of about 22 days enables a long-range transport between continents all year long and hemispheric transport except in summer (Akimoto, 2003; Stevenson et al., 2006; Derwent et al., 2002) where increased atmospheric water vapour concentrations decrease its lifetime (Parrish et al., 2012). Climate change might reduce ozone lifetimes due to an increased ozone loss via the reaction with increasing water vapour concentrations in the atmosphere (Stevenson et al., 2006).

The stronger convective activity over China compared to other industrialised regions in the world facilitates the transport of ozone into the free atmosphere and can cause an increase of background levels in the downwind direction (Fusco and Logan, 2003). In the case of ozone, the transport of ozone precursors is an important issue in addition to ozone transport itself. Carbon monoxide possesses an atmospheric lifetime allowing for intercontinental and hemispheric transport (Akimoto, 2003) whereas nitrogen oxides possess shorter lifetimes.  $\text{NO}_x$  is in general only transported regionally and thus causes for example low and rather constant ozone concentrations over the oceans (Derwent et al., 2002).

### 1.2.2 Background concentrations

Local ozone background concentrations are to a large extent determined by the hemispheric baseline but are additionally affected by the geographic location and elevation. These concentrations are further altered (increased or decreased) by local and regional processes, for example the extent of anthropogenic influence (Vingarzan, 2004; Jenkin, 2008). Knowing the background ozone concentration is essential to get an estimate of longer-term concentration changes due to the effects of local and regional anthropogenic emissions. Measurements in urban areas include anthropogenic impacts and are important to assess the immediate exposure and damage for the biosphere. Average surface mixing ratios for the year 2000 for the Northern Hemisphere are estimated to  $33.7 \pm 3.8$  ppb (40 to 50 ppb over large parts of North America, southern Europe, and Asia) and  $23.7 \pm 3.7$  ppb for the Southern hemisphere (background values range from 15-25 ppb) (Akimoto, 2003; Vingarzan, 2004; Dentener et al., 2006). Assuming that in pre-industrial times surface ozone concentrations were mainly produced by natural sources and constitute a natural background, the comparison of pre-industrial and

present day concentrations indicates the anthropogenic impact on today's ozone concentrations. Present day ozone surface mixing ratios are measured at thousands of surface stations around the globe. Vertical ozone profiles are obtained from measurements of sondes, lidars, especially equipped aircraft and over a large part of the globe by satellites (Cooper et al., 2014).

### 1.2.3 Trends

Surface ozone concentrations in 1860 amounted 15-25 ppb over the mid- and high-latitudes of Eurasia and North America, and increased to 40-50 ppb in the present (Akimoto, 2003). In Western Europe, tropospheric O<sub>3</sub> levels have increased approximately by a factor 2 to 5 from pre-industrial values to the 1990s (Cooper et al., 2014; Marenco et al., 1994; Staehelin et al., 1994), although the low values at the start of this period are very uncertain. Between 1950 and the 1990s tropospheric O<sub>3</sub> levels approximately doubled in the Northern Hemisphere (Parrish et al., 2012; Cooper et al., 2014). In the last decades, the yearly rate of increase has been approximately 0.5-2% in the mid latitudes of the Northern Hemisphere (Vingarzan, 2004; Parrish et al., 2012). The observed increase in ozone concentrations coincides with an increase in its precursor NO<sub>x</sub> by a factor of 4.5 between 1955 and 1985 (Cooper et al., 2014; Staehelin et al., 1994). The longest quantitative measurements of O<sub>3</sub> were conducted in Europe what restricts statements on long-term changes to this region (Cooper et al., 2014).

The major causes for increased O<sub>3</sub> formation are the increased emission of O<sub>3</sub> precursor trace gases such as NO<sub>x</sub> and CO, primarily from combustion sources, non-methane volatile organic compounds from anthropogenic sources (combustion, solvents), and methane emissions from agriculture and industry (Fusco and Logan, 2003; Vingarzan, 2004). Increased NO<sub>x</sub> and methane emissions seem to account for 10-20% and 3-4% increase in O<sub>3</sub> background levels since 1970, respectively (Vingarzan, 2004). Model runs by Fusco and Logan (2003) suggest that 40% of the increase in O<sub>3</sub> concentrations can be attributed to increased NO<sub>x</sub> emissions and less than 20% to increases in methane concentrations between 1970 and 1994. The stratospheric ozone influx into the troposphere on the contrary seems to have declined during the modelling period of 1970 to 1994 (Fusco and Logan, 2003). Intercontinental transport of ozone increases background concentrations downwind of polluted sites and might account for increased ozone concentrations by 3-10 ppb in the western United States during spring due to Asian pollution (Vingarzan, 2004).

An increase in tropospheric ozone concentrations is not observed everywhere and trends vary between locations. Many background stations measured increasing levels of ozone between the 1960s and 2000s, however some stations report declining levels (Vingarzan, 2004). On average an upward trend can be observed due to the increasing baseline trend and a decreasing trend of the removal of ozone by locally emitted nitric oxide (Jenkin, 2008). Intercontinental transport seems to be an important factor influencing locally observed ozone trends (Vingarzan, 2004; Jenkin, 2008). For instance, air cleaning policies to reduce anthropogenic NO<sub>x</sub> and VOC emissions have decreased the occurrence of very high peak ozone concentrations in the UK, in spite of the in-

crease of ozone concentrations at background sites due to the increasing global baseline concentration (Jenkin, 2008).

Projections suggest worldwide increasing background ozone concentrations of  $1.5 \pm 1.2$  ppb by 2030 under the CLE scenario (Current Legislation scenario: implementation of current air quality legislation around the world) and  $4.3 \pm 2.2$  ppb under the more pessimistic IPCC SRES A2 scenario (Dentener et al., 2006). By 2100 mean monthly ozone concentrations are projected to exceed 70 ppb in the summer months in large parts of the Northern Hemisphere when applying the IPCC SRES A2 emission scenario (Sitch et al., 2007). However, future trends of ozone concentrations are highly dependent on the location.

### 1.3 Ozone effects on plants

Ozone occurring in the near-surface atmosphere enters plants primarily through the leaf stomata, a process which is limited by the leaf boundary layer conductance and the stomatal conductance (Musselman et al., 2006). Factors that control stomatal conductance for example photosynthetic capacity, incident light, vapour pressure deficit (VPD), and temperature can thus be assumed to affect foliar ozone uptake. After entering the leaf internal air spaces, ozone quickly dissolves into the aqueous phase surrounding the cells and is rapidly consumed in the cell walls and/or the plasma membrane. This results in a near zero leaf internal ozone concentration (Laisk et al., 1989). Initial target sites for reactions are plasma membrane lipids, susceptible amino acids in proteins, plasma membranes, apoplastic enzymes, or cell wall components (Fiscus et al., 2005). In these reactions, reactive oxygen species (ROS) such as hydroxyl radicals ( $\text{OH}^-$ ), superoxide anions ( $\text{O}_2^-$ ) and hydrogen peroxide ( $\text{H}_2\text{O}_2$ ) are produced (Kangasjärvi et al., 1994). These ROS then cause an abundance of observed effects: Amongst others they can act as messengers and trigger hypersensitivity reaction resulting in programmed cell death (Tausz et al., 2007) or induce stomatal closure (McAinsh et al., 2002; Fiscus et al., 2005).

#### 1.3.1 Overview of types of effects

Effects of ozone on plants are generally investigated by ozone filtration/fumigation experiments where plants exposed to different ozone concentrations are compared. Charcoal filtered air is often used to simulate pre-industrial conditions, whereas a fumigation with elevated ozone concentrations can be used to assess impacts at ozone hotspots or under possible future conditions. The available empirical studies to investigate ozone effects differ in their length, i.e. investigation of short-term effects versus the consequences of chronic exposure, and in the exposure method, for instance using open top chambers (Heagle et al., 1973; Fuhrer, 1994), or free air ozone fumigation systems (FACE), such as combined free air ozone and  $\text{CO}_2$  enrichment experiments (Karnosky et al., 2003). The observed injuries in the experiments cover a wide range of effects. Prominent adverse effects are visible injury like lesion or chlorosis (Langebartels et al., 1991; Wohlgemuth et al., 2002), reductions in photosynthetic capacity (Tjoelker et al., 1995; Wittig et al.,

2007) and growth and yield (Grantz et al., 2006; Hayes et al., 2007; Feng and Kobayashi, 2009; Wittig et al., 2009; Leisner and Ainsworth, 2012). There is some evidence for a shifted carbon allocation with a reduced allocation to roots, resulting in an altered root:shoot-ratio (Grantz et al., 2006; Hayes et al., 2012). Conflicting results exist regarding altered respiration rates, including reports of increasing, decreasing and unaltered respiration rates (Tjoelker et al., 1995; Wittig et al., 2009; Lombardozzi et al., 2012b). Many symptoms of ozone injury resemble senescence like chlorosis, chloroplast degradation, protein loss, ethylene emissions and decreases in photosynthetic capacity (see Pell et al. (1997); Fuhrer and Booker (2003) and section 1.3.3). The commonly observed decline in photosynthesis (Wittig et al., 2007) is often related to a decline in carboxylation efficiency (Farage et al., 1991), electron transport as well as direct and indirect effects on stomatal conductance (see Paoletti and Grulke (2005); Lombardozzi et al. (2012b) and section 1.3.4). Reductions in carboxylation efficiency are assumed to be caused by reduced RuBisCO levels and activation, which in return can be caused either by enhanced degradation or reduced production (Fiscus et al., 2005). Since stomatal conductance and photosynthesis are affected, ozone has a direct effect on the plant's transpiration rate, and in the case of stomatal damage also on the plant's water use efficiency (WUE) (Wittig et al., 2007; Mills et al., 2009; Lombardozzi et al., 2012b). Not all ozone that is taken up into the plants however directly damages them. Plants can activate defence mechanism and physiological pathways to produce protective compounds like ascorbate and polyamines which can detoxify at least part of the ozone (see Kangasjärvi et al. (1994); Kronfuß et al. (1998); Tausz et al. (2007) and section 1.3.2).

### 1.3.2 Detoxification, respiration, repair

Defence mechanisms can detoxify at least part of the ozone that enters the plants stomata. The effective ozone flux constitutes the remaining fraction that could not be detoxified and has the potential to injure the plant cells (Musselman et al., 2006). The ozone dose (integral of instantaneous ozone stomatal flux over a period of time) thus can be very different to the effective dose (integral of the effective flux over a period of time), depending on the plant's specific defence capabilities (Musselman et al., 2006).

Oxidative stress in plants occurs due to the uptake of pollutants like ozone, but also occurs naturally under photo-oxidative stress. Plants have developed an antioxidant defence system to control ROS which are produced by either process (Tausz et al., 2007).

Detoxification agents can be classified in two broad categories - constitutive and inductive - according to their mode of action (Musselman et al., 2006; Wieser and Matyssek, 2007). Constitutive agents are present already when ozone enters the leaf and directly detoxifies it. Ascorbate is often termed 'the first line of defence, as it is present in the plant's cell walls and directly detoxifies entering ozone (Smirnov, 1996; Tausz et al., 2007; Wieser and Matyssek, 2007). Other compounds additionally acting as detoxifying agents are for instance polyamines (Langebartels et al., 1991; Kangasjärvi et al., 1994), jasmonates (Overmyer et al., 2000) and isoprenoids (Vickers et al., 2009; Fares et al., 2010). Inductive agents are produced on demand if the detoxifying capacity

of the constitutive defence is insufficient. Since their production has to be induced, a time lag occurs until they can act as protective agents.

Ozone injury is assumed to occur when the anti-oxidant system becomes overwhelmed (Wieser and Matyssek, 2007). The level of ascorbate is considered as an indicator for tolerance, but is also known to be insufficient for determining varying ozone tolerances between species (Tausz et al., 2007). Dizengremel et al. (2008) suggests to consider the cells ability to regenerate antioxidants and hence amongst others the level of reducing power (NADPH) provided by photosynthesis additional to the ascorbate content. Independent on the exact mechanism, detoxification of ozone and/or repair of ozone induced injury likely increases the plant's respiration costs and hence progressively reduces net primary production with increasing cumulative ozone uptake (Wieser and Matyssek, 2007).

### 1.3.3 Injury

Ozone injury in plants can either manifest themselves in visible injury like chlorotic spots of the leaf surface, or in an altered physiology without any visible symptoms (Heath, 1994). An altered physiology in general develops due to chronic exposure to low concentrations, and includes symptoms such as inhibition of photosynthesis, altered stomatal conductance, a lack of responsiveness to abscisic acid (ABA) and accelerated senescence (Kangasjärvi et al., 1994; Dizengremel, 2001; Mills et al., 2009). Visible injury in general results from unregulated or programmed cell death either due to short-term exposure to high ozone concentrations that occurs within hours after the exposure (acute effects), but can also be the consequence of chronic exposure to lower concentrations, where the lesions develop over days or weeks (Fiscus et al., 2005).

Injury occurs when the amount of absorbed ozone exceeds the capacity of the anti-oxidative defence system to detoxify it (see Musselman et al. (2006) and section 1.3.2). This might happen if the costs for building up defence compounds exceeds the supply with assimilates provided by photosynthesis (Wieser and Matyssek, 2007). The magnitude of the injury might be determined by the amount of ozone that is not detoxified. For example, lesion formation was found to linearly increase with the ozone dose in tobacco plants (Langebartels et al., 1991).

Injury formation results from triggering the pathogen-defence pathway, which leads to a hypersensitivity response and can induce cell death due to a ROS accumulation in the tissue termed an 'oxidative burst' (Wohlgemuth et al., 2002). Existing lesions expand by triggering ROS accumulation in neighbouring cells (Wohlgemuth et al., 2002). Injury formation also correlates with an increase in ethylene levels after ozone exposure in ozone-sensitive plants, whereas ethylene contents remain low at insensitive plants (Tingey et al., 1976; Langebartels et al., 1991; Kangasjärvi et al., 1994). Ethylene is involved in controlling the natural senescence of a leaf; it modulates pathogen defence pathways and has the potential to prevent stomatal closure (Burg, 1968; Wilkinson and Davies, 2009; McManus, 2012).

High ozone concentrations have the potential to cause direct adverse effects (Reich, 1987; Fiscus et al., 2005; Noormets et al., 2010). Peak ozone events might play an

important role to determine potential injury. Several studies showed that plants exposed to peak concentrations were more impacted than those exposed to smooth concentrations (Stan and Schicker, 1982; Musselman et al., 1994). However crop responses seem to be better related to intermediate ozone concentrations (hourly averages between 50-90 ppb) because they occurred at times when atmospheric conditions favour a high stomatal conductance and hence ozone uptake Krupa et al. (1995).

#### 1.3.4 Impacts on stomatal conductance

Stomata control the leaf gas exchange and stomatal conductance is a major factor determining the amount of ozone uptake besides the foliar area of a plant (Wieser and Havranek, 1995). The near-surface atmospheric ozone concentration and the aerodynamic and stomatal resistance to ozone transport determine the ozone dose [nmol O<sub>3</sub> m<sup>-2</sup> over a defined period of time] a plant experiences. Species with higher stomatal conductance are subjected to higher ozone doses and are shown to be more prone to injury (Reich, 1987; Wittig et al., 2009), what suggests a strong correlation between the ozone dose and realised injury. Stomatal conductance is generally highest in the mid-morning hours, due to high irradiance and low vapour pressure deficit (VPD), and decreases in the afternoon. A mid-day-dip in stomatal conductance can result from a high midday VPD (Pathre et al., 1998). Near-surface ozone concentrations are generally highest in the late afternoon, as a result of the photochemical production process. Peak ozone concentrations thus do not generally coincide with peak values of ozone uptake (Musselman et al., 2006; Heath et al., 2009; Fares et al., 2010). Night-time stomatal conductance is often omitted in ozone assessments, because plants are assumed to have minimal stomatal conductance at night and because the lower turbulent air exchange between the free atmosphere and the surface boundary layer during night-time additionally reduces gas exchange. However it was shown for many species that stomata remain partly open during the night, and that the nocturnal stomatal ozone flux can be an important factor in the total plant ozone uptake (Musselman and Minnick, 2000; Musselman et al., 2006).

In general it is assumed that stomata close at high concentrations of ozone following an inhibition of photosynthesis (Darrall, 1989), as both processes are tightly coupled. However, stomata respond in general 10-100 times slower to changes in external conditions than photosynthesis (Morison, 1998). Ozone induced reductions in stomatal conductance are mediated by an increase in the leaf internal CO<sub>2</sub> concentration caused by an impaired photosynthetic apparatus (Darrall, 1989; Paoletti and Grulke, 2005, 2010). Besides such indirect effects on stomatal conductance, stomata can also be directly effected. Ozone-affected stomata respond much slower to environmental stimuli than unaffected cells (Paoletti and Grulke, 2005), what can delay closure. In this case, stomatal conductance and photosynthesis can become 'uncoupled' (Reich, 1987; Tjoelker et al., 1995; Lombardozzi et al., 2012b). This decoupling, also known as 'sluggishness', causes a higher ozone uptake and transpiration rates (Mills et al., 2009; Paoletti and Grulke, 2010; Lombardozzi et al., 2012b). The increased transpiration and hence water loss due to stomatal sluggishness can increase the risk of hydraulic failure under drought stress (Sun et al., 2012). Exposure to short-term high concentrations of ozone can cause

immediate reductions in photosynthesis and a parallel decline in stomatal conductance whereas chronic exposure is assumed to lead to stomatal sluggishness (Farage et al., 1991; Paoletti and Grulke, 2005).

### 1.3.5 Exposure indices

To assess the potential detrimental effect of tropospheric ozone on the biosphere, exposure indices were developed starting with concentration based indices (see LRTAP-Convention, 2017, for an overview). The classical example is the AOTX [ppm h], where the free-air ozone concentration is related to observed plant damage. When calculating the AOTX, the mean hourly ozone concentration exceeding a threshold of X ppb (generally 30 or 40 ppb) are summed for all daylight hours (radiation  $> 50 \text{ W m}^{-2}$ ) for a specified time period, for example the months when the vegetation is active. The advantage of a concentration-based metric is that it relies exclusively on easily observable quantities like the ground level ozone concentration.

Models assessing ozone damage to gross or net primary production based on AOTX have been used for many years and indicate that substantial reduction in plant growth and carbon sequestration occurs globally and may reach reductions of more than 40% at  $\text{O}_3$  hotspots (Felzer et al., 2004, 2005; Ren et al., 2011; Anav et al., 2011).

However, different species and their regional provenances differ vastly in their stomatal conductance and hence the amount of ozone uptake per time interval ('dose') (Reich, 1987). The  $\text{O}_3$  dose has been observed to strongly correlate with the amount of injury of a plant, suggesting that plants with a higher stomatal conductance are subject to higher doses and hence are more susceptible to injury (Reich, 1987; Wittig et al., 2009). Stomatal flux-based models, such as for instance the  $\text{DO}_3\text{SE}$  model (Emberson et al., 2000a), estimate the uptake of ozone per time period as a function of surface ozone concentration and the plant's stomatal conductance. The latter is affected by various factors such as incident light, atmospheric vapour pressure deficit (VPD), air temperature and phenology. A commonly used flux-based index is the  $\text{POD}_y$  [ $\text{nmol m}^{-2} \text{s}^{-1}$ ], which gives the accumulated ozone flux above a threshold of  $y \text{ nmol m}^{-2} \text{s}^{-1}$  for all daylight hours and a given time period. Common threshold values for  $\text{POD}_y$  range from 1-6  $\text{nmol m}^{-2} \text{s}^{-1}$  (Pleijel et al., 2007; LRTAP-Convention, 2017; Mills et al., 2011b), depending on the specific species sensitivity to  $\text{O}_3$ . The AOTX and  $\text{POD}_y$  both calculate a cumulated value, which is then related to plant damage. Regions of high risk for potential damage generally differ between both indices (Simpson et al., 2007; Emberson et al., 2000a). Contrary to the exposure based AOTX, the uptake based  $\text{POD}_y$  suggests high ozone effects not only in for example southern Europe, but also in central and northern Europe, where climatic conditions favour a high stomatal ozone uptake (Mills et al., 2011a; Simpson et al., 2007). Observed ozone damage in the field seems to be better correlated to flux-based risk assessment compared to concentration based methods (Mills et al., 2011a). Following this the, UNECE Convention on Long-range Transboundary Air Pollution (LRTAP Convention) recommends flux based methods as the preferred tool for risk assessment (see LRTAP-Convention, 2017).

A recent study by Feng et al. (2018) suggest that relating ozone uptake to leaf mass

(termed PODx) better explains inter-specific ozone sensitivity compared to the already established damage index PODy, where ozone uptake is related to the leaf area. However, an independent confirmation of this observation is still missing and it is yet unclear if this index will generally be used in future risk assessments.

## 1.4 Impacts of elevated CO<sub>2</sub> concentrations on plants

Increasing atmospheric CO<sub>2</sub> concentrations are a key aspect of climate change. As CO<sub>2</sub> is a nutrient for plants, changes in the atmospheric abundance of CO<sub>2</sub> impact plants. A multitude of experiments with herbaceous and woody plants, exposed to elevated CO<sub>2</sub> (eCO<sub>2</sub>) concentrations for short or medium time spans, fumigated in chambers or Free Air CO<sub>2</sub> Enrichment systems (FACE) over the last decades suggests a multitude of effects on plants, soil microbes and soil properties. It is shown that elevated eCO<sub>2</sub> for example stimulates photosynthesis (Curtis and Wang, 1998; Medlyn et al., 1999; Ainsworth and Long, 2005), increases total biomass (Curtis and Wang, 1998; King et al., 2005; De Graaff et al., 2006), alters stomatal conductance (Medlyn et al., 2001; Paoletti and Grulke, 2005), and thus possibly impacts soil moisture and run-off (Field et al., 1995). There is some evidence that the biochemical composition of leaves is altered, including an increase in starch content and a reduction in nitrogen content (Drake et al., 1997; Curtis and Wang, 1998; Medlyn et al., 1999), and that dark respiration is decreased (Drake et al., 1997). Foliar senescence might be delayed (Karnosky et al., 2003). Both, an altered chemical foliar composition and soil moisture pattern, might impact litter decomposition (Field et al., 1995). However a meta-analysis by Norby et al. (2001) showed that despite a significant reduction in leaf nitrogen in the litter and an increased lignin concentration no significant effect on decomposition was found.

Studies using different species and exposure systems (FACE or fumigation chambers) or life stages observed different and sometimes contradictory effects (Ainsworth and Long, 2005; De Graaff et al., 2006; Leakey et al., 2009, see for example). A meta-analysis of FACE studies shows that functional groups differ in their response to FACE and that trees responded stronger compared to herbaceous species (Ainsworth and Long, 2005). Trees showed little photosynthetic acclimation to eCO<sub>2</sub> and exhibited the largest increase in dry matter production (Ainsworth and Long, 2005). Increases in the leaf area index (LAI) could be observed in trees but not in herbaceous plants (Ainsworth and Long, 2005). However when considering these results one has to take into account that the trees in the experiment were generally young and rapidly growing, what might impact these findings (Ainsworth and Long, 2005). A general finding by Ainsworth and Long (2005) is that light-saturated carbon uptake and carbon assimilation, growth and above-ground production is increased, whereas specific leaf area and stomatal conductance is decreased in eCO<sub>2</sub>. Increased growth induced by eCO<sub>2</sub> induces a concurrent demand for nutrients and might cause a depletion of for example soil nitrogen and ensued a reduction in NPP (Hyvönen et al., 2007). The eCO<sub>2</sub> induced stimulation of NPP is also found to stimulate root growth and to increase the root:shoot ratio (Luo et al., 2006). The probably expanded rooting system might increase the nitrogen uptake which has the

potential to increase NPP (Hyvönen et al., 2007). Furthermore evidence exists for an increased nitrogen use efficiency of plants under eCO<sub>2</sub> (Leakey et al., 2009). Increases in NPP simultaneously increase litter production and soil organic matter (Hyvönen et al., 2007). Increased biomass and litter production under eCO<sub>2</sub> is assumed to increase soil respiration and hence CO<sub>2</sub> release to the atmosphere (Hyvönen et al., 2007; De Graaff et al., 2006). This CO<sub>2</sub> release at least partly counterbalances increased rates of CO<sub>2</sub> uptake due to the stimulated plant carbon uptake.

The CO<sub>2</sub> fertilisation effect (increases in photosynthesis and carbon uptake induced by eCO<sub>2</sub>) is generally assumed to only develop if CO<sub>2</sub> is the most limiting resource (Field et al., 1995). The stimulating effect of eCO<sub>2</sub> on NPP might get severely reduced or completely eliminated if other resources like water or nitrogen are limited (Reich et al., 2014; De Graaff et al., 2006). The deposition of anthropogenic produced reactive nitrogen thus has the potential to at least partly maintain the CO<sub>2</sub> fertilisation effect in nutrient poor ecosystems (Ciais et al., 2013). A study by Zak et al. (2011) indicates that under eCO<sub>2</sub> microbial decay and net N mineralisation are accelerated, which increases the soil N-cycling and sustains increased rates of NPP (Zak et al., 2011). A greater below ground plant growth induced by eCO<sub>2</sub> hastened the organic matter decay and enhanced the N supply to plants (Zak et al., 2011). If these increased rates of soil N cycling are able to maintain increased rates of NPP is yet uncertain (Zak et al., 2011).

Stomata open or close depending on the leaf internal CO<sub>2</sub> concentrations (Mott, 1988; Paoletti and Grulke, 2005), where photosynthesis (CO<sub>2</sub> fixation) acts as a CO<sub>2</sub> sink and stomatal opening as a CO<sub>2</sub> source. meta-analyses indicate a reduction in stomatal conductance under eCO<sub>2</sub> (Curtis and Wang, 1998; Medlyn et al., 2001), what might reduce transpiration, increase the plants water-use efficiency (WUE) and cause less water uptake from the soil and hence an increase in soil water content (Drake et al., 1997) and river runoff (Gedney et al., 2006). Where water is a limiting factor for productivity, this increased soil moisture has the potential to increase productivity and foliar area (Field et al., 1995). Increases in LAI can in return elevate stand-level transpiration rates to levels comparable to ambient CO<sub>2</sub> even though transpiration on a leaf-level basis is reduced (Drake et al., 1997). The increase in WUE and leaf-level transpiration potentially increases leaf temperatures due to a reduced loss of latent heat (Drake et al., 1997), which through a feedback to near leaf VPD might cause an increase in transpiration.

#### 1.4.1 Coupled effects of elevated CO<sub>2</sub> and O<sub>3</sub>

The coupled effects of elevated CO<sub>2</sub> and elevated ozone (eO<sub>3</sub>) on plant traits and performance are less well understood than the single effects. The stomatal closure induced by eCO<sub>2</sub> (Paoletti and Grulke, 2005) has the potential to limit O<sub>3</sub> uptake and hence damage. Contradictory evidence exists showing that either eCO<sub>2</sub> ameliorated the negative effects of O<sub>3</sub> on plants (Barnes and Pfirrmann, 1992; Broadmeadow and Jackson, 2000; Isebrands et al., 2001; Riikonen et al., 2004) or that there was little interaction between both gases and the stimulating effect of eCO<sub>2</sub> on NPP persisted (Talhelm et al., 2014; Zak et al., 2011). However, results from the Aspen FACE indicate that stomatal

conductance and ozone uptake were not reduced by eCO<sub>2</sub> in their experiment (Uddling et al., 2010).

Some studies observed reductions in injury (Barnes and Pfirrmann, 1992; Wustman et al., 2001) and chlorophyll degradation (Broadmeadow and Jackson, 2000) under the joint fumigation of eCO<sub>2</sub> and eO<sub>3</sub> (eCO<sub>2</sub>+eO<sub>3</sub>). Several studies find species specific positive or negative impacts of eCO<sub>2</sub>+eO<sub>3</sub> on photosynthesis (Noormets et al., 2001), growth (Isebrands et al., 2001) and biomass (King et al., 2005). Ozone fumigation completely offset the growth enhancement observed in the eCO<sub>2</sub> treatment for ozone sensitive and tolerant clones in the ASPEN FACE (Karnosky et al., 2003). An amplification of the negative effects of O<sub>3</sub> under eCO<sub>2</sub> on leaf chlorophyll content, nitrogen content and electron transport capacity ( $J_{max}$ ) was observed in ozone sensitive and tolerant aspen clones (Noormets et al., 2010). A possible reason for the amplification of ozone induced negative effects under eCO<sub>2</sub> is a possible down regulation or suppression of antioxidant production under eCO<sub>2</sub> and hence increased injury (Wustman et al., 2001; Karnosky et al., 2003). All in all, a clear picture of the joint effects of eCO<sub>2</sub>+eO<sub>3</sub> on plants or plant groups is still lacking.

#### 1.4.2 Coupled effects of elevated CO<sub>2</sub>, O<sub>3</sub> and N availability

The coupled effects of O<sub>3</sub> and N availability are rarely investigated. Nitrogen fertilisation can stimulate plant photosynthesis and through this increase stomatal conductance. Increased rates of stomatal conductance can enhance ozone uptake and hence ozone induced injury what in return can reduce photosynthesis. Some studies find no or less severe adverse effects of O<sub>3</sub> in nitrogen limited treatments (Cardoso-Vilhena and Barnes, 2001; Utraiainen and Holopainen, 2001). However, a meta-analyses on the combined effects of N-availability and O<sub>3</sub> showed that above-ground biomass, leaf area and root biomass were stronger negatively affected by O<sub>3</sub> when nitrogen was limited compared to sufficient N-treatments (Yendrek et al., 2013). The joint impacts of CO<sub>2</sub>, O<sub>3</sub> and N availability are even less well investigated. A study with spring wheat showed that for all tested nitrogen levels eCO<sub>2</sub> counteracted the harmful effects of O<sub>3</sub> on photosynthesis and growth (Cardoso-Vilhena and Barnes, 2001). The observed reduction in damage was associated with a decline in O<sub>3</sub> uptake (Cardoso-Vilhena and Barnes, 2001).

### 1.5 Future projections of climate change

To investigate potential future impacts of air pollution and climate change on the terrestrial biosphere models need to be driven by potential future climate and atmospheric compositions. Climate scenarios have been developed for several decades and are regularly updated. Over the last decades the IPCC commissioned the development of several scenarios, like the IS92 and SRES scenario (Nakicenovic et al., 2000; Moss et al., 2010). Climate models have become more complex over the last decades and need an extended and more detailed set of input (Moss et al., 2010) to create updated climate scenarios. The climate modelling community developed a set of scenarios, the 'representative

concentration pathways (RCPs)', which contain possible future emissions and concentrations of greenhouse gases and air pollutants as well as land-use trajectories necessary to run Climate models and Integrated Assessment Models (van Vuuren et al., 2011). The use of a common set of drivers of climate change facilitates the comparison of results from different models.

### 1.5.1 Representative concentration pathways (RCPs)

The RCPs are trajectories of major drivers of climate change, that are developed to span the full range (extreme and intermediate) of possible future climate scenarios in the scientific literature (van Vuuren et al., 2011). Four pathways were produced for the period 1850-2100 that lead to a radiative forcing of 2.6, 4.5, 6 and 8.5  $\text{W m}^{-2}$  by the year 2100 (van Vuuren et al., 2011). The RCP8.5 is a high emission scenario containing a high baseline of greenhouse gas emissions and medium-high air pollution (van Vuuren et al., 2011). The RCP6 and RCP4.5 are intermediate emission scenarios with both containing medium levels of air pollution and a medium and very low baseline of greenhouse gas emissions, respectively (van Vuuren et al., 2011). The low emissions scenario RCP2.6 assumes very low emissions of greenhouse gases and medium-low levels of air pollution (van Vuuren et al., 2011). All RCPs show declining trends of air pollution owed to the assumption of more strict air pollution control and thus do not account for the possibility of very little or no reduction of air polluting emissions (van Vuuren et al., 2011). The global nitrogen deposition is projected to remain relatively constant in all RCP scenarios, except RCP2.6, but changes occur on a regional basis (Ciais et al., 2013).

The RCP scenarios can be used by climate models to develop new climate scenarios (Moss et al., 2010). Integrated Assessment Models can use the RCPs to investigate various technological, socio-economic and policy futures that might lead to each of the RCPs and the resulting change in radiative forcing (Moss et al., 2010).

### 1.5.2 Simulated changes during the 21st century

Within the Coupled Model Intercomparison Project Phase 5 (CMIP5) of the World Climate Research Programme a large number of Earth system Models (ESM) and Atmosphere–Ocean General Circulation Models (AOGCMs) conducted new climate model simulations which constitute the core of the climate system projections (Stocker, 2014). The models participating in the CMIP5 project base their simulations on the RCP scenarios described in the above section. The simulation results indicate with very high confidence that by the end of the 21st century temperature changes over land will be higher compared to over the ocean with the highest warming occurring in the Arctic region (Stocker, 2014). With increasing global mean surface temperatures global precipitation will certainly increase on a global mean, where different regions will experience decreases, increases or no changes (Stocker, 2014).

The ocean uptake of  $\text{CO}_2$  is projected to continue until the end of 21st century with very high confidence (Stocker, 2014). The land carbon sink is projected to continue until 2100 by most CMIP5 models but a minority of models predicts the terrestrial bio-

sphere to become a net CO<sub>2</sub> source, due to the effects of climate and land-use change (Stocker, 2014). The CMIP5 simulations furthermore suggests that elevated CO<sub>2</sub> increases the land carbon sink and climate effects will reduce CO<sub>2</sub> uptake in the tropics and mid-latitudes, both with medium confidence (Ciais et al., 2013). Since none of the models included a representation of permafrost pools the sign and magnitude of climate responses in high-latitudes is of low confidence (Ciais et al., 2013).

Nutrient availability will very likely limit the effect of rising atmospheric CO<sub>2</sub> levels on land carbon storage (Ciais et al., 2013; Stocker, 2014). Climate warming is projected to increase soil organic matter decomposition and nitrogen mineralisation with high confidence (Ciais et al., 2013). An enhanced availability of reactive nitrogen species might increase carbon storage by vegetation (Ciais et al., 2013). With high confidence nitrogen is projected to limit terrestrial carbon sequestration even when anthropogenic nitrogen deposition is considered (Ciais et al., 2013; Stocker, 2014).

The simulation of future surface ozone concentrations based on the RCP scenarios projects annual global mean reductions of 2 ppb by 2050 (compared to the levels of the year 2000) contrary to a 4-6 ppb increase when applying the IPCC SRES scenarios (Wild et al., 2012). Over most regions a substantial reduction in annual mean ozone concentrations is expected except for South Asia where increases might be as high as 5 ppb (Wild et al., 2012).

## 1.6 Global terrestrial biosphere models

The impact of the terrestrial biosphere on the global climate is difficult to estimate through direct observations (Bonan, 2008). Biosphere-atmosphere interactions can for example be investigated by eddy covariance flux towers and field experiments on a local scale. Large scale estimates of GPP can for example be derived from remote sensing products like MODIS (Heinsch et al., 2006). The most common approach to investigate the global interaction between atmosphere and biosphere is by applying models (Bonan, 2008). In this thesis the terrestrial biosphere model O-CN model is used to investigate air pollution impacts on the terrestrial carbon and nitrogen cycling.

### 1.6.1 The O-CN model

O-CN is a further development of the land-surface-scheme ORCHIDEE (O) (Krinner et al., 2005), and simulates the terrestrial coupled carbon (C), nitrogen (N) and water cycles for twelve plant functional types driven by climate data, atmospheric composition (N deposition, as well as atmospheric CO<sub>2</sub> and O<sub>3</sub> burden), and land use information (land cover and fertiliser application).

In O-CN net photosynthesis is calculated for shaded and sun-lit leaves in a multi-layer canopy with up to 20 layers (each with a thickness of up to 0.5 leaf area index). Photosynthesis is calculated following a modified Farquhar-scheme in chapter 2 and the Ball and Berry formulation in chapters 3 and 4. In both approaches the light profiles of diffuse and direct radiation is considered (Zaehle and Friend, 2010). Photosynthetic

capacity depends on leaf nitrogen concentration and leaf area, which are both affected by ecosystem available N. Increases in the leaf nitrogen content increase  $V_{cmax}$  and  $J_{max}$  (nitrogen-specific rates of maximum light harvesting, electron transport) and hence maximum net photosynthesis and stomatal conductance per leaf area. This in turn affects transpiration as well as  $O_3$  uptake and ozone damage estimates. The leaf N content is highest at the top of the canopy and exponentially decreases with increasing canopy depth (Friend, 2001; Niinemets et al., 2015). Following this, stomatal conductance and  $O_3$  uptake is generally highest in the upper canopy and lowest in the bottom of the canopy.

Canopy-integrated assimilated carbon enters a labile non-structural carbon pool, which can either be used to fuel maintenance respiration (a function of tissue nitrogen), storage (for seasonal leaf and fine root replacement and buffer of inter-annual variability of assimilation) or biomass growth. The labile pool responds within days to changes in GPP, the long-term reserve has a response time of several months, depending on its use to support seasonal foliage and fine root development or sustain growth in periods of reduced photosynthesis. After accounting for reproductive production (flowers and fruits), biomass growth is partitioned into leaves, fine roots, and sapwood according to a modified pipe-model (Zaehle and Friend, 2010), accounting for the costs of biomass formation (growth respiration). In other words, changes in leaf-level productivity affect the build-up of plant pools and storage, and thereby feed back on the ability of plants to acquire carbon through photosynthesis, or nutrients through fine root uptake.

### 1.6.2 Modelling air pollution impacts in O-CN

As before this thesis the O-CN model accounted for nitrogen deposition and its effects on plant growth but it did not account for the effects of ozone damage. To investigate the impact of both air pollutants, nitrogen deposition and ozone, on the terrestrial carbon and nitrogen cycling, an extended version of the O-CN model had to be developed which accounts for ozone damage on plants. Crucial steps to simulate ozone damage are the simulation of ozone uptake into the plants and the relation of the taken up ozone to plant damage. To simulate ozone uptake into the plants a realistic estimate of canopy level ozone concentrations is essential. The ozone concentrations provided by chemical transport models as input for terrestrial biosphere models report ozone concentrations in approximately 45 m above the surface. The canopy level ozone concentration is estimated by including an ozone deposition scheme. The canopy level ozone concentration is used to calculate ozone uptake into the leaf via the gas exchange between the plant and the canopy air. The taken up ozone is assumed to accumulate in the plants and represents potential accumulating damage. As plants are able to detoxify part of the taken up ozone (see section 1.3.2) a flux threshold is implemented and only ozone uptake rates which exceed the threshold are accumulated and thus accounted for in the damage calculation. The accumulated ozone in the plants is related to plant damage via an injury function. Different injury functions are evaluated in terms of their ability to reproduce observed biomass damage relationships in fumigation/filtration experiments. The evaluation of the injury functions finalised the model development and enabled the simulation of past,

present and future impacts of both air pollutants (nitrogen deposition and ozone) on the terrestrial carbon and nitrogen cycling.

The structure of the thesis is explained in the next section 1.7 together with the investigated research questions during the development, evaluation and application of the extended model.

## 1.7 Thesis structure and objectives

The objective of this thesis is to investigate the influence of air pollution, especially tropospheric ozone and nitrogen deposition, on the ability of the terrestrial biosphere to store carbon dioxide. Main research questions of the thesis are:

- What are key factors in the simulation of ozone damage that might explain the strong variation in estimated ozone induced damage estimates found in the literature and how can they be improved to obtain more reliable damage estimates?
- How much impacted ozone damage and nitrogen deposition the terrestrial carbon uptake and storage in the past since pre-industrial times?
- What is the extend of ozone damage and nitrogen deposition on the terrestrial carbon uptake and storage during the 21st century in simulations based on RCP scenarios?

To answer these question the thesis is structured into three main chapters (chapters 2-4). Each chapter consists of a brief introduction to the specific topic of the chapter, a description of the methods used in the chapter, a presentation of the results, their discussion and a conclusion.

In particular chapter 2 (Development and evaluation of an ozone deposition scheme for coupling to a terrestrial biosphere model) describes the implementation, testing and evaluation of a detailed ozone deposition included into the terrestrial biosphere model O-CN. Specific research questions investigated in this chapter are:

- To which extend impacts the deposition scheme the estimates of ozone uptake and hence potential damage estimates?
- What are key factors that determine the simulation of ozone uptake in the extended model?
- How much ozone induced damage to carbon uptake (GPP) and transpiration is estimated for the present when applying the new developed model version?

In chapter 3 the impact of different leaf-level injury functions, which relate simulated ozone uptake to plant injury, on simulated ozone effects on forests are investigated and evaluated. The addressed research questions are:

- Can observed biomass damage relationships be reproduced in simulations run by the O-CN model if previously published injury functions are applied in the damage calculation?
- Do linear injury functions exist whose application permit a reproduction of observed biomass damage relationships?
- Can injury functions developed from experiments with young trees be reliably applied to estimate ozone damage of mature trees?

The model developed in chapter 2 and evaluated and updated in chapter 3 is applied in chapter 4 to assess past and future impacts of air pollution on the terrestrial carbon uptake and storage. The addressed research questions are:

- To which extent reduced ozone damage carbon uptake and storage in the past and what are projected damage values for the 21st century?
- How much does the application of the ozone deposition scheme impact damage estimates?
- What is the net effect of nitrogen deposition and ozone damage on carbon uptake and storage?

Chapters 2 and 3 base on previously published papers which have been slightly adapted to fit into the thesis. Chapter 2 is based on the paper 'Development and evaluation of an ozone deposition scheme for coupling to a terrestrial biosphere model' by Franz et al. (2017) published in Biogeosciences. Chapter 3 builds upon the paper 'Evaluation of simulated ozone effects in forest ecosystems against biomass damage estimates from fumigation experiments' by Franz et al. (2018) published in Biogeosciences. Both papers are attached in the Appendix of this thesis. As chapters 2 and 3 involve input from co-authors on the previously published versions of the chapters, I will use the term 'we' instead of 'I' in both chapters.

The final chapter 5 presents a general conclusion by summarising the answers to the three main research questions of the thesis, indicating limitations and giving an outlook to possible future work.

## Chapter 2

# Development and evaluation of an ozone deposition scheme for coupling to a terrestrial biosphere model

### 2.1 Introduction

A number of O<sub>3</sub> exposure indices have been proposed to assess the potential detrimental effect of tropospheric O<sub>3</sub> on the plants (LRTAP-Convention, 2017; Mills et al., 2011b). In Europe, the standard method of these indices is the concentration-based AOTX [ppb h] (accumulated O<sub>3</sub> concentration over a threshold of  $X$  ppb), which relates the free-air O<sub>3</sub> concentration to observed plant damage. Models assessing ozone damage to gross or net primary production based on AOTX have been used for many years and indicate that substantial reduction in plant growth and carbon sequestration occurs globally and may reach reductions of more than 40% at O<sub>3</sub> hotspots (Felzer et al., 2004, 2005; Ren et al., 2011; Anav et al., 2011).

Accounting for the O<sub>3</sub> dose rather than the O<sub>3</sub> exposure in assessments of ozone damage results in diverging regional patterns of ozone damage, as regions with the highest exposure (O<sub>3</sub> concentrations) do not always coincide with regions of high uptake (Emberson et al., 2000a; Mills et al., 2011a; Simpson et al., 2007). Observed ozone damage in the field seems to be better correlated with flux-based risk assessment compared to concentration-based methods (Mills et al., 2011a). Following this the LRTAP Convention recommends flux-based methods (e.g. PODy [Phytotoxic Ozone Dose, nmol m<sup>-2</sup> s<sup>-1</sup>]) as the preferred tool for risk assessment (LRTAP-Convention, 2017).

When calculating the O<sub>3</sub> uptake into the plants, it is important to consider that stomatal uptake is not the only surface sink of O<sub>3</sub>. O<sub>3</sub> destruction also occurs at non-stomatal surfaces such as the leaves' cuticle and soil surface. The stomatal flux represents approximately half of the total O<sub>3</sub> flux to the surface (Gerosa et al., 2004; Fowler et al., 2009;

Cieslik, 2004; Simpson et al., 2003). Accounting for this non-stomatal O<sub>3</sub> deposition reduces the amount of O<sub>3</sub> uptake into the plants by reducing the surface O<sub>3</sub> concentration (Tuovinen et al., 2009) and thus has the potential to affect flux-based ozone damage estimates.

Only a few terrestrial biosphere models have adopted the flux approach to relate O<sub>3</sub> exposure to plant damage and thus estimate O<sub>3</sub> induced reductions in terrestrial carbon sequestration in a process-based manner. Sitch et al. (2007) developed a version of the JULES model in which stomatal O<sub>3</sub> uptake directly affects net primary production (NPP), thereby ignoring the effect of reduced photosynthesis under elevated levels of O<sub>3</sub> on water fluxes. Lombardozzi et al. (2015) proposed a revised version of the Community Land Model (CLM), in which O<sub>3</sub> imposes fixed reductions to net photosynthesis for two out of three modelled plant types. Atmospheric O<sub>3</sub> concentrations and the amount of cumulated O<sub>3</sub> uptake directly affect net photosynthesis only for one plant type.

In this chapter, a new, globally applicable model is presented to calculate O<sub>3</sub> uptake and damage in a process-oriented manner, coupled to the terrestrial energy, water, carbon, and nitrogen budget of the O-CN terrestrial biosphere model (Zaehle and Friend, 2010).

In this model, the canopy O<sub>3</sub> abundance is calculated using aerodynamic resistance and surface resistances to soil surface, vegetation surfaces, and stomatal cavities to take account of non-stomatal O<sub>3</sub> destruction. Canopy O<sub>3</sub> abundance is used to simulate stomatal O<sub>3</sub> uptake given instantaneous values of net photosynthesis and stomatal conductance. O<sub>3</sub> uptake and its effect on net photosynthesis is then calculated based on an extensive meta-analysis across 28 tree species by Wittig et al. (2007) considering the ability of plants to detoxify a proportion of the O<sub>3</sub> dose (Sitch et al., 2007).

We first give a detailed overview of the ozone scheme (Section 2.2.1); evaluate modelled gross primary production (GPP), canopy conductance, latent heat fluxes, and leaf area index (LAI) against data from the FLUXNET database (Baldocchi et al., 2001) to test the ability of the model to simulate observed values of key components affecting calculate O<sub>3</sub> uptake (Section 2.3.1); evaluate the simulated O<sub>3</sub> metrics against reported values in the literature (Section 2.3.2); provide a sensitivity analysis of critical variables and parameters of the deposition model to evaluate the reliability of simulated values of O<sub>3</sub> uptake (Section 2.3.3); give an estimate of the effect of the present-day O<sub>3</sub> burden on European GPP and transpiration (Section 2.3.4); and estimate the impact of using the O<sub>3</sub> deposition scheme on O<sub>3</sub> uptake and cumulated uptake (Section 2.3.5).

## 2.2 Methods

We developed an ozone deposition and leaf-uptake module for the terrestrial biosphere model O-CN (see section 1.6.1 for details).

The O<sub>3</sub> and N-deposition data used for this study are provided by the EMEP MSC-W (European Monitoring and Evaluation Programme Meteorological Synthesizing Centre - West) chemical transport model (CTM) (Simpson et al., 2012). The O<sub>3</sub> flux and deposition modules used in the EMEP model are advanced compared to most CTMs, and have

been documented in a number of papers (Emberson et al., 2001; Tuovinen et al., 2004, 2009; Simpson et al., 2007, 2012; Klingberg et al., 2008). The ozone deposition scheme for O-CN is adapted from the model used by EMEP MSC-W (Simpson et al., 2012) to fit the land-surface characteristics and process descriptions of the ORCHIDEE model. The leaf-level ozone concentrations computed by EMEP can not directly be used by O-CN, since EMEP and O-CN differ in a number of properties, as for instance in the number of simulated PFTs, and importantly their ecophysiological process representation. Both models differ in the simulation of various ecosystem processes (e.g. phenology, canopy processes, biogeochemical cycles, and vegetation dynamics, which are more explicitly represented in O-CN), which in sum impact stomatal and non-stomatal ozone deposition and through this the leaf-level ozone concentration. A possible further development of the updated O-CN model is the coupling to a CTM to allow for a consistent simulation of tropospheric O<sub>3</sub> burden and vegetation O<sub>3</sub> uptake.

### 2.2.1 Ozone module

The ozone deposition scheme calculates O<sub>3</sub> deposition to the leaf surface from the free atmosphere, represented by the O<sub>3</sub> concentration at the lowest level of the atmospheric chemistry transport model (CTM), taken to be at 45 m above the surface. The total O<sub>3</sub> dry deposition flux ( $F_g$ ) to the ground surface is calculated as

$$F_g = V_g \chi_{atm}^{O_3} \quad (2.1)$$

where  $\chi_{atm}^{O_3}$  is the O<sub>3</sub> concentration at 45 m and  $V_g$  is the deposition velocity at that height. In O-CN  $V_g$  is taken to be dependent on the aerodynamic resistance ( $R_a$ ), canopy-scale quasi-laminar layer resistance ( $R_b$ ) and the compound surface resistance ( $R_c$ ) to O<sub>3</sub> deposition.

$$V_g = \frac{1}{R_a + R_b + R_c}. \quad (2.2)$$

$R_b$  is calculated from the friction velocity ( $u_*$ ) as

$$R_b = \frac{6}{u_*}. \quad (2.3)$$

The  $R_a$  between 45 m height and the canopy is not computed by O-CN and is inferred from the logarithmic wind profile. To calculate the O<sub>3</sub> deposition of the free atmosphere at the lowest level of the CTM (approximately 45 m) to the vegetation canopy, it is necessary to know the aerodynamic resistance between these heights ( $R_{a,45}$ ). These data are model- and land-cover-specific, and thus not provided by the CTM. Instead, we approximate  $R_{a,45}$  from the wind speed at 45 m height ( $u_{45}$ ) and the friction velocity  $u_*$  according to

$$R_{a,45} = \frac{u_{45}}{u_*^2} \quad (2.4)$$

where  $u_*$  is calculated from the wind speed at 10 m height ( $u_{10}$ ) using the atmospheric resistance calculations of the ORCHIDEE model (Krinner et al., 2005). The wind at 45 m ( $u_{45}$ ) is approximated by assuming the logarithmic wind profile for neutral atmospheric conditions (Monteith and Unsworth, 2007) due to the lack of information on any other relevant atmospheric properties at 45 m height:

$$u_{45} = u_{10} \frac{\log(\frac{45}{z_0})}{\log(\frac{10}{z_0})} \quad (2.5)$$

where  $z_0$  is the roughness length.

$R_c$  is calculated as the sum of the parallel resistances to stomatal/canopy ( $1/G_c^{O_3}$ ) and non-stomatal  $O_3$  uptake ( $1/G_{ns}$ ) (Simpson et al., 2012, Eq. 55)

$$R_c = \frac{1}{G_c^{O_3} + G_{ns}}. \quad (2.6)$$

The stomatal conductance to  $O_3$   $G_{st}^{O_3}$  ( $m s^{-1}$ ) is computed by O-CN (Zaehle and Friend, 2010) as

$$G_{st}^{O_3} = g_1 \frac{f(\Theta)f(q_{air})f(C_i)f(height)A_{n,sat}}{1.51} \quad (2.7)$$

where  $G_{st}^{O_3}$  is calculated as a function of net photosynthesis at saturating  $C_i$  ( $A_{n,sat}$ ), where  $g_1$  is the intrinsic slope between  $A_n$  and  $G_{st}$ . It further depends on a number of scalars to account for the effect of soil moisture ( $f(\Theta)$ ), water transport limitation with canopy height ( $f(height)$ ), and atmospheric drought ( $f(q_{air})$ ), as well as an empirical non-linear sensitivity to the internal leaf  $CO_2$  concentration ( $f(C_i)$ ), all as described in Friend and Kiang (2005). The factor 1.51 accounts for the different diffusivity of  $O_3$  from water vapour (Massman, 1998). The canopy conductance to  $O_3$   $G_c^{O_3}$  is calculated by summing the  $G_{st}^{O_3}$  of all canopy layers. To yield reasonable conductance values in O-CN compared to FLUXNET data (see Sect. 2.3.1), the original intrinsic slope between  $A_n$  and  $G_c$  called  $\alpha$  in Friend and Kiang (2005) is adapted such that  $g_1 = 0.7\alpha$ .

The non-stomatal conductance  $G_{ns}$  follows the EMEP approach (Simpson et al., 2012, Eq. 60) and represents the  $O_3$  fluxes between canopy-air space and surfaces other than the stomatal cavities. The model accounts for  $O_3$  destruction on the leaf surface ( $r_{ext}$ ), within-canopy resistance to  $O_3$  transport ( $R_{inc}$ ), and ground surface resistance ( $R_{gs}$ )

$$G_{ns} = \frac{SAI}{r_{ext}} + \frac{1}{R_{inc} + R_{gs}} \quad (2.8)$$

where the surface area index ( $SAI$ ) is equal to the  $LAI$  for herbaceous PFTs (grasses and crops) and  $SAI = LAI + 1$  for tree PFTs according to Simpson et al. (2012) in order to account for  $O_3$  destruction on branches and stems. Unlike EMEP, we do not apply a day of the growing season constraint for crop exposure to  $O_3$ , which in O-CN is accounted for by the simulated phenology and seasonality of photosynthesis. The external leaf resistance ( $r_{ext}$ ) per unit surface area is calculated as

$$r_{ext} = r_{ext,b} F_T \quad (2.9)$$

where the base external leaf resistance ( $r_{ext,b}$ ) of  $2500 \text{ m s}^{-1}$  is scaled by a low-temperature correction factor  $F_T$  and

$$F_T = e^{-0.2(1+T_s)} \quad (2.10)$$

with  $1 \leq F_T \leq 2$  and  $T_s$  the 2 m air temperature ( $^{\circ}\text{C}$  Simpson et al., 2012, Eq. 60). For temperatures below  $-1 \text{ }^{\circ}\text{C}$  non-stomatal resistances are increased up to two times (Simpson et al., 2012; Zhang et al., 2003). The within-canopy resistance ( $R_{inc}$ ) is calculated as

$$R_{inc} = bSAI \frac{h}{u_*} \quad (2.11)$$

where  $b$  is an empirical constant (set to  $14 \text{ s}^{-1}$ ) and  $h$  is the canopy height in m. The ground-surface resistance  $R_{gs}$  is calculated as

$$R_{gs} = \frac{1 - 2f_{snow}}{F_T \hat{R}_{gs}} + \frac{2f_{snow}}{R_{snow}} \quad (2.12)$$

(Simpson et al., 2012, Eq. 59).  $\hat{R}_{gs}$  represents base values of  $R_{gs}$  and takes values of  $2000 \text{ s m}^{-1}$  for bare soil,  $200 \text{ s m}^{-1}$  for forests and crops, and  $1000 \text{ s m}^{-1}$  for non-crop grasses (Simpson et al., 2012, Suppl.). As in EMEP, the ground-surface resistance of  $\text{O}_3$  to snow ( $R_{snow}$ ) is set to a value of  $2000 \text{ s m}^{-1}$  according to Zhang et al. (2003).  $f_{snow}$  is calculated from the actual snow depth ( $s_d$ ) simulated by O-CN, and the maximum possible snow depth ( $s_{d,max}$ ):

$$f_{snow} = \frac{s_d}{s_{d,max}} \quad (2.13)$$

with the constraint of  $0 \leq f_{snow} \leq 0.5$  to prevent negative values in the first fraction of Eq. 2.12.  $s_{d,max}$  is taken to be  $10 \text{ kg m}^{-2}$  (Ducoudré et al., 1993).

Given these resistances, the canopy  $\text{O}_3$  concentration ( $\chi_c^{O_3}$ ,  $\text{nmol m}^{-3}$ ) is then calculated based on a constant flux assumption:

$$\chi_c^{O_3} = \chi_{atm}^{O_3} \left(1 - \frac{R_a}{R_a + R_b + R_c}\right). \quad (2.14)$$

$\chi_c^{O_3}$  and the stomatal conductance to  $\text{O}_3$  ( $G_{st}^{O_3}$  in  $\text{m s}^{-1}$ ) are used to calculate the  $\text{O}_3$  flux into the leaf cavities ( $F_{st}$ ,  $\text{nmol m}^{-2} \text{ s}^{-1}$ ):

$$F_{st} = (\chi_c^{O_3} - \chi_i^{O_3}) G_{st}^{O_3}. \quad (2.15)$$

According to Laisk et al. (1989) the leaf internal  $\text{O}_3$  concentration ( $\chi_i^{O_3}$ ) is assumed to be zero.

The O-CN implementation of deposition and flux described above is a simplification of the deposition system used by EMEP in order to fit the process representation of

ORCHIDEE, from which O-CN has inherited its biophysical modules. The external leaf resistance is not included in the calculation of  $F_{st}$  (Tuovinen et al., 2007, 2009), which results in an overestimation of stomatal  $O_3$  uptake. Further, O-CN's calculation of  $R_a$  is based upon neutral stability conditions, whereas the EMEP model makes use of rather detailed stability correction factors. However, a series of calculations with the full EMEP model have shown that the uncertainties associated with these simplifications are small, typically 0.5-5  $\text{mmol m}^{-2}$ . As base-case values of  $POD_0$  are typically ca. 30-50  $\text{mmol m}^{-2}$  in EU regions, these approximations do not seem to be a major cause of error, at least in regions with substantial ozone (and carbon) uptake. The full coupling of O-CN to a CTM would be desirable to eliminate this bias and allow for a consistent calculation of tropospheric and surface near  $O_3$  burdens.

### 2.2.2 Relating stomatal uptake to leaf injury

An accumulation of  $F_{st}$  over time gives the accumulated uptake of  $O_3$  for a particular canopy layer ( $CUO_l$ ,  $\text{mmol m}^{-2}$ ), or for  $l = 1$  (top canopy layer) the phytotoxic  $O_3$  dose ( $POD$ ,  $\text{mmol m}^{-2}$ ):

$$\frac{dCUO_l}{dt} = (1 - f_{new})CUO_l + cF_{st,l} \quad (2.16)$$

where  $c = 10^{-6}$  converts from  $\text{nmol}$  to  $\text{mmol}$  and the integration time step is 1800 seconds.

The phenology of leaves is accounted for by assuming that emerging leaves are undamaged and by reducing the  $CUO_l$  by the fraction of newly developed leaves per time step and layer ( $f_{new}$ ). Furthermore, deciduous PFTs shed all CUO at the end of the growing season and grow uninjured leaves the next spring. Evergreen PFTs shed proportionate amounts of CUO during the entire year whenever new leaves are grown.

The full canopy cumulative uptake of  $O_3$  is calculated by summing  $CUO_l$  over all present canopy layers ( $n$ ):

$$CUO = \sum_{l=1}^n CUO_l. \quad (2.17)$$

The  $CUO_l$  is used to approximate the injury to net photosynthesis ( $A_n$ ) by using the injury relationship of Wittig et al. (2007):

$$d_l^{O_3} = \frac{0.22CUO_l + 6.16}{100}, \quad (2.18)$$

where the factor 100 scales the percentage values of injury to fractions. Net photosynthesis accounting for ozone injury ( $A_n^{O_3}$ ) is then calculated by subtracting the injury fraction from the uninjured value of  $A_n$ :

$$A_{n,l}^{O_3} = A_{n,l}(1 - d_l^{O_3}). \quad (2.19)$$

Since  $G_{st}$  and  $A_n$  are tightly coupled (see Eq. 2.7), an injury of  $A_n$  results in a simultaneous reduction in  $G_{st}$ . The canopy-scale  $O_3$  flux into the leaf cavities ( $F_{stC}$ ) is calculated by summing  $F_{st}$  of all canopy layers, similar to the aggregation of  $A_{n,l}$  and  $G_{st}$  and  $CUO_l$ . Canopy  $O_3$  concentration,  $O_3$  uptake, canopy cumulative  $O_3$  uptake (CUO), and injury to net photosynthesis are solved iterative to account for the feedbacks between ozone injury, canopy conductance and canopy-air  $O_3$  concentrations.

Note that CUO and POD can be directly compared to estimates according to the LRTAP-Convention (2017) notation when analysing only the top canopy layer (Mills et al., 2011b).

### 2.2.3 Sensitivity analysis

A sensitivity analysis is conducted to estimate the sensitivity of the modelled plant  $O_3$  uptake to the parameterisation of the model, to establish the robustness of the model, and to identify the most influential parameters. Three parameters (ground-surface resistance ( $\hat{R}_{gs}$ ), external leaf resistance ( $r_{ext}$ ), and empirical constant ( $b$ ); see Eq. 2.12, 2.8, and 2.11, respectively) and three modelled quantities (canopy conductance ( $G_c$ ), aerodynamic resistance ( $R_a$ ), and canopy-scale quasi-laminar layer resistance ( $R_b$ ); see Eq. 2.7, 2.2), with considerable uncertainty due to the underlying parameters used to calculate these quantities, are perturbed within  $\pm 20\%$  of their central estimate.

A set of 100 parameter combinations is created with a Latin hypercube sampling method (McKay et al., 1979), simultaneously perturbing all six parameter values (R-package: FME; function: Latinhyper). For each parameter combination, a transient run (see subsection 2.2.4) is performed creating an ensemble of estimates for the key prognostic variables  $F_{stC}$  (Eq. 3.3),  $R_c$  (Eq. 2.6),  $V_g$  (Eq. 2.2) and the  $O_3$  flux ratio ( $F_R$ ) calculated as the ratio of  $F_{stC}$  and the total  $O_3$  flux to the surface ( $F_g$ , Eq. 2.1).

The summer months June, July, and August (JJA) are selected from the simulation output and used for further analysis. For each prognostic variable ( $F_{stC}$ ,  $R_c$ ,  $V_g$ ,  $F_R$ ), the sensitivity to changes in all six perturbed parameters/variables is estimated by calculating partial correlation coefficients (PCCs) and partial ranked correlation coefficients (PRCCs) (Helton and Davis, 2002). PCCs record the linear relationship between two variables where the linear effects of all other variables in the analysis are removed (Helton and Davis, 2002). In the case of nonlinear relationships, RPCCs can be used, which implies a rank transformation to linearise any monotonic relationship, such that the regression and correlation procedures as in the PCCs can follow (Helton and Davis, 2002). We estimate the magnitude of the parameter effect by creating mean summer values of the four prognostic variables for each sensitivity run, and regressing these values against the corresponding parameter/variable scaling values of the respective model run.

### 2.2.4 Modelling protocol and data for site-level simulations

The site-level simulations (single-point simulations) at the FLUXNET sites are run using observed metrological forcing, soil properties, and land cover from the La Thuile

Dataset (<http://fluxnet.fluxdata.org/data/la-thuile-dataset/>) of the FLUXNET project (Baldocchi et al., 2001). Data on atmospheric CO<sub>2</sub> concentrations are obtained from Sitch et al. (2015). Reduced and oxidised nitrogen deposition in wet and dry forms and hourly O<sub>3</sub> concentrations at 45 m height are provided by the EMEP model (see Sect. 2.2.5).

O-CN is brought into equilibrium in terms of the terrestrial vegetation and soil carbon and nitrogen pools in a first step with the forcing of the year 1900. In the next step, the model is run with a progressive simulation of the period 1900 up until the start year of the respective site. For this period atmospheric O<sub>3</sub> and CO<sub>2</sub> concentrations as well as N-deposition of the respective simulated years are used. Due to lack of observed climate for the sites for this period, the site-specific observed meteorology from recent years is iterated for these first two steps. The observation years (see Tab. 2.1) are simulated with the climate and atmospheric conditions (N deposition, CO<sub>2</sub> and O<sub>3</sub> concentrations) of the respective years.

For the evaluation of the model output, net ecosystem exchange (NEE), and latent heat flux (LE), as well as meteorological observations are obtained for 11 evergreen needle-leaved forest sites, 10 deciduous broadleaved forest sites, and 5 C<sub>3</sub> grassland sites in Europe (see Tab. 2.1) from the La Thuile Dataset of the FLUXNET project (Baldocchi et al., 2001). Leaf area indices (LAIs) based on discrete point measurements are obtained from the La Thuile ancillary database.

NEE measurements are used to estimate gross primary production (GPP) by the flux-partitioning method according to Reichstein et al. (2005). Canopy conductance ( $G_c$ ) is derived by inverting the Penman-Monteith equation given the observed LE and atmospheric conditions as described in Knauer et al. (2015).

The half-hourly FLUXNET and model fluxes are filtered prior to deriving average growing-season fluxes (bud break to litter fall) to reduce the effect of model biases on the model-data comparison. Night-time and morning/evening hours are excluded by removing data with lower than 20% of the daily maximum shortwave downward radiation. To avoid any biases associated with the soil moisture or atmospheric drought response of O-CN, we further exclude data points with a modelled soil moisture constraint factor (range between 0 and 1) below 0.8 and an atmospheric vapour pressure deficit larger than 0.5 kPa.

Daily mean values are calculated from the remaining time steps only where both modelled and observed values are present. The derived daily values are furthermore constrained to the main growing season by excluding days where the daily GPP is less than 20% of the yearly maximum daily GPP.

To derive representative diurnal cycles, data for the month July are filtered for daylight hours (taken as incoming shortwave radiation  $\geq 100 \text{ W m}^{-2}$ ), with periods of soil or atmospheric drought stress excluded as above. This is done for modelled  $F_{stC}$ ,  $R_c$ ,  $V_g$ , and  $F_R$  and for both modelled and FLUXNET observed  $GPP$  and  $G_c$ .

Table 2.1: Characteristics of the FLUXNET sites used in this study.

Sites	Latitude	Longitude	Climate <sup>a</sup>	PFT <sup>b</sup>	Years	Reference
AT-Neu	47.12	11.32	Cfb	TeH	2002-2005	(Wohlfahrt et al., 2008b)
CH-Oe1	47.29	7.73	Cfb	TeH	2002-2006	(Ammann et al., 2007)
DE-Bay	50.14	11.87	Cfb	CEF	1997-1998	(Rebmann et al., 2004)
DE-Hai	51.08	10.45	Cfb	TeBDF	2000-2006	(Kutsch et al., 2008)
DE-Meh	51.28	10.66	Cfb	TeH	2004-2006	(Scherer-Lorenzen et al., 2007)
DE-Tha	50.96	13.57	Cfb	CEF	2004-2006	(Grünwald and Bernhofer, 2007)
DK-Lva	55.68	12.08	Cfb	TeH	2005-2006	(Gilmanov et al., 2007)
DK-Sor	55.49	11.65	Cfb	TeBDF	1997-2006	(Lagergren et al., 2008)
ES-ES1	39.35	-0.32	Csa	CEF	1999-2004	(Sanz et al., 2004)
FI-Hyy	61.85	24.29	Dfc	CEF	2001-2006	(Suni et al., 2003)
FR-Hes	48.67	7.06	Cfb	TeBDF	2001-2006	(Granier et al., 2000)
FR-LBr	44.72	-0.77	Cfb	CEF	2003-2006	(Berbigier et al., 2001)
FR-Pue	43.74	3.60	Csa	TeBEF	2001-2006	(Keenan et al., 2010)
IL-Yat	31.34	35.05	BSh	CEF	2001-2002	(Grünzweig et al., 2003)
IT-Cpz	41.71	12.38	Csa	TeBEF	2001-2006	(Tirone et al., 2003)
IT-Lav	45.96	11.28	Cfb	CEF	2006-2006	(Marcolla et al., 2003)
IT-MBo	46.02	11.05	Cfb	TeH	2003-2006	(Wohlfahrt et al., 2008a)
IT-PT1	45.20	9.06	Cfa	TeBDF	2003-2004	(Migliavacca et al., 2009)
IT-Ro1	42.41	11.93	Csa	TeBDF	2002-2006	(Rey et al., 2002)
IT-Ro2	42.39	11.92	Csa	TeBDF	2002-2006	(Tedeschi et al., 2006)
IT-SRo	43.73	10.28	Csa	CEF	2003-2006	(Chiesi et al., 2005)
NL-Loo	52.17	5.74	Cfb	CEF	1997-2006	(Dolman et al., 2002)
PT-Esp	38.64	-8.60	Csa	TeBEF	2002-2006	(Pereira et al., 2007)
PT-Mi1	38.54	-8.00	Csa	TeS	2003-2005	(Pereira et al., 2007)
SE-Fla	64.11	19.46	Dfc	CEF	2000-2002	(Lindroth et al., 2008)
SE-Nor	60.09	17.48	Dfb	CEF	1996-1997	(Lagergren et al., 2008)

<sup>a</sup> Koeppen-Geiger climate zone (BSh = hot arid steppe; Cfa = humid, warm temperate, hot summer; Cfb = humid, warm temperate, warm summer; Csa = summer dry, warm temperate, hot summer; Dfb = Cold, humid, warm summer; Dfc = Cold, humid, cold summer).

<sup>b</sup> Plant functional type (TeBEF = Temperate broadleaf evergreen forest, TeBDF = Temperate broadleaf deciduous forest, CEF = Coniferous evergreen forest, TeS = Temperate open woodland with C<sub>3</sub> grass, TeH = C<sub>3</sub> grassland).

### 2.2.5 Modelling protocol and data for regional simulations

For the regional simulations, O-CN is run at a spatial resolution of  $0.5^\circ \times 0.5^\circ$  on a spatial domain focused on Europe. Daily meteorological forcing (temperature, precipitation, shortwave and long-wave downward radiation, atmospheric specific humidity, and wind speed) for the years 1961 to 2010 is obtained from RCA3 regional climate model (Samuelsson et al., 2011; Kjellstrom et al., 2011), nested in the ECHAM5 model (Roeckner et al., 2006), and has been bias-corrected for temperatures and precipitation using the CRU climatology (New et al., 1999). Reduced and oxidised nitrogen deposition in wet and dry forms and  $O_3$  concentrations at 45 m height for the same years are obtained from the EMEP model, which is also run with RCA3 meteorology (as in Simpson et al., 2014b). Emissions for the EMEP runs in current years are as described in Simpson et al. (2014b), and are scaled back to 1900 using data from UNECE and van Aardenne et al. (2001) – see subsection 2.2.6. Further details of the EMEP model setup for this grid and meteorology can be found in Simpson et al. (2014b) and Engardt et al. (2017). For O-CN, land cover, soil, and N fertiliser application are used as in Zaehle et al. (2011) and kept at 2005 values throughout the simulation. Data on atmospheric  $CO_2$  concentrations are obtained from Sitch et al. (2015).

O-CN is brought into equilibrium in terms of the terrestrial vegetation and soil carbon and nitrogen pools by randomly iterating the forcing from the period 1961-1970. This is followed by a simulation for the years 1961-2011 with time-varying climate and atmospheric conditions (N deposition,  $CO_2$ , and  $O_3$  concentrations) but with static land cover and land-use information (kept at year 2005 levels). An upscaled FLUXNET-MTE product of GPP (Jung et al., 2011), using the model tree ensembles (MTE) machine learning technique, is used to evaluate modelled GPP.

### 2.2.6 Emissions inventory

Emissions for the EMEP model were derived by merging data from three main sources. Firstly, emissions for 2005 and 2010 were taken from the ECLIPSE database produced by IIASA for various EU Projects and the Task Force on Hemispheric Transport of Air Pollution (Amann et al., 2013; Stohl et al., 2015), although with improved spatial resolution over Europe by making use of the 7 km resolution MACC-2 emissions produced by TNO (Kuenen et al., 2011). For 1990, emissions from land-based sources were taken directly from the EMEP database for that year, since 1990 had been the subject of recent review and quality control (e.g. Mareckova et al., 2013). Emissions between 1990 and 2005 were estimated via linear interpolation between these 2005 and EMEP 1990 values. Emissions prior to 1990 were derived by scaling the EMEP 1990 emissions by the emissions ratios found in the historical data series of Lamarque et al. (2010).

Emissions of the biogenic hydrocarbon isoprene from vegetation are calculated using the model's land cover and meteorological data (Simpson et al., 2012, 1999). Emissions of NO from biogenic sources (soils, forest fires, etc.) were set to zero given both their uncertainty and sporadic occurrence. Tests have shown that this approximation has only a small impact on annual deposition totals to the EU area, even for simulations at

the start of the 20th century. Volcanic emissions of sulphur dioxide ( $\text{SO}_2$ ) were set to a constant value from the year 2010.

### 2.2.7 Impacts of using the ozone deposition scheme

In contrast to other terrestrial biosphere models, the O-CN ozone module accounts for the effects of aerodynamic, stomatal and non-stomatal resistance to  $\text{O}_3$  deposition. Due to these resistances, the deposition of  $\text{O}_3$  to leaf level is reduced, and the canopy  $\text{O}_3$  concentration is lower than the atmospheric  $\text{O}_3$  concentration. Thus, using such a deposition scheme reduces modelled  $\text{O}_3$  uptake into plants and accumulation. To get an estimate of the magnitude of this impact we compare simulations with the standard deposition scheme as described above (D) with a simulation where  $\text{O}_3$  surface resistance is only determined by stomatal resistance and the non-stomatal depletion of  $\text{O}_3$  is zero (D-STO). Furthermore, the standard deposition model D is compared to a simulation where no deposition scheme is used and the canopy  $\text{O}_3$  concentration is equal to the atmospheric concentration (ATM).

## 2.3 Results

### 2.3.1 Evaluation against daily eddy-covariance data

Figure 2.1 a shows that, for most sites, modelled and observation-based GPP agree well (see Tab. 2.2 for  $R^2$  and RMSE values). The standard deviation is larger for the observation-based estimates because of the high level of noise in the eddy-covariance data. For sites dominated by needle-leaved trees, the modelled and observation-based GPP values are very close, with only slight under- and overestimates by the model at some sites. At sites dominated by broadleaved trees, modelled GPP deviates more strongly from the observation-based GPP, underestimating the observations in 7 out of 10 cases. However, the results are within the range of standard deviation except for the drought-prone PT-Mi1 site (see Fig. 2.2 a for an explicit site comparison). At  $C_3$  grassland sites, modelled GPP is in good agreement with the observation-based GPP except for AT-Neu, which has the highest mean GPP of all sites observed by FLUXNET with a large standard deviation, which may reflect the effect of site management (e.g. mowing and fertilisation), for which no data were readily available as model forcing.

When comparing modelled and observed latent heat flux (LE), the model fits the observations best at the needle-leaved forest sites (Fig. 2.1 c). However, LE is overestimated at nine out of ten broadleaved forest sites, but remains within the range of the large observational standard deviation. At sites dominated by  $C_3$  grasses the modelled  $LE$  differs considerably from observed value, at two sites overestimating and two underestimating the fluxes, again within the observational standard deviation.

In agreement with the comparison of GPP and LE, the comparison of modelled to observation-based canopy conductance ( $G_c$ ) shows the best agreement for sites dominated by needle-leaved trees (Fig. 2.1 b). At sites dominated by broadleaved trees, the modelled  $G_c$  varies more widely from the FLUXNET  $G_c$ . The modelled  $G_c$  at sites

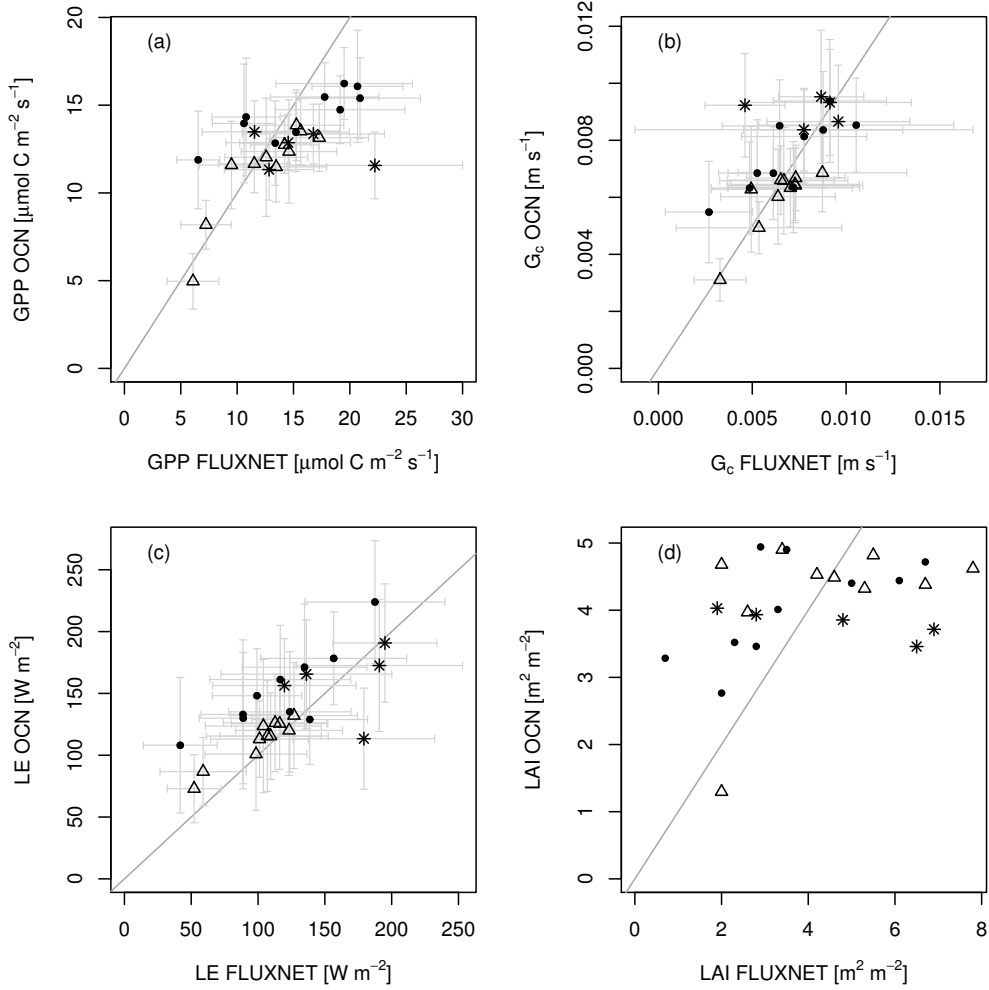


Figure 2.1: Comparison of measured a) GPP, b) canopy conductance ( $G_c$ ), c) latent heat flux (LE), and d) LAI at 26 European FLUXNET sites and simulations by O-CN. Displayed are means and standard deviations of daily means of the measuring/simulation period, with the exception of FLUXNET-derived LAI, which is based on point measurements. Dots symbolise sites dominated by broadleaved trees, triangles sites dominated by needle-leaved trees and asterisks sites dominated by  $C_3$  grasses. The grey line constitutes the 1:1 line.

dominated by  $C_3$  grasses is in very good agreement with FLUXNET  $G_c$ , with slight overestimation of  $G_c$  at two out of three sites, except for the DE-Meh site, where means differ outside the standard deviation (see Fig. 2.2b).

Table 2.2: Coefficient of determination ( $R^2$ ) and root mean square error (RMSE) for  $GPP$ , canopy conductance ( $G_c$ ), and latent heat flux ( $LE$ ) for all sites and for sites dominated by broadleaved trees, needle-leaved trees,  $C_3$  grass, and  $C_3$  grass excluding the AT-Neu site (outlier).

	All sites	Broadleaved	Needle-leaved	$C_3$ grass	$C_3$ grass (excluding AT-Neu)
$R^2$ : $GPP$	0.465	0.714	0.8	0.139	0.058
RMSE: $GPP$	3.495	3.771	1.944	5.175	2.257
$R^2$ : $G_c$	0.458	0.69	0.722	0.013	0.01
RMSE: $G_c$	0.001	0.002	0.001	0.002	0.002
$R^2$ : $LE$	0.566	0.725	0.9	0.022	0.002
RMSE: $LE$	30.897	39.725	13.977	37.124	40.493

The comparison of the average modelled summertime LAI and point measurements at the FLUXNET illustrates that the variability in the measured LAI is much greater than that of O-CN (Fig. 2.1 d). The modelled LAI values approach light-saturating, maximum LAI values and are not able to reproduce between-site differences in, for example the growth stage, site history, or maximum possible LAI values. Furthermore, it should be borne in mind that the observed LAI values are averages of point measurements, which are not necessarily representative of the modelled time period, and that the model had not been parameterised specifically for the sites. Modelled GPP depends not only on LAI, but also on light availability, temperature, and soil moisture. The much better represented values of GPP,  $G_c$ , and LE compared to FLUXNET data (Fig. 2.1 a-c) indicate that O-CN is able to adequately transform available energy into carbon uptake and water loss and thus simulate key variables impacting ozone uptake within a reasonable range.

### 2.3.2 Mean diurnal cycles of key $O_3$ parameters.

For further evaluation of the modelled  $O_3$  uptake, we analysed the diurnal cycles of  $O_3$  uptake ( $F_{stC}$ ),  $O_3$  surface resistance ( $R_c$ ),  $O_3$  deposition velocity ( $V_g$ ), and flux ratio ( $F_R$ ) as well as  $GPP$  and  $G_c$ . We selected three sites (a broadleaved, a needle-leaved, and a  $C_3$  grass site) based on the selection criteria that modelled and FLUXNET GPP and LAI agree well and a minimum of five observation years is available to reduce possible biases from the inability of the model to simulate short-term variations from the mean. The selected sites are a temperate broadleaved summer green forest (IT-Ro1), a boreal needle-leaved evergreen forest (FI-Hyy), and a temperate  $C_3$  grass land (CH-Oe1). We evaluate modelled  $GPP$  and  $G_c$  against observations from the FLUXNET sites. The modelled mean diurnal cycles of  $O_3$  related variables ( $F_{stC}$ ,  $R_c$ ,  $V_g$ ,  $F_R$ ) are compared to reported values in the literature since we did not have access to site-specific observations.

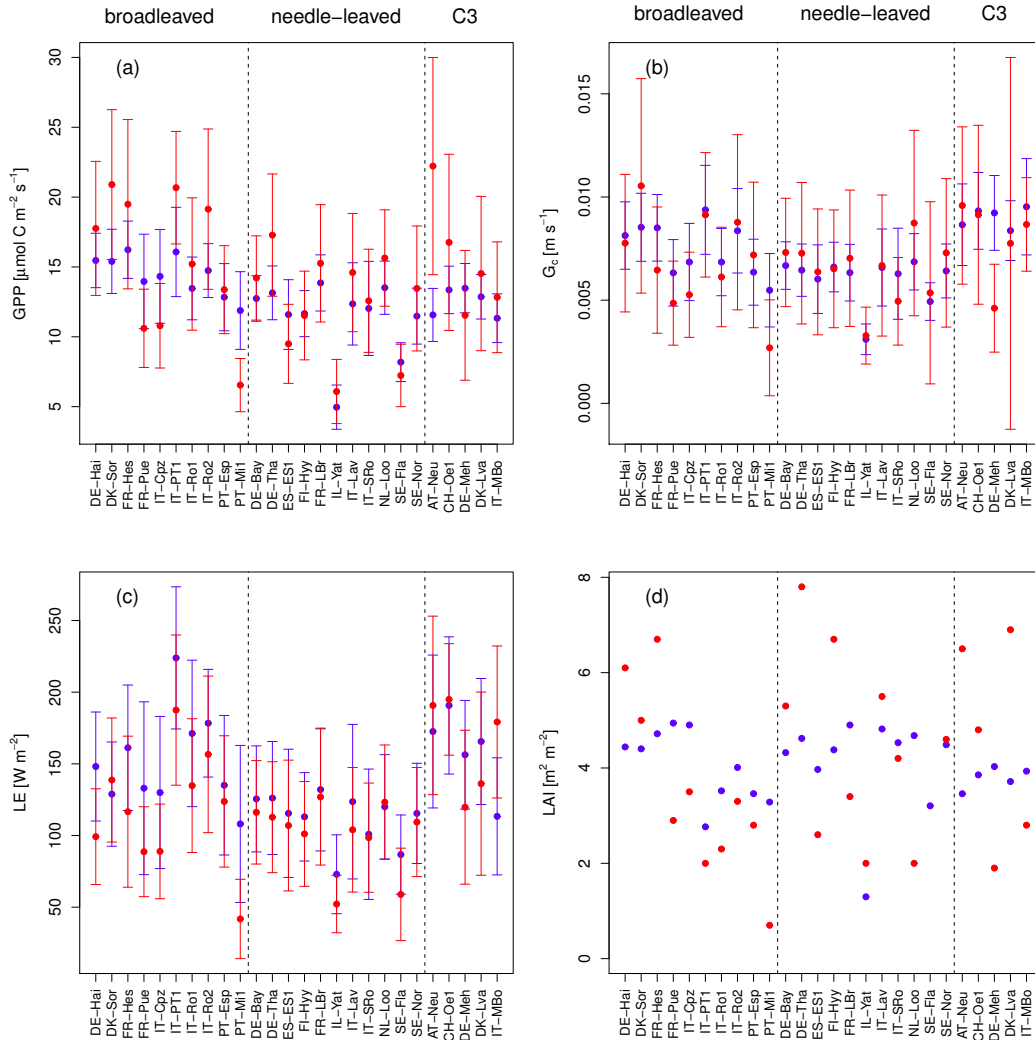


Figure 2.2: Comparison of measured (a) GPP, (b)  $G_c$ , (c) latent heat flux (LE), and (d) LAI at 26 European FLUXNET sites (red) and simulations by O-CN (blue). Displayed are means and standard deviation of daily means of the measuring/simulation period, with the exceptions of FLUXNET-derived LAI, which is based on point measurements.

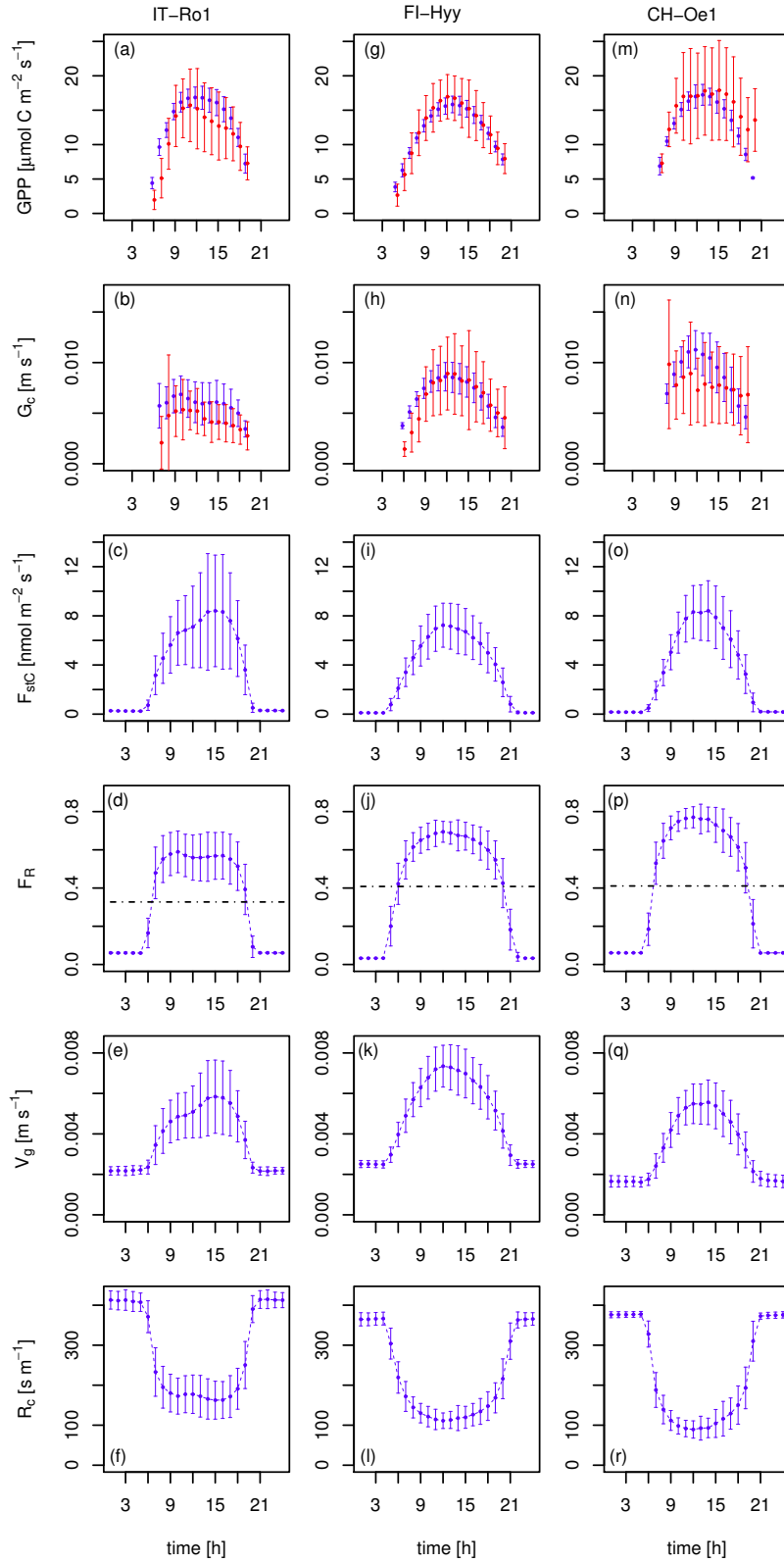


Figure 2.3: Simulated and observed hourly means over all days of the months of July of 2002-2006 for CH-Oe1 and IT-Ro1, as well as for 2001-2006 for FI-Hyy. Plotted are mean hourly values (local time) of a,g,m) GPP (blue: O-CN; red: FLUXNET), b,h,n) canopy conductance ( $G_c$ ) (blue: O-CN, red: FLUXNET), c,i,o)  $\text{O}_3$  uptake ( $F_{stc}$ ), d,j,p) the flux ratio ( $F_R$ ), e,k,q)  $\text{O}_3$  deposition velocity ( $V_g$ ), and f,l,r)  $\text{O}_3$  surface resistance ( $R_c$ ). The error bars indicate the standard deviation from the hourly mean. The dotted line in panel (d),(j), and (p) indicates the daily mean value.

Modelled and observed mean diurnal cycles of  $GPP$  and  $G_c$  are in general agreement at the three selected FLUXNET sites (see Fig. 2.3 a,g,m and b,h,n) with particularly good agreement for the mean diurnal cycle of  $GPP$  at the needle-leaved site FI-Hyy, where the hourly means are very close and the observational standard deviation is narrow (see Fig. 2.3 g). At the grassland site IT-Ro1 the overall daytime magnitude of the fluxes is reproduced in general except for the observed afternoon reduction in  $GPP$  (see Fig. 2.3 a). The modelled hourly values fall in the range of the observed values. Modelled and observation-based hourly means of  $GPP$  at the site CH-Oe1 agree well except for the evening hours, where the observed values increase again. The mean diurnal cycles of  $G_c$  derived from the FLUXNET data are again best matched at the site FI-Hyy, whereas the model generally overestimates the diurnal cycle of  $G_c$  slightly at the site IT-Ro1, and overestimates peak  $G_c$  at the CH-Oe1 site. The fact that O-CN does not always simulate the observed midday depression of  $G_c$ , suggests that the response of stomata to atmospheric and soil drought in O-CN requires further evaluation and improvement. Similar to the daily mean values (see Fig. 2.1 a,b) the mean hourly values show the best match of  $GPP$  and  $G_c$  for the needle-leaved tree site and stronger deviations for the sites covered by broadleaved trees and  $C_3$  grasses.

The stomatal  $O_3$  uptake  $F_{stC}$  (Fig. 2.3 c,i,o) is close to zero during night-time when the stomata are assumed to be closed, because gross photosynthesis is zero. At FI-Hyy and CH-Oe1, peak uptake occurred at noon, when photosynthesis (Fig. 2.3 g,m) and stomatal conductance (Fig. 2.3 h,n) are highest, at values between 8-9  $\text{nmol m}^{-2} \text{s}^{-1}$ . At the Italian site IT-Ro1, maximum uptake occurs in the afternoon hours around 15 h, with much larger standard deviation compared to the other two sites (Fig. 2.3 c)). The magnitude of stomatal  $O_3$  uptake corresponds well to some values for example, for crops (Gerosa et al., 2003, 2004, daily maxima of 4-9  $\text{nmol m}^{-2} \text{s}^{-1}$ ) and holm oak (Vitale et al., 2005, approx. 7-8  $\text{nmol m}^{-2} \text{s}^{-1}$ ). Lower daily maximum values have been reported for an evergreen Mediterranean forest dominated by Holm Oak of 4  $\text{nmol m}^{-2} \text{s}^{-1}$  under dry weather conditions (Gerosa et al., 2005) and 1-6  $\text{nmol m}^{-2} \text{s}^{-1}$  for diverse southern European vegetation types (Cieslik, 2004). Much higher values are reported for *Picea abies* (50-90  $\text{nmol m}^{-2} \text{s}^{-1}$ ), *Pinus cembra* (10-50  $\text{nmol m}^{-2} \text{s}^{-1}$ ) and *Larix decidua* (10-40  $\text{nmol m}^{-2} \text{s}^{-1}$ ) at a site near Innsbruck Austria (Wieser et al., 2003), where canopy  $O_3$  uptake was estimated by sap-flow measurements in contrast to the studies mentioned before where the eddy-covariance technique was applied. The much higher  $F_{stC}$  values in that study result from a much higher canopy conductance to  $O_3$  ( $G_c^{O_3}$ ), which are up to 12 times higher than the modelled  $G_c^{O_3}$  values in our study (see Fig. 2.3,  $G_c^{O_3} = \frac{G_c}{1.51}$ ).

The ratio between the stomatal  $O_3$  uptake and the total surface uptake ( $F_R$ ) is close to zero during night-time hours and increases steeply in the morning hours (Fig. 2.3 d,j,p). The 24 h average is approximately 0.3 for IT-Ro1 and 0.4 for FI-Hyy and CH-Oe1 (Fig. 2.3 d,j,p). Peak hourly mean values are close to 0.6 at IT-Ro1, around 0.7 at FI-Hyy and close to 0.8 at CH-Oe1. These values are comparable to the ratios reported for crops (Gerosa et al., 2004; Fowler et al., 2009, 0.5-0.6), Norway spruce (Mikkelsen et al., 2004, 0.3-0.33) and various southern European vegetation types (Cieslik, 2004, 0.12 - 0.69). The modelled flux ratios here show slightly higher daily maximum flux

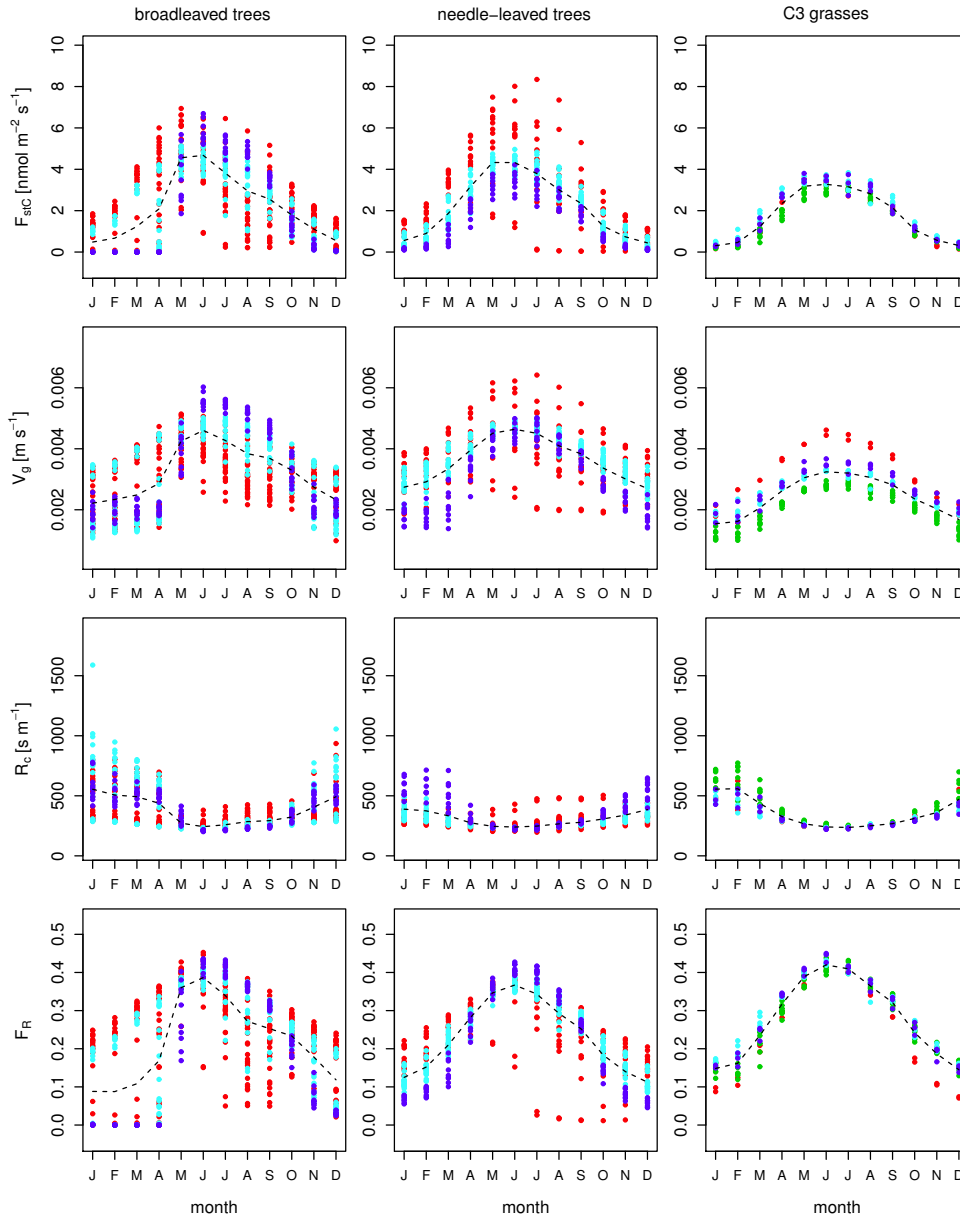


Figure 2.4: Simulated monthly mean values of O<sub>3</sub> uptake ( $F_{stC}$ ), O<sub>3</sub> deposition velocity ( $V_g$ ), O<sub>3</sub> surface resistance ( $R_c$ ), and the flux ratio ( $F_R$ ) for sites dominated by broadleaved trees (left column), needle-leaved trees (central column) and C<sub>3</sub> grasses (right column). The colour indicates the location of the site. Dark blue: Denmark, Sweden and Finland.; light blue: Germany, France and Netherlands; green: Austria and Switzerland; red: Italy, Portugal, Spain, and Israel. Broken line: mean of all sites and years of the 12 months.

ratios than reported in the listed studies. Daily mean flux ratios are well within the reported range.

The modelled deposition velocities  $V_g$  are lowest during night-time with values of approximately  $0.002 \text{ m s}^{-1}$  (Fig. 2.3 e,k,q). These values increase to maximum hourly means of  $0.006\text{-}0.007 \text{ m s}^{-1}$  during daytime. These values compare well with reported values of deposition velocities, which range from  $0.003$  to  $0.009 \text{ m s}^{-1}$  at noon (Gerosa et al., 2004) for a barley field, approximately  $0.006 \text{ m s}^{-1}$  at noon for a wheat field (Tuovinen et al., 2004), and approximately  $0.009 \text{ m s}^{-1}$  at noon at a potato field (Coyle et al., 2009). The estimates for FI-Hyy also agree well with maximum deposition velocities reported for Scots pine site of  $0.006 \text{ m s}^{-1}$  (Keronen et al., 2003; Tuovinen et al., 2004) and noon values from Danish Norway spruce sites of  $0.006\text{-}0.010 \text{ m s}^{-1}$  (Mikkelsen et al., 2004; Tuovinen et al., 2001). Mean daytime deposition velocities of  $0.006 \text{ m s}^{-1}$  (range  $0.003\text{-}0.008 \text{ m s}^{-1}$ ) are reported at a Finish mountain birch site (Tuovinen et al., 2001). Simulated monthly mean values of  $V_g$  differ substantially between the sites (see Fig. 2.4). When comparing the monthly means over all sites (Fig. 2.4 dashed line) of a functional group (broadleaved, needle-leaved,  $C_3$  grasses) to the ensemble mean of 15 CTMs (Hardacre et al., 2015), the values simulated here are higher for needle-leaved tree sites. For broadleaved tree sites and grassland sites, higher values, but which are still within the observed ensemble range, are found for the summer months.

The modelled hourly mean  $\text{O}_3$  surface resistance  $R_c$  is highest during night-time, at approximately  $400 \text{ sm}^{-1}$ , and decreases during daytime to values of  $100$  to  $180 \text{ sm}^{-1}$ , where the lowest surface resistance of approximately  $100 \text{ sm}^{-1}$  is modelled at the grassland site CH-Oe1 (Fig. 2.3 f,l,r). These values are slightly higher than independent estimates (for grasses and crops obtained for other sites) of noon surface resistances ranging from  $50$  to  $100 \text{ sm}^{-1}$  (Padro, 1996; Coyle et al., 2009; Gerosa et al., 2004; Tuovinen et al., 2004). Tuovinen et al. (2004) reported noon values of approximately  $140 \text{ sm}^{-1}$  for a Scots pine forest and  $70\text{-}140 \text{ sm}^{-1}$  for a Norway spruce forest site (Tuovinen et al., 2001), which compares well with the modelled  $R_c$  values at the needle-leaved forest site (FI-Hyy; Fig. 2.3 l). Higher noon values of approximately  $250 \text{ sm}^{-1}$  are reported at a Danish Norway spruce site (Mikkelsen et al., 2004). For a mountain birch forest, noon values of  $110$  to  $140 \text{ sm}^{-1}$  (Tuovinen et al., 2001) are observed which is slightly lower than the modelled value at the IT-Ro1 site (dominated by broadleaved tree PFT).

### 2.3.3 Sensitivity analysis

We assess the sensitivity of the modelled  $\text{O}_3$  uptake and deposition, represented by  $F_g$ ,  $F_{stC}$ ,  $V_g$ , and  $R_c$  to uncertainty in six weakly constrained variables and parameters of the  $\text{O}_3$  deposition scheme ( $R_a$ ,  $b$ ,  $r_{ext}$ ,  $\hat{R}_{gs}$ ,  $G_c$ , and  $R_b$ ). Fig. 2.5 a shows, for example, the results for the boreal needle-leaved forest FI-Hyy. As expected, all uptake/deposition variables, except for the flux ratio ( $F_R$ ) are negatively correlated with the aerodynamic resistance  $R_a$ , which describes the level of decoupling of the atmosphere and land surface. Increasing  $R_a$  decreases the canopy internal  $\text{O}_3$  concentration and hence stomatal ( $F_{stC}$ ) and total ( $F_g$ ) deposition as well as the deposition velocity ( $V_g$ ). The flux ratio  $F_R$  is slightly positively correlated with changes in  $R_a$  due to the stronger negative correlation

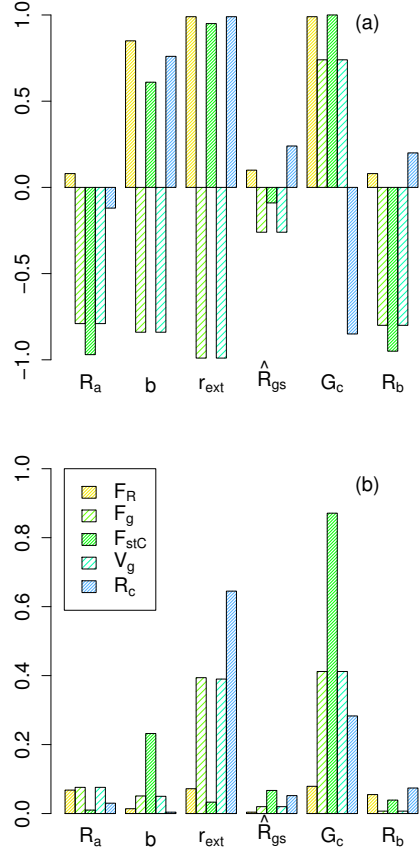


Figure 2.5: a) Mean partial correlation coefficients and b) strength of the correlation in % per %.  $R_a$ ,  $b$ ,  $r_{ext}$ ,  $\hat{R}_{gs}$  and  $G_c$  are perturbed within  $\pm 20\%$  of their central estimate. Results from simulations at the FLUXNET site FI-Hyy for the simulation period 2001-2006.

of  $F_{stC}$  relative to  $F_g$ .

In decreasing order, but as expected, the level of external leaf resistance ( $r_{ext}$ ), the scaling factor  $b$  (Eq. 2.11), the soil resistance ( $\hat{R}_{gs}$ ), and the canopy-scale quasi-laminar layer resistance ( $R_b$ ) increase  $R_c$  and consequently reduce  $F_g$  and  $V_g$ . Reducing the non-stomatal deposition by increasing  $r_{ext}$ ,  $b$ ,  $\hat{R}_{gs}$ , and  $R_b$  increases the canopy internal  $O_3$  concentration and thus stomatal  $O_3$  uptake ( $F_{stC}$ ). The combined effects of a reduction in total deposition  $F_g$  and an increase in  $F_{stC}$  cause a positive correlation of  $F_R$  to  $r_{ext}$ ,  $b$ ,  $\hat{R}_{gs}$ , and  $R_b$ .

Increasing canopy conductance ( $G_c$ ) increases stomatal  $O_3$  uptake ( $F_{stC}$ ) and thereby also increases  $V_g$  and  $F_g$ . The increased total  $O_3$  uptake ( $F_g$ ) decreases the surface resistance to  $O_3$  uptake  $R_c$ , resulting in a negative correlation of  $R_c$  with  $G_c$ . The stronger increase in  $F_{stC}$  relative to  $F_g$  results in a positive correlation of  $F_R$ .

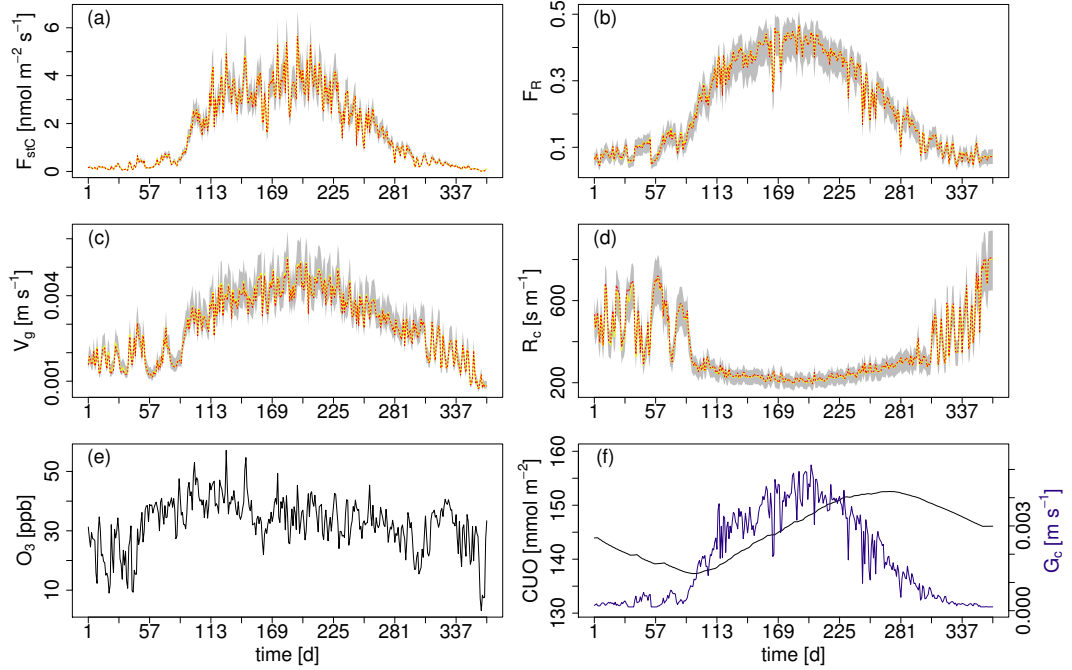


Figure 2.6: Ensemble range of key O<sub>3</sub> uptake/deposition variables resulting from the perturbation of  $R_a$ ,  $b$ ,  $r_{ext}$ ,  $\hat{R}_{gs}$  and  $G_c$  within  $\pm 20\%$  of their central estimate. Shown are simulated daily mean values of a) O<sub>3</sub> uptake ( $F_{stC}$ ), b) the O<sub>3</sub> flux ratio ( $F_R$ ), c) O<sub>3</sub> deposition velocity ( $v_g$ ) and d) O<sub>3</sub> surface resistance ( $R_c$ ) for the boreal needle-leaved evergreen forest at the finish FLUXNET site FI-Hyy for the year 2001. Red dashed: unperturbed model; yellow: median of all sensitivity runs; light-grey area: min-max range off all sensitivity runs. Simulated daily mean values for the respective site and year of e) atmospheric O<sub>3</sub> concentrations O<sub>3</sub> and f) cumulative uptake of O<sub>3</sub> (CUO) and canopy conductance  $G_c$ .

Despite these partial correlations, only changed values for  $r_{ext}$  and  $G_c$  have a notable effect on the predicted fluxes (Fig. 2.5 b), whereas for the other factors ( $R_a$ ,  $b$ , and  $\hat{R}_{gs}$ ) the impact on the simulated fluxes is less than 0.1% due to a 1% change in the variables/parameters of the deposition scheme.

The flux ratio  $F_R$  is very little affected by varying  $r_{ext}$  and  $G_c$ .

Notwithstanding the perturbations, all four O<sub>3</sub> related flux variables show a fairly narrow range of simulated values (Fig. 2.6). For all four variables the unperturbed model and the ensemble mean lie on top of each other (see dashed red and yellow line in Fig. 2.6 a-d). The seasonal course of the surface resistances and fluxes is maintained. The simulations show a strong day-to-day variability in  $F_{stC}$ , which is conserved with different parameter combinations and which is largely driven by the day-to-day variations in  $G_c$  and the atmospheric O<sub>3</sub> concentration (see Fig. 2.6 f and e respectively). Ozone uptake

by the leaves reduces the  $O_3$  surface resistance during the growing season such that  $R_c$  becomes lowest. The cumulative uptake of  $O_3$  (CUO) is lowest at the beginning of the growing season but not zero because the evergreen pine at the Hyytiälä site accumulates  $O_3$  over several years (Fig. 2.6 f). The CUO increases during the growing season and declines in autumn when a larger fraction of old needles are shed.

The minor impact of the perturbations on the simulated  $O_3$  uptake and deposition variables suggests that the calculated  $O_3$  uptake is relatively robust against uncertainties in the parameterisation of some of the lesser known surface properties.

### 2.3.4 Regional simulations

We used the model to simulate the vegetation productivity,  $O_3$  uptake, and associated ozone damage of plant production over Europe for the period 2001-2010 (see Section 2.2.5 for modelling protocol).

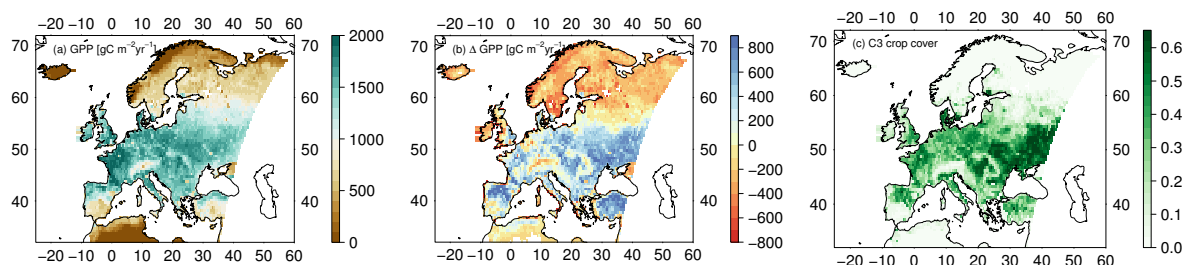


Figure 2.7: Europe-wide simulated GPP and difference between modelled GPP by O-CN and a GPP estimate by a FLUXNET-MTE product. Plotted, for the years 1982-2011, are (a) the simulated mean GPP accounting for ozone damage in  $g C m^{-2} yr^{-1}$ , (b) the mean differences for O-CN minus MTE GPP in  $g C m^{-2} yr^{-1}$ , and (c) the mean simulated grid cell cover of the  $C_3$ -crop PFT in O-CN, given as fractions of the total grid cell area.

Simulated mean annual GPP for the years 1982-2011 shows in general good agreement with an independent estimate of GPP based on upscaled eddy-covariance measurements (MTE; see Section 2.2.5), with O-CN on average underestimating GPP by 16% (European mean). A significant exception are cropland dominated areas (Fig. 2.7) in parts of eastern Europe, southern Russia, Turkey, and northern Spain, which show consistent overestimation of GPP by O-CN of  $400-900 g C m^{-2} yr^{-1}$  (58% overestimation on average). Regions with a strong disagreement coincide with high simulated LAI values by O-CN and a higher simulated GPP in summer compared to the summer GPP by MTE. In addition, O-CN simulates a longer growing season for croplands since sowing and harvest dates are not considered. It is worth noting, nevertheless, that there are no FLUXNET stations present in the regions of disagreement hotspots, making it difficult to assess the reliability of the MTE product in these regions.

North of  $60^\circ N$ , O-CN has the tendency to produce lower estimates of GPP than

inferred from the observation-based product, which is particularly pronounced in low-productivity mountain regions of Norway and Sweden. It is unclear whether this bias is indicative of a N limitation that is too strong in the O-CN model.

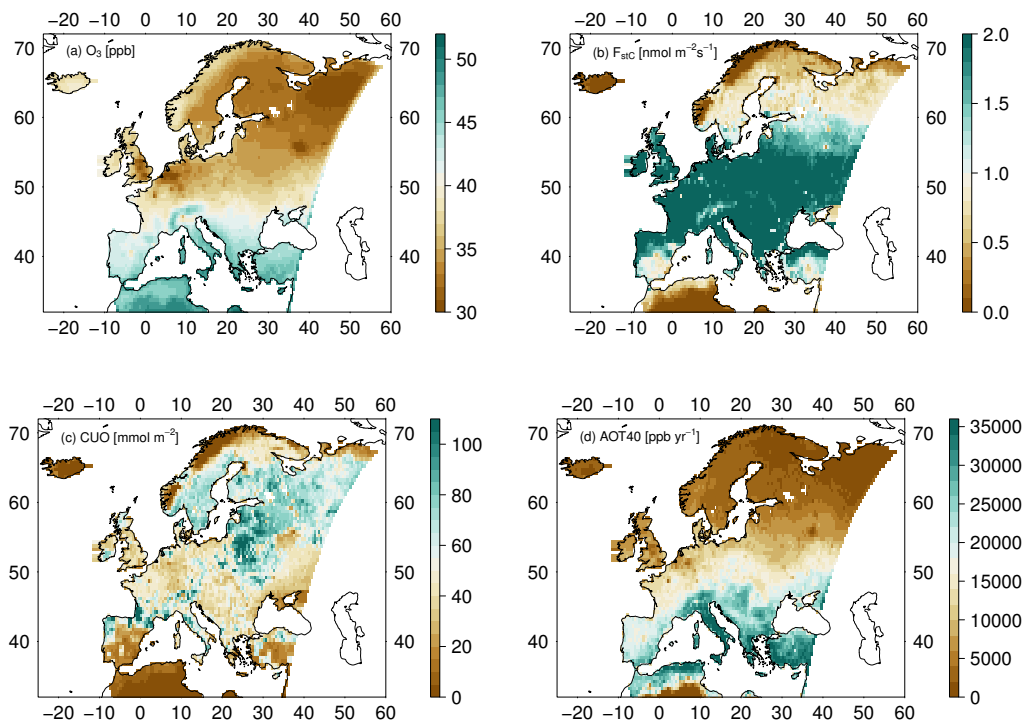


Figure 2.8: Mean decadal (a)  $\text{O}_3$  concentration [ppb], (b) canopy-integrated  $\text{O}_3$  uptake into the leaves [ $\text{nmol m}^{-2} \text{s}^{-1}$ ], (c) canopy-integrated cumulative uptake of  $\text{O}_3$  (CUO) [ $\text{mmol m}^{-2}$ ], and (d) AOT40 [ $\text{ppm yr}^{-1}$ ], for Europe of the years 2001-2010.

Average decadal  $\text{O}_3$  concentrations generally increase from northern to southern Europe (Fig. 2.8 a) and with increasing altitude, with local deviations from this pattern in centres of substantial air pollution. The pattern of foliar  $\text{O}_3$  uptake differs distinctly from that of the  $\text{O}_3$  concentrations, showing highest uptake rates in central and eastern Europe and parts of southern Europe (Fig. 2.8 b), associated with centres of high rates of simulated gross primary production (Fig. 2.7 a) and thus canopy conductance. The cumulative  $\text{O}_3$  uptake reaches values of 40-60  $\text{mmol m}^{-2}$  in large parts of central Europe (Fig. 2.8 c). The highest accumulation rates of 80-110  $\text{mmol m}^{-2}$  are found in eastern Europe and parts of Scandinavia as well as in Italy, the Alps and the Bordeaux region. The concentration-based exposure index AOT40 (Fig. 2.8 d) shows a strong north-south gradient similar to the  $\text{O}_3$  concentration (Fig. 2.8 a) and is distinctly different to the flux-based CUO pattern (Fig. 2.8 c).

Simulated reductions in mean decadal GPP due to  $\text{O}_3$  range from 80 to 160  $\text{g C m}^{-2} \text{yr}^{-1}$  over large areas of central, eastern, and south-eastern Europe (Fig. 2.9 a) and are gen-

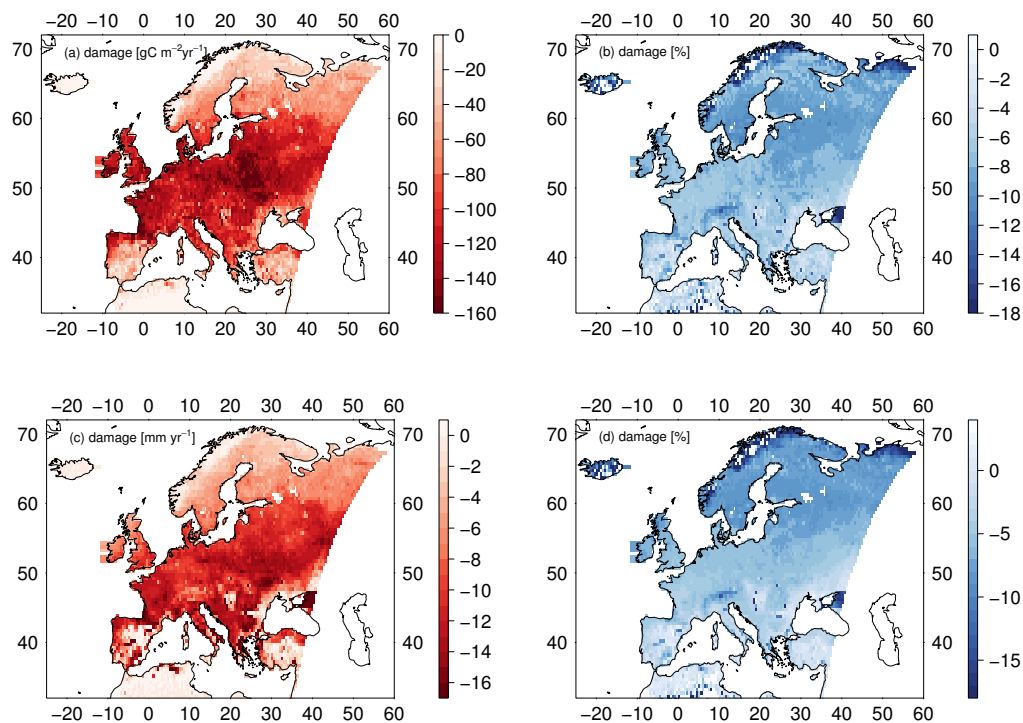


Figure 2.9: Mean decadal (a) reduction in GPP [ $\text{g C m}^{-2} \text{yr}^{-1}$ ], (b) percent reduction in GPP, (c) reduction in transpiration [ $\text{mm yr}^{-1}$ ] and (d) percent reduction in transpiration due to ozone damage averaged for the years 2001-2010.

erally largest in regions of high productivity. The relative reduction in GPP is fairly consistent across large areas in Europe and averages 6-10% (Fig. 2.9 b). Higher reductions in relative terms are found in regions with high cover of  $C_4$  PFTs, e.g. the Black Sea area. Lower relative reductions are found in northern Europe and parts of southern Europe, where productivity is low and stomatal  $\text{O}_3$  uptake is reduced by, for example, low  $\text{O}_3$  concentrations or drought control on stomatal fluxes respectively. Slight increases or strong decreases in relative terms are found in regions with very small productivity like in northern Africa and the mountainous regions of Scandinavia. A slight increase in GPP might be caused by feedbacks of GPP damage on LAI, canopy conductance and soil moisture content such that water savings, for example, enable a prolonged growing season and thus a slightly higher GPP. Overall, simulated European productivity has been reduced from  $10.6 \text{ Pg C yr}^{-1}$  to  $9.8 \text{ Pg C yr}^{-1}$  corresponding to a 7.6% reduction.

The  $\text{O}_3$  induced reductions in GPP are associated with a reduction in mean decadal transpiration rates of  $8\text{-}15 \text{ mm yr}^{-1}$  over large parts of central and eastern Europe (Fig. 2.9 c). These reductions correspond to 3-6% of transpiration in central Europe and 6-10 % in northern Europe. As expected, the relative reductions in transpiration rates are therefore slightly lower than for GPP due to the role of aerodynamic resistance in

controlling water fluxes in addition to canopy conductance. Very high reductions in transpiration are found in the eastern Black Sea area associated with strong reductions in GPP and in the mountainous regions of Scandinavia where absolute changes in transpiration are very small. Regionally (in particular in eastern Spain, northern Africa and around the Black Sea) lower reductions in transpiration or even slight increases are found (Fig. 2.9 d). These are related to  $O_3$ -induced soil moisture savings during the wet growing season, leading to lower water stress rates during the drier season. The very strong reduction in transpiration west of the Crimean Peninsula are related to the strong reductions in GPP mentioned above. Overall, simulated European mean transpiration has been reduced from 170.4 mm to 163.3 mm corresponding to a 4.2% reduction.

### 2.3.5 Impacts of using the ozone deposition scheme

At the FI-Hyy site the canopy  $O_3$  concentration, uptake and accumulated uptake (CUO) increases approximately 10-15% for the D-STO model (non-stomatal depletion of  $O_3$  is zero) and 20-25% for the ATM model version (canopy  $O_3$  concentration is equal to the atmospheric concentration) compared to the standard deposition scheme (D) used here (Fig. 2.10a-c and Fig. 2.11). The exact values however are site- and PFT-specific (see Fig. 2.11 for the CH-Oe1 and IT-Ro1 site).

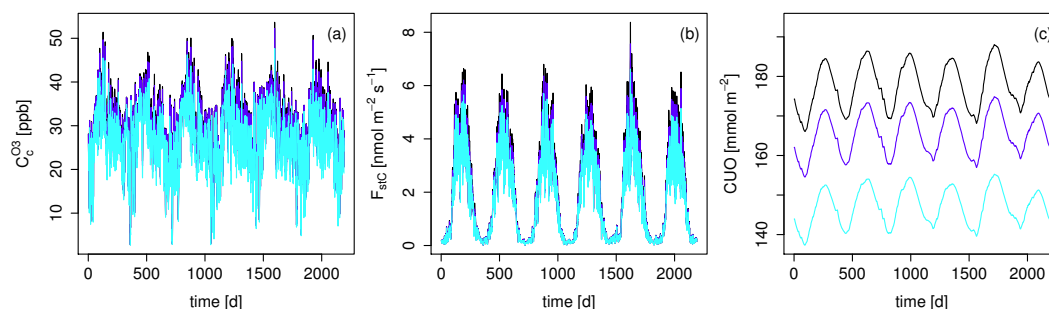


Figure 2.10: Mean daily values of the (a)  $O_3$  surface concentration [ppb], (b) canopy-integrated  $O_3$  uptake into the leaves [ $\text{nmol m}^{-2} \text{s}^{-1}$ ], and (c) canopy-integrated cumulative uptake of  $O_3$  (CUO) [ $\text{mmol m}^{-2}$ ] at the FLUXNET site FI-Hyy. Black: ATM model, Dark blue: D-STO model, Light blue: standard deposition model (D).

The regional impact of using the ozone deposition scheme on CUO is shown in Fig. 2.12. CUO substantially decreases for the D-STO (Fig. 2.12b) compared to the ATM model (Fig. 2.12a). Using the standard deposition model D (Fig. 2.12c) further reduces the CUO compared to the ATM version where the stomata respond directly to the atmospheric  $O_3$  concentration.

Calculating the canopy  $O_3$  concentration with the help of a deposition scheme that accounts for stomatal and non-stomatal  $O_3$  deposition thus reduces  $O_3$  accumulation in the vegetation.

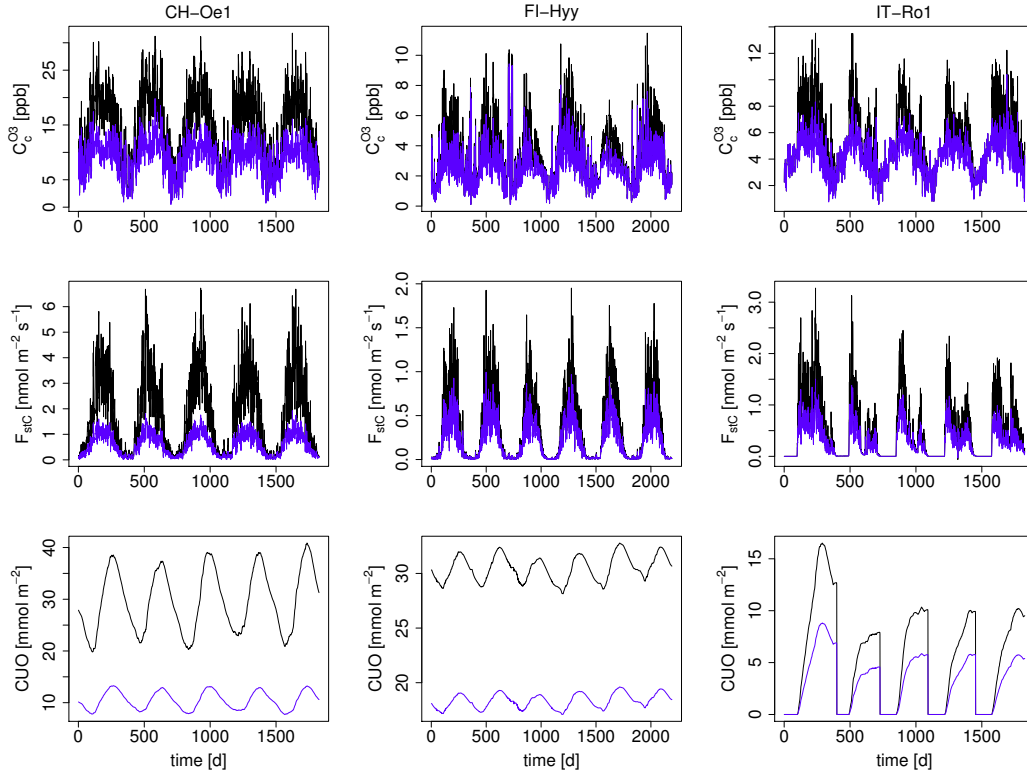


Figure 2.11: Differences in mean daily values of the (a)  $\text{O}_3$  surface concentration [ppb], (b) canopy-integrated  $\text{O}_3$  uptake into the leaves [ $\text{nmol m}^{-2} \text{s}^{-1}$ ], and (c) canopy integrated cumulative uptake of  $\text{O}_3$  (CUO) [ $\text{mmol m}^{-2}$ ] for the three FLUXNET sites CH-Oe1, FI-Hyy and IT-Ro1. Blue: difference between the D-STO model and the standard model (D); black: difference between the ATM model and the standard model (D).

## 2.4 Discussion

We extended the terrestrial biosphere model O-CN by a scheme to account for the atmosphere–leaf transfer of  $\text{O}_3$  in order to better account for air pollution effects on net photosynthesis and hence regional to global water, carbon, and nitrogen cycling. This ozone deposition scheme calculates canopy  $\text{O}_3$  concentrations and uptake into the leaves depending on surface conditions and vegetation carbon uptake.

Estimates of the regional damage to annual average GPP (- 7.6%) and transpiration (- 4.2%) simulated by O-CN for 2001-2010 are lower than previously reported estimates. Meta-analyses suggest on average a 11% (Wittig et al., 2007) and a 21% (Lombardozzi et al., 2013) reduction in instantaneous photosynthetic rates. However, because of carry-over effects this does not necessarily translate directly into reductions in annual GPP. Damage estimates using the CLM model suggest GPP reductions of 10-25% in Europe and 10.8% globally (Lombardozzi et al., 2015). Reductions in transpiration have been

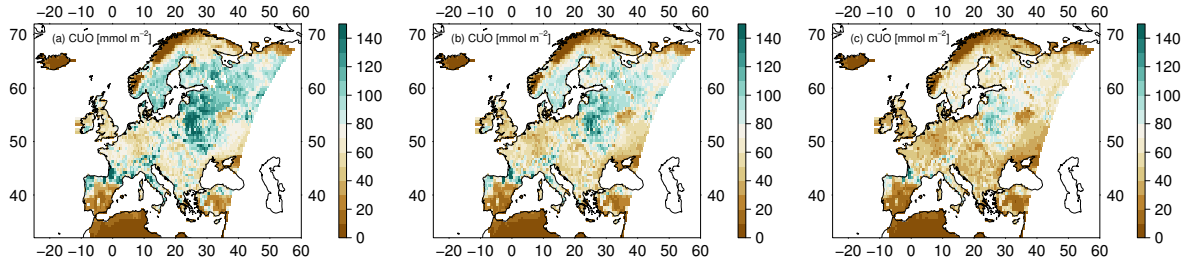


Figure 2.12: Mean decadal canopy-integrated cumulative uptake of  $O_3$  (CUO) [ $\text{mmol m}^{-2}$ ] for Europe of the years 2001–2010. (a) Canopy  $O_3$  concentration is equal to the atmospheric concentration (ATM) and (b)  $O_3$  surface resistance is only determined by stomatal resistance (D-STO). (c) Standard ozone deposition scheme (D).

estimated to amount 5-20% for Europe and 2.2% globally (Lombardozzi et al., 2015). Lombardozzi et al. (2015) however, used fixed reductions of photosynthesis (12-20%) independent of cumulative  $O_3$  uptake for two out of three simulated plant types. Damage was only related to cumulative  $O_3$  uptake for one plant type with a very small slope and hence little increase in damage due to increases in cumulative  $O_3$  uptake. Sitch et al. (2007) simulated global GPP reductions of 8-14% (under elevated and fixed  $CO_2$  respectively) for low plant ozone sensitivity and 15-23% (under elevated and fixed  $CO_2$  respectively) for high plant ozone sensitivity for the year 2100 compared to 1901. For the Euro-Mediterranean region an average GPP reduction of 22% was estimated by the ORCHIDEE model for the year 2002 using an AOT40-based approach (Anav et al., 2011).

Possible causes for the discrepancies are differences in the applied injury functions, flux thresholds accounting for the detoxification ability of the plants, atmospheric  $O_3$  concentrations, simulation periods, and simulation of climate change (elevated  $CO_2$ ) and air pollution (nitrogen deposition). We discuss the most important aspects below. To elucidate the reasons for the substantial differences in the damage estimates further studies are necessary to disentangle the combined effects of differing flux thresholds; injury relationships; climate change; and deposition of nitrogen.

#### 2.4.1 Atmosphere-leaf transport of ozone

The sensitivity analysis in Section 2.3.3 demonstrates that the estimate of canopy conductance ( $G_c$ ) is crucial for calculating plant ozone uptake; therefore, reliable observations to constrain modelled canopy conductance are highly important. The site-level evaluation shows that O-CN produces reasonable estimates of simulated gross primary productivity (GPP), canopy conductance, and latent heat flux (LE) compared to FLUXNET observations. This agreement has to be seen in the light of the diverse set of random and systematic errors in the eddy-covariance measurements as well as derived

flux and conductance estimates (Richardson et al., 2012; Knauer et al., 2017). Next to uncertainties about the strength of the aerodynamic coupling between atmosphere and canopy, problems exist at many sites with respect to the energy balance closure (Wilson et al., 2002). Failure to close the energy balance can cause underestimation of sensible and latent heat, as well as an overestimation of available energy, with mean bias of 20% where the imbalance is greatest during nocturnal periods (Wilson et al., 2002). This imbalance propagates to estimates of canopy conductance, which is inferred from latent and sensible heat fluxes. The energy imbalance furthermore appears to affect estimates of CO<sub>2</sub> uptake and respiration (Wilson et al., 2002). Flux partitioning algorithms which extrapolate night-time ecosystem respiration estimates to daytime introduce an additional potential for bias in the estimation of GPP (Reichstein et al., 2005). Nevertheless, the general good agreement of  $G_c$  compared to FLUXNET estimates, together with the finding that modelled values of key ozone variables are within observed ranges, supports the use of the extended O-CN model for determining the effect of air pollution on terrestrial carbon, nitrogen, and water cycling.

A key difference from previous studies is our use of the use of the ozone deposition scheme, which reduces O<sub>3</sub> surface concentrations and hence also the estimated O<sub>3</sub> uptake and accumulation (see Fig. 2.12). Accounting for stomatal and non-stomatal deposition in the calculation of the surface O<sub>3</sub> concentrations considerably impacts the estimated plant uptake of O<sub>3</sub>. O<sub>3</sub> uptake and cumulated uptake are considerably overestimated when atmospheric ozone concentrations are used to calculate O<sub>3</sub> uptake or when in the calculation of leaf-level O<sub>3</sub> concentrations only stomatal destruction of O<sub>3</sub> is regarded (see subsection 2.3.5). Compared to the values that would have been obtained if the CTM O<sub>3</sub> concentrations of the atmosphere (from ca. 45 m height) had been used directly at the leaf surface, our simulations yield a decrease in CUO by 31% (European means for the years 2001-2010). A significant fraction of the decreases is associated with non-stomatal O<sub>3</sub> uptake and destruction at the surface, which decreased the simulated cumulative O<sub>3</sub> uptake by 16%. To obtain an estimate of CUO that is as accurate as possible, stomatal and non-stomatal destruction of O<sub>3</sub> and their impacts on canopy O<sub>3</sub> concentrations should be accounted for in terrestrial biosphere models (Tuovinen et al., 2009). Flux-based ozone damage assessment models may overestimate ozone-related damage unless they properly account for non-stomatal O<sub>3</sub> uptake at the surface.

We note that vegetation type and dynamics also impact the stomatal and non-stomatal deposition of O<sub>3</sub>, and hence the calculation of the leaf-level O<sub>3</sub> concentrations. This impedes the use of CTM-derived leaf-level O<sub>3</sub> concentration, as CTM and vegetation specifications may differ strongly. Using the O<sub>3</sub> from the lowest level of the atmosphere reduces this problem, but running a terrestrial biosphere with a fixed atmospheric boundary condition (and not coupled to a atmospheric CTM) is still a simplification that prevents biosphere-atmosphere feedbacks and therefore to potential discrepancies between vegetation and CTM. Not accounting for this feedback and stomatal and non-stomatal O<sub>3</sub> deposition might result in an overestimation of O<sub>3</sub> uptake and hence potential damage in the vegetation model. The deposition scheme in O-CN offers the potential to couple vegetation and chemical transport modelling and is thus a step

forward towards coupled atmosphere-vegetation simulations.

### 2.4.2 Estimating vegetation damage from ozone uptake

A key aspect of ozone damage estimates are the assumed dose-response relationships, which relate  $O_3$  uptake to plant damage. The use of flux-based relationships is generally thought to improve damage estimates compared to concentration-based metrics (e.g. AOT40), since stomatal constraints on  $O_3$  uptake are taken into account, yielding very different spatial patterns of exposure hotspots (Simpson et al., 2007). Similar to Simpson et al. (2007), we find strongly differing patterns between cumulative  $O_3$  uptake (CUO) and AOT40 in our simulations here (see Fig. 2.8), where highest exposure is found not only in southern Europe, where the  $O_3$  concentration is highest, but also in eastern Europe.

Several dose-response relationships exist for biomass or yield damage (see LRTAP-Convention (2017), for an overview), however there are few estimates of the likely cause of this damage, i.e. the reduction in net photosynthesis. In this study, the injury relationship to net photosynthesis proposed by Wittig et al. (2007) is used. The major advantage of this relationship is that it has been obtained by meta-analysis of many different tree species and thus might indicate an average response. This relationship is therefore used for all modelled PFTs. However, a substantial disadvantage is that the meta-analysis implies an injury of 6.16% at zero accumulated  $O_3$  uptake with a rather minor increase in injury with increasing  $O_3$  uptake. This might be an important factor explaining the lower ozone damage estimates of O-CN compared to other terrestrial biosphere models. In Lombardozzi et al. (2015) also an injury relationship derived from a meta-analysis is used; however, the disadvantage of predicted ozone injury at zero accumulated  $O_3$  uptake there is even greater compared to Wittig et al. (2007). Two out of three modelled PFTs assume ozone induced injury values of -12.5% and -16.1% at zero accumulated  $O_3$  uptake (broadleaved and needle-leaved species respectively) and the third PFT (grass and crop) assumes -19.8% at zero accumulated  $O_3$  uptake together with a small increase in injury with increasing  $O_3$  uptake (Lombardozzi et al., 2015). An evaluation of the different proposed injury functions implemented in terrestrial biosphere models (e.g. Wittig et al. (2007); Lombardozzi et al. (2015); Sitch et al. (2007)) is necessary to elucidate which are able to reproduce, for example, observed patterns of biomass damage and hence might be suitable to predict regional or global damage estimates. Furthermore, new injury relationships for different plant groups would be desirable for use in dynamic vegetation models to improve the ozone damage estimates, for example by ensuring an intercept close to one (zero injury at zero accumulated  $O_3$ ).

The use of a (possibly PFT-specific) flux threshold and its magnitude naturally also impacts the CUOY (canopy cumulative  $O_3$  uptake above a threshold of  $Y \text{ nmol m}^{-2} \text{ s}^{-1}$ ) and possible damage estimates (Tuovinen et al., 2007). The included injury function by Wittig et al. (2007) is designed for the CUO without a flux threshold ( $Y = 0$ ). The impacts of using different flux thresholds on regional estimates of  $O_3$  uptake, accumulation and damage are still poorly understood and need further research.

It should be noted that using plant  $O_3$  uptake based on leaf-level  $O_3$  concentrations,

as done here, together with empirical ozone injury functions, where  $O_3$  uptake is calculated from atmospheric  $O_3$  concentrations, introduces a discrepancy. The  $O_3$  uptake rates of the experiments forming the injury relationship however are calculated from mean ozone concentrations, for example, over the exposure period and the respective average stomatal conductance (Wittig et al., 2007) such that the estimated  $O_3$  uptake and cumulated uptake used to derive the injury relationship are coarse approximations and underlie considerable uncertainty. The error introduced in O-CN by using leaf-level  $O_3$  concentrations instead of atmospheric concentrations seems small, especially since the use of the leaf-level  $O_3$  concentration is the physiologically more appropriate approach.

In the current version of O-CN only ozone injury to net photosynthesis is accounted for. Other processes like detoxification of  $O_3$  and injury repair (Wieser and Matyssek, 2007; Ainsworth et al., 2012), stomatal sluggishness (Paoletti and Grulke, 2010) and early senescence (Gielen et al., 2007; Ainsworth et al., 2012) are not accounted for. Decoupling of photosynthesis and stomatal conductance (e.g. through stomatal sluggishness) might impact GPP and transpiration damage estimates and requires further analysis. Accounting for direct impairment of the stomata might reduce the reported reductions in transpiration or even cause an increase compared to simulations with no ozone injury. Reduced carbon gain due to early senescence might impact the growth and biomass accumulation of plants (Gielen et al., 2007; Ainsworth et al., 2012) and ought to also be included in terrestrial biosphere models.

## 2.5 Conclusion

Estimates of  $O_3$  impacts on plant gross primary productivity vary substantially. This uncertainty in the magnitude of damage and hence the potential impact on the global carbon budget is related to different approaches to model ozone damage. The use of a comparatively detailed ozone deposition scheme that accounts for non-stomatal as well as stomatal deposition when calculating surface  $O_3$  concentrations substantially affects  $O_3$  uptake in our model. We therefore recommend that non-stomatal  $O_3$  uptake be routinely included in model assessments of ozone damage to obtain a better estimate of ozone uptake and accumulation. We show that  $O_3$  uptake into the stomata is mainly determined by the canopy conductance in the ozone deposition scheme used here. This highlights the importance of reliable modelling of canopy conductance as well as realistic surface  $O_3$  concentrations to obtain as accurate as possible estimates of  $O_3$  uptake, which are the basis for plant damage estimates. Suitable ozone injury relationships to net photosynthesis for different plant groups are essential to relate the accumulated  $O_3$  uptake to plant damage in a model. Mean responses of plant groups similar to commonly modelled PFTs are also desirable. Only a few relationships exist which indicate mean responses of several species (e.g. Wittig et al. (2007); Lombardozzi et al. (2013), which however, propose very different relationships). Furthermore, the impact of the plants ability to detoxify  $O_3$  should be considered by using, for example, flux thresholds, as well as the combined effects of  $O_3$  with air pollution (nitrogen deposition) and climate change (elevated  $CO_2$ ) on the plants carbon uptake.



## Chapter 3

# Evaluation of simulated ozone effects in forest ecosystems against biomass damage estimates from fumigation experiments

### 3.1 Introduction

Simulated reductions in GPP due to ozone-induced injury vary substantially between models and model versions (Lombardozzi et al., 2012a, 2015; Franz et al., 2017; Sitch et al., 2007). This uncertainty is predominantly due to the different approaches that these models use to relate ozone uptake (or ozone exposure) to reductions in whole-tree biomass, and in the exact parameterisation of the injury functions and dose-response relationships applied (Karlsson et al., 2004; Pleijel et al., 2004; Wittig et al., 2007; Lombardozzi et al., 2012a, 2013). The injury functions employed by current terrestrial biosphere models differ decidedly in their slope (i.e. the change in injury per unit of time-integrated ozone uptake), intercept (ozone injury at zero time-integrated ozone uptake) and their assumed threshold, below which the ozone uptake rate is considered sufficiently low that ozone will be detoxified before any injury occurs (Karlsson et al., 2004; Pleijel et al., 2004; Lombardozzi et al., 2012a). For example, Sitch et al. (2007) relates the instantaneous ozone uptake exceeding a flux threshold to net photosynthetic injury via an empirically derived factor. An alternative approach has been to relate ozone injury to net photosynthesis in response to the accumulated ozone uptake rather than to the instantaneous ozone uptake as in Sitch et al. (2007), e.g. by using the *CUOY*, which refers to the cumulative canopy O<sub>3</sub> uptake above a flux threshold of  $Y \text{ nmol m}^{-2} \text{ s}^{-1}$  (Wittig et al., 2007; Lombardozzi et al., 2012a, 2013; Cailleret et al., 2018).

The effect of ozone on plant growth has been investigated by ozone filtration/fumigation experiments either at the individual experimental level or by pooling data from multiple experiments that have been conducted according to a standardised experimental

method. These experiments typically rely on young trees because of their small size. A challenge in developing and testing process-based models of ozone damage from these ozone fumigation experiments is that often only the difference in biomass accumulation between plants grown in an ozone treatment and in ambient or charcoal-filtered air at the end of the experiment are reported. Data from these studies provide evidence for a linear, species-specific relationship between accumulated ozone uptake and reductions in plant biomass (Pleijel et al., 2004; Mills et al., 2011b; Nunn et al., 2006, e.g.). Sitch et al. (2007) for instance calibrated their instantaneous leaf-level injury function between ozone uptake and photosynthesis by relating simulated annual net primary production and accumulated ozone uptake to observed biomass dose-response relationships developed by Karlsson et al. (2004) and Pleijel et al. (2004), where biomass/yield damage is related to the phytotoxic ozone dose ( $POD_y$ ). The  $POD_y$  refers to the accumulated ozone uptake above a flux threshold of  $y \text{ nmol m}^{-2} \text{ s}^{-1}$  by the leaves representative of the upper-canopy leaves of the plant. Such an approach applies biomass dose-response relationships of young trees to mature trees. However, the effects of ozone on leaf physiology (e.g. net photosynthesis and stomatal conductance) or plant carbon allocation may differ between juvenile and adult trees (Hanson et al., 1994; Samuelson and Kelly, 1996; Kolb and Matyssek, 2001; Paoletti et al., 2010). Whether or not biomass dose-response relationships can be used to calibrate injury functions for mature trees is uncertain.

An alternative approach is to directly simulate ozone injury to photosynthesis, which may have been a major cause for the observed decline in plant biomass production (Ainsworth et al., 2012). Possible injury targets in the simulations can be, for example the net photosynthesis or leaf-specific photosynthetic activity (such as represented by the maximum carboxylation capacity of RuBisCO,  $V_{cmax}$ ). For instance Lombardozzi et al. (2012a) based their injury function on an experimental study involving a single forest tree species, whereas more recent publications (e.g. Lombardozzi et al. (2015) and Franz et al. (2017)) have used injury functions from meta-analyses of a far larger set of filtration/fumigation studies. Meta-analyses have attempted to summarise the responses of plant performance to ozone exposure across a wider range of experiments and vegetation types (Wittig et al., 2007; Lombardozzi et al., 2013; Feng and Kobayashi, 2009; Li et al., 2017; Wittig et al., 2009) and to develop injury functions for plant groups that might provide an estimate of mean plant group responses to ozone. However, these meta-analyses suffer from a lack of consistency in the derivation of either plant injury or ozone exposure, and generally report a large amount of unexplained variance. A further complication in the meta-analyses of ozone injury (e.g. Wittig et al., 2007; Lombardozzi et al., 2013) is that they have to indirectly estimate the cumulative ozone uptake underlying the observed ozone injury based on a restricted amount of data, which causes uncertainty in the derived injury functions.

Büker et al. (2015) provides an independent data set of whole-tree biomass plant responses to ozone uptake which is independent of data sets that were used to describe injury functions by Wittig et al. (2007) and Lombardozzi et al. (2013). This data set has been collected from experiments that follow a more standardised methodology to assess dose-responses and has associated meteorological and ozone data at a high time

resolution that allow more accurate estimates of modelled ozone uptake to be made. These dose-response relationships describe whole-tree biomass reductions in young trees derived from standardised ozone filtration/fumigation methods for eight European tree species at 10 locations across Europe (see Tab. 3.2 for details and Büker et al., 2015). These data thus provide an opportunity to evaluate simulations of biosphere models that use leaf-level injury functions (describing the effect of ozone uptake on photosynthetic variables) to estimate carbon (C) assimilation, growth and ultimately whole-tree biomass against these robust empirical dose-response relationships that relate ozone exposure directly to whole-tree biomass response.

Here we test four alternative, previously published ozone injury functions that target either net photosynthesis or the leaf carboxylation capacity ( $V_{cmax}$ ), which have been included in state-of-the-art terrestrial biosphere models (Lombardozzi et al., 2012a, 2015; Franz et al., 2017) against these new biomass dose-response relationships by Büker et al. (2015). We incorporate these injury functions into a single modelling framework, the O-CN model (Zaehle and Friend, 2010; Franz et al., 2017). To reduce model-data mismatch, we test the functions in simulations that mimic to the extend possible the conditions of each of the experiments in the Büker et al. (2015) data-set. In particular we simulate the young age of the trees, such that we can directly compare the simulated to the observed whole-tree biomass reductions in the empirically derived dose-response relationships. This allows us to identify the contribution of these alternative injury function formulations on the simulated whole-tree biomass response. The simulated biomass dose-response relationships are then compared to the data from the experiments to evaluate the capability of the different model versions to reproduce observed dose-response relationships. Based on these comparisons we use a similar approach to that of Sitch et al. (2007) and develop alternative parameterisations of the injury functions to improve the capability of the O-CN model to simulate the whole-tree biomass responses observed in the fumigation experiments, with the notable exception that we explicitly simulate in-fumigation experiments and the approximate age of the trees. Finally, we explore whether or not there is a substantial difference in the biomass response to ozone of young or mature trees by using a sequence of model simulations and comparing the response both in terms of whole-tree biomass as well as net primary production.

## 3.2 Methods

We use the O-CN terrestrial biosphere model (see section 1.6.1 for details) to simulate the ozone fumigation experiments described in Büker et al. (2015). The simulations of the fumigation experiments are repeated with different model versions, where each model version contains a different ozone injury function.

### 3.2.1 Ozone injury calculation in O-CN

Throughout this chapter we refer to the biological response to  $O_3$  uptake at the leaf level as 'injury' and to responses of plant production, growth and biomass at the ecosystem

level as 'damage' following Guderian (1977). The relationship between ozone uptake and injury is called 'injury function'; the relationship between ozone uptake and damage is called 'dose-response relationship'.

Leaf-level ozone uptake is determined by stomatal conductance and atmospheric  $O_3$  concentrations, as described in Franz et al. (2017). To mimic the conditions of the fumigation experiments with plot-level controlled atmospheric  $O_3$  concentrations, simulations are conducted with a model version of O-CN, in which atmospheric  $O_3$  concentrations are directly used to calculate ozone uptake into the leaves, and the transfer and destruction of ozone between the atmosphere and the surface is ignored (ATM model version in chapter 2 and Franz et al. (2017)). Deviating from Franz et al. (2017), stomatal conductance  $g_{st}$  here is calculated based on the Ball and Berry formulation (Ball et al., 1987) as

$$g_{st,l} = g_0 + g_1 \times \frac{A_{n,l} \times RH \times f(\text{height}_l)}{C_a} \quad (3.1)$$

where net photosynthesis ( $A_{n,l}$ ) is calculated as described in Zaehle and Friend (2010) as a function of the leaf-internal partial pressure of  $CO_2$ , absorbed photosynthetic photon flux density on shaded and sunlit leaves, leaf temperature, the nitrogen-specific rates of maximum light harvesting, electron transport ( $J_{max}$ ) and carboxylation rates ( $V_{cmax}$ ).  $RH$  is the atmospheric relative humidity,  $f(\text{height}_l)$  the water-transport limitation with canopy height,  $C_a$  the atmospheric  $CO_2$  concentration,  $g_0$  the residual conductance when  $A_n$  approaches zero, and  $g_1$  the stomatal-slope parameter as in Krinner et al. (2005). The index  $l$  indicates that  $g_{st}$  is calculated separately for each canopy layer.

The stomatal conductance to ozone  $g_{st,l}^{O_3}$  is calculated as

$$g_{st,l}^{O_3} = \frac{g_{st,l}}{1.51} \quad (3.2)$$

where the factor 1.51 accounts for the different diffusivity of  $O_3$  from water vapour (Massman, 1998).

For each canopy layer, the  $O_3$  stomatal flux ( $f_{st,l}$ ,  $\text{nmol m}^{-2}(\text{leaf area}) \text{s}^{-1}$ ) is calculated from the atmospheric  $O_3$  concentration the plants in the field experiments were fumigated with ( $\chi_{atm}^{O_3}$ ), and  $g_{st,l}$  is calculated as

$$f_{st,l} = (\chi_{atm}^{O_3} - \chi_i^{O_3}) g_{st,l}^{O_3}. \quad (3.3)$$

where the leaf-internal  $O_3$  concentration ( $\chi_i^{O_3}$ ) is assumed to be zero (Laisk et al., 1989).

The accumulation of ozone fluxes above a threshold of  $Y$   $\text{nmol m}^{-2}(\text{leaf area}) \text{s}^{-1}$  ( $f_{st,l,Y}$ ,  $\text{nmol m}^{-2}(\text{leaf area}) \text{s}^{-1}$ ) with

$$f_{st,l,Y} = \text{MAX}(0, f_{st,l} - Y) \quad (3.4)$$

gives the  $CUOY_l$ . The canopy value of  $CUOY$  is calculated by summing  $CUOY_l$  over all canopy layers (Franz et al., 2017).

For comparison to observations, the  $POD$  ( $\text{mmol m}^{-2}$ ) can be diagnosed by the accumulation of  $f_{st,l}$  for the top canopy layer ( $l = 1$ ), in accordance with LRTAP-Convention

(2017) and B ker et al. (2015). The accumulation of ozone fluxes of the top canopy layer above a threshold of  $y \text{ nmol m}^{-2}(\text{leaf area}) \text{ s}^{-1}$  gives the  $PODy$ . The estimates of  $PODy$  (both  $POD2$  and  $POD3$ ) can be used offline to re-construct dose-response relationships equivalent to those described in B ker et al. (2015). These modelled dose-response relationships can then be compared with the empirically derived dose-response relationships to assess the ability of the model to estimate injury. As such, the  $POD2$  and  $POD3$  used for the formation of these modelled dose-response relationships are purely diagnostic variables and not involved in the injury calculation of the model. The flux thresholds (2 and 3  $\text{nmol m}^{-2}(\text{leaf area}) \text{ s}^{-1}$ ) are not the flux thresholds that are used to estimate biomass response in the O-CN model simulations.

Ozone injury, i.e. the fractional loss of carbon uptake associated with ozone uptake  $d_l^{O_3}$ , is calculated as a linear function of the cumulative leaf-level uptake of ozone above a threshold of  $Y \text{ nmol m}^{-2}(\text{leaf area}) \text{ s}^{-1}$  ( $CUOY_l$ )

$$d_l^{O_3} = a - b \times CUOY_l \quad (3.5)$$

where  $a$  is the intercept and  $b$  is the slope of the injury function. The injury fraction ( $d_l^{O_3}$ ) is calculated separately for each canopy layer  $l$  based on the specific accumulated ozone uptake of the respective canopy layer ( $CUOY_l$ ), and takes values between 0 and 1. The magnitude of  $d_l^{O_3}$  in Eq. 3.5 varies between the canopy layers because  $CUOY_l$  varies driven by within-canopy gradients in stomatal conductance and photosynthetic capacity.

The effect of ozone injury on plant carbon uptake is calculated by

$$x_l^{O_3} = x_l(1 - d_l^{O_3}). \quad (3.6)$$

where  $x_l$  is either leaf-level net photosynthesis  $A_{n,l}$  or the maximum photosynthetic capacity ( $J_{max,l}$  and  $V_{cmax,l}$ ), which is used in the calculation of  $A_{n,l}$ .  $J_{max,l}$  and  $V_{cmax,l}$  are reduced in proportion such that the ratio between the two is not altered. While there is some evidence that ozone can affect the ratio between  $J_{max}$  and  $V_{cmax}$ , we believe that for the purpose of this paper, it is justifiable to assume a fixed ratio between them.

Reductions in  $A_{n,l}$  cause a decline in stomatal conductance ( $g_{st,l}$ ) due to the tight coupling between both. Other stress factors that impact  $g_{st,l}$  are accounted for in the preceding calculation of the  $g_{st,l}$  uninjured by ozone (see Eq. 3.1). Reductions in  $g_{st,l}$  decrease the  $O_3$  uptake into the plant ( $f_{st,l}$ ) and slow the increase in  $CUOY_l$  and thus ozone injury.

### 3.2.2 Model set-up

Four published injury functions were applied within the O-CN model (see Tab. 3.1 for the respective slopes, intercepts and flux thresholds). As shown below in Fig. 3.1 and explained in the results section, these did not match well with the observed biomass dose-response relationships by B ker et al. (2015). Following this we manually calibrated two additional injury relationships one each for  $A_n$  or  $V_{cmax}$  based on the data presented in B ker et al. (2015) (see Tab. 3.1 for slopes and intercepts). For these calibrated injury

Table 3.1: Slopes and intercepts, partly PFT specific, of all four published (W07 $_{PS}$ , L12 $_{PS}$ , L12 $_{VC}$ , L13 $_{PS}$ ) and two tuned (tun $_{PS}$ , tun $_{VC}$ ) injury functions included in O-CN. Targets of ozone injury are net photosynthesis (PS) or  $V_{cmax}$ . Injury calculations base on the  $CTOY$  with a specific flux threshold for each injury function.

ID	Target	Slope	Intercept	Plant group	Flux threshold [mmol m <sup>-2</sup> (leaf area) s <sup>-1</sup> ]	Reference
		(b)	(a)			
W07 $_{PS}$	PS	0.0022	0.9384	All	0	Wittig et al. (2007)
L12 $_{PS}$	PS	0.2399	1.0421	All	0.8	Lombardozzi et al. (2012a)
L12 $_{VC}$	$V_{cmax}$	0.1976	0.9888	All	0.8	Lombardozzi et al. (2012a)
L13 $_{PS}$	PS	0	0.8752	Broadleaf	0.8	Lombardozzi et al. (2013)
L13 $_{PS}$	PS	0	0.839	Needleleaf	0.8	Lombardozzi et al. (2013)
tun $_{PS}$	PS	0.065	1	Broadleaf	1	Tuned here
tun $_{PS}$	PS	0.021	1	Needleleaf	1	Tuned here
tun $_{VC}$	$V_{cmax}$	0.075	1	Broadleaf	1	Tuned here
tun $_{VC}$	$V_{cmax}$	0.025	1	Needleleaf	1	Tuned here

functions, we chose a flux threshold value of  $1 \text{ nmol m}^{-2}(\text{leaf area}) \text{ s}^{-1}$ , as suggested by the LRTAP-Convention (2017). We forced the intercept ( $a$ ) of these relationships to 1 to simulate zero ozone injury at zero accumulated  $\text{O}_3$  (for ozone levels that cause less than  $1 \text{ nmol m}^{-2}(\text{leaf area}) \text{ s}^{-1}$  instantaneous ozone uptake). As described above, in all model versions, ozone injury is calculated independently for each canopy layer based on the accumulated  $\text{O}_3$  uptake ( $CUOY_i$ ) in that layer, above a specific flux threshold of  $Y \text{ nmol m}^{-2}(\text{leaf area}) \text{ s}^{-1}$  for the respective injury function (see Tab. 3.1).

### 3.2.3 Model and protocol for young trees

Single-point simulations were run for each fumigation experiment using meteorological input from the daily CRU-NCEP climate data set (CRU-NCEP version 5; LSCE ([http://dods.extra.cea.fr/store/p529viov/cruncep/V5\\_1901\\_2013/](http://dods.extra.cea.fr/store/p529viov/cruncep/V5_1901_2013/))) at the nearest grid cell to the coordinates of the experiment sites. The meteorological data provided by the experiments incompletely described the atmospheric boundary conditions required to drive the O-CN model. Atmospheric  $\text{CO}_2$  concentrations were taken from Sitch et al. (2015), and reduced as well as oxidised nitrogen deposition in wet and dry forms was provided by the EMEP model (Simpson et al., 2014b). Hourly  $\text{O}_3$  concentrations were obtained from the experiments, as in Büker et al. (2015).

Büker et al. (2015) report data for eight tree species at 11 sites across Europe (see Tab. 3.2 for experiment and simulation details). The O-CN model simulates 12 plant functional types (PFTs) rather than explicit species therefore, the species from the experiments were assigned to the corresponding PFT: all broadleaved species except *Quercus ilex* were assigned to the temperate broadleaved summer-green PFT. *Quercus ilex* was classified as temperate broadleaved evergreen PFT. All needleleaf species were assigned to the temperate needleleaf evergreen PFT.

The fumigation experiments were conducted on young trees or cuttings. Prior to the simulation of the experiment, the model was run in an initialisation phase from bare ground until the simulated stand-scale tree age was stable and representative of 1-2 year old trees. During this initialisation, O-CN was run with the climate of the years preceding the experiment and zero atmospheric  $\text{O}_3$  concentrations. Using ambient ozone concentrations during the initialisation phase would have resulted in different initial biomass values for the different response functions, which would have reduced the comparability of the different model runs. The impact of the ozone concentrations in the initialisation phase on our results here can be considered negligible since we only evaluate the simulated biomass from different treatments in relation to each other and do not evaluate it in absolute terms.

The duration of the initialisation phase depends on the site and PFT and averages 7.8 years (mean over all simulated experiments). Some of the published injury functions and/or parameterisations applied have intercepts unequal to 1 ( $a$  in Eq. 3.5; see Tab. 3.1), which induces reductions ( $a < 1$ ) or increases ( $a > 1$ ) in photosynthesis at zero ozone concentration and thus causes a bias in biomass and in particular foliage area at the end of the initialisation phase. To eliminate this bias, the nitrogen-specific photosynthetic capacity of a leaf was adjusted for each of the six parameterisations of the model

Table 3.2: List of fumigation experiments used by Bülker et al. (2015) and simulated here.

Site	Longitude [°E]	Latitude [°N]	Species	O <sub>3</sub> treatment start year	Fumigation [yrs]
Östad (S)	12.4	57.9	<i>Betula pendula</i>	1997	2
Birmensdorf (CH)	8.45	47.36	<i>Betula pendula</i>	1989	1
Birmensdorf (CH)	8.45	47.36	<i>Betula pendula</i>	1990	1
Birmensdorf (CH)	8.45	47.36	<i>Betula pendula</i>	1992	1
Birmensdorf (CH)	8.45	47.36	<i>Betula pendula</i>	1993	1
Kuopio (FIN)	27.58	62.21	<i>Betula pendula</i>	1994	2
Kuopio (FIN)	27.58	62.21	<i>Betula pendula</i>	1996	3
Kuopio (FIN)	27.58	62.21	<i>Betula pendula</i>	1994	5
Schönenbuch (CH)	7.5	47.54	<i>Fagus sylvatica</i>	1991	2
Zugerberg (CH)	8.54	47.15	<i>Fagus sylvatica</i>	1987	2
Zugerberg (CH)	8.54	47.15	<i>Fagus sylvatica</i>	1989	3
Zugerberg (CH)	8.54	47.15	<i>Fagus sylvatica</i>	1991	2
Curno (I)	9.03	46.17	<i>Populus spec.</i>	2005	1
Grignon (F)	1.95	48.83	<i>Populus spec.</i>	2008	1
Ebro Delta (SP)	0.5	40.75	<i>Quercus ilex</i>	1998	3
Col-du-Donon (F)	7.08	48.48	<i>Quercus robur or petraea</i>	1999	2
Headley (U.K.)	-0.75	52.13	<i>Quercus robur or petraea</i>	1997	2
Ebro Delta (SP)	0.5	40.75	<i>Pinus halepensis</i>	1993	4
Col-du-Donon (F)	7.08	48.48	<i>Pinus halepensis</i>	1997	2
Schönenbuch (CH)	7.5	47.54	<i>Picea abies</i>	1991	2
Zugerberg (CH)	8.54	47.15	<i>Picea abies</i>	1991	2
Östad (S)	12.4	57.9	<i>Picea abies</i>	1992	5
Headley (U.K.)	-0.75	52.13	<i>Pinus sylvestris</i>	1995	2

Table 3.3: Original and adapted values of the nitrogen-specific photosynthetic capacity of a leaf (npl) for three out of four different O-CN versions (ID) including published injury functions. The intercept of the fourth O-CN version (L12<sub>VC</sub>) is very close to 1 and simulations produce comparable LAI values without an adaption of npl.

ID	PFT	npl original	npl adapted
W07 <sub>PS</sub>	Broadleaf	1.50	1.60
W07 <sub>PS</sub>	Needleleaf	0.75	0.80
L12 <sub>PS</sub>	Broadleaf	1.50	1.45
L12 <sub>PS</sub>	Needleleaf	0.75	0.70
L13 <sub>PS</sub>	Broadleaf	1.50	1.75
L13 <sub>PS</sub>	Needleleaf	0.75	0.90

to obtain comparable leaf area index (LAI) values at the beginning of the experiment (see Tab. 3.3). This adaption of the nitrogen-specific photosynthetic capacity of a leaf only counterbalances the fixed increases or decreases in the calculation of photosynthesis implied by the intercepts unequal to 1 and has no further impact on ozone uptake and injury calculations.

The simulations of the experiments relied on the meteorological and atmospheric forcing of the experiment years. Simulations were made for all reported O<sub>3</sub> treatments of the specific experiment, including the respective control treatments. B ker et al. (2015) obtained estimates of biomass reductions due to ozone by calculating the hypothetical biomass at zero ozone uptake for all experiments that reported ozone concentrations greater than zero for the control group (e.g. for charcoal-filtered or non-filtered air) and calculated the biomass damage from the treatments against a completely undamaged biomass. Our model allows us to run simulations with zero ozone concentrations and skip the calculation of the hypothetical biomass at zero ozone concentrations as done by B ker et al. (2015). Following this, we ran additional reference simulations with zero O<sub>3</sub> and based our biomass damage calculations upon them.

### 3.2.4 Modelling protocol for mature trees

To test whether biomass dose-response relationships of mature forests will show a similar relationship as observed in the simulations of young trees, we ran additional simulations with mature trees. To allow the development of a mature forest where biomass accumulation reached a maximum, and high, and medium turnover soil pools reached an equilibrium, the model was run for 300 years in the initialisation phase. The simulations were conducted with the respective climate previous to the experiment period and zero atmospheric O<sub>3</sub> concentration. For the simulation years previous to 1901 the yearly climate is randomly chosen from the years 1901-1930. Constant values of atmospheric CO<sub>2</sub> concentrations are used in simulated years previous to 1750 followed by increasing con-

centrations up to the experiment years. The subsequent experiment years are simulated in the same way as the simulations with the young trees. The ozone injury for mature trees is calculated based on the same  $tun_{VC}$  injury function (see Tab. 3.1) that is used in the simulation of young trees (see subsection 3.2.5 for details on the development of  $tun_{VC}$ ).

### 3.2.5 Calculation of the biomass damage relationships

The ozone-induced biomass damage is calculated from the difference between a treatment and a control simulation. At each experiment site and for all treatments the annual reduction in biomass due to ozone ( $RB$ ) is calculated as in B ker et al. (2015):

$$RB = \left( \frac{BM_{treat}}{BM_{zero}} \right)^{\frac{1}{n}}, \quad (3.7)$$

where  $BM_{treat}$  represents the biomass of a simulation, which experienced an  $O_3$  treatment and  $BM_{zero}$  the biomass of the control simulation with zero atmospheric  $O_3$  concentration. The exponent imposes an equal fractional biomass reduction across all simulation years for experiments lasting longer than 1 year.

B ker et al. (2015) report the dose-response relationships for biomass reduction with reference to the  $PODy$  with flux thresholds  $y$  of 2 and 3  $\text{nmol m}^{-2}(\text{leaf area}) \text{s}^{-1}$  ( $POD_2$  and  $POD_3$ ) for the needleleaf and broadleaf category, respectively, where the  $PODy$  values were derived from simulations with the  $DO_3SE$  model (Emberson et al., 2000b) given site-specific meteorology and ozone concentrations. To be able to compare the simulated biomass reduction by O-CN with these estimates, we also diagnosed these  $PODy$  values for each simulation from the accumulated ozone uptake of the top canopy layer ( $PODy_{O-CN} = CUOY_{l=1}$ ). Note that the  $PODy_{O-CN}$  is purely diagnostic, and not used in the injury calculations, which are based on the  $CUOY_l$  (see Eq. 3.5). As O-CN computes continuous, half-hourly values of ozone uptake (see Franz et al. (2017), for details), the  $PODy_{O-CN}$  values have to be transformed to be comparable to the simulated mean annual  $PODy$  values reported in B ker et al. (2015). For deciduous species, the yearly maximum of  $PODy_{O-CN}$  was taken as a yearly increment  $PODy_{O-CN,i}$ . The  $PODy_{O-CN}$  of evergreen species was continuously accumulated over several years. To obtain the yearly increment  $PODy_{O-CN,i}$ , the  $PODy_{O-CN}$  at the beginning of the year  $i$  is subtracted from the  $PODy_{O-CN}$  at the end of the year  $i$ .

The selected yearly  $PODy_{O-CN,i}$  was used to calculate mean annual values necessary for the formation of the dose-response relationships integrating all simulation years ( $PODy^{dr}$ ) as

$$PODy_i^{dr} = \frac{\sum_{k=1}^i PODy_{O-CN,i}}{i} \quad (3.8)$$

where  $PODy_{O-CN,i}$  is the  $PODy$  of the  $i$ -th year calculated by O-CN. The  $PODy^{dr}$  values are used to derive biomass dose-response relationships.

Separate biomass dose-response relationships were estimated by grouping site data for broadleaved and needleleaf species. The biomass dose-response relationships are

obtained from the simulation output by fitting a linear model to the simulated values of  $RB$  and  $PODy^{dr}$  (with flux thresholds of 2 and 3  $\text{nmol m}^{-2}(\text{leaf area})\text{s}^{-1}$  for needleleaf and broadleaved species, respectively), where the regression line is forced through 1 at zero  $PODy^{dr}$ . B ker et al. (2015) report two alternative dose-response relationships for their data set: the simple and the standard model  $B_{SI}$  and  $B_{ST}$ , respectively. We evaluate our different model versions regarding their ability to reach the area between those two functions (target area) with the biomass-dose-response relationships computed from their output. The tuned injury relationships  $tun_{PS}$  and  $tun_{VC}$  were obtained by adjusting the slope  $b$  in Eq. 3.5 such that the corresponding biomass dose-response relationships fits the target area. The intercept of the injury relationships are forced to 1 to simulate zero ozone injury at ozone fluxes lower than 1  $\text{nmol m}^{-2}(\text{leaf area})\text{s}^{-1}$ .

### 3.3 Results

#### 3.3.1 Testing published injury functions

None of the versions where ozone injury is calculated based on previously published injury functions fit the observations well. Some versions strongly overestimate the simulated biomass dose-response relationship and others strongly underestimate it (see Fig. 3.1) compared to the dose-response relationships developed by B ker et al. (2015).

In the  $W07_{PS}$  simulations, where injury is calculated based on the injury function by Wittig et al. (2007), biomass damage is strongly underestimated compared to the estimates from B ker et al. (2015). Ozone injury estimates are mainly driven by the intercept of the relationship, which assumes a reduction in net photosynthesis by 6.16% at zero ozone uptake. Little additional ozone damage occurs due to the accumulation of ozone uptake. As a consequence, the ozone treatments and reference simulations differ little in their simulated biomass. Similarly, the Lombardozzi et al. (2013) injury function ( $L13_{PS}$ ) calculates ozone injury as a fixed reduction in net photosynthesis independent of the actual accumulated ozone uptake. The reference simulations with zero atmospheric ozone thus equal the simulations with ozone treatments and result in an identical simulated biomass. We tested accounting for effects of ozone on stomatal conductance besides net photosynthesis as suggested by Lombardozzi et al. (2013). However, this additional direct injury to stomatal conductance yielded a minimal decrease in simulated biomass accumulation in needleleaf trees, but did not qualitatively change the results (results not shown). These results indicate that injury functions, with a large intercept and a very shallow (or non-existing) slope cannot simulate the impact of spatially varying  $O_3$  concentrations or altered atmospheric  $O_3$  concentrations.

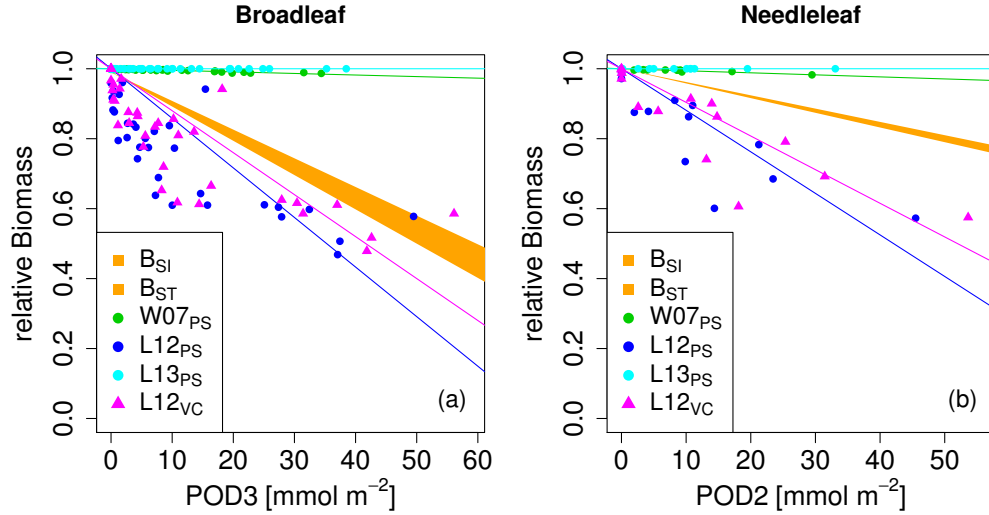


Figure 3.1: Biomass dose-response relationships for simulations based on published injury relationships, separate for a) broadleaved species and b) needleleaf species. The dose-response relationships by Büker et al. (2015) ( $B_{SI}$  and  $B_{ST}$ ) define the target area (orange). The displayed dose-response relationships are simulated by model versions which base injury calculations either on net photosynthesis  $W07_{PS}$  (Wittig et al., 2007),  $L12_{PS}$  (Lombardozzi et al., 2012a), and  $L13_{PS}$  (Lombardozzi et al., 2013), or on  $V_{cmax}$   $L12_{VC}$  (Lombardozzi et al., 2012a) (see Tab. 3.1 for more details). See Tab. 3.4 for slopes, intercepts,  $R^2$  and p values of the displayed regression lines. Injury calculation in the simulations is based on  $CUOY$  (see Tab. 3.1) and not on  $POD2$  or  $POD3$  (see Sec. 3.2.5 for more details).

Table 3.4: Slopes and intercepts of biomass dose-response relationships for broadleaf and needleleaf species simulated by O-CN versions based on published injury functions to net photosynthesis or  $V_{cmax}$  (see Tab. 3.1).  $B_{SI}$  and  $B_{ST}$  represent the simple and standard model of Büker et al. (2015).

ID	Intercept (a)	Slope (b)	$R^2$	p value
Broadleaf				
$B_{SI}$	0.99	0.0082	0.34	<0.001
$B_{ST}$	0.99	0.0098	0.38	<0.001
$W07_{PS}$	1	0.00045	0.93	$1 \times 10^{-24}$
$L12_{PS}$	1	0.0142	0.77	$2 \times 10^{-14}$
$L15_{PS}$	1	0.0000	-	-
$L12_{VC}$	1	0.0120	0.80	$1.9 \times 10^{-15}$
Needleleaf				
$B_{SI}$	1	0.0038	0.46	<0.001
$B_{ST}$	1	0.0042	0.52	<0.001
$W07_{PS}$	1	0.00058	0.93	$1.5 \times 10^{-09}$
$L12_{PS}$	1	0.0119	0.83	$9.4 \times 10^{-07}$
$L15_{PS}$	1	0.0000	-	-
$L12_{VC}$	1	0.0096	0.85	$3.5 \times 10^{-07}$

The simulations L12 $_{PS}$  and L12 $_{VC}$  (net photosynthesis and  $V_{max}$  injury according to Lombardozzi et al. (2012a), respectively) strongly overestimate biomass damage compared to B ker et al. (2015). Both injury functions assume an extensive injury to carbon fixation at low ozone accumulation values ( $CUOY$ ) of about 5 mmol O $_3$ . This results in a very steep decline in relative biomass at low values of  $POD3$ . Notably, despite a linear injury function, the very steep initial decline in biomass of broadleaved trees at low values of  $POD3$  is not continued at higher exposure, resulting in a non-linear biomass dose-response relationships. Higher accumulation of ozone doses does not result in higher injury rates beyond a threshold of about 5 mmol O $_3$  m $^{-2}$  leaf area, and relative biomass declines remain at 50% to 70%. Whereas non-linear dose-response relationships are observed in experiments e.g. for leaf injury (Marzuoli et al., 2009), such a non-linear relationship is not produced in the biomass dose-response relationship by B ker et al. (2015).

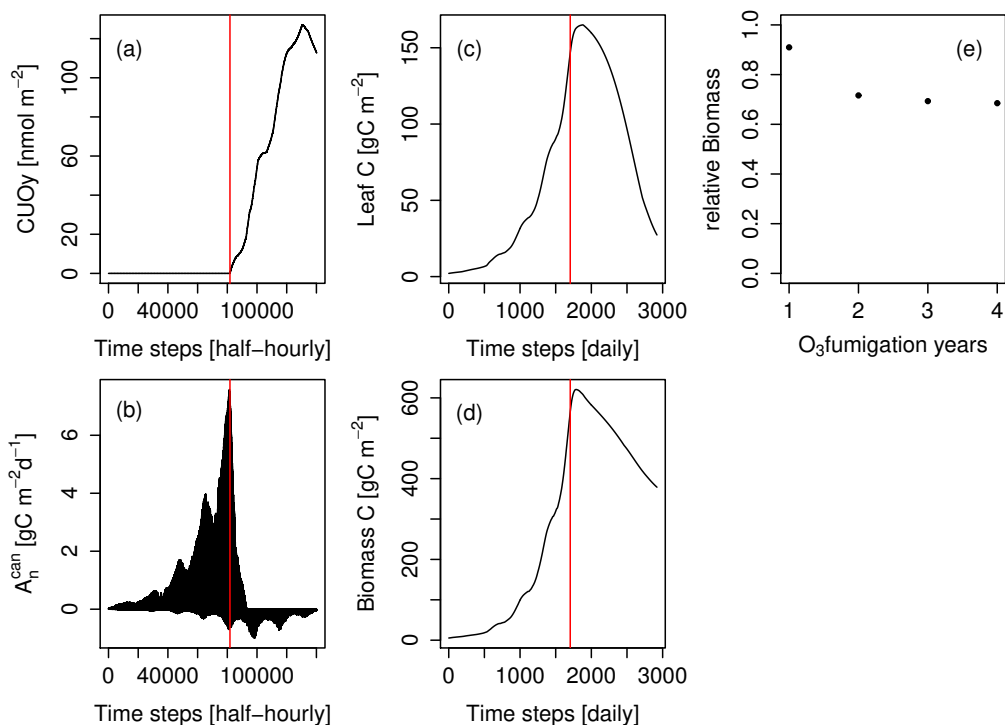


Figure 3.2: Simulated cumulative ozone uptake above a threshold of 0.8 nmol m $^{-2}$ (leaf area) s $^{-1}$  ( $CUOY$ ), canopy-integrated net photosynthesis ( $A_n^{can}$ ), leaf carbon content ( $Leaf$  C), total carbon in biomass ( $biomass$  C) and relative biomass ( $RB$ ) of *Pinus halepensis* at the Ebro Delta fumigated with the NF+ ozone treatment. Simulations are conducted with the L12 $_{PS}$  model version. Panels (a-d) display the entire simulation period. The red line indicates the onset of O $_3$  fumigation (NF+) in the fifth of eight simulation years. The relative biomass compared to a control simulation with zero O $_3$  concentration (panel e) is displayed for the O $_3$  fumigation years.

We investigated the cause for this using the example of the *Pinus halepensis* stand in the Ebro Delta with a high ozone treatment as shown in Fig. 3.2. The simulated  $CUOY$  quickly increases after the onset of fumigation (Fig. 3.2a) and is paralleled by a rapid decline in canopy-integrated net photosynthesis ( $A_n^{can}$ , see Fig. 3.2b). Once all canopy layers accumulated more than 5 mmol O<sub>3</sub> m<sup>-2</sup>, the canopy photosynthesis is fully reduced, and  $A_n^{can}$  becomes negative as a consequence of ongoing leaf maintenance respiration. Thereafter, leaf and total biomass steadily decline (Fig. 3.2c,d), and the plants are kept alive only by the consumption of stored non-structural carbon reserves. Despite the 100% reduction in gross photosynthesis, the biomass compared to a control simulation (relative biomass,  $RB$ ) reaches only values of approximately 0.7 (Fig. 3.2e), because of the remaining woody and root tissues (see Eq. 3.7 for the calculation of  $RB$ ).

### 3.3.2 Tuned injury relationships

We next tested whether a linear injury function is in principle able to reproduce the observed biomass dose-response relationships. Simulations conducted with our tuned injury relationships produce biomass dose-response relationships which fit the target area defined by the  $B_{SI}$  and  $B_{ST}$  dose-response relationships by B ker et al. (2015) (see Fig. 3.3 and Tab. 3.5).

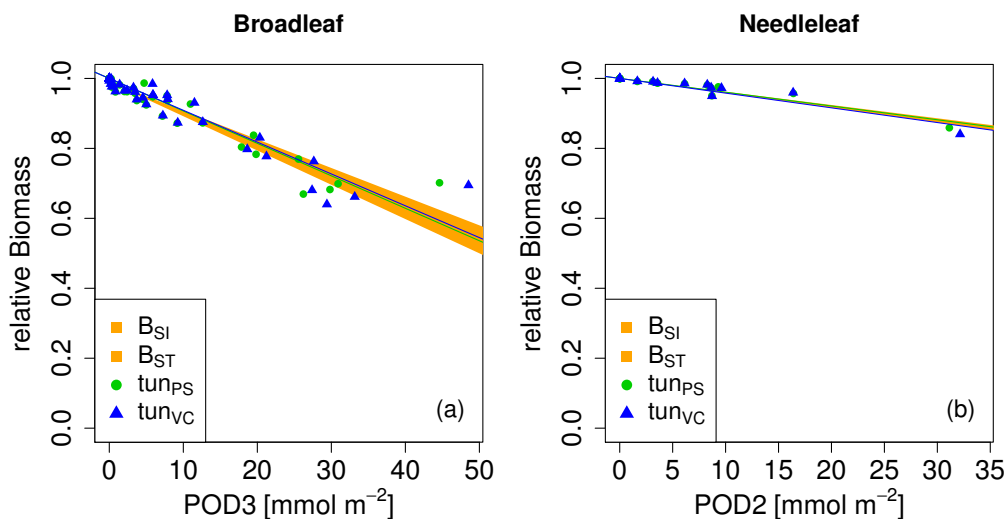


Figure 3.3: Biomass dose-response relationships for simulations based on tuned injury functions (see Tab. 3.1 for abbreviations), separate for a) broadleaved species, and b) needleleaf species. The dose-response relationships by B ker et al. (2015) ( $B_{SI}$  and  $B_{ST}$ ) define the target area (orange). See Tab. 3.5 for slopes, intercepts,  $R^2$  and p values of the displayed regression lines. Injury calculation in the simulations is based on  $CUO1$  (see Tab. 3.1) and not on  $POD2$  or  $POD3$  (see Sec. 3.2.5 for more details).

Table 3.5: Slopes and intercepts of biomass dose-response relationships for broadleaf and needleleaf species simulated by O-CN versions based on tuned injury functions to net photosynthesis or  $V_{cmax}$  (see Tab. 3.1).  $B_{SI}$  and  $B_{ST}$  represent the simple and standard model by B ker et al. (2015).

ID	Intercept (a)	Slope (b)	R <sup>2</sup>	p value
Broadleaf				
$B_{SI}$	0.99	0.0082	0.34	<0.001
$B_{ST}$	0.99	0.0098	0.38	<0.001
$tun_{PS}$	1	0.0093	0.94	$1.4 \times 10^{-26}$
$tun_{VC}$	1	0.0091	0.93	$5 \times 10^{-25}$
Needleleaf				
$B_{SI}$	1	0.0038	0.46	<0.001
$B_{ST}$	1	0.0042	0.52	<0.001
$tun_{PS}$	1	0.0039	0.94	$4.8 \times 10^{-10}$
$tun_{VC}$	1	0.0042	0.93	$2.2 \times 10^{-09}$

For the calibrated relationships used in these simulations, we chose a flux threshold value of  $1 \text{ nmol m}^{-2}(\text{leaf area}) \text{ s}^{-1}$ , as suggested by LRTAP-Convention (2017). We forced the intercept ( $a$ ) of these relationships through 1, to simulate zero ozone injury at ozone fluxes lower than  $1 \text{ nmol m}^{-2}(\text{leaf area}) \text{ s}^{-1}$ . The resulting slope of the  $tun_{PS}$  function for broadleaved PFTs is approximately 30 times higher compared to the slope suggested by Wittig et al. (2007) and a fourth of the slope by Lombardozzi et al. (2012a). For the needleleaf PFT, the tuned slope ( $tun_{PS}$ ) is approximately 10 times higher (lower) than the slopes by Wittig et al. (2007) and Lombardozzi et al. (2012a), respectively. Notably, we did not observe any difference in the model performance irrespective of whether net photosynthesis or photosynthetic capacity ( $V_{cmax}$  and simultaneously  $J_{max}$ ) was reduced.

### 3.3.3 Ozone injury to mature trees

The simulation of young trees (simulated as in the previous section) compared to adult trees with the same model version reveals a distinct difference between the simulated-versus-observed dose-response relationship when expressed as reduction in biomass. Ozone injury causes a much shallower simulated biomass dose-response relationship for adult trees ( $tun_{VC}^{mature}$  in Fig. 3.4a,b) compared to young trees ( $tun_{VC}^{young}$  in Fig. 3.4a,b), both for broadleaved and needleleaf species. It is worth noting that this is primarily the consequence of the higher initial biomass of the adult trees before ozone fumigation starts ( $tun_{VC}^{mature}$ ).

Comparing the dose-response relationship of young and mature trees based on the

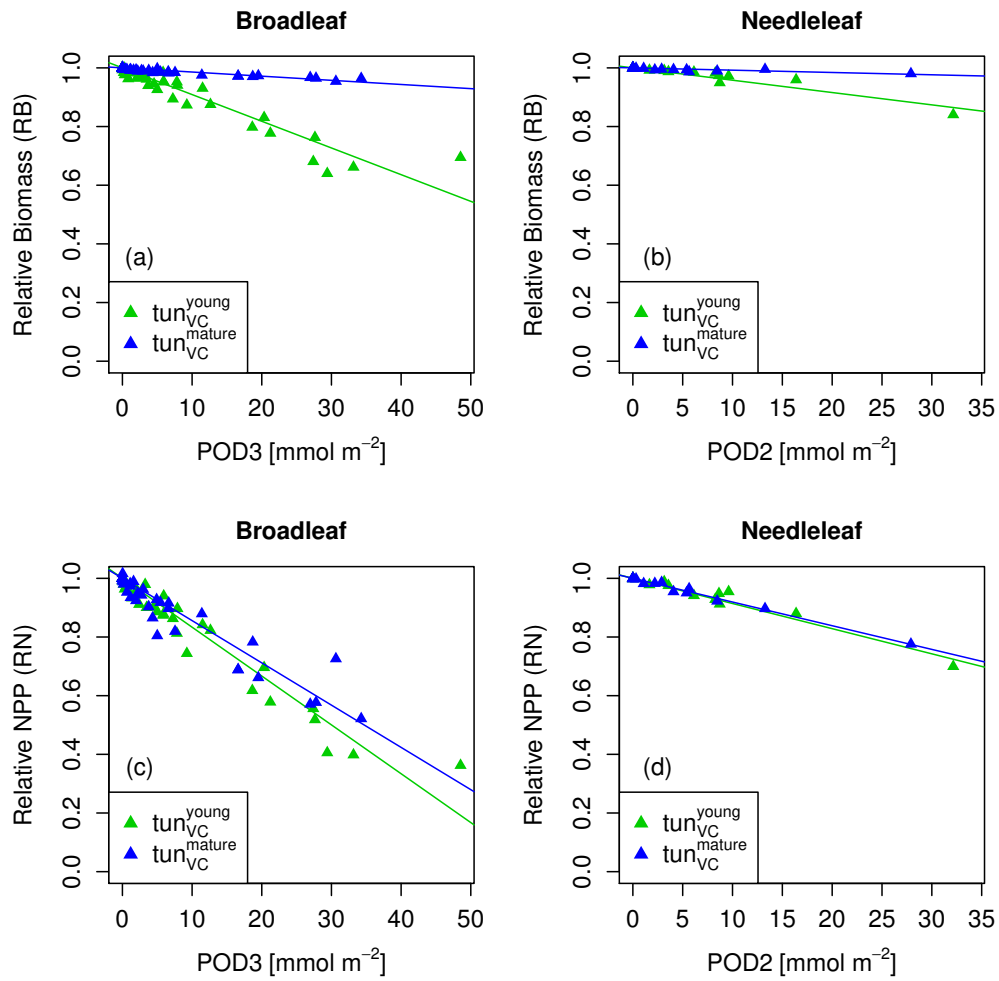


Figure 3.4: Biomass (RB) and NPP (RN) dose-response relationships of simulations with young ( $tun_{VC}^{young}$ ) and mature trees ( $tun_{VC}^{mature}$ ) separately for a,c) broadleaf species and b,d) needleleaf species.

annual NPP shows nearly identical slopes for needleleaf species (Fig. 3.4d and Tab. 3.6), whereas the slopes for broadleaved tree species (Fig. 3.4c and Tab. 3.6) suggest only a slightly lower reduction in NPP in mature compared to young trees, likely related to the larger amount of non-structural reserves that increases the resilience of mature versus young trees.

Table 3.6: Slopes and intercepts of biomass (RB) and NPP (RN) dose-response relationships (DRRs) for broadleaf and needleleaf species simulated by the  $\text{tun}_{VC}$  model version (see Tab. 3.1). The fumigation of young trees ( $\text{tun}_{VC}^{young}$ ) with  $\text{O}_3$  is compared to the fumigation of mature trees ( $\text{tun}_{VC}^{mature}$ ).

DRR	ID	Intercept (a)	Slope (b)	R <sup>2</sup>	p value
Broadleaf					
RB	$\text{tun}_{VC}^{young}$	1	0.0091	0.93	$5 \times 10^{-25}$
RB	$\text{tun}_{VC}^{mature}$	1	0.00142	0.91	$9.8 \times 10^{-23}$
RN	$\text{tun}_{VC}^{young}$	1	0.0167	0.96	$6.2 \times 10^{-30}$
RN	$\text{tun}_{VC}^{mature}$	1	0.0144	0.93	$1.4 \times 10^{-24}$
Needleleaf					
RB	$\text{tun}_{VC}^{young}$	1	0.0042	0.93	$2.2 \times 10^{-09}$
RB	$\text{tun}_{VC}^{mature}$	1	0.000785	0.79	$4.2 \times 10^{-06}$
RN	$\text{tun}_{VC}^{young}$	1	0.00858	0.97	$2.3 \times 10^{-12}$
RN	$\text{tun}_{VC}^{mature}$	1	0.00808	0.99	$3.7 \times 10^{-16}$

### 3.4 Discussion

Injury functions that relate accumulated ozone uptake to fundamental plant processes such as photosynthesis are a key component for models that aim to estimate the potential impacts of ozone pollution on forest productivity, growth and carbon sequestration. We tested four published injury functions for net photosynthesis and  $V_{cmax}$  within the framework of the O-CN model to assess their ability to reproduce the empirical whole-tree biomass dose-response relationships derived by B uker et al. (2015). The biomass dose-response relationships calculated from the O-CN simulations show that the parameterisation of the injury functions included in the model has a large impact on the simulated whole-tree biomass. The published injury functions either substantially over- or substantially underestimated whole-tree biomass reduction compared to the data presented by B uker et al. (2015). Our results highlight the importance for improved evaluation of injury functions applied in the simulation of ozone damage for large-scale risk assessments, and we discuss a number of important considerations for an improved parameterisation below.

The simulation results from the O-CN version applying an injury function based on a single, ozone-sensitive species (Lombardozzi et al., 2012a) to a range of European tree species leads to a strong overestimation of the simulated biomass damage compared to the observations used in this study. The problem of using such injury parameterisations based on short-term experiments of ozone-sensitive species is further highlighted when applying them in simulations of multiple season fumigation experiments and/or high ozone concentrations. Under such conditions, fumigation with high  $\text{O}_3$  concentrations can lead to lethal doses, which might not be observed in field experiments due to

restricted experiment lengths. Previous studies have suggested that in large areas of Europe, the eastern US and southeast Asia average growing season values of  $CUOY$  for recent years range between 10 and 100  $\text{mmol O}_3 \text{ m}^{-2}$  (Lombardozzi et al., 2015; Franz et al., 2017). The injury relationships  $L12_{PS}$  and  $L12_{VC}$  by Lombardozzi et al. (2012a) assume a 100% injury to net photosynthesis or  $V_{cmax}$  at accumulation values of about 5  $\text{mmol O}_3 \text{ m}^{-2}$ . This would imply that in these large geographic regions, photosynthesis would have been completely impaired by ozone, which is clearly not the case. This result highlights the need for a representative set of species for the development of injury functions for large-scale biosphere models. Overall, our results suggest that the estimates by Lombardozzi et al. (2012a) of global GPP reduction as a result of ozone pollution are strongly overestimated.

Meta-analyses (Wittig et al., 2007; Lombardozzi et al., 2013) are designed to minimise the effect of species-specific ozone sensitivities and provide estimates of the average species response. However, we found that the relationships derived by these meta-analyses substantially underestimate biomass damage. Technically, the reasons for this are a weak or non-existent increase in the ozone injury with increased ozone uptake (shallow or non-existent slopes) and/or high ozone injury at zero accumulated ozone uptake (intercept lower than 1). Apparently, the diversity of species responses and experimental settings that are assembled in the meta-analyses by Wittig et al. (2007) and Lombardozzi et al. (2013), together with uncertainties in precisely estimating accumulated ozone uptake in these databases preclude the identification of injury functions that are consistent with the damage estimates by Büker et al. (2015). The high intercepts in the meta-analyses by Wittig et al. (2007) and Lombardozzi et al. (2013), which assume a considerable injury fraction even when no ozone is taken up at all, seem to be ecologically illogical and suggest that an alternative approach is necessary to simulate ozone injury. As a consequence of these points, the Europe-wide GPP reduction estimates by Franz et al. (2017), which have been based on the injury function by Wittig et al. (2007), may substantially underestimate actual GPP reduction. Similarly, global estimates as well as spatial variability in ozone damage to GPP by Lombardozzi et al. (2015), based on Lombardozzi et al. (2013), are virtually independent of actual ozone concentrations or uptake for all tree plant functional types and should be interpreted with caution.

A crucial aspect in forming dose-response relationships is the calculation of the accumulated ozone uptake (e.g.  $PODy$  or  $CUOY$ ). The calculation of accumulated ozone uptake is realised in different ways in the meta-analyses and the study by Büker et al. (2015) as well as in our approach here. Experiments synthesised in the meta-analyses generally do not have access to stomatal conductance values at high resolution measured throughout the experiment, which impedes precise determination of  $O_3$  uptake. The uncertainty in the necessary approximations of accumulated ozone uptake can be assumed to be considerable, and it is thus highly recommendable to measure and report required observations in future ozone fumigation experiments. Büker et al. (2015) use the  $DO_3SE$  model to simulate ozone uptake and accumulation in a similar way as in our model here. These modelled values for ozone uptake and accumulation can be assumed to be more reliable since both models simulate processes that determine ozone uptake continuously

for the entire experiment length at high temporal resolution. They account for diurnal changes in stomatal conductance as well as climate factors restricting stomatal conductance and hence ozone uptake. However, both models (DO<sub>3</sub>SE and O-CN) vary in their complexity of the simulated plants, carbon assimilation, and growth processes, which will also impact the estimates of ozone accumulation (*PODy*) and hence their suggested biomass dose-response relationships.

The meta-analyses do not account for non-stomatal ozone deposition (e.g. to the leaf cuticle or soil), which imposes a bias towards overestimating ozone uptake and accumulation contrary to the DO<sub>3</sub>SE model used by B ker et al. (2015), which accounts for this. The O-CN model in principle can simulate non-stomatal ozone deposition from the free atmosphere to ground level (see chapter 2 or Franz et al. (2017)). The leaf boundary layer is implicitly included in the calculation of the aerodynamic resistance of O-CN and included in Franz et al. (2017). However, for the simulation of the chamber experiments we used the observed chamber O<sub>3</sub> concentrations, rather than estimating the canopy-level O<sub>3</sub> concentration based on the free atmosphere (approximately 45 m above the surface) and atmospheric turbulence. This required not accounting for aerodynamic resistance and therefore also the leaf-boundary layer resistance as it prevented the calculation of the non-stomatal deposition, which may lead to a slight overestimation of ozone uptake and accumulation in our simulations.

The calibration of injury functions to net photosynthesis and  $V_{cmax}$  shows that in principle, the linear structure of Eq. 3.5 is sufficient to simulate biomass dose-response relationships comparable to B ker et al. (2015) in O-CN. An advantage of the injury functions derived here compared to previously published injury functions (Wittig et al., 2007; Lombardozzi et al., 2012a, 2013) is the intercept of 1, implying that simulated ozone injury is zero at zero accumulated O<sub>3</sub> and steadily increases with increased ozone accumulation. The flux threshold used in the simulations is  $1 \text{ nmol m}^{-2}(\text{leaf area}) \text{ s}^{-1}$  as suggested by the LRTAP-Convention (2017). Since the tuned injury functions are structurally identical to previously published injury functions based on accumulated ozone uptake they can be directly compared to them. Slopes of the tuned injury functions lie in between the values proposed by Wittig et al. (2007) and Lombardozzi et al. (2012a) and thus take values in an expected range. We did not find any significant difference in simulated biomass responses between the use of net photosynthesis or leaf-specific photosynthetic capacity ( $V_{cmax}$ ) as a target for the ozone injury function, although we do note that the slopes were slightly lower for the net photosynthesis-based functions. The simulation of ozone effects on leaf-specific photosynthetic capacity ( $V_{cmax}$ ) seems preferable over the adjustment of net photosynthesis because  $V_{cmax}$  and  $J_{max}$  are parameters in the calculation of net photosynthesis and thus are likely more easily transferable between models. Models with different approaches to simulate net photosynthesis might obtain better comparable results by using injury relationships that target  $V_{cmax}$  instead of net photosynthesis.

All injury functions included in the O-CN model base injury calculations on the injury index *CUOY* (canopy value) rather than *PODy*, as used by some other models, e.g. the DO<sub>3</sub>SE model (Emberson et al., 2000b). We tested the effect of basing the injury

calculation on *POD1* rather than *CUO1*, and found that these produced comparable biomass dose-response relationships as the injury relationships based on *CUO1* presented in Fig. 3.3 (results not shown). The slopes of injury functions based on *POD1* are approximately two-thirds and half compared to the slopes based on *CUO1* for broadleaved and needleleaf species, respectively. The difference in the slope values associated with *POD1* and *CUO1* results from the different calculation and application of them. *PODy* is calculated in the top canopy layer and the respective injury fraction is then applied uniformly to all canopy layers. *CUOY* and the associated injury fraction is calculated separately for each canopy layer and varies with the canopy profile of stomatal conductance and therefore the distribution of light and photosynthetic capacity (other factors such as vertical gradients of temperature or ozone are currently not represented in O-CN). More analysis of the gradients of ozone injury within deep canopies are required to evaluate whether the scaling of top-of-the-canopy injury to whole-canopy injury is appropriate or if alternative simulation approaches need to be developed. Higher-frequency data on the ozone injury incurred by plants are required to disentangle whether an ozone injury parameterisation based on instantaneous (e.g. similar to the approach by Sitch et al. (2007)) or accumulated ozone uptake results in a more accurate simulation of the seasonal effects of ozone fumigation.

Further aspects that determine ozone sensitivity and damage to the carbon gain of plants, like leaf morphology (Calatayud et al., 2011; Bussotti, 2008), different sensitivity of sunlit and shaded leaves (Tjoelker et al., 1995; Wieser et al., 2002), early senescence (Gielen et al., 2007; Ainsworth et al., 2012), and costs for the detoxification of ozone and/or the repair of ozone injury that likely increases the plant’s respiration costs (Dizengremel, 2001; Wieser and Matyssek, 2007), are not considered by either approach. Marzuoli et al. (2016) observed an ozone-induced reduction in biomass but no significant reduction in physiological parameters like  $V_{cmax}$ . They suggest that the reduced growth is caused by higher energy investments and reducing power for the detoxification of ozone whereas the photosynthetic apparatus remained uninjured (Marzuoli et al., 2016).

Species within the same plant functional type are known to exhibit different sensitivities to ozone (Wittig et al., 2007, 2009; Mills et al., 2011b; B ker et al., 2015). This suggests that the application of a single injury function for a large set of species and plant functional types may not be sufficient to yield reliable estimates of large-scale damage estimates. Species interaction and competition, differing genotypes, and individuals ontogeny may further alter ozone impacts on plants and ecosystems (Matyssek et al., 2010). For instance, a modelling study using an individual-based forest model showed that ozone may not reduce the carbon sequestration capacity in forests if at the ecosystem level the reduced carbon fixation of ozone-sensitive species is compensated for by an increased carbon fixation of less ozone-sensitive species (Wang et al., 2016). First-generation dynamic global vegetation models such as O-CN do not simulate separate species but are based on plant functional types, which combine a large set of species. This restricts per se the ability of global models to simulate ozone-induced community dynamics and may therefore lead to overestimates of the net ozone impact if the parameterisation of the damage functions is entirely based on ozone-sensitive species. In

our study, we have presented an approach to use the existing experimental evidence to parameterise a globally applicable model in a simple design to generate injury functions which are based on a relevant range of species rather than relying on species-specific injury functions as a first step towards a more reliable parameterisation of large-scale ozone damage.

Some studies have found that ozone-affected stomata respond much more slowly to environmental stimuli than unaffected cells (Paoletti and Grulke, 2005), which can delay closure and trigger stomatal sluggishness, an uncoupling of stomatal conductance and photosynthesis (Reich, 1987; Tjoelker et al., 1995; Lombardozzi et al., 2012b) and thus impact transpiration rates (Mills et al., 2009; Paoletti and Grulke, 2010; Lombardozzi et al., 2012b) and the plant's water use efficiency (Wittig et al., 2007; Mills et al., 2009; Lombardozzi et al., 2012b). The O-CN model is able to directly impair stomatal conductance, by uncoupling injury to net photosynthesis from the subsequent injury to stomatal conductance. In this version of the O-CN model both net photosynthesis and stomatal conductance can directly be injured by individual injury functions. The simulation of this kind of direct injury to stomatal conductance additional to the injury of net photosynthesis, both according to the injury functions by Lombardozzi et al. (2013), have a negligible impact on biomass production compared to not accounting for direct injury to the stomata (results not shown). However, our above-mentioned concerns regarding the structure of the injury relationships by Lombardozzi et al. (2013) should be taken into account when considering this result.

A key challenge for the use of fumigation experiments to parameterise ozone-injury in models is that trees (as opposed to grasses fumigated from seeds) typically possess a certain amount of biomass at the beginning of the fumigation experiment. Even at lethal ozone doses, the relative biomass thus cannot decline to zero, and tree death may occur at values of a relative biomass greater than zero. The relative biomass is positive even if carbon fixation is fully reduced and the plants survive due to the use of stored carbon. The higher the initial biomass and the slower the annual biomass growth rate of the tree is, the harder it is to obtain low values of  $RB$ . When comparing  $RB$  values obtained from trees with substantially different initial biomass and tree species with different growth rates proportionate damage rates thus cannot be directly inferred. This indicates that the explanatory value of the relative biomass between a control and a treatment to estimate long-term plant damage at a given  $O_3$  concentration is limited. This is particularly the case when evaluating the damage of more mature forests. The simulated biomass dose-response relationships of adult trees are much more shallow than dose-response relationships of young trees (see Fig. 3.4) because of the high initial biomass prior to fumigation. This suggests that the use of biomass injury functions derived from experiments with young trees to parameterise the biomass loss of adult trees, as done in Sitch et al. (2007), will likely lead to an overestimation of plant damage and loss of carbon storage. Dose-response relationships based on biomass increments or growth rates might be better transferable between young and mature trees and hence better suitable for parameterising global terrestrial biosphere models.

Our approach to overcome this challenge was to alter the vegetation model to sim-

ulate the ozone damage of young trees, where we could directly compare simulated biomass reductions to observations. Since we used injury relationships that are based on the calculation of leaf-level photosynthesis, we are able to apply the calibrated model also for mature stands. Our simulations have demonstrated that despite the different sizes of young and mature trees, and associated changes in the wood growth rate and the available amount of non-structural carbon reserves to repair incurred injury, the simulated effect of ozone on the net annual biomass production (NPP) was very similar when using an injury function associated with leaf-level photosynthesis. Overall our findings support the idea that the photosynthesis-based injury relationships developed here and evaluated against fumigation experiments of young trees, might be useful to estimate effect on forest production of older trees. Monitoring approaches of ozone damage that are either capable of measuring the actual increment of biomass or quantify at the leaf and canopy level the change in net photosynthesis over the growing season would allow us to develop injury/damage estimates that could be more readily translated into modelling frameworks.

The extrapolation of results from short-term experiments with young trees to estimate responses of adult trees grown under natural conditions is subject to several issues, e.g. due to the differing environmental conditions and changing ozone sensitivities with increasing tree size or age (Schaub et al., 2005; Cailleret et al., 2018). It is still uncertain whether the simulation of injury to photosynthesis based on experiments with young trees can indeed be transferred to adult trees to yield realistic biomass damage estimates. The sparse knowledge of ozone effects on the biomass of adult forest trees prevents an evaluation of simulated ozone damage of adult trees. Ozone fumigation is mostly found to reduce the biomass or diameter of adult trees (e.g. Matyssek et al. (2010) for an overview), but this is not always the case (Samuelson et al., 1996; Percy et al., 2007). Results from phytotron and free-air fumigation studies suggest that in natural forests a multitude of abiotic and biotic factors exist that have the potential to impact the plants ozone effects (Matyssek et al., 2010). If more data become available, e.g. regarding the changes in ozone sensitivity between young and mature trees a more realistic damage parameterisation of mature forests in terrestrial biosphere models might become possible.

Terrestrial biosphere models in general assume that plant growth is primarily determined by carbon uptake. However, an alternative concept proposes that plant growth is more limited by direct environmental controls (temperature, water and nutrient availability) than by carbon uptake and photosynthesis (Fatichi et al., 2014). The O-CN model provides a first step into this direction because it separates the step of carbon acquisition from biomass production, both in terms of a non-structural carbon buffer as well as a stoichiometric nutrient limitation on growth independent of the current photosynthetic rate. This would in principle allow us to account for ozone effects on the carbon sink dynamics within plants. However, it is not clear that data readily exist to parameterise such effects. Instead of targeting net photosynthesis as done in our approach here, ozone injury might be better simulated by targeting biomass growth rates or processes that limit these, e.g. stomatal conductance, which impacts the plants' water balance,

assuming that suitable data to parameterise a large-scale model become available.

All in all, a multitude of aspects that impact ozone damage to plants has not yet been incorporated into global terrestrial biosphere models. The ongoing discussion of which processes are major drivers for observed damage, how they interact and impact different species and plant types, and the lack of suitable data needed to parameterise a global model are reasons why the simulation of ozone damage has up to now focused only on a few aspects where suitable data are available, as presented in our study.

### 3.5 Conclusion

The inclusion of previously published injury functions in the terrestrial biosphere model O-CN led to a strong over- or underestimation of simulated biomass damage compared to the biomass dose-response relationship by Büker et al. (2015). Injury functions included in terrestrial biosphere models are a key aspect in the simulation of ozone damage and have a great impact on the estimated damage in large-scale ozone risk assessments. The calibration of injury functions performed in this study provides the advantage of calculating ozone injury close to where the actual physiological injury might occur (photosynthetic apparatus) and simultaneously reproduces observed biomass damage relationships for a range of European forest species used by Büker et al. (2015). The calibration of ozone injury functions similar to our approach here in other ozone sub-models of terrestrial biosphere models might improve damage estimates compared to previously published injury functions and might lead to better estimates of terrestrial carbon sequestration. The comparison of simulated biomass dose-response relationships of young and mature trees shows strongly different slopes. This suggests that observed biomass damage relationships from young trees might not be suitable for estimating the biomass damage of mature trees. The comparison of simulated NPP dose-response relationships of young and mature trees shows similar slopes and suggests that they might more readily be transferred between trees differing in age.



## Chapter 4

# Simulated air pollution impacts from 1850-2099

### 4.1 Introduction

Ozone concentrations in 1860 were 15-25 ppb over the mid- and high-latitudes of Eurasia and North America, and increased to 40-50 ppb in the present (Akimoto, 2003). Tropospheric ozone concentrations in Western Europe increased by a factor 2 to 5 from pre-industrial values to the 1990s (Cooper et al., 2014; Marenco et al., 1994; Staehelin et al., 1994). The increases are paralleled by an increase in its precursor nitrogen oxides ( $\text{NO}_x$ ) by a factor of 4.5 between 1955 and 1985 (Cooper et al., 2014; Staehelin et al., 1994).

Ozone ( $\text{O}_3$ ) is a toxic air pollutant that can injure plant leaves and substantially affect the plant's gross primary production (GPP). Part of the reactive nitrogen produced in or emitted to the atmosphere, like the  $\text{O}_3$  precursors  $\text{NO}_x$ , are deposited back on land where they might be taken up by plants and stimulate plant growth in nitrogen limited regions. Both pollutants ( $\text{O}_3$  and  $\text{NO}_x$ ) are linked in their occurrence but impose opposing effects on plants.

During the 21st century the global nitrogen deposition is projected to remain relatively constant in all scenarios of the Representative concentration pathways (RCP), except in the most optimistic scenario RCP2.6, but changes occur on a regional basis (Ciais et al., 2013). In Fig. 4.1 past nitrogen deposition rates for the decades of 1850 and 1990 are displayed and projected rates suggested by RCP2.6 and RCP8.5 for the middle and end of the 21st century.

Due to stringent air pollution control ozone levels are projected to decline until the end of the 21st century (van Vuuren et al., 2011). See Fig. 4.2 for past and projected tropospheric  $\text{O}_3$  concentrations suggested by RCP2.6 and RCP8.5. The application of the RCP scenarios (Moss et al., 2010; van Vuuren et al., 2011) in 14 global chemistry transport models results in the projection of declining annual global mean surface  $\text{O}_3$  concentrations of as much as 2 ppb by 2050 in most regions of the globe except South Asia where increases are simulated (Wild et al., 2012). Contrary to this the application

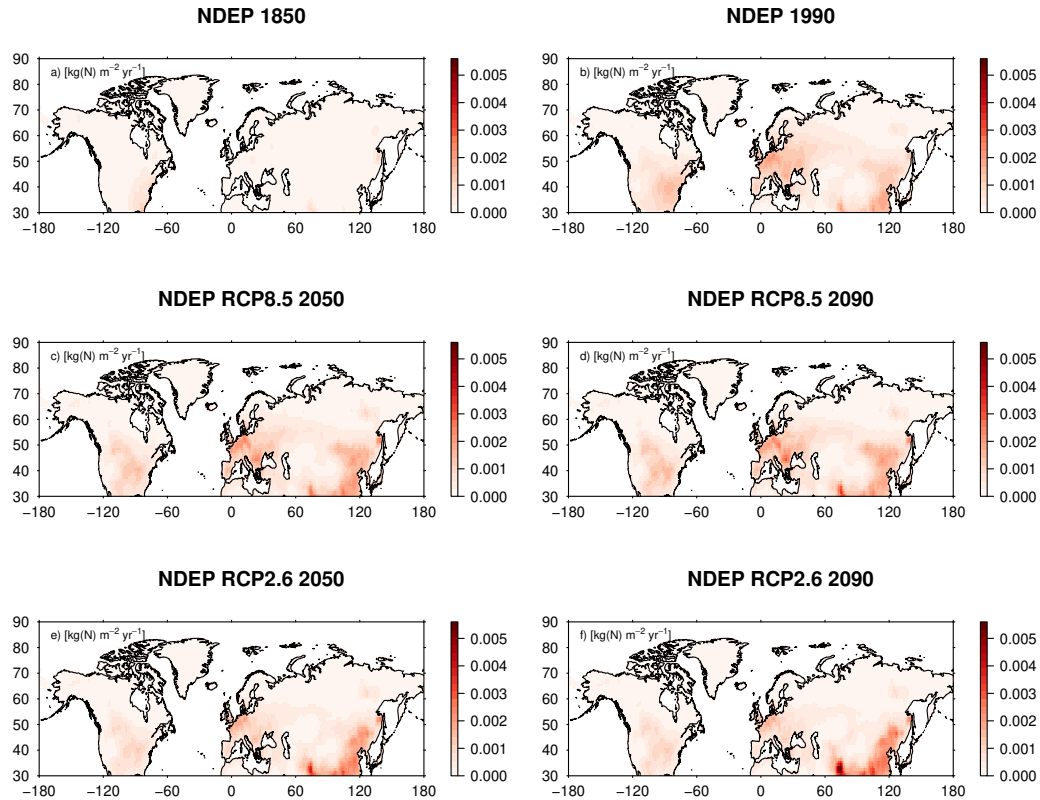


Figure 4.1: Mean nitrogen deposition rates for the temperate and boreal Northern Hemisphere ( $\geq 30^{\circ}\text{N}$ ) in the decades of the years of 1850, 1990, 2050 and 2090, each according to the RCP2.6 and RCP8.5 pollution scenario.

of the IPCC SRES scenarios (which assume a large increase in  $\text{O}_3$  precursor emissions) results in a simulated increase in annual global mean surface  $\text{O}_3$  concentrations by 4–6 ppb which highlights the importance of emission control (Wild et al., 2012). The ensemble of six global atmospheric chemistry transport models driven by the emission scenarios RCP2.6 (most optimistic scenario), RCP4.5 and RCP8.5 (most pessimistic scenario) project changes in surface  $\text{O}_3$  concentrations by 2010 compared to values in the early 2000s. The projected changes range from increases of 4–5 ppb in simulations based on the RCP8.5 scenario to reductions of 2–10 ppb based on the RCP2.6 scenario (Sicard et al., 2017). A similar pattern is found for the temperate and boreal Northern Hemisphere  $\geq 30^{\circ}\text{N}$ . Time series of the regional mean canopy  $\text{O}_3$  concentration show increasing values until late in the 21st century for RCP8.5 and considerable decreases during the 21st century for RCP2.6 (see Fig. 4.3a).

Driven by projected reductions in surface  $\text{O}_3$  concentrations the potential threat to vegetation under the emissions of the RCP4.5 scenario is projected to decline as well (Klingberg et al., 2014). By 2050 the ozone exposure index AOT40 (Accumulated expo-

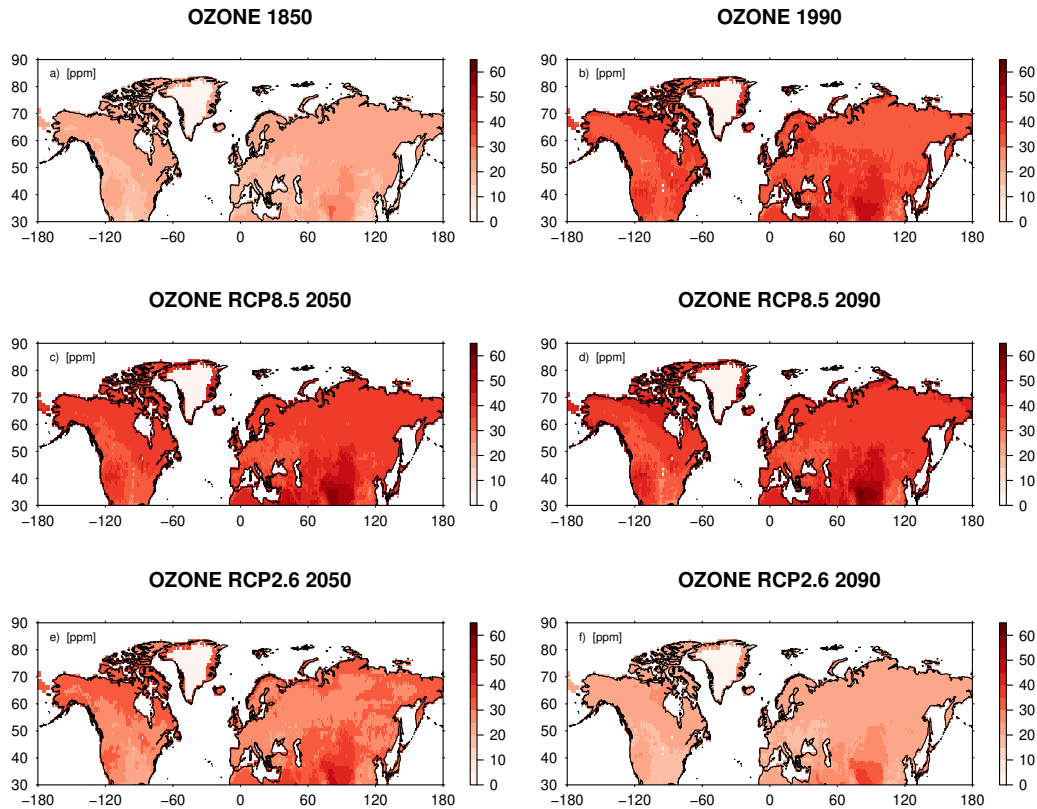


Figure 4.2: Projected mean canopy level  $O_3$  concentration for the temperate and boreal Northern Hemisphere ( $\geq 30^\circ N$ ) in the decades of the years of 1850, 1990, 2050 and 2090, each according to the RCP2.6 and RCP8.5 pollution scenario.

sure Over a Threshold of 40 ppb  $O_3$ ) is projected to decrease over wide areas of Europe below critical levels defined by the EU directive 2008/50/EC and the LRTAP convention in simulations of a chemical transport model (CTM) driven by the RCP4.5 emission scenario (Klingberg et al., 2014). The more physiological based ozone damage index POD1 (Phytotoxic Ozone Dose above a threshold of  $1 \text{ nmol m}^{-2} \text{ s}^{-1}$ ) is projected to decline less compared to the AOT40 index and not below critical levels defined for forest trees (Klingberg et al., 2014). The ensemble of six global atmospheric chemistry transport models project improvements of the AOT40 index under the RCP2.6 and RCP4.5 but an exceedance of critical levels over many areas in the Northern Hemisphere by 2099 (Sicard et al., 2017). In these simulations the potential impact of  $O_3$  on photosynthesis and carbon assimilation by 2099 is projected to decline by 61% under the RCP2.6 scenario, by 47% under RCP4.5 and increase by 70% under the RCP8.5 scenario compared to the early 2000s (Sicard et al., 2017).

Several models simulated present day or future impacts of ozone damage on GPP/NPP on regional and global scale (Felzer et al., 2005; Sitch et al., 2007; Franz et al., 2017;

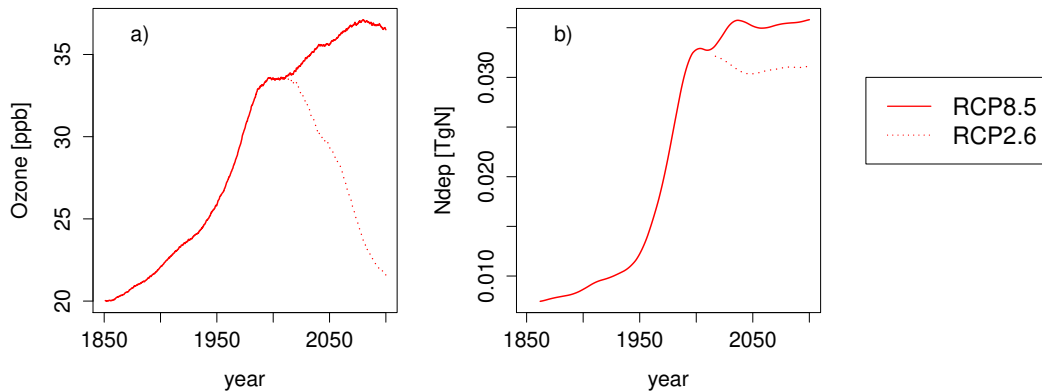


Figure 4.3: Time series of the regional mean (temperate and boreal Northern Hemisphere ( $\geq 30^\circ\text{N}$ )) ozone concentration and summed nitrogen deposition according to the RCP2.6 and RCP8.5 pollution scenario.

Lombardozi et al., 2015; Oliver et al., 2018) and found substantial ozone induced detrimental impacts. The models differ in various aspects which might affect simulated damage estimates. Franz et al. (2017) investigates the importance of the simulation of  $\text{O}_3$  transport from the free atmosphere into the stomates on simulated  $\text{O}_3$  uptake and accumulation (see chapter 2). Different models furthermore include non-identical injury functions which are applied to calculate ozone damage. Franz et al. (2018) investigated the ability of various injury functions to reproduce biomass damage relationships observed in a range of fumigation/filtration experiments with European tree species (see chapter 3). The injury function applied in Franz et al. (2017) was found to considerably underestimate biomass damage compared to the observed biomass damage relationships. The injury function applied by Lombardozi et al. (2015) was found to be not able to reproduce the observed biomass damage relationships at all due to the lack of a dependence on the actual ozone concentration/ uptake into the plant.

The combined air pollution effect of  $\text{O}_3$  and nitrogen deposition has not yet been addressed. Models that account for the growth stimulating effect of nitrogen deposition but not the detrimental effect induced by ozone might overestimate the stimulating effect on plant growth. The new RCP scenarios, which project stronger pollution control and lower tropospheric ozone concentrations compared to the IPCC SRES scenarios (Wild et al., 2012) are yet little applied to investigate future ozone impacts.

Here, the terrestrial biosphere of the Northern Hemisphere is simulated from pre-industrial times (year 1850) until the end of the 21st century. Ozone damage is calculated based on injury functions tuned to reproduce observed biomass damage of a range of European tree species in fumigation/filtration experiments (see chapter 3 and Franz et al. (2018)). As the applied injury functions are based on experiments with boreal and temperate European tree species, the simulation scope is restricted to the temperate and

boreal region of the Northern Hemisphere  $\geq 30^\circ\text{N}$ . Two pollution scenarios are simulated with different combinations of transient or fixed  $\text{CO}_2$ , climate, nitrogen deposition, and  $\text{O}_3$  for the most optimistic and most pessimistic RCP scenario (RCP2.6 and RCP8.5 respectively). In a factorial analysis the impact of the single drivers on plant growth, biomass and selected soil properties is calculated. The possible impact of  $\text{O}_3$  to offset growth enhances induced by nitrogen deposition is evaluated as well as the interaction between  $\text{O}_3$  and  $\text{CO}_2$ .

## 4.2 Methods

Simulations are conducted with the O-CN model (see section 1.6.1 for details) version  $\text{tun}_{VC}$  where ozone damage is calculated based on injury functions to  $V_{cmax}$ . The  $\text{tun}_{VC}$  injury functions were calibrated to reproduce observed biomass damage relationships of experiments with a range of European tree species in fumigation/filtration experiments (see chapter 3 or Franz et al. (2018) for details). As in chapter 3 a flux threshold  $1 \text{ nmol m}^{-2} \text{ s}^{-1}$  is applied in the simulations here to account for the plants ability to detoxify part of the taken up  $\text{O}_3$ . The cumulative canopy  $\text{O}_3$  uptake above a flux threshold of  $1 \text{ nmol m}^{-2} \text{ s}^{-1}$  (CUO1) is used to calculate ozone induced damage to  $V_{cmax}$ . Contrary to Franz et al. (2018), in the simulations run for this study the ozone deposition scheme described in Franz et al. (2017) is applied (D-model version in Franz et al. (2017) or chapter 2).

### 4.2.1 Modelling protocol

The model is run at a spatial resolution of  $1^\circ \times 1^\circ$  on a spatial domain focused on the temperate region of the Northern Hemisphere ( $30^\circ\text{N} - 90^\circ\text{N}$ ). The model is driven by climate model output of the Institute Pierre Simon Laplace (IPSL) general circulation model IPSL-CM5A-LR (Dufresne et al., 2013), bias-corrected according to the Inter-Sectoral Impact Model Intercomparison Project (Hempel et al., 2013). Downward nitrogen deposition velocity and near surface ozone concentrations are provided by CAM, the community atmosphere model (Lamarque et al., 2010; Cionni et al., 2011). Land cover, soil, and N fertiliser application are used as in Zaehle et al. (2011) and kept at 2000 values throughout the simulation. Data on atmospheric  $\text{CO}_2$  concentrations are obtained from Meinshausen et al. (2011). Through all simulations present day land-use information are applied for the year 2000 (Hurtt et al., 2011). O-CN is run for 1291 years to achieve an equilibrium in terms of the terrestrial vegetation and soil carbon and nitrogen pools by using the forcing data of the year 1850 data where available. The climate years are randomly iterated from the period of 1901 to 1930. The subsequent simulation years run from the year 1850 to 2099 with either transient forcing or fixed forcing to the reference values of the year 1850 (1901-1930 for climate), depending on the specific simulated factorial run (see Tab. 4.1). The period up to the year 2005 is simulated identical for both RCPs. Between 2005 and 2099 simulations are run using the forcing according to the RCP2.6 and are repeated using the RCP8.5 forcing (Moss

Table 4.1: Forcing setting of the factorial runs. Transient forcing indicates that the forcing of the respective simulation year is used (1850-2099 except for the climate forcing where the period 1850-1899 is simulated based on the years 1901-1930). Fixed indicates that the forcing of the reference year 1850 is used (1901-1930 for climate).

Factorial run	CO <sub>2</sub>	Climate	Nitrogen deposition	O <sub>3</sub>
S1	transient	fixed	fixed	fixed
S2	transient	fixed	fixed	transient
S3	transient	transient	fixed	fixed
S4	transient	transient	transient	fixed
S5	transient	transient	transient	transient

et al., 2010; van Vuuren et al., 2011).

To investigate the impact of the ozone deposition scheme on the simulation results the factorial runs are repeated with a model version where the ozone deposition scheme is turned off (see ATM model version in chapter 2). In simulations where the ozone deposition module is turned off the canopy ozone concentration equals the O<sub>3</sub> concentration at 45 m above the surface which is the lowest level of the atmospheric chemistry transport model (CTM) that deliver the forcing for our runs here.

#### 4.2.2 Factorial simulation runs

Five factorial simulation runs are simulated where key drivers of plant growth and carbon sequestration (CO<sub>2</sub>, climate, nitrogen deposition, O<sub>3</sub>) are simulated transient (progressively changing within the simulation period) or fixed to the reference year (see Tab. 4.1). The simulations are conducted for the Representative concentration pathway scenarios RCP2.6 and repeated for RCP8.5. To obtain an indication of the impact of the single forcing drivers on different output variables the simulation results are subtracted from each other.

#### 4.2.3 Factorial analysis

The impact of a single forcing driver on the simulation results is of great interest and approximated by subtracting the simulation results of suitable factorial runs from one another (see Tab.4.2). In the following the term 'forcing driver' is used to refer to the input variables of the conducted simulations and 'single driver' refers to the approximated impact of a single forcing driver on the simulation results. The impact of increasing atmospheric CO<sub>2</sub> concentrations on the simulation results from the factorial run S1 is obtained by subtracting the mean value of the period 1850-1859 from each simulation year (1850-2099) of each output variable of interest. To obtain the impact of the other three drivers (climate, nitrogen deposition, O<sub>3</sub>) on the simulation results suitable factorial runs are subtracted from each other (see Tab. 4.2). The described approach constitutes an approximation of the impact of the single drivers and assumes that the

Table 4.2: Calculation of the single driver effects (CO<sub>2</sub>, climate, nitrogen deposition, O<sub>3</sub>) from the conducted simulations. The term 'mean(S1(1850:1859))' refers to the mean value of the years 1850 to 1859 of the S1 factorial run. The relative change for CO<sub>2</sub> is only calculated for the time intervals displayed below in Tab. 4.3. *yr* and *refYr* constitute the years which span the respective time periods. The single drivers are calculated for multiple output variables.

Single driver	Calculation absolute value	Calculation relative value
CO <sub>2</sub>	$S1 - \text{mean}(S1(1850 : 1859))$	$(S1_{yr} - S1_{refYr})/S1_{refYr}$
O <sub>3</sub> approach 1	$S2 - S1$	$(S2 - S1)/S1$
O <sub>3</sub> approach 2	$S5 - S4$	$(S5 - S4)/S4$
Climate	$S3 - S2$	$(S3 - S2)/S2$
Nitrogen deposition	$S5 - S3$	$(S5 - S3)/S3$

drivers effect on the analysed output variables is additive. The assumption of additive effects is a necessary simplification to restrict the number of simulations and computation time. For O<sub>3</sub>, a main driver of interest, two different approaches to calculate the single driver can be realised. In one approach the O<sub>3</sub> impact is calculated from the two factorial runs with only one/ two transient drivers (S1 and S2), and a second time from the factorial runs where all and all but one driver (S5 and S4 respectively) are simulated transient. The comparison of these two approaches to calculate the single driver might indicate the extend of impact of interacting forcing drivers on the estimate of the O<sub>3</sub> single driver.

## 4.3 Results

A strong increase in GPP and carbon storage in biomass and soils can be observed in the Northern Hemisphere  $\geq 30^\circ\text{N}$  during the simulation period in the simulation of the 5 different factorial runs (S1-S5) (see Fig. 4.6a,d,g and Tab. 4.3). The major fraction of the observed increase can be attributed to increasing levels of atmospheric CO<sub>2</sub> concentrations and climate impacts as the second most import factor (see Fig. 4.6b,e and Tab. 4.3). The impact of air pollution (nitrogen deposition and tropospheric O<sub>3</sub> concentrations) on terrestrial carbon uptake and storage is presented in detail in the following subsections.

### 4.3.1 Regional means and sums of air pollution impacts

The regional means and sums reported in section 4.3.1 are based on simulations driven by RCP8.5, if not explicitly stated otherwise. In section 4.3.1.3 simulation results based on RCP8.5 are compared to results based on RCP2.6.

### 4.3.1.1 Ozone uptake and accumulation

The simulated change in ozone uptake ( $F_{st}$ ) is mainly controlled by transient increasing  $O_3$  concentrations through the entire simulation period (see Fig. 4.4b,c). Climate change induces a small increase in  $F_{st}$  and increasing  $CO_2$  levels slightly decreases  $F_{st}$ , because of reduced rates of canopy conductance. Contrary to the  $F_{st}$ , cumulative canopy  $O_3$  uptake above a flux threshold of  $1 \text{ nmol m}^{-2} \text{ s}^{-1}$  (CUO1) does not keep relative constant values during the 21st century but reaches a maximum at the end of the 20th century and steadily declines afterwards. The CUO1 is mainly impacted by the increased  $O_3$  in the first 150 simulation years (see Fig. 4.4a,b). In the last 100 simulation years the impact of the altered  $O_3$  concentration decreases (see Fig. 4.4e,f). In the decade of 2090 the atmospheric  $CO_2$  concentration and climate impact the CUO1 in a similar magnitude like the increased  $O_3$  concentration compared to simulations based on pre-industrial  $O_3$  concentrations (see Fig. 4.4f).

The steady decline of CUO1 during the 21st century is caused by a less frequent

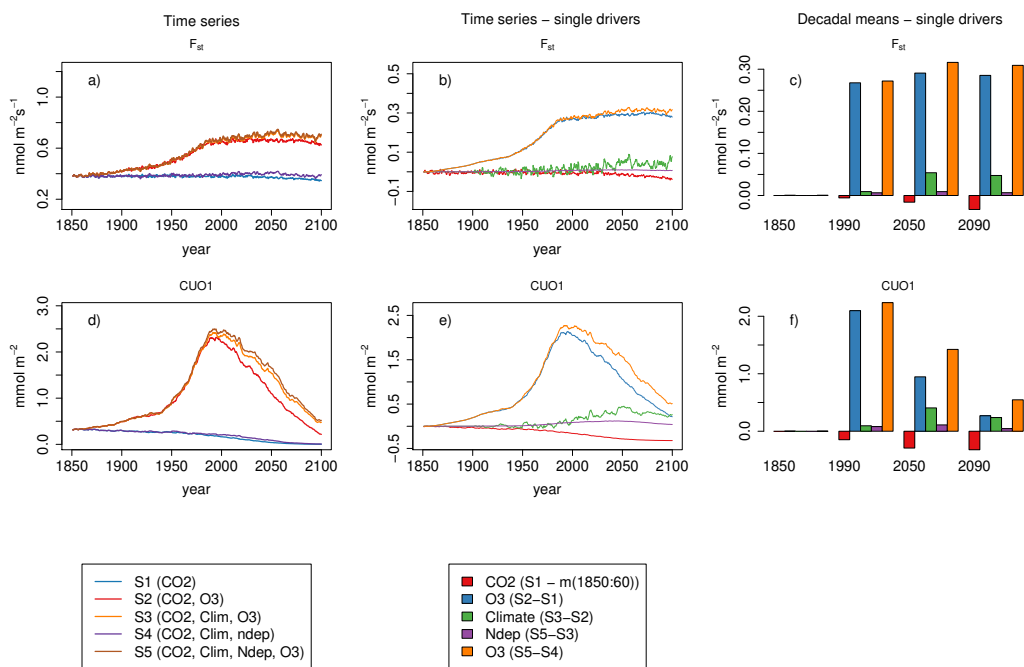


Figure 4.4: Simulated regional mean ozone uptake ( $F_{st}$ ) and regional mean cumulative canopy  $O_3$  uptake above a flux threshold of  $1 \text{ nmol m}^{-2} \text{ s}^{-1}$  (CUO1) of the simulations based on RCP8.5. The effect of the seasonal cycle is smoothed by the application of a moving average of 12 months(a,b,d,e). (a,d): Time series of all factorial runs (S1-S5), (b,e): Single drivers obtained by subtracting factorial runs, (c,f): Decadal means of the years 1850,1990,2050, and 2090 of the single drivers.

exceedance of the flux threshold of  $1 \text{ nmol m}^{-2} \text{ s}^{-1}$ . The simulated regional mean  $F_{st}$  remains at relative constant values during the 21st century, however the seasonal cycle is narrowing (see Fig. 4.5b). Simulated changes in the cumulative  $\text{O}_3$  uptake without a flux threshold (CUO0) strongly follow changes in the  $\text{O}_3$  concentrations during the entire simulation period. The narrowing seasonal cycle does not considerably impact CUO0, since all taken up  $\text{O}_3$  is accumulated and the mean  $F_{st}$  remains constant. However the cumulative  $\text{O}_3$  uptake above a flux threshold of  $1 \text{ nmol m}^{-2} \text{ s}^{-1}$  (CUO1) strongly declines during the 21st century (see Fig. 4.4 and 4.5). The narrowing of the seasonal cycle of  $F_{st}$  causes a less frequent exceeding of the flux threshold of  $1 \text{ nmol m}^{-2} \text{ s}^{-1}$  and hence a decline in CUO1. The increasing atmospheric  $\text{CO}_2$  concentrations during the simulation period decrease the plants stomatal conductance and increase the plants water-use-efficiency (results not shown). Lower values of stomatal conductance reduce  $F_{st}$  and CUO1, even if though the  $\text{O}_3$  concentrations slightly increase in simulations based on RCP8.5.

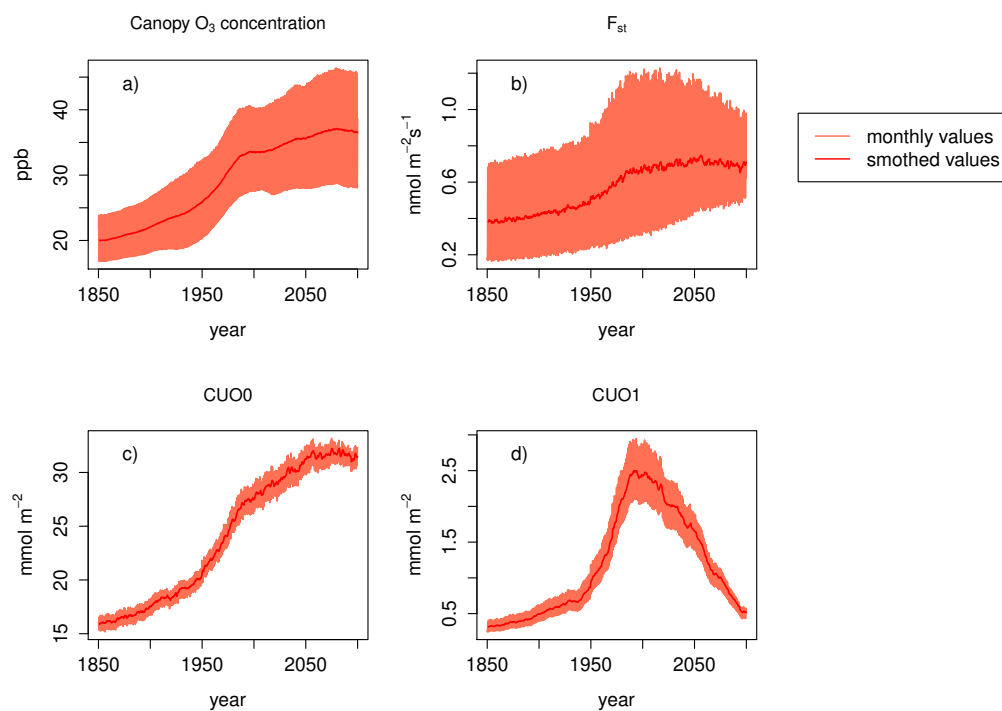


Figure 4.5: Simulated canopy  $\text{O}_3$  concentration, ozone uptake ( $F_{st}$ ), cumulative  $\text{O}_3$  uptake without a flux threshold (CUO0) and cumulative  $\text{O}_3$  uptake above a flux threshold of  $1 \text{ nmol m}^{-2} \text{ s}^{-1}$  (CUO1) of the factorial run S5 (all forcing variables are simulated transient) based on RCP8.5. Light red lines: monthly values, dark red lines: the effect of the seasonal cycle is smoothed by the application of a moving average of 12 month.

### 4.3.1.2 Carbon fixation and biomass production

Highest levels of GPP and C-biomass are simulated in the factorial run S4 (see Fig. 4.6a,d), which simulates all forcing drivers transient except O<sub>3</sub>. In all five factorial runs the simulated GPP increases strongly between 1850 and 2099 and approximately doubles for the runs S3-S5 (see Fig. 4.6a). The primary cause for this simulated increase is the CO<sub>2</sub> fertilisation effect and the increasing atmospheric CO<sub>2</sub> concentrations (see Fig. 4.6b and Tab. 4.3). In the period of 1970-1990 the growth stimulating effect induced by rising CO<sub>2</sub> concentrations equals roughly the detrimental impact of O<sub>3</sub> (see Fig. 4.6b). The negative impact of O<sub>3</sub> on GPP shows a maximum approximately in the 1990s and steadily decreases in subsequent decades (see Fig. 4.6b,c). The growth stimulating effect induced by N-deposition is lower compared to negative impact induced by O<sub>3</sub> during the decade of 1990 and higher by the end of the 21st century (see Fig. 4.6b,c).

Ozone damage considerably impacts the simulated carbon above- and below-ground biomass (C-biomass) in the simulation area. In the simulations with transient O<sub>3</sub> (S2,S3,S5) the regional summed C-biomass ceases to grow in the 1950s for 30-50 years (see in Fig. 4.6d). The impact of ozone damage on the C-biomass is stronger in magnitude compared to GPP and shows a maximum in the middle of the 21st century (compare Fig. 4.6b,c and Fig. 4.6e,f).

The carbon soil organic matter (SOM C) is strongly impacted by the atmospheric CO<sub>2</sub> concentration (see Fig. 4.6h). Highest levels of SOM C are simulated for the factorial run S1 (see Fig. 4.6g) where only CO<sub>2</sub> is simulated transient. The SOM C is less impacted by N-deposition (slightly increased) compared to O<sub>3</sub> (decreased) until the end of the 21st century when they approximately balance themselves (see Fig. 4.6h,i).

### 4.3.1.3 Magnitude of impact and differences between the RCPs

The two different approaches (approach 1: (S2-S1)/S1 and approach 2:(S5-S4)/S4) to calculate the O<sub>3</sub> impact on the simulation results yield similar but not identical results (see Fig. 4.7). Approach 1 suggests smaller reductions for GPP and C-biomass compared to approach 2. The extend of the differences varies between the variables. Maximal differences do not exceed approximately 1% except for CUO1 where absolute changes are small (see Fig. 4.8).

The mean ozone uptake ( $F_{st}$ ) increases about 70% until the year 2000 (see Fig. 4.7a). In simulations based on RCP8.5  $F_{st}$  increases until the end of the 21st century and reaches values of more than 90% increase compared to simulations based on pre-industrial O<sub>3</sub> concentrations. In simulations based on RCP2.6  $F_{st}$  declines strongly and by the end of the 21st century comparable values to simulations based on pre-industrial O<sub>3</sub> concentrations are reached. The mean CUO1 increases by approximately 1000% until the year 2000 and increases to values about 7000-14000% by 2099 in simulations based on RCP8.5 (see Fig. 4.7b). In simulations based on RCP2.6 the CUO1 values decline during the 21st century and reach comparable values to simulations based on pre-industrial O<sub>3</sub> concentrations by 2099. The strong relative increases in  $F_{st}$  and CUO1 results from small to moderate absolute changes of less than 0.4 nmol m<sup>-2</sup> s<sup>-1</sup> and less than 2.5

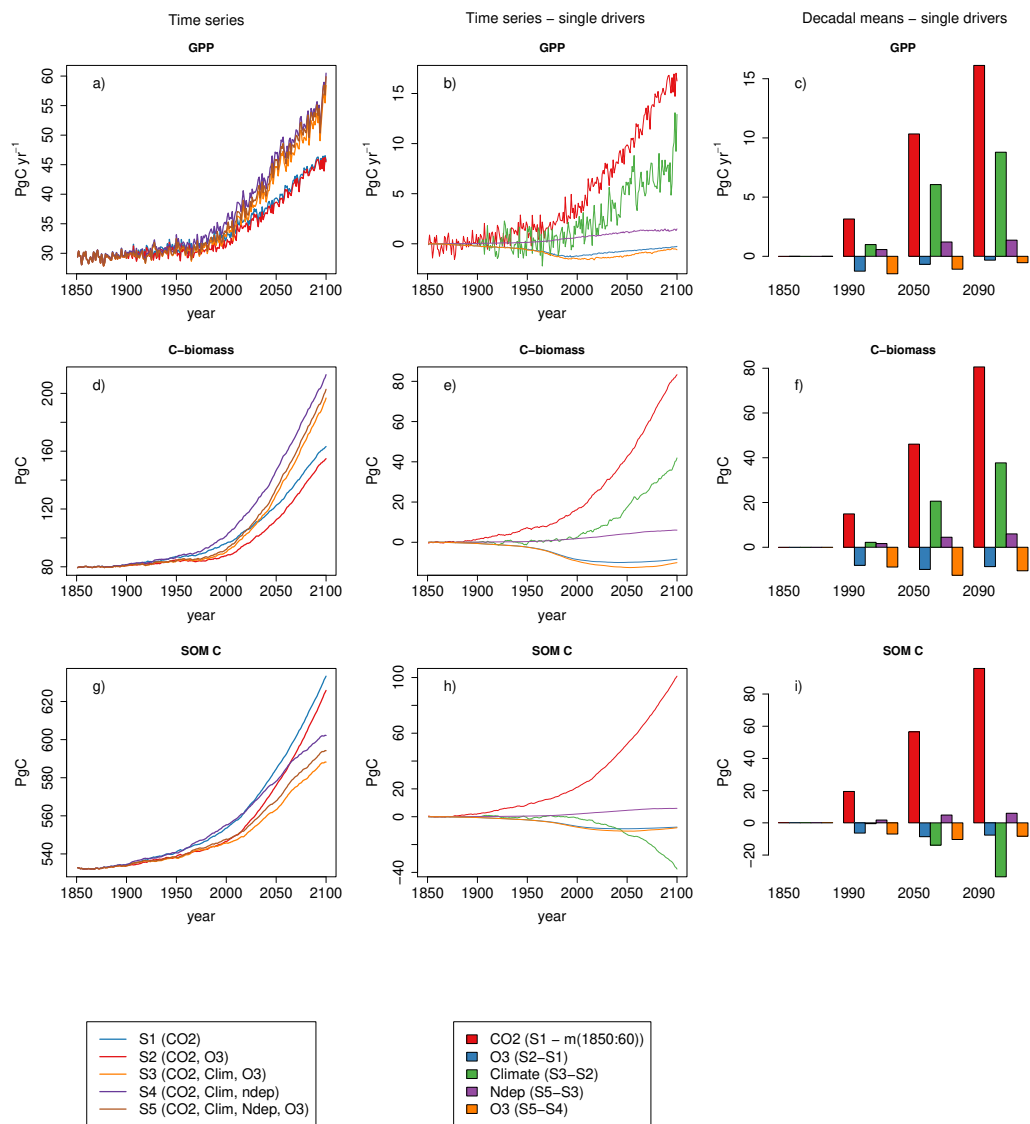


Figure 4.6: The amount of simulated regional summed GPP, regional summed stocks of total carbon biomass (C-biomass) and soil organic matter carbon (SOM C) of the simulations based on RCP8.5. (a,d,g): Time series of all factorial runs (S1-S5), (b,e,h): Single drivers obtained by subtracting factorial runs, (c,f,i): Decadal means of the years 1850,1990,2050, and 2090 of the single drivers.

Table 4.3: Absolute and relative change in GPP, total carbon biomass (C-biomass) and soil organic matter carbon (SOM C) induced by changing atmospheric CO<sub>2</sub> concentrations, climate, nitrogen deposition (Ndep), and O<sub>3</sub> concentrations. The differences in GPP, C-biomass and SOM C are presented for simulations of the past years of 1850 to 2004, simulations based on RCP8.5 and RCP2.6 for the time spans of 2005 to 2099, and for the entire simulation period 1850 to 2099.

RCP and time span	CO <sub>2</sub>	CO <sub>2</sub>	Climate	Climate	Ndep	Ndep	O <sub>3</sub>	O <sub>3</sub>
GPP	[PgC yr <sup>-1</sup> ]	[%]	[PgC yr <sup>-1</sup> ]	[%]	[PgC yr <sup>-1</sup> ]	[%]	[PgC yr <sup>-1</sup> ]	[%]
Past 1850:2004	4.4	14.8	1.1	3.2	0.7	2.2	-1.2...-1.5	-3.5...-4.1
RCP2.6 1850:2099	6.3	21.5	5.2	14.6	1	2.5	0...0.1	0...0.1
RCP8.5 1850:2099	16.3	55.6	12.9	28.4	1.5	2.6	-0.3...-0.6	-0.6...-1
RCP2.6 2005:2099	3.5	11	1.5	2.6	0.3	0.4	1.2...1.5	3.6...4.2
RCP8.5 2005:2099	13	39.6	9.8	18.6	0.7	0.4	0.9	2.8...3.1
C-biomass	[PgC]	[%]	[PgC]	[%]	[PgC]	[%]	[PgC]	[%]
Past 1850:2004	18.1	22.7	4.3	4.9	2	2.2	-8.9...-10	-9.1...-9.5
RCP2.6 1850:2099	42.7	53.7	20.2	17.2	4.4	3.2	-4.5...-5.1	-3.5...-3.7
RCP8.5 1850:2099	83.8	105.4	41.9	27.1	6.1	3.1	-8.4...-10.1	-4.8...-5.1
RCP2.6 2005:2099	25.2	26	15	11.2	2.4	1	4.4...4.9	5.5...6
RCP8.5 2005:2099	65.5	67	37	21.6	4	0.9	0...0.6	4...4.8
SOM C	[PgC]	[%]	[PgC]	[%]	[PgC]	[%]	[PgC]	[%]
Past 1850:2004	22.7	4.3	-1.8	-0.3	2.2	0.4	-7.4...-8.1	-1.3...-1.5
RCP2.6 1850:2099	64.8	12.2	-8.4	-1.4	5.7	1	-4.7...-5.5	-0.8...-0.9
RCP8.5 1850:2099	100.5	18.9	-37.6	-6	6	1	-7.5...-8	-1.2...-1.3
RCP2.6 2005:2099	42	7.6	-6.3	-1	3.5	0.6	2.5...2.7	0.5
RCP8.5 2005:2099	77.2	13.9	-35.5	-5.6	3.7	0.6	0...0.2	0.1...0.2

mmol  $\text{O}_3 \text{ m}^{-2}$  respectively (see Fig. 4.4a,d for  $F_{st}$  and CUO1 of the different factorial runs and Fig. 4.8 for the change). During the 21st century the absolute difference in CUO1 between simulations based on RCP8.5 compared to simulations based on pre-industrial  $\text{O}_3$  declines (see Fig. 4.7b), the relative difference however keeps increasing (see Fig. 4.8b). This increasing relative difference is caused by a decline of CUO1 during the 21st century in the simulations using pre-industrial ozone concentrations (see S1 and S4 in Fig. 4.4d). The decrease of CUO1 is caused by increasing atmospheric  $\text{CO}_2$  concentrations (see Fig. 4.4e,f), which reduce stomatal conductance and ozone uptake.

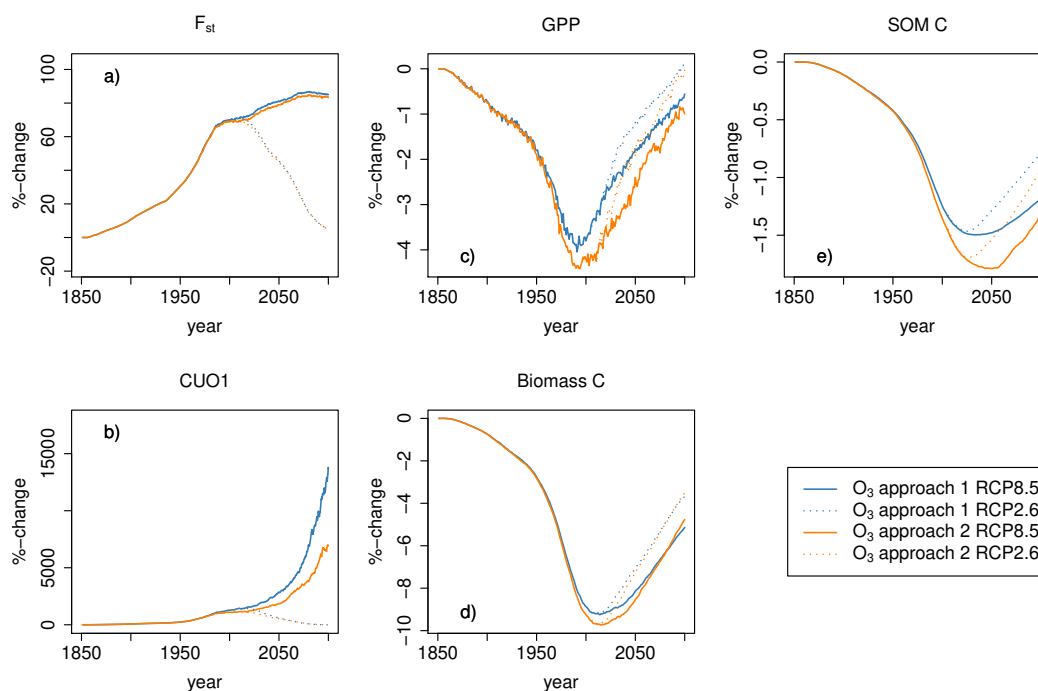


Figure 4.7: Ozone induced %-change of regional mean ozone uptake ( $F_{st}$ ), mean cumulative  $\text{O}_3$  uptake above a flux threshold of  $1 \text{ nmol m}^{-2} \text{ s}^{-1}$  (CUO1), summed GPP, summed carbon biomass (C-biomass) and summed carbon soil organic matter (SOM C) compared to pre-industrial values in the simulation region. Different colors indicate different approaches to calculate the ozone induced change from the factorial runs. Orange lines represent approach 1:  $(S2-S1)/S1$ , blue lines approach 2:  $(S5-S4)/S4$ . Solid lines indicate results from simulations based on RCP8.5, dotted lines results from simulations based on RCP2.6. The effect of the seasonal cycle is smoothed by the application of a moving average of 12 months.

The maximal  $\text{O}_3$  induced reduction of the mean GPP in the simulation area compared to pre-industrial values occurs in the 1990 and constitutes approximately 4% (see Fig. 4.7c and Tab. 4.4). In the following decades the simulated ozone induced reduction in GPP declines to 1% by the end of the 21st century for RCP8.5 and to close to zero

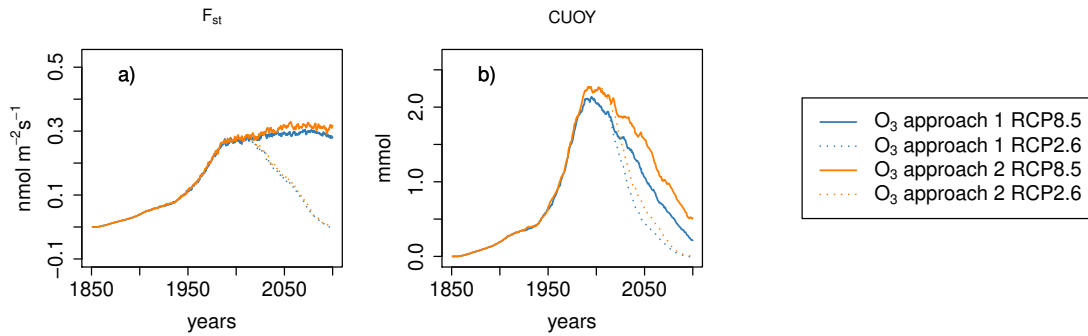


Figure 4.8: Ozone induced absolute change of regional mean ozone uptake ( $F_{st}$ ) and mean cumulative  $\text{O}_3$  uptake above a flux threshold of  $1 \text{ nmol m}^{-2} \text{ s}^{-1}$  (CUO1) compared to pre-industrial values in the simulation region. Different colours indicate different approaches to calculate the ozone induced change from the factorial runs. Orange lines represent approach 1:  $(S2-S1)/S1$ , blue lines approach 2:  $(S5-S4)/S4$ . Solid lines indicate results from simulations based on RCP8.5, dotted lines results from simulations based on RCP2.6. The effect of the seasonal cycle is smoothed by the application of a moving average of 12 months.

for RCP2.6. The simulated stocks of carbon in the simulation area exhibit the strongest ozone induced reduction in the period of 2000-2020 of approximately 9% and decline to 5% by 2099 for RCP8.5 and 4% for RCP2.6 (see Fig. 4.7d and Tab. 4.4). The SOM C is less strongly impacted by  $\text{O}_3$  with simulated maximal reductions of approximately 1.7%.

Nitrogen deposition slightly increases  $F_{st}$  and induces an up to 12% increase in CUO1 in the second half of the 21st century (see Fig. 4.9a,b). Nitrogen deposition stimulates GPP and C-biomass to a similar amount. Peak increases of about 3% for GPP and 3.5% for C-biomass are simulated in the second half of the 21st century (see Fig. 4.9c,d and Tab. 4.5). The increasing effect of nitrogen deposition on GPP and C-biomass keeps growing in China until the end of the 21st century (see Tab. 4.5). In Europe and the USA the GPP and C-biomass at the end of the 21st century is less enhanced by nitrogen deposition compared to during the middle of the 21st century. The SOM C is impacted less by nitrogen deposition and maximal increases of 1% compared to pre-industrial values are simulated at the end of the 21st century (see Fig. 4.9e and Tab. 4.3). Simulations based on RCP2.6 and RCP8.5 produce similar effects of nitrogen deposition on the displayed variables.

The magnitude of ozone induced damage on GPP exceeded the growth stimulating effect induced by nitrogen deposition until the end of the 20th century and the beginning of the 21st century (see Fig. 4.6b,c). Contrary to the tropospheric  $\text{O}_3$  concentrations, the regional mean nitrogen deposition does not decline during the 21st century but slightly increases in RCP8.5 and RCP2.6. The growth stimulating effect on GPP induced by nitrogen deposition becomes higher in magnitude during the 21st century compared to the detrimental effect of ozone (see Fig. 4.6b,c and Tabs. 4.4 and 4.5).

The growth stimulating effect of nitrogen deposition on C-biomass remains lower in magnitude compared to the detrimental effects of ozone for both pollution scenarios throughout the entire simulation period (see Fig. 4.6e,f and Tab. 4.3). However, in simulations based on RCP2.6 the ozone induced reduction on C-biomass is only slightly higher in magnitude compared to the growth stimulating effect induced by nitrogen deposition (see Tabs. 4.4 and 4.5).

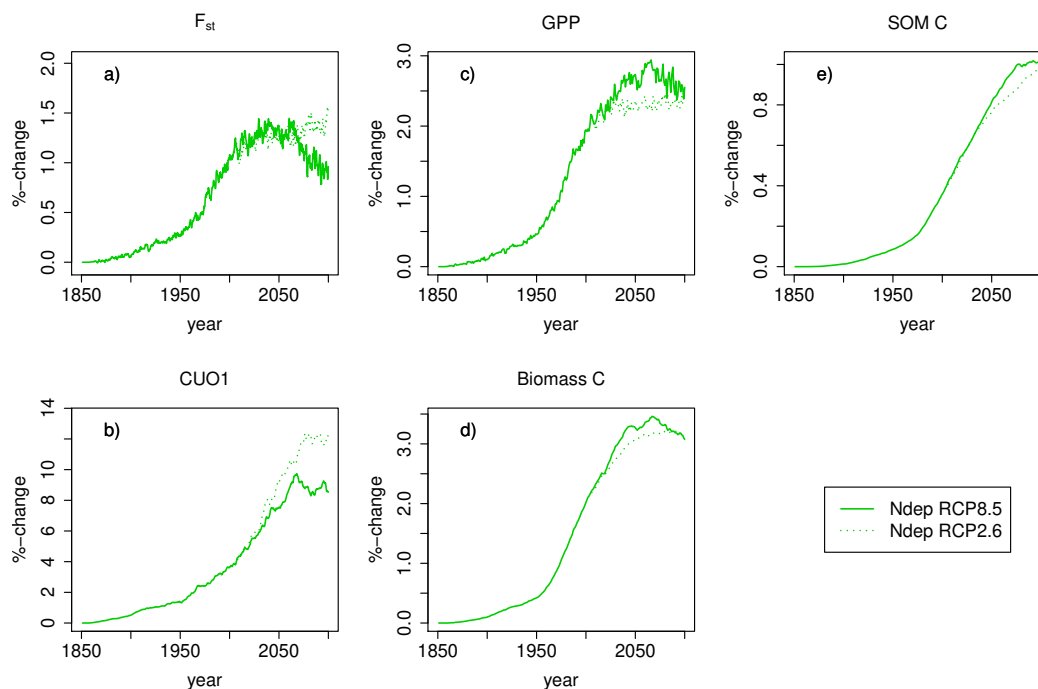


Figure 4.9: Nitrogen deposition induced %-change of regional mean ozone uptake ( $F_{st}$ ), mean cumulative  $O_3$  uptake above a flux threshold of  $1 \text{ nmol m}^{-2} \text{ s}^{-1}$  (CUO1), summed GPP, summed carbon biomass (C-biomass), and summed carbon soil organic matter (SOM C) compared to pre-industrial values in the simulation region. Solid lines indicate results from simulations based on RCP8.5, dotted lines results from simulations based on RCP2.6. The effect of the seasonal cycle is smoothed by the application of a moving average of 12 months (a,b).

Table 4.4: Mean percent change in GPP and C-biomass induced by ozone during the decades of 1990 (1990-1999), 2050 (2050-2059) and 2090 (2090-2099) compared to pre-industrial values for the Northern Hemisphere north of 30°N (NH<sub>30</sub>), Europe, USA and China. The given range indicates the estimates according to both approaches to calculate the ozone impact.

Region	1990	2050 RCP8.5	2050 RCP2.6	2090 RCP8.5	2090 RCP2.6
GPP					
NH <sub>30</sub>	-3.8...-4.3	-1.7...-2.3	-1.1...-1.6	-0.7...-1.0	0...-0.2
Europe	-4.5...-4.9	-1.8...-2.1	-1.0...-1.4	-0.8	-0.2...-0.3
USA	-4.7...-5.0	-1.8...-2.0	-1.3...-1.6	-0.8...-1.1	0.3...1.0
China	-9.2...-10.1	-6.5...-8.8	-7.2...-7.9	-1.6...-2.8	-3.8...-5.7
C-biomass					
NH <sub>30</sub>	-8.5...-8.9	-7.9...-8.1	-6.7...-6.9	-5.1...-5.4	-3.8...-3.9
Europe	-10.8...-11.5	-9.2...-9.8	-8.0...-8.4	-6.1...-6.4	-4.9
USA	11.9...-12.5	-10.0...-10.7	-8.6...-9.0...	-6.5...-6.8	-4.1...-4.3
China	-15.1...-15.9	-24.7...-27.5	-22.0...-23.4	-15.8...-18.5	-16.2...-16.4

Table 4.5: Mean percent change in GPP and C-biomass induced by nitrogen deposition during the decades of 1990 (1990-1999), 2050 (2050-2059) and 2090 (2090-2099) compared to pre-industrial values for the Northern Hemisphere north of 30°N (NH<sub>30</sub>), Europe, USA and China.

Region	1990	2050 RCP8.5	2050 RCP2.6	2090 RCP8.5	2090 RCP2.6
GPP					
NH <sub>30</sub>	1.8	2.7	2.3	2.5	2.4
Europe	2.7	3.7	2.9	2.9	2.5
USA	1.4	1.1	0.7	0.6	0.9
China	2.9	5.7	6.6	6.4	7
C-biomass					
NH <sub>30</sub>	1.8	3.3	3.1	3.2	3.2
Europe	3.2	4.6	4.3	3.6	4
USA	1.6	1.7	1.6	1.5	1.3
China	1.6	3.2	4.4	3.9	6.2

#### 4.3.1.4 Impact of the ozone deposition scheme

Simulations run with a model version where the ozone deposition scheme is turned off result in considerably higher estimates of  $F_{st}$  and CUO1 what induces higher damage

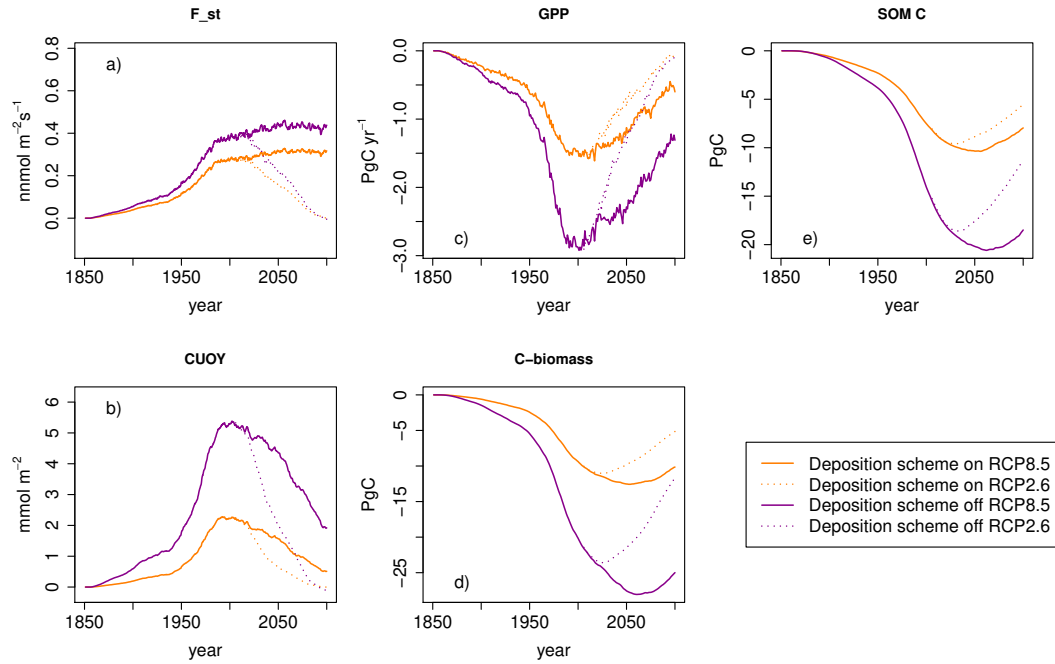


Figure 4.10: Ozone impacts on the regional mean ozone uptake ( $F_{st}$ ), mean cumulative  $\text{O}_3$  uptake above a flux threshold of  $1 \text{ nmol m}^{-2} \text{ s}^{-1}$  (CUO1), summed GPP, summed carbon biomass (C-biomass), and summed carbon soil organic matter (SOM C) compared to pre-industrial values in the simulation region. The displayed ozone impact is calculated based on approach 2. Orange lines: Results based on a model version where the ozone deposition scheme is turned on. Magenta lines: Results based on a model version where the ozone deposition scheme is turned off. Solid lines indicate results from simulations based on RCP8.5, dotted lines results from simulations based on RCP2.6. The effect of the seasonal cycle is smoothed by the application of a moving average of 12 months (a,b).

estimates (see Fig. 4.10). In simulations where the ozone deposition scheme is turned off ozone induced reductions in GPP and C-biomass are approximately twice as high compared to simulations where the ozone deposition scheme is turned on. Reductions in GPP in simulations where the ozone deposition scheme is turned off reach peak values of about  $3 \text{ PgC yr}^{-1}$  ( $\approx 8\%$ ) compared to approximately  $1.5 \text{ PgC yr}^{-1}$  ( $\approx 4\%$ ) in simulations where the deposition scheme is turned on. By the end of the 21st century simulations with the ozone deposition scheme turned on produce very similar estimates for GPP damage compared to simulations where the deposition scheme is turned off for RCP2.6. In simulations based on RCP8.5 where the deposition scheme is turned off estimated reductions to GPP at the end of the 21st century amount  $1.3 \text{ PgC yr}^{-1}$  ( $\approx 2\%$ ) compared to  $0.6 \text{ PgC yr}^{-1}$  ( $\approx 1\%$ ) for simulations where the deposition scheme is turned on. For C-biomass the difference between both model versions in simulations

based on RCP8.5 at the end of the 21st century is even more pronounced. For C-biomass estimated reductions at the end of the 21st century for simulations based on RCP8.5 constitute 25 PgC ( $\approx 11\%$ ) in runs where the deposition scheme is turned off and 10 PgC ( $\approx 5\%$ ) in runs where the deposition scheme is turned on.

### 4.3.2 Simulated spatial differences of air pollution impacts

In this section ozone damage calculated only according to approach 2 (see Tab. 4.2) is displayed to minimise the amount of figures. Both approaches to calculate the ozone impact produce similar results where approach 2 indicates slightly higher ozone induced reductions compared to approach 1. Since in approach 2 all climate drivers are simulated transient contrary to approach 1 where one  $\text{CO}_2$  and  $\text{O}_3$  are simulated transient, approach 2 might indicate more realistic results.

Simulated values of CUO1 strongly vary in the simulated region. Highest values are found during the decade of 1990 in the eastern and north-eastern US, large parts of Europe central and eastern Asia (see Fig. 4.11a). Regions of peak increases in CUO1 (compared to pre-industrial values) coincide with regions of high cover fraction of the boreal needleleaf evergreen PFT (in Canada, the northern US and northern Eurasia) and the temperate broadleaved summer-green as well as the temperate needleleaf evergreen PFT (in Europe, eastern Asia, eastern and western US). The CUO1 values decline strongly during the 21st century in simulations based on both RCPs, though stronger for RCP2.6 (see Fig. 4.11). At the end of the 21st century simulated CUO1 values reach comparable values to pre-industrial times in large parts of the simulation region and slightly lower values in large parts of the US and Eurasia in simulations based on RCP2.6. Increased atmospheric  $\text{CO}_2$  concentrations compared to values in 1850 decrease the stomatal conductance, limit the  $\text{O}_3$  uptake and cause lower values of CUO1.

The extend of simulated impact of ozone and nitrogen deposition on the terrestrial carbon uptake (GPP) and storage (C-biomass) differs strongly within the simulated region. Nitrogen deposition stimulates GPP compared to simulations run with pre-industrial deposition values mainly in Europe and Eastern Asia. Simulated increases of GPP in these regions constitute about  $80\text{-}140 \text{ gC m}^2 \text{ yr}^{-1}$  for simulations run based on RCP8.5 (see left column in Fig. 4.12). In relative terms peak increases of 10-16% are found in parts of eastern, central and northern Asia and small parts of Europe (see left column in Fig. 4.13). Simulated increases in GPP are higher, and hotspot areas more extended, in the decade of 2090 compared to the 2050 decade for both RCPs. Simulations based on RCP2.6 exhibit similar patterns compared to simulations based on RCP8.5 but show a less strong increase in GPP induced by to nitrogen deposition.

The highest ozone induced absolute reductions in GPP occur in Europe, Eastern US and Eastern Asia where the respective increase in CUO1 is highest. Peak reductions of about  $150\text{-}220 \text{ gC m}^2 \text{ yr}^{-1}$  are simulated in the eastern US, southern Europe and eastern Asia during the decade of 1990.

Simulated ozone induced damage to GPP declines in the decades of 2050 and 2090 for both RCPs but considerable ozone induced reductions in GPP are simulated until the end of the 21st century in eastern Asia. Simulations based on RCP2.6 indicate

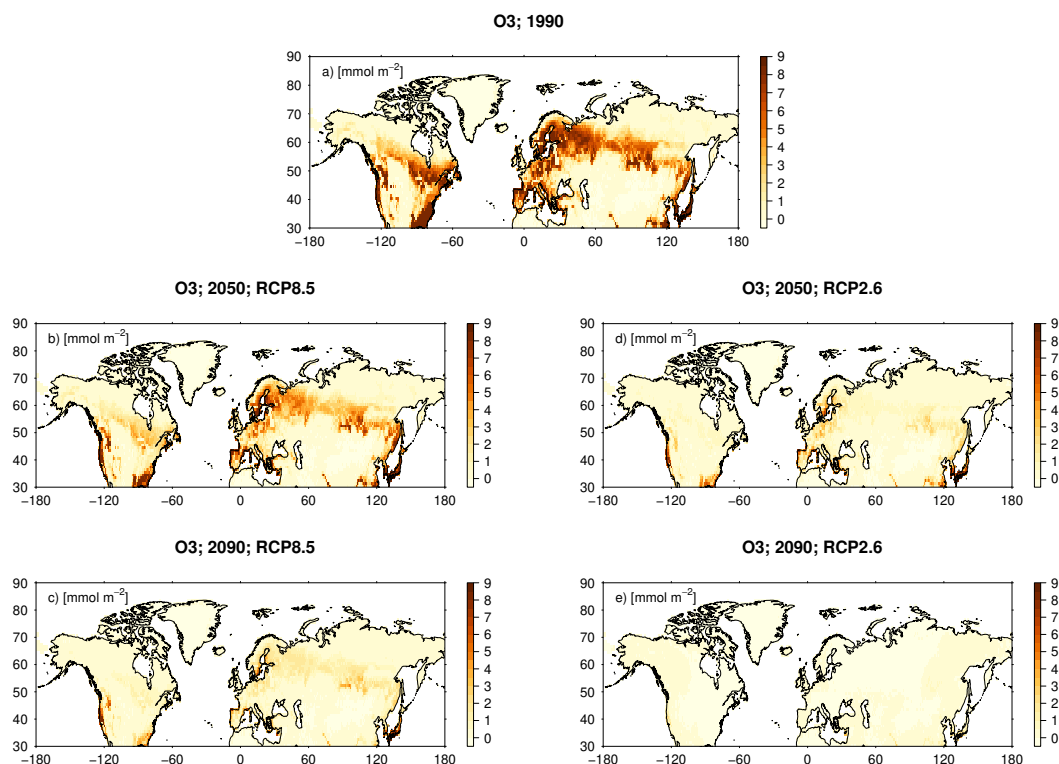


Figure 4.11: Absolute change in CUO1 compared to pre-industrial values induced by ozone, calculated according to approach 2. Displayed are the decade 1990 (mean of the years 1990-1999), 2050 (mean of the years 2050-2059) and of 2090 (mean of the years 2090-2099). For the decades 2050 and 2090 results from simulations based on RCP8.5 and RCP2.6 are displayed. See Tab. 4.2 for details on the calculation of the ozone impact.

for the end of the 21st century close to no ozone induced damage compared to pre-industrial values over large parts of the simulation scope. Small absolute reductions are observed in parts of Europe and small absolute increases are simulated in the Eastern US induced by lower CUO1 values compared to pre-industrial values (see Fig. 4.11). Increased atmospheric CO<sub>2</sub> concentrations compared to pre-industrial values reduce the stomatal conductance, restrict ozone uptake and enable the increased GPP values.

The relative reductions in GPP exhibit a scattered pattern of increases and decreases in large areas of central Asia and the central US, where the simulated vegetation cover is dominated by grasses and crops. Peak values of relative reductions in GPP of 8-11% are simulated in the decade of 1990 in the eastern US, Europe and eastern Asia. In the decade of 2050 relative reductions in GPP of 4-8% are simulated in southern Europe, parts of the eastern and western US in simulations based on RCP8.5 (see Fig. 4.13). Peak relative decreases of 8-11% are simulated in eastern Asia. At the end of the 21st

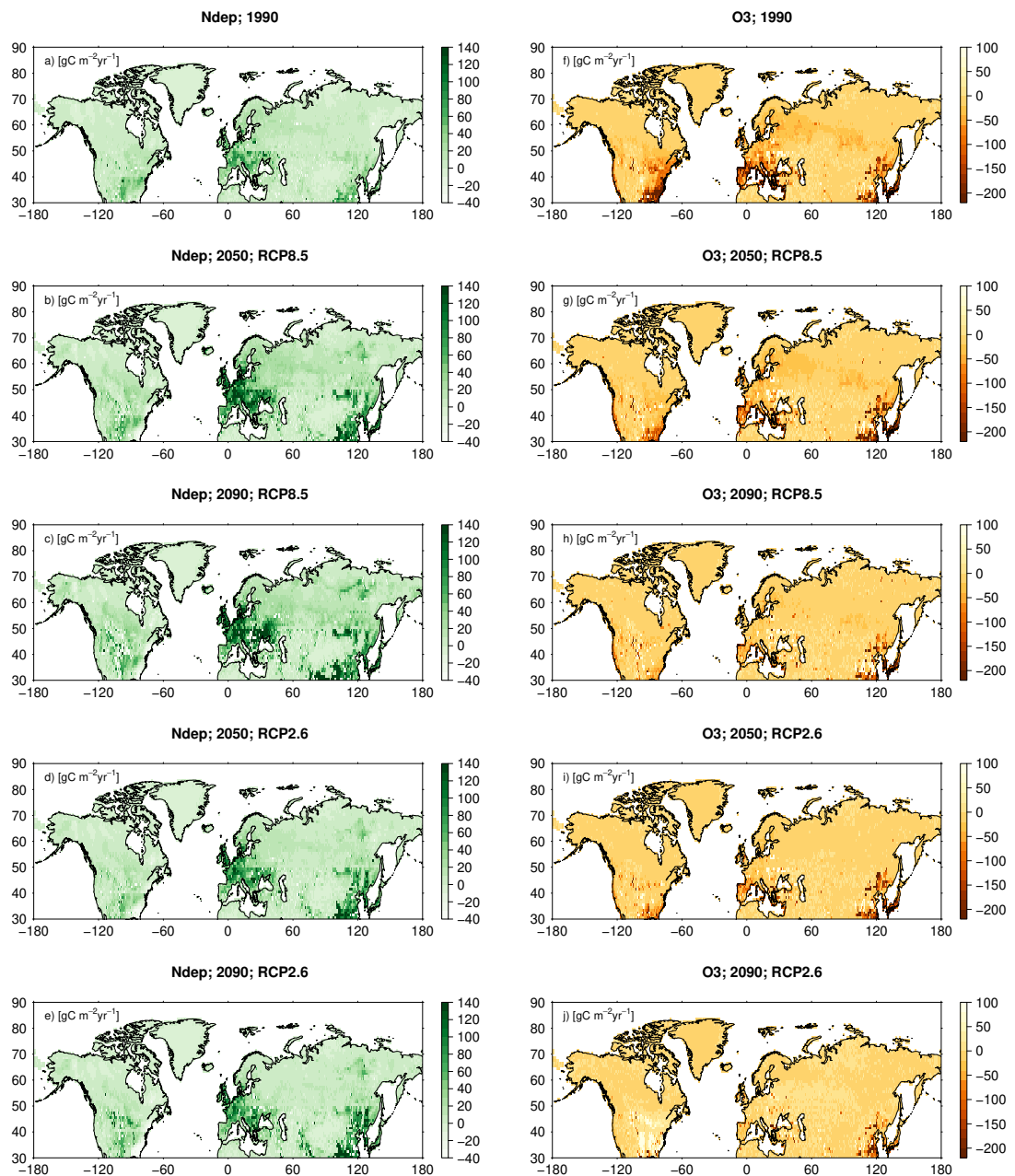


Figure 4.12: Absolute change in GPP compared to pre-industrial values induced by nitrogen deposition (left column) and ozone calculated according to approach 2 (right column). The induced change in GPP is displayed for the decades 1990 (mean of the years 1990-1999), 2050 (mean of the years 2050-2059) and 2090 (mean of the years 2090-2099). For the decades 2050 and 2090 results from simulations based on RCP8.5 and RCP2.6 are displayed. See Tab. 4.2 for details on the calculation of the single drivers.

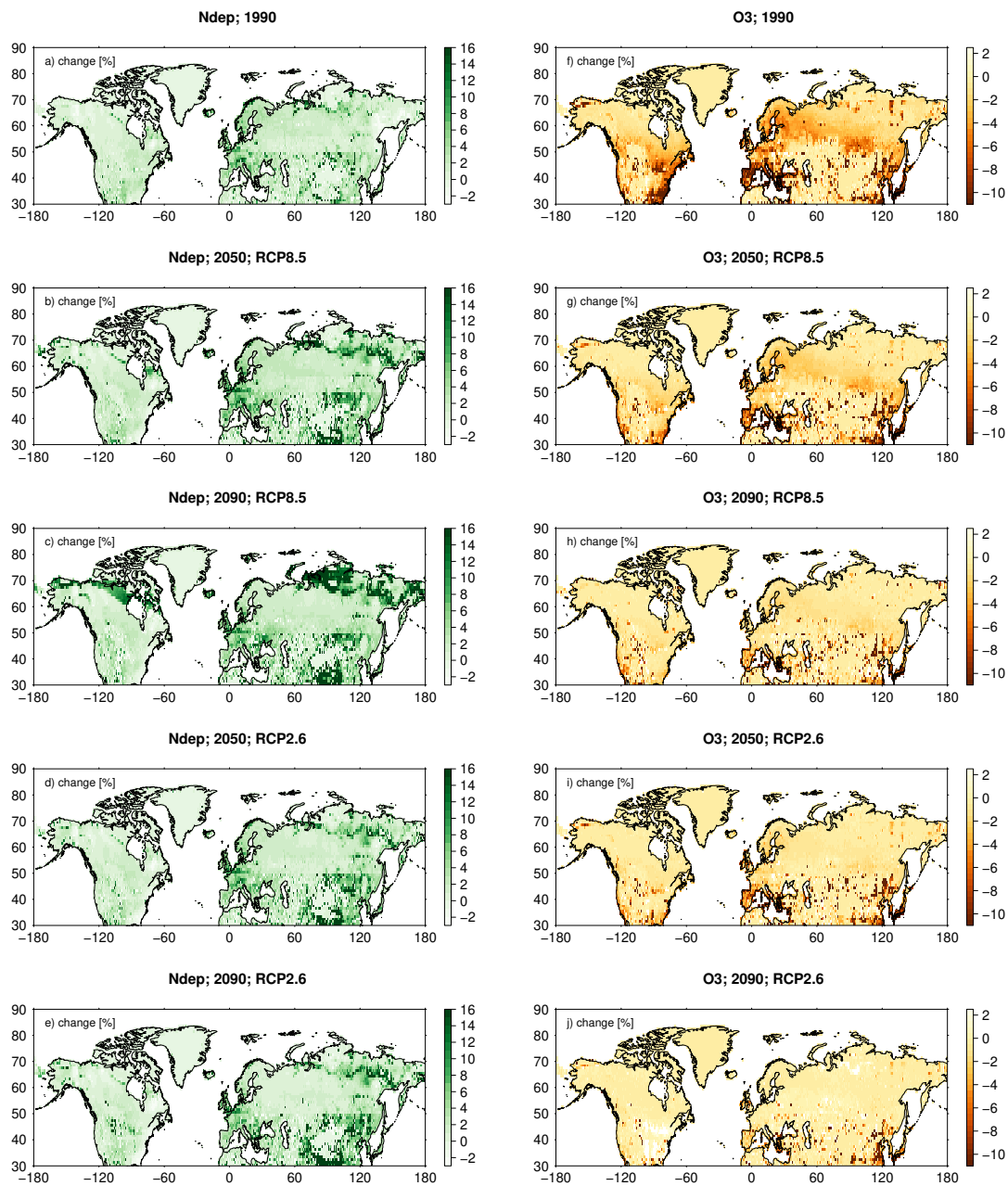


Figure 4.13: Relative change in GPP compared to pre-industrial values induced by nitrogen deposition (left column) and ozone calculated according to approach 2 (right column). The induced change in GPP is displayed for the decades 1990 (mean of the years 1990-1999), 2050 (mean of the years 2050-2059) and 2090 (mean of the years 2090-2099). For the decades 2050 and 2090 results from simulations based on RCP8.5 and RCP2.6 are displayed. See Tab. 4.2 for details on the calculation of the single drivers.

century ozone induced reductions in GPP decline, but reductions of above 8% are still simulated in small parts of eastern Asia. Slight increases in GPP are simulated in a large fraction of the Eastern US and small scattered areas in Asia.

Nitrogen deposition induces peak increases in C-biomass of 500-600 gCm<sup>-2</sup> compared to pre-industrial values in parts of Europe and eastern Asia (see left column of Fig. 4.14). Highest relative increases in C-biomass of 14-17% are simulated in the decades of 2050 and 2090 in regions of southern and northern Asia, where absolute changes are mostly small (see left column of Fig. 4.14 and Fig. 4.15). Simulations based on RCP8.5 exhibit slightly higher increases in C-biomass compared to RCP2.6. For both scenarios nitrogen deposition increases C-biomass stronger in 2090 compared to 2050.

Hotspots of ozone induced damage to C-biomass during the decade of 1990 are southern Europe and the eastern US with simulated decreases of 20-23% (see right column of Fig. 4.15). For both pollution scenarios, RCP2.6 and RCP8.5, the strongest ozone induced absolute reductions in C-biomass of 1400-1600 gCm<sup>-2</sup> occur in the decade of 2050 in the eastern US, southern Europe and eastern Asia (see right column of Fig. 4.14). By the end of the 21st century the hotspots of C-biomass reduction attenuate for both RCPs and abate stronger in simulations based on RCP2.6. The ozone induced C-biomass reductions in relative terms exceed 20% in parts of Europe, eastern and western US and eastern Asia in the middle of the 21st century for both RCPs (see right column of Fig. 4.15). By the end of the 21st century simulated decreases in these hotspots become smaller for both RCPs where attenuations are stronger for RCP2.6.

## 4.4 Discussion

The simulation of the Northern Hemisphere biosphere from 1850-2099 according to the Representative concentration pathway scenarios RCP8.5 and RCP2.6 indicates that air pollution (ozone and nitrogen deposition) might have considerably impacted carbon uptake and plant growth in the past and has the potential to continue a considerable impact during the 21st century.

### 4.4.1 Air pollution impacts on GPP and total carbon biomass

The ozone induced mean regional (Northern Hemisphere  $\geq 30^\circ\text{N}$ ) reductions in GPP increase from 1850 until the decade of 1990 where GPP is reduced by approximately 4% compared to simulations based on pre-industrial O<sub>3</sub> concentrations. Damage hotspots in southern Europe, eastern Asia and the eastern US exhibit ozone induced reductions of 8-11% for the decade of 1990. The regional mean value is lower compared to net photosynthesis damage estimated by meta-analyses of ozone damage to trees. In a meta-analyses by Wittig et al. (2009) net photosynthesis damage of trees grown in ambient O<sub>3</sub> concentrations vs. charcoal filtered air is estimated to amount 11% and 19% for trees grown in elevated O<sub>3</sub> concentrations vs. charcoal filtered air. Lombardozzi et al. (2013) estimates damage to net photosynthesis of temperate deciduous trees to amount 12% and 16% for temperate evergreen trees. A reduction of 28% in net photosynthesis

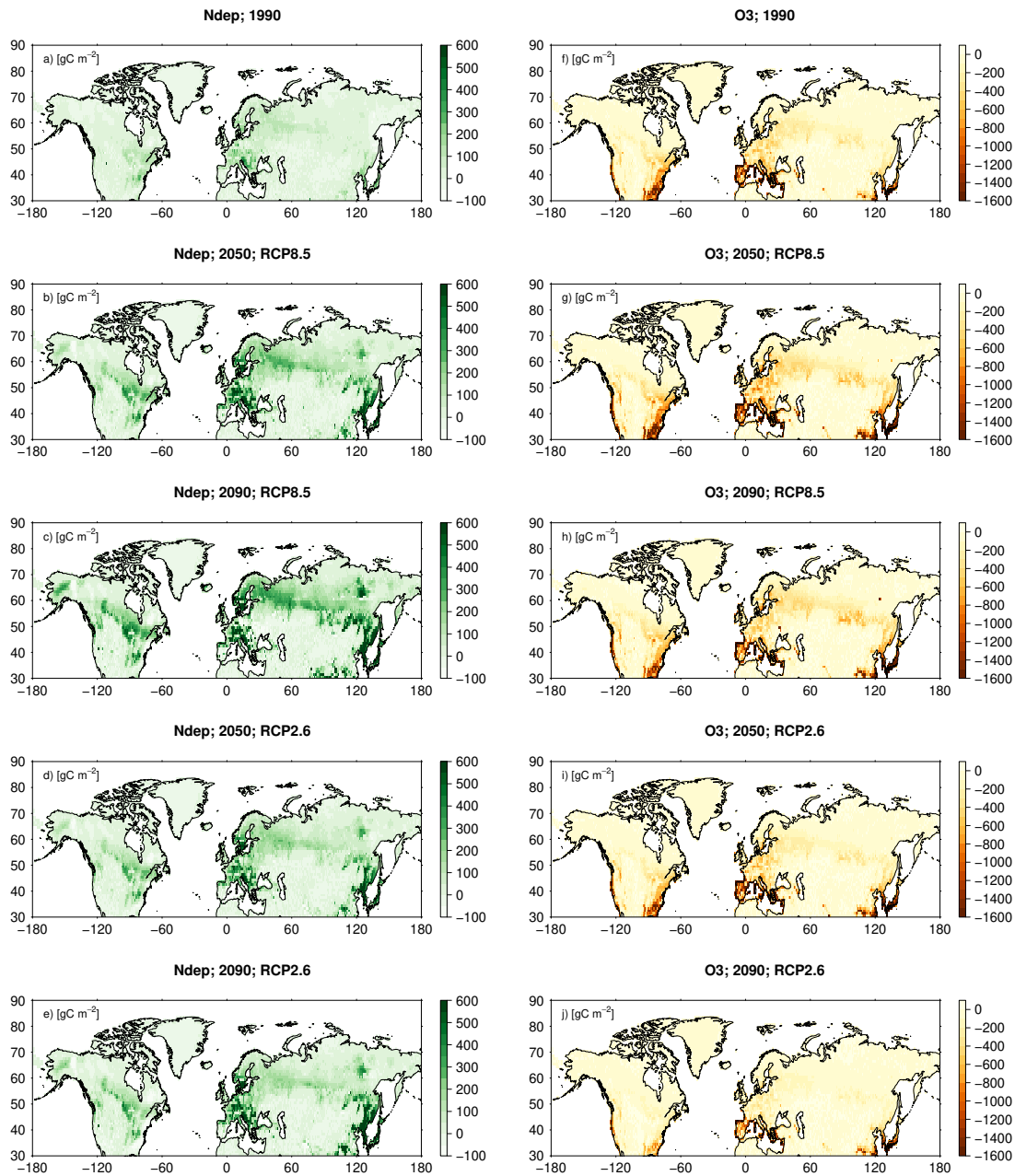


Figure 4.14: Absolute change in C-biomass compared to pre-industrial values induced by nitrogen deposition (left column) and ozone calculated according to approach 2 (right column). The induced change in C-biomass is displayed for the decades 1990 (mean of the years 1990-1999), 2050 (mean of the years 2050-2059) and 2090 (mean of the years 2090-2099). For the decades 2050 and 2090 results from simulations based on RCP8.5 and RCP2.6 are displayed. See Tab. 4.2 for details on the calculation of the single drivers.

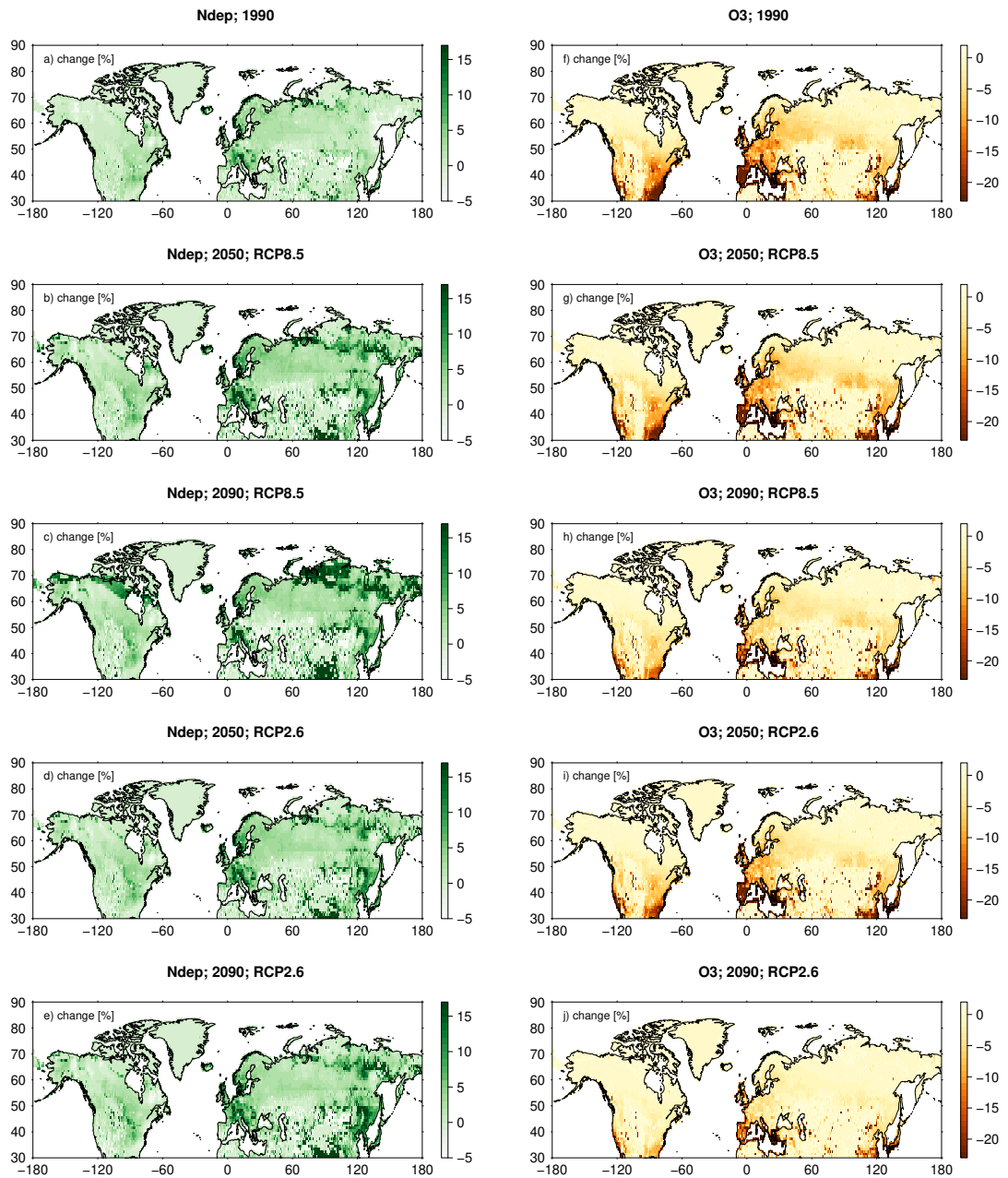


Figure 4.15: Relative change in C-biomass compared to pre-industrial values induced by nitrogen deposition (left column) and ozone calculated according to approach 2 (right column). The induced change in C-biomass is displayed for the decades 1990 (mean of the years 1990-1999), 2050 (mean of the years 2050-2059) and 2090 (mean of the years 2090-2099). For the decades 2050 and 2090 results from simulations based on RCP8.5 and RCP2.6 are displayed. See Tab. 4.2 for details on the calculation of the single drivers.

is estimated for woody plants grown in elevated  $O_3$  compared to a control by Li et al. (2017). Simulated ozone damage values in hotspot areas take values close to the lower damage estimates suggested by Wittig et al. (2009) and Lombardozzi et al. (2013).

Several process based models estimated ozone induced damage to NPP/GPP on global or regional scale. A mean global ozone induced reduction in NPP of 0.8 -2.9% from 1989 to 1993 is estimated by the Terrestrial Ecosystem Model (Felzer et al., 2005). Simulations with the Community Land Model suggest a 10.8% reduction of global mean GPP for present day  $O_3$  concentrations (Lombardozzi et al., 2015). A mean reduction in NPP of 4.5% in China between 1961-2000 is estimated by a process-based Dynamic Land Ecosystem Model (Ren et al., 2007). The simulation of ozone damage to China's forests suggest a 0.2-1.6% decrease in NPP from the 1960s to 2000-05 (Ren et al., 2011). Simulations using the Terrestrial Ecosystem Model estimate a mean reduction in NPP of 2.6-6.8% in the United States for the period of the late 1980s to early 1990s (Felzer et al., 2004). In the Euro-Mediterranean region a reduction in GPP of 22% is estimated for the year 2002 by the ORCHIDEE model (Anav et al., 2011). The mean GPP of the years 2001-2010 in Europe is simulated to be reduced by 7.6% compared to not accounting for ozone damage by the O-CN model (Franz et al., 2017).

During the 21st century the cumulative  $O_3$  uptake above a flux threshold of  $1 \text{ nmol m}^{-2} \text{ s}^{-1}$  (CUO1), on which the damage calculations base, declines due to the impact of the  $CO_2$  fertilisation effect on stomatal conductance and ozone uptake. This result is in agreement with Oliver et al. (2018), who found in Europe-wide simulations that elevated future  $CO_2$  levels and reductions in  $O_3$  concentrations result in reduced  $O_3$  induced damage values by 2050. Induced by the simulated decline in CUO1 the mean regional reduction in GPP decreases in the decade of 2050 to approximately 2% in simulations based on RCP8.5 and 1-1.5% in simulations based on RCP2.6. By the end of the 21st century damage induced by elevated levels of  $O_3$  decreases to approximately 1% in simulations based on RCP8.5 and close to zero for RCP2.6. Simulations with the JULES model estimate a 14-23% reduction in global GPP between 1901-2100 (Sitch et al., 2007). A more recent version of the JULES model suggest a 4 to 9% reduction in European GPP due to ozone by 2050 (Oliver et al., 2018). Both estimates are higher compared to the simulation results here (see Tab. 4.4). A possible reason for the higher estimates by Sitch et al. (2007) and Oliver et al. (2018) is the absence of an ozone deposition scheme in JULES, what might have caused higher surface ozone concentrations and hence increased ozone uptake and incurred damage.

On a regional mean basis very small ozone induced reductions are simulated by O-CN at the end of the 21st century, however in eastern Asia peak decreases amount more than 8% for both RCPs.

The stimulating effect of nitrogen deposition on regional mean GPP is lower in magnitude compared to the detrimental effect of  $O_3$  during most of the simulation period for both RCPs (results for RCP2.6 not shown). Both effects approximately even out in their impact on the mean regional GPP by 2030-2050. By the end of the 21st century nitrogen deposition stronger increases GPP than  $O_3$  impacts decline it. However, regions that experience strong ozone induced negative effects do not always coincide with

regions that benefit from the stimulating effect of nitrogen deposition.

The ozone induced simulated mean regional reduction in total above- and below-ground carbon biomass (C-biomass) reaches peak values of 8-10% at the end of the 20th and first half of the 21st century. Damage values of 20-23% are simulated in damage hotspots in southern Europe, eastern Asia and the eastern and western US for the decade of 1990. A meta-analyses with tree suggests a 7% reduction in total biomass for trees grown in ambient air compared to charcoal filtered air and a 17% reduction for trees grown in elevated O<sub>3</sub> concentrations compared to charcoal filtered air (Wittig et al., 2009). In a meta-analyses by Li et al. (2017) a 14% reduction in total biomass is calculated for trees grown in elevated O<sub>3</sub> concentrations (mean of 116 ppb) compared to controls grown in a mean O<sub>3</sub> concentration of 21 ppb. The simulated regional mean estimate of ozone induced damage to C-biomass is higher compared to the estimate of trees grown in ambient vs. charcoal filtered air by Wittig et al. (2009) and lower compared to trees grown in elevated O<sub>3</sub> vs. charcoal filtered air or a mean of 21 ppb O<sub>3</sub> (Wittig et al., 2009; Li et al., 2017). Simulated damage values in the hotspots are higher compared to the estimates by the meta-analyses.

The stimulating effect of nitrogen deposition on regional mean C-biomass is lower in magnitude compared to the detrimental effects induced by O<sub>3</sub> for the entire simulation period for RCP8.5. In simulations based on RCP2.6 both effects approximately even out by 2099, and O<sub>3</sub> induced damage is only slightly higher compared to the stimulation induced by nitrogen deposition (results not shown).

#### 4.4.2 Limitations of comparisons between publications

When interpreting the comparison of the results here and previously published simulation results one has to keep in mind that the different modelling approaches usually differ in several aspects that might considerably impact the damage estimate. Simulations often differ in the simulated time period, e.g. Sitch et al. (2007) (1901-2100), Lombardozzi et al. (2015) 25 years with an average O<sub>3</sub> concentration of the years 2002-2009, Franz et al. (2017) (1961-2011), and Oliver et al. (2018) (1901-2050). They differ in e.g. the representation of changing CO<sub>2</sub> concentrations, nitrogen deposition and land-cover/land-use change. Sitch et al. (2007) simulate changing CO<sub>2</sub> concentrations, Lombardozzi et al. (2015) do include neither, Franz et al. (2017) account for changing CO<sub>2</sub> concentrations, nitrogen deposition but use static land-cover (kept fixed at 2005 levels), and Oliver et al. (2018) simulate changing CO<sub>2</sub> concentrations and a partly fixed land-cover. Furthermore damage estimates are calculated based on different references. Damage might be given as the difference between a simulation accounting for O<sub>3</sub> damage compared to a reference simulation not accounting for ozone damage (Lombardozzi et al., 2015; Franz et al., 2017). Another approach is to report the damage simulated between a specific time period. Sitch et al. (2007) calculate ozone induced damage between 1901-2100 and Oliver et al. (2018) between 1901-2001 and 2001-2050.

A further difference between the published results is the time resolution of the ozone forcing applied in the simulations. Some studies used hourly ozone forcing (e.g. Lombardozzi et al. (2015), Franz et al. (2017), and Oliver et al. (2018)) and others are forced

by monthly diurnal mean values (e.g. Sitch et al. (2007) and the simulations here). As the formation of ozone shows a pronounced diurnal cycle (Sanz et al., 2007), the use of monthly mean ozone concentrations probably impacts the simulated estimates of ozone uptake. However, to which extent the omission of a diurnal cycle impacts ozone uptake, accumulation and damage estimates is yet uncertain.

#### 4.4.3 Potential impacts of vegetation dynamics

Ozone sensitivity differs between plant groups, plant species and between genotypes (Wittig et al., 2007; Lombardozzi et al., 2013; Li et al., 2017; Hayes et al., 2007; Karnosky et al., 2003). These differences ought to be reflected in injury functions included into models to be able to simulate average responses as attempted in global models. The injury function is a key aspect of the simulation of ozone damage and has a large impact on the extent of the estimate damage (see chapter 3). The scarcity of suitable data restricts the possibility to parameterise injury functions for all simulated PFTs (e.g. 12 PFTs in O-CN) and furthermore restricts the evaluation of ozone-submodels and the included injury functions. The injury functions used for the simulations here are tuned to reproduce observed biomass damage from filtration/fumigation experiments of broadleaved and needle-leaved tree species (see chapter 3 for more details).

Differing ozone sensitivities might induce changes in community composition (Barbo et al., 1998; Kubiske et al., 2007; Zak et al., 2011) as well as the interactive effects of changed CO<sub>2</sub> and O<sub>3</sub> concentrations (Karnosky et al., 2003). The responses of plants grown under interspecific competition, e.g. in forests, may not be transferred from results of filtration/fumigation experiments (with elevated CO<sub>2</sub> and/or O<sub>3</sub>) of plants grown in monoculture (Kozovits et al., 2005). Zak et al. (2011) found that initial declines in forest productivity induced by elevated levels of O<sub>3</sub> were compensated for by the growth of ozone tolerant individuals resulting in an equivalent NPP between ambient and elevated levels of O<sub>3</sub>. Simulations by an individual-based forest model indicate that the carbon sequestration capacity in forests might not be reduced by ozone damage if at the ecosystem level the reduced carbon fixation of ozone-sensitive species is compensated for by an increased carbon fixation of less ozone-sensitive species (Wang et al., 2016).

First generation dynamic global vegetation models such as O-CN simulate plant functional types (PFTs) rather than explicit species. The simulation of community dynamics is restricted in O-CN and might lead to an overestimation of simulated damage if the injury function is parametrised based on ozone-sensitive species. The injury function here is parameterised based on a relevant range of European tree species, rather than being a species-specific injury functions. Furthermore, the simulations are restricted to the Northern Hemisphere  $\geq 30^\circ\text{N}$  to secure the simulation of temperate/boreal forest and thus similar species as used for the tuning of the injury functions. However, the biomass damage experiments used to parameterise the injury function are conducted with young trees grown in monocultures. The common attempt to estimate responses of adult trees grown under natural conditions by the extrapolation of results from short-term experiments with young trees is subject to several issues, e.g. due to the differing environmental conditions and changing ozone sensitivities with increasing tree size or

age (Schaub et al., 2005; Cailleret et al., 2018). It is yet uncertain if the simulation of injury to photosynthesis based on experiments with young trees can be transferred to adult trees to obtain realistic biomass damage estimates. The effect of interspecific competition on ozone damage is not reflected in the used injury function as the experiments are conducted with monocultures. A possible shift in the community composition to more ozone tolerant species can not be simulated by O-CN or other PFT based models. This might induce an overestimation of the simulated damage.

The included injury functions are parameterised for needle-leaved and broadleaved trees (see chapter 3). Simulated grasses and crops are damaged based on the injury function for broadleaved trees because of the lack of a suitable injury function for either of them. This simplification induces a considerable error of the damage estimate in non-forest/ agricultural areas.

#### 4.4.4 Impact of the ozone deposition scheme

The tropospheric  $O_3$  concentrations used in the simulations here to force the model are provided by CTMs which report  $O_3$  concentrations in a height of approximately 45 m above the surface. The ozone deposition scheme included into O-CN uses the  $O_3$  concentration of the free atmosphere to calculate the  $O_3$  concentration at canopy level. If this step is omitted and the  $O_3$  concentration provided by the CTMs is directly used as if being at canopy level the O-CN model simulates a higher ozone uptake and twice as high damage values to GPP and C-biomass compared to simulations where the deposition scheme is applied to calculate the canopy level  $O_3$  concentration. This highlights the importance of using canopy level  $O_3$  concentrations to calculate ozone uptake and damage to prevent a considerable overestimation of ozone induced damage.

## 4.5 Conclusion

$O_3$  damage considerably reduced simulated carbon uptake (GPP) and storage (total carbon biomass) in the simulation area where the maximal impact occurs at the end of the 20th century and beginning of the 21st century respectively. The detrimental ozone impact declines during the 21st century and reaches mean regional reductions of 0-1% for GPP and 4-5% for total carbon biomass by the end of the 21st century compared to pre-industrial values. However in damage hotspots decreases in GPP of more than 8% (eastern Asia) and decreases in total carbon biomass of more than 15% (parts of Europe, eastern and western US and eastern Asia) are simulated at the end of the 21st century. Nitrogen deposition increases GPP less than  $O_3$  impacts decrease it for most of the simulated period. The increasing effect of nitrogen deposition on total carbon biomass is lower compared to the decreasing effect of  $O_3$  for the entire simulation period. Accounting for the stimulating effects of nitrogen deposition but omitting the detrimental effect of  $O_3$  might lead to an over estimation of carbon uptake and storage.

## Chapter 5

# General conclusion and outlook

This thesis studied the importance of air pollution impacts on the terrestrial carbon and nitrogen cycling. A focus is placed on the impact of tropospheric ozone concentrations and nitrogen deposition on terrestrial carbon uptake and storage.

Ozone concentrations strongly increased since pre-industrial times over the mid- and high-latitudes of Eurasia and North America from 15-25 ppb in 1860 to 40-50 ppb in the present (Akimoto, 2003). Ozone is a toxic substance that can damage plant leaves and cause a wide range of effects. Prominent adverse effects are the formation of lesions or chlorosis (Langebartels et al., 1991; Wohlgemuth et al., 2002), reductions in photosynthetic capacity (Tjoelker et al., 1995; Wittig et al., 2007) as well as in growth and yield (Grantz et al., 2006; Hayes et al., 2007; Feng and Kobayashi, 2009; Wittig et al., 2009; Leisner and Ainsworth, 2012). Previously published modelling studies estimate substantial differing damage values for the present and the future (Anav et al., 2011; Lombardozzi et al., 2015; Franz et al., 2017; Sitch et al., 2007; Oliver et al., 2018). Present day ozone induced damage is for example estimated in the range of about 8-22% (Anav et al., 2011; Lombardozzi et al., 2015; Franz et al., 2017). Future projections of ozone damage are estimated to amount about 4-23% (Sitch et al., 2007; Oliver et al., 2018).

Observed increases in ozone coincide with an increase in its precursor  $\text{NO}_x$  (nitrogen oxides) which increased for example between 1955 and 1985 by a factor of 4.5 (Cooper et al., 2014; Staehelin et al., 1994). Part of the reactive nitrogen produced in or emitted to the atmosphere is deposited back on land where it might be taken up by plants and stimulate their growth. However, the role of  $\text{NO}_x$  as precursors for ozone formation might significantly reduce the mitigating effect of anthropogenic nitrogen deposition on climate change due decreases in terrestrial net primary production caused by ozone damage to plants (Zaehle et al., 2011).

This thesis presents results acquired by the application of the updated terrestrial biosphere model O-CN. The updated version of O-CN simulates the detrimental effects of ozone as well as the growth enhancing effects of nitrogen deposition. I included an ozone deposition scheme into O-CN to obtain more realistic estimates of ozone uptake. To improve damage estimates an injury function was included into O-CN which is able to

reproduce biomass damage relationships observed in fumigation/filtration experiments.

In the subsequent sections the answers to the key research questions addressed in this thesis are summarised, limitations of the findings given and an outlook to possible future research on the topic proposed.

## 5.1 Answers to the underlying research questions

Answers to the three main research questions of this thesis is presented below. Detailed answers to the questions of this thesis are provided in chapters 2 to 4.

**What are key factors in the simulation of ozone damage that might explain the strong variation in estimated ozone induced damage estimates found in the literature and how can they be improved to obtain more reliable damage estimates?** Ozone damage to plants is simulated in this thesis by relating accumulated ozone uptake to injury in net photosynthesis or the maximum carboxylation capacity of the leaf ( $V_{cmax}$ ). The simulation of ozone uptake and the relation of the accumulated ozone uptake to plant injury are key aspects in the estimation of ozone induced damage.

Chapter 2 has demonstrated that the estimation of ozone uptake is especially sensitive to the simulated canopy conductance and the canopy ozone concentration. The ozone concentrations provided by chemical transport models (CTMs) as input for terrestrial biosphere models report ozone concentrations in approximately 45 m height and not at canopy level. Up to now a common approach has been to directly use these forcing data to calculate ozone uptake into the plant. However, to consistently simulate the transport of ozone from the atmosphere into the plant leaves, the canopy ozone concentration can be calculated from the ozone concentrations provided by CTMs by applying a ozone deposition scheme that accounts for stomatal and non-stomatal deposition of ozone. An evaluation of key parameters of the deposition scheme can indicate the reliability of the implemented scheme. The inclusion of an ozone deposition scheme into the O-CN model showed that estimates of the cumulative canopy O<sub>3</sub> uptake (CUO) are reduced by 31% compared to simulations where O<sub>3</sub> concentrations provided by a CTM are directly used to calculate ozone uptake. A scheme that accounts for both stomatal and non-stomatal ozone deposition is highly recommendable since accounting for non-stomatal deposition alone reduces the CUO by 16% (see chapter 2). Results presented in chapter 4 indicate that not using an ozone deposition scheme can lead to a doubling of the estimated ozone induced damage.

Ozone is taken up into the plant leaves via stomatal conductance. An evaluation of the modelled canopy conductance (canopy integrated stomatal conductance) can indicate if the model can simulate realistic values for this key variable in the calculation of ozone uptake. In this thesis the simulated canopy conductance was evaluated against eddy covariance data from the FLUXNET database (Baldocchi et al., 2001) and a general good agreement of the simulated and measured data could be observed (see chapter 2). However, one ought to keep in mind that canopy conductance values derived from

eddy covariance measurements are subject to a considerable range of uncertainties too (Knauer et al., 2018).

To calculate plant damage the calculated ozone uptake needs to be related to plant damage. A common approach to simulate plant damage is to injure photosynthesis. However, data that relate ozone uptake to injury in photosynthesis are scarce and only a few damage relationships are reported in the literature which relate accumulated ozone uptake to photosynthesis parameters. These damage relationships are subject to a large amount of uncertainty since the fumigation/ filtration experiments on which they base can not directly measure ozone uptake and incurred damage. Stomatal conductance and for instance net photosynthesis are measured at certain time intervals, like once per day, to estimate ozone uptake and plant injury during the experiment period. Despite the substantial inherent uncertainty in these data and damage relationships, several such damage relationships have been included into terrestrial biosphere models as injury functions to relate accumulated ozone uptake to injury of net photosynthesis or  $V_{cmax}$ . Whether the application of these injury functions enables the models to simulate realistic values of biomass damage has up to now not been investigated. The publication of the biomass dose-response relationships by Büker et al. (2015) provided an independent dataset to, for the first time, evaluate injury functions previously applied in terrestrial biosphere models. The results presented in chapter 3 show that the use of differing damage relationships as injury functions in a terrestrial biosphere model can strongly impact the estimates of incurred plant damage. No damage relationship which was previously used as an injury function in a terrestrial biosphere model was able to reproduce the biomass dose-response relationships by Büker et al. (2015). To enable improved estimates of ozone damage, I tuned injury functions to net photosynthesis and  $V_{cmax}$  which reproduce the biomass dose-response relationships by Büker et al. (2015).

The use of an injury function which is evaluated against an independent set of data and found to be able to reproduce observed damage relationships can prevent strong over- or underestimations of damage. Multi-season fumigation/ filtration experiments with trees where besides stomatal conductance and photosynthesis parameters also the change in biomass is measured, for example by measuring changes in tree diameter, could possibly help to better understand and simulate ozone impacts on carbon uptake and plant growth.

**How much impacted ozone damage and nitrogen deposition the terrestrial carbon uptake and storage in the past since pre-industrial times?** The terrestrial biosphere model O-CN, which was updated to account for ozone damage (see chapter 2) and reproduce realistic biomass damage relationships observed in fumigation/filtration experiments (see chapter 3), was applied to simulate air pollution impacts during the past period from the years 1850 to 2004.

The results presented in chapter 4 show that the effects of ozone damage on carbon uptake (GPP) and storage (total carbon biomass) of the temperate and boreal Northern Hemisphere have increased since pre-industrial times and reached peak values at the end of the 20th century and beginning of the 21st century, respectively. Compared to other

drivers of climate change like increased atmospheric CO<sub>2</sub> concentrations, air pollution impacts exert only a small impact on GPP. In the simulation of the past period, GPP was increased by atmospheric CO<sub>2</sub> concentrations by 4.4 PgC yr<sup>-1</sup> (14.8%) in 2004 compared to the reference year 1850 (mean over the simulation region 30°N to 90°N). In 2004, the last year of the simulation of the past period, ozone damage reduced GPP by ≈1.5 PgC yr<sup>-1</sup> (≈4%) compared to GPP values in 1850. The stimulating effect of nitrogen deposition on GPP and total carbon biomass steadily increases from 1850 to 2004. In the year 2004 GPP is stimulated by nitrogen deposition by 0.7 PgC yr<sup>-1</sup> (2.2%). At the end of the 20th century peak values of ozone induced damage to GPP of 8-11% are simulated to occur in the eastern US, southern Europe and eastern Asia. Regions of simulated peak increases in GPP due nitrogen deposition are located in central Europe and parts of Asia.

The simulated mean regional (30°N to 90°N) damage to GPP at the beginning of the 21st century is lower compared to estimates of net photosynthesis damage to trees estimated by meta-analyses which suggest damage values of 11% to 19% (Wittig et al., 2009; Lombardozzi et al., 2013). Simulated peak damage values in polluted areas take values close to the lowest value observed in the meta-analyses. Previous simulations by terrestrial biosphere model suggest higher reductions in GPP compared to the results presented here. Anav et al. (2011) suggest a 22% reduction in GPP for the year 2002 in the Euro-Mediterranean region, (Lombardozzi et al., 2015) estimate a 10.8% reduction of global mean GPP for present day O<sub>3</sub> concentrations and Franz et al. (2017) estimate the ozone induced reduction in GPP to amount 7.6% in Europe during the years 2001-2010.

Carbon storage is impacted stronger by elevated levels of CO<sub>2</sub> and O<sub>3</sub> compared to the simulated changes in GPP. The CO<sub>2</sub> fertilisation effect induced an increase in total carbon biomass by 18.1 PgC (22.7%) in 2004 compared to the values in 1850. Ozone is simulated to have decreased total carbon biomass by about ≈9.5 PgC (≈9%) in 2004 compared to reference year 1850. Nitrogen deposition is simulated to increase total carbon biomass by 2 PgC (2.2%) in 2004 compared to 1850 values. Nitrogen deposition exerts in relative terms an equal effect on GPP and total carbon biomass during this simulation period. Hotspot regions of air pollution impacts (nitrogen deposition and ozone) on total carbon biomass at the the end of the 20th century are southern Europe and the eastern US. Peak increases induced by nitrogen deposition amount 12-17% and peak decreases due to ozone damage 20-23%.

The simulated regional mean estimate of ozone induced damage to C-biomass is higher compared to the estimated 7% of trees grown in ambient vs. charcoal filtered air by Wittig et al. (2009) and lower compared to estimated 17% for trees grown in elevated O<sub>3</sub> vs. charcoal filtered air or a mean of 21 ppb O<sub>3</sub> (Wittig et al., 2009; Li et al., 2017). Simulated peak damage values in polluted regions are higher compared to the estimates by the meta-analyses.

During the simulation of the past period from 1850 to 2004 the stimulating effect of nitrogen deposition on GPP and total carbon biomass was outweighed by the detrimental effects of ozone damage.

**What is the extend of ozone damage and nitrogen deposition on the terrestrial carbon uptake and storage during the 21st century in simulations based on RCP scenarios?** The application of the updated O-CN model, to simulate future effects of air pollution on carbon uptake and storage, indicates that GPP is impacted less than expected from previous studies (see chapter 4). The simulated impact of air pollution by ozone and nitrogen deposition on Northern Hemisphere (30°N - 90°N) carbon uptake and storage at the end of the 21st century is minor compared to the effect of for instance elevated CO<sub>2</sub> concentrations. In the simulations here, GPP is stimulated by the CO<sub>2</sub> fertilisation effect by 22% in simulations based on RCP2.6 and by 56% in simulations based on RCP8.5 at the end of the 21st century compared to pre-industrial values. Total carbon biomass is increased by 54% under RCP2.6 and 105% under RCP8.5.

The maximum impact of ozone damage on GPP occurs at the end of the 20th century. During the simulation of the future projections period (the years 2005 to 2099) simulated ozone damage steadily decreases for both simulated pollution scenarios, RCP2.6 and RCP8.5. By the end of the 21st century GPP is increases by  $\approx 3\%$  for RCP8.5 and  $\approx 4\%$  for RCP2.6 due to reduced ozone damage compared to the values in 2005. By the end of the 21st century ozone damage is simulated to have close to zero effect on GPP on a regional mean (30°N - 90°N) compared to pre-industrial values for both investigated pollution scenarios. Only in damage hotspots, like eastern Asia, considerable damage values of more than 8% are simulated. These strongly declined regional mean ozone damage values occur because of the increased atmospheric CO<sub>2</sub> concentrations. The CO<sub>2</sub> fertilisation effect reduces stomatal conductance and peak ozone uptake rates. This causes a reduction in the cumulative canopy O<sub>3</sub> uptake above a flux threshold of 1 nmol m<sup>-2</sup> s<sup>-1</sup>, on which the damage calculations base. Even though the mean regional ozone concentrations slightly increase during the 21st century under RCP8.5, simulated damage declines due the impact of elevated levels of CO<sub>2</sub> on stomatal conductance and ozone uptake.

Previously published estimates of future ozone induced reductions in GPP amount for example 14-23% in global GPP between 1901–2100 (Sitch et al., 2007) and 4-9% in Europe by 2050 (Oliver et al., 2018). The lower estimates of future ozone induced damage here might be caused by the implementation of an ozone deposition scheme into the O-CN model. The ozone abundances provided by chemical transport models are not directly used to calculate ozone uptake, the ozone deposition scheme calculates ozone surface concentrations which are used in the calculation of ozone uptake.

Total carbon biomass is impacted stronger by ozone damage compared to GPP. Similar to GPP, total carbon biomass increases during the period of 2005 to 2099 due to reduced ozone accumulation above the flux threshold and hence reduced ozone induced damage. Total carbon biomass increases by  $\approx 4.5\%$  compared to the values in 2005 in simulations based on RCP8.5 und by  $\approx 6\%$  in simulations based on RCP2.6. The regional mean damage estimate of carbon biomass constitutes approximately  $\approx 5$  PgC ( $\approx 3.5\%$ ) and  $\approx 9$  PgC ( $\approx 5\%$ ) at the 21st century compared to pre-industrial values for RCP2.6 and RCP8.5 respectively.

Nitrogen deposition stimulated GPP in the simulation of the future projections be-

tween the years 2005-2099 by  $0.7 \text{ PgCyr}^{-1}$  (0.4%) for RCP8.5 and by  $0.3 \text{ PgCyr}^{-1}$  (0.4%) for RCP2.6. Compared to pre-industrial values (of the year 1850) nitrogen deposition stimulates GPP at the end of the 21st century by  $1.5 \text{ PgCyr}^{-1}$  (2.6%) for RCP8.5 and  $1 \text{ PgCyr}^{-1}$  (2.5%) for RCP2.6. Nitrogen deposition stimulates GPP compared to simulations run with pre-industrial deposition values mainly in Europe and Eastern Asia. At the end of the 21st century simulated increases of GPP in these regions constitute about  $80\text{-}140 \text{ gCm}^2\text{yr}^{-1}$  for simulations run based on RCP8.5. In relative terms peak increases of 10-16% are found in parts of eastern, central and northern Asia and small parts of Europe. Simulations based on RCP2.6 exhibit similar patterns compared to simulations based on RCP8.5 but show a less strong increase in GPP induced by to nitrogen deposition.

Carbon biomass is impacted stronger than GPP by nitrogen deposition between the years 2005-2099. For simulations based on RCP8.5 total carbon biomass is increased by  $4 \text{ PgC}$  (0.9%) and for simulations based on RCP2.6 by  $2.4 \text{ PgC}$  (1%). Compared to pre-industrial values total carbon biomass at the end of the 21st century is stimulated by  $6.1 \text{ PgC}$  (3.1%) under RCP8.5 and by  $4.4 \text{ PgC}$  (3.2%) under RCP2.6.

The combined impact of nitrogen deposition and ozone damage on the terrestrial carbon uptake in the Northern Hemisphere ( $30^\circ\text{N} - 90^\circ\text{N}$ ) changes during the simulation of the future projections according to the RCP scenarios. At the beginning of the simulation period ozone damage outweighs the stimulating impact of nitrogen deposition on GPP. The effects of both air pollutants on GPP approximately evens out during the period of 2030-2050. In the second half of the 21st century nitrogen deposition stronger increases GPP than  $\text{O}_3$  impacts decline it for both RCP scenarios. The impact of both air pollutants on total carbon biomass is dominated by the detrimental effects of ozone during the entire simulation period. All in all, accounting for the stimulating effects of nitrogen deposition but omitting the detrimental effect of  $\text{O}_3$  might lead to an over estimation of carbon uptake and storage.

## 5.2 Limitations

The results presented in this thesis are subject to several sources of uncertainty caused by limited understanding of the involved processes, limited computational resources and most importantly limited data availability.

Terrestrial biosphere models simulate global/ regional plant growth and nutrient cycling. The terrestrial biosphere involves a diverse set of species and a complex set of processes, but the models can only include a restricted set of both. Simplifications like grouping species into plant functional types aim to simulate mean responses of plant groups, but prevent the simulation of species interaction and composition. The necessary adaptations of O-CN to simulate ozone damage are suspect to a range of uncertainties as well. These involve approximations in the parametrisation of the deposition scheme and the injury functions and uncertainties regarding the representation of ozone damage in the model (for more details see the discussion sections in chapters 2 to 4).

Aspects which have to be neglected in the simulation approach here are that species

interaction and competition, differing genotypes, and individuals ontogeny may alter ozone impacts on plants and ecosystems (Matyssek et al., 2010). A potential ozone induced shift in forest community compositions, where ozone tolerant species or genotypes replace sensitive ones, can not be simulated by first-generation dynamic global vegetation models such as O-CN. This may lead to an overestimation of the net ozone impact on carbon storage if the parameterisation of the injury functions is entirely based on ozone-sensitive species. Furthermore, terrestrial biosphere models generally base their ozone damage calculations on injury functions derived from experiments with young trees. However, it is still uncertain whether ozone injury observed in short-term experiments with young trees can indeed be transferred to adult trees grown under natural conditions.

Forcing data used to run terrestrial biosphere models (e.g. the atmosphere composition and climate) are output data created by other models (e.g. chemical transport models or climate models) and thus are subject to a range of uncertainties as well. Furthermore as the future development of emission of air pollutants is uncertain, future projections of ozone concentrations are regularly updated and can differ considerably between different types of scenarios. Considerable differences in the projected tropospheric ozone concentrations can for example be found between the IPCC SRES scenarios and the representative concentration pathway (RCP) scenarios (Wild et al., 2012). The application of a common set of scenarios in different climate models results in different magnitudes and differing spatial patterns of future carbon uptake and storage (Ciais et al., 2013). Possible causes for this are differing representations of simulated processes in the models and their parameterisation. This suggests that the choice of model used for the simulations in this thesis also impacted the simulated estimates of ozone damage, since stomatal conductance links carbon uptake to ozone uptake and hence to potential damage.

To sum up the results presented in this thesis are obtained by using a state-of-the-art terrestrial biosphere model which as explained above is subject to a large range of uncertainties. Simulations run with such a model try to simulate the most important processes in the real world and approximate implications of induced changes in the drivers e.g. in the atmosphere composition and climate change. The simulation results by definition yield approximations of past, present or future plant growth and nutrient cycling.

### 5.3 Outlook

To better constrain the future impact of ozone damage on the terrestrial carbon sequestration and hence on climate change, a more realistic simulation of ozone induced damage, where injury calculations are based on damage-relationships for a larger set of plant types, is necessary.

The representation of ozone damage effects in terrestrial biosphere models is very basic. The availability of suitable data to parameterise ozone damage effects in terrestrial biosphere models is generally sparse and restricts up to now the inclusion of important

factors/ processes. For instance processes of ozone damage like detoxification of  $O_3$ , injury repair (Wieser and Matyssek, 2007; Ainsworth et al., 2012) and early senescence (Gielen et al., 2007; Ainsworth et al., 2012) are not accounted for in O-CN. The state-of-the-art approach to simulate the plants ability to detoxify part of the taken up ozone by the inclusion of a flux threshold is a very simplistic approach. A more realistic approach would be desirable which accounts for the need of resources to produce antioxidants, a consequent increase in respiration costs and incurred damage if the damage capacity of antioxidant production is exceeded. The collection of data on this topic are a crucial aspect in the development of more realistic ozone damage calculations. Furthermore, if more data become available on the change in ozone sensitivity between young and mature trees, the damage simulation and parameterisation of mature forests in terrestrial biosphere models might become more realistic.

The simulations of future ozone impacts in this thesis are constrained to the temperate and boreal Northern Hemisphere as the applied injury functions are derived from tree species of the respective region. More ozone fumigation/filtration experiments that focus on for instance tropical tree species are necessary to develop more suitable injury functions for terrestrial biosphere models. The development of such injury functions could enable an extension of the simulation scope and yield an updated global estimate of present day and potential future ozone damage. However, if and when such injury functions become available is up to now uncertain.

Aspects of ozone induced damage that could be investigated directly now are for instance stomatal sluggishness. Ozone induced stomatal sluggishness causes a decoupling of photosynthesis and stomatal conductance and might impact GPP and transpiration damage estimates (Paoletti and Grulke, 2010). Accounting for direct impairment of the stomata might reduce the reported reductions in transpiration (for example in Franz et al. (2017)) or even cause an increase compared to simulations with no ozone damage. Increases in stomatal conductance can decrease the plants water use efficiency and through this impact carbon uptake and storage. A basic representation of stomatal sluggishness is already now included into the O-CN model. The comparison of simulations where stomatal sluggishness is accounted for or not accounted for might indicate to which extend the terrestrial carbon and water cycle could be impacted by this process.

The impact of diurnal cycling of ozone concentrations on damage estimates is an important aspect that still lacks investigation. In our simulations here monthly mean ozone concentrations are used to force the O-CN model. However, the formation of ozone exhibits a pronounced diurnal cycle (Sanz et al., 2007), and the impact of not accounting for this diurnal cycling on ozone damage estimates is yet unclear. The comparison of simulations applying monthly mean  $O_3$  concentrations compared to simulations using hourly ozone concentrations might indicate whether the low estimates of future ozone induced damage presented in this thesis might partly be caused by the application of monthly mean ozone concentrations.

## 5.4 Final remarks

Climate change displays a major challenge for humanity. The ability of the terrestrial biosphere to store part of the carbon emitted to the atmosphere slows the growth of the atmospheric CO<sub>2</sub> concentration and thus ameliorates climate change. This thesis shows that air pollution impacts considerably decreased terrestrial carbon uptake and storage in the past. A reduction of future tropospheric ozone concentrations has the potential to lessen the ozone induced constraint on future carbon uptake and storage of the terrestrial biosphere. Air cleansing programs thus have the potential to improve human health in polluted areas as well as to a small amount mitigate climate change.



# Acknowledgements

I would like to thank all the people who made this thesis possible. In particular I would like to thank:

First of all I am very grateful to my day-to-day supervisor at the MPI for biogeochemistry Sönke Zaehle. Many thanks for the guidance, sharing your knowledge and patience especially during the extended interruptions of my work on the thesis. You have been a great supervisor.

I am very grateful to Almut Arneht for supervising my thesis and the patience during the extended interruptions of my work on the thesis.

I am grateful to Julia Pongratz and Laurens Ganzeveld for reviewing this thesis.

Many thanks goes to David Simpson for advice on the inclusion of the EMEP deposition scheme into the O-CN model.

I would like to thank everyone who shared biomass damage data of their fumigation/filtration experiments and especially Patrick Büker for mediating the sharing of the data.

Many thanks to my colleagues who created a productive work environment.

This thesis was funded by the EU Framework programme through grant no. 282910 (ECLAIRE) and the Max Planck Society for the Advancement of Science e.V. through the ENIGMA project.



# Bibliography

- Ainsworth, E. A. and Long, S. P. (2005). What have we learned from 15 years of free-air  $CO_2$  enrichment (FACE)? A meta-analytic review of the responses of photosynthesis, canopy properties and plant production to rising  $CO_2$ . *New Phytologist*, 165(2):351–372.
- Ainsworth, E. A., Yendrek, C. R., Sitch, S., Collins, W. J., and Emberson, L. D. (2012). The Effects of Tropospheric Ozone on Net Primary Productivity and Implications for Climate Change. *Annual Review of Plant Biology*, 63:637–661.
- Akimoto, H. (2003). Global Air Quality and Pollution. *Science*, 302(5651):1716–1719.
- Amann, M., Klimont, Z., and Wagner, F. (2013). Regional and Global Emissions of Air Pollutants: Recent Trends and Future Scenarios. *Annual Review of Environment and Resources*, 38:31–55.
- Ammann, C., Flechard, C., Leifeld, J., Neftel, A., and Fuhrer, J. (2007). The carbon budget of newly established temperate grassland depends on management intensity. *Agriculture, Ecosystems & Environment*, 121(1):5–20.
- Anav, A., Menut, L., Khvorostyanov, D., and Viovy, N. (2011). Impact of tropospheric ozone on the Euro-Mediterranean vegetation. *Global Change Biology*, 17(7):2342–2359.
- Arnth, A., Harrison, S. P., Zaehle, S., Tsigaridis, K., Menon, S., Bartlein, P. J., Feichter, J., Korhola, A., Kulmala, M., O’donnell, D., Schurgers, G., Sorvari, S., and Vesala, T. (2010). Terrestrial biogeochemical feedbacks in the climate system. *Nature Geoscience*, 3(8):525–532.
- Baldocchi, D., Falge, E., Gu, L., Olson, R., Hollinger, D., Running, S., Anthoni, P., Bernhofer, C., Davis, K., Evans, R., Fuentes, J., Goldstein, A., Katul, G., Law, B., Lee, X., Malhi, Y., Meyers, T., Munger, W., Oechel, W., Paw U, K. T., Pilegaard, K., Schmid, H. P., Valentini, R., Verma, S., Vesala, T., Wilson, K., and Wofsy, S. (2001). FLUXNET: A New Tool to Study the Temporal and Spatial Variability of Ecosystem-Scale Carbon Dioxide, Water Vapor, and Energy Flux Densities. *Bulletin of the American Meteorological Society*, 82(11):2415–2434.
- Ball, J., Woodrow, I., and Berry, J. (1987). A Model Predicting Stomatal Conductance and its Contribution to the Control of Photosynthesis under Different Environmental

- Conditions. In Biggins, J., editor, *Prog. Photosynthesis Res. Proc. Int. Congress 7th, Providence. 10-15 Aug 1986*, pages 221–224. Progress in Photosynthesis Research.
- Barbo, D., Chappelka, A., Somers, G., Miller-Goodman, M., and Stolte, K. (1998). Diversity of an early successional plant community as influenced by ozone. *The New Phytologist*, 138(4):653–662.
- Barnes, J. and Pfirrmann, T. (1992). The influence of  $CO_2$  and  $O_3$ , singly and in combination, on gas exchange, growth and nutrient status of radish (*Raphanus sativus* L.). *New Phytologist*, 121(3):403–412.
- Beer, C., Reichstein, M., Tomelleri, E., Ciais, P., Jung, M., Carvalhais, N., Rödenbeck, C., Arain, M. A., Baldocchi, D., Bonan, G. B., Bondeau, A., Cescatti, A., Lasslop, G., Lindroth, A., Lomas, M., Luyssaert, S., Margolis, H., Oleson, K. W., Roupsard, O., Veenendaal, E., Viovy, N., Williams, C., Woodward, F. I., and Papale, D. (2010). Terrestrial Gross Carbon Dioxide Uptake: Global Distribution and Covariation with Climate. *Science*, 329(5993):834–838.
- Berbigier, P., Bonnefond, J.-M., and Mellmann, P. (2001).  $CO_2$  and water vapour fluxes for 2 years above Euroflux forest site. *Agricultural and Forest Meteorology*, 108(3):183–197.
- Bonan, G. B. (2008). Forests and Climate Change: Forcings, Feedbacks, and the Climate Benefits of Forests. *Science*, 320(5882):1444–1449.
- Bouwman, A. F., Beusen, A. H. W., Griffioen, J., Van Groenigen, J. W., Hefting, M. M., Oenema, O., Van Puijenbroek, P. J. T. M., Seitzinger, S., Slomp, C. P., and Stehfest, E. (2013). Global trends and uncertainties in terrestrial denitrification and  $N_2O$  emissions. *Philosophical Transactions of the Royal Society of London B: Biological Sciences*, 368(1621).
- Broadmeadow, M. S. and Jackson, S. (2000). Growth responses of *Quercus petraea*, *Fraxinus excelsior* and *Pinus sylvestris* to elevated carbon dioxide, ozone and water supply. *The New Phytologist*, 146(3):437–451.
- Büker, P., Feng, Z., Uddling, J., Briolat, A., Alonso, R., Braun, S., Elvira, S., Gerosa, G., Karlsson, P., Le Thiec, D., Marzuoli, R., Mills, G., Oksanen, E., Wieser, G., , Wilkinson, M., and Emberson, L. (2015). New flux based dose-response relationships for ozone for European forest tree species. *Environmental Pollution*, 206:163–174.
- Burg, S. (1968). Ethylene, Plant Senescence and Abscission. *Plant Physiology*, 43(9 Pt B):1503–1511.
- Bussotti, F. (2008). Functional leaf traits, plant communities and acclimation processes in relation to oxidative stress in trees: a critical overview. *Global Change Biology*, 14(11):2727–2739.

- Cailleret, M., Ferretti, M., Gessler, A., Rigling, A., and Schaub, M. (2018). Ozone effects on European forest growth—Towards an integrative approach. *Journal of Ecology*, 106(4):1377–1389.
- Calatayud, V., Cerveró, J., Calvo, E., García-Breijo, F.-J., Reig-Armiñana, J., and Sanz, M. J. (2011). Responses of evergreen and deciduous *Quercus* species to enhanced ozone levels. *Environmental Pollution*, 159(1):55–63.
- Cardoso-Vilhena, J. and Barnes, J. (2001). Does nitrogen supply affect the response of wheat (*Triticum aestivum* cv. Hanno) to the combination of elevated  $CO_2$  and  $O_3$ ? *Journal of Experimental Botany*, 52(362):1901–1911.
- Chiesi, M., Maselli, F., Bindi, M., Fibbi, L., Cherubini, P., Arlotta, E., Tirone, G., Matteucci, G., and Seufert, G. (2005). Modelling carbon budget of Mediterranean forests using ground and remote sensing measurements. *Agricultural and Forest Meteorology*, 135(1-4):22–34.
- Ciais, P., Sabine, C., Bala, G., Bopp, L., Brovkin, V., Canadell, J., Chhabra, A., DeFries, R., Galloway, J., Heimann, M., Jones, C., Le Quéré, C., Myneni, R. B., Piao, S., and Thornton, P. (2013). Carbon and other biogeochemical cycles. In *Climate Change 2013: The Physical Science Basis. Contribution of Working Group I to the Fifth Assessment Report of the Intergovernmental Panel on Climate Change [Stocker, T.F., D. Qin, G.-K. Plattner, M. Tignor, S.K. Allen, J. Boschung, A. Nauels, Y. Xia, V. Bex and P.M. Midgley (eds.)]*, chapter 6, pages 465–570. Cambridge University Press, Cambridge, United Kingdom and New York, NY, USA.
- Cieslik, S. A. (2004). Ozone uptake by various surface types: a comparison between dose and exposure. *Atmospheric Environment*, 38(15):2409–2420.
- Cionni, I., Eyring, V., Lamarque, J.-F., Randel, W., Stevenson, D., Wu, F., Bodeker, G., Shepherd, T., Shindell, D., and Waugh, D. (2011). Ozone database in support of CMIP5 simulations: results and corresponding radiative forcing. *Atmospheric Chemistry and Physics*, 11(21):11267–11292.
- Collins, W., Derwent, R., Garnier, B., Johnson, C., Sanderson, M., and Stevenson, D. (2003). Effect of stratosphere-troposphere exchange on the future tropospheric ozone trend. *Journal of Geophysical Research: Atmospheres*, 108(D12).
- Cooper, O. R., Parrish, D., Ziemke, J., Balashov, N., Cupeiro, M., Galbally, I., Gilge, S., Horowitz, L., Jensen, N., Lamarque, J.-F., Naik, V., Oltmans, S., Schwab, J., Shindell, D., Thompson, A., Thouret, V., Wang, Y., and Zbinden, R. (2014). Global distribution and trends of tropospheric ozone: An observation-based review. *Elementa: Science of the Anthropocene*, 2(1):000029.
- Coyle, M., Nemitz, E., Storeton-West, R., Fowler, D., and Cape, J. N. (2009). Measurements of ozone deposition to a potato canopy. *Agricultural and Forest Meteorology*, 149(3-4):655–666.

- Curtis, P. and Wang, X. (1998). A meta-analysis of elevated  $CO_2$  effects on woody plant mass, form, and physiology. *Oecologia*, 113(3):299–313.
- Darrall, N. (1989). The effect of air pollutants on physiological processes in plants. *Plant, Cell & Environment*, 12(1):1–30.
- De Graaff, M., Van Groenigen, K., Six, J., Hungate, B., and Van Kessel, C. (2006). Interactions between plant growth and soil nutrient cycling under elevated  $CO_2$ : A meta-analysis. *Global Change Biology*, 12(11):2077–2091.
- Dentener, F., Stevenson, D., Ellingsen, K., van Noije, T., Schultz, M., Amann, M., Atherton, C., Bell, N., Bergmann, D., Bey, I., Bouwman, L., Butler, T., Cofala, J., Collins, B., Drevet, J., Doherty, R., Eickhout, B., Eskes, H., Fiore, A., Gauss, M., Hauglustaine, D., Horowitz, L., Isaksen, I. S. A., Josse, B., Lawrence, M., Krol, M., Lamarque, J. F., Montanaro, V., Müller, J. F., Peuch, V. H., Pitari, G., Pyle, J., Rast, S., Rodriguez, J., Sanderson, M., Savage, N. H., Shindell, D., Strahan, S., Szopa, S., Sudo, K., Van Dingenen, R., Wild, O., and Zeng, G. (2006). The Global Atmospheric Environment for the Next Generation. *Environmental Science & Technology*, 40(11):3586–3594.
- Derwent, R., Collins, W., Johnson, C., and Stevenson, D. (2002). Global Ozone Concentrations and Regional Air Quality. *Environmental Science & Technology*, 36(19):379–382.
- Dizengremel, P. (2001). Effects of ozone on the carbon metabolism of forest trees. *Plant Physiology and Biochemistry*, 39(9):729–742.
- Dizengremel, P., Le Thiec, D., Bagard, M., and Jolivet, Y. (2008). Ozone risk assessment for plants: Central role of metabolism-dependent changes in reducing power. *Environmental Pollution*, 156(1):11–15.
- Dlugokencky, E. and Tans, P. (2016). Trends in atmospheric carbon dioxide. *Earth System Research Laboratory, National Oceanic and Atmospheric Administration, USA*: <https://www.esrl.noaa.gov/gmd/ccgg/trends/global.html>.
- Dolman, A., Moors, E., and Elbers, J. (2002). The carbon uptake of a mid latitude pine forest growing on sandy soil. *Agricultural and Forest Meteorology*, 111(3):157–170.
- Drake, B., González-Meler, M., and Long, S. (1997). MORE EFFICIENT PLANTS: A Consequence of Rising Atmospheric  $CO_2$ ? *Annual Review of Plant Physiology and Plant Molecular Biology*, 48(1):609–639.
- Ducoudré, N. I., Laval, K., and Perrier, A. (1993). SECHIBA, a New Set of Parameterizations of the Hydrologic Exchanges at the Land-Atmosphere Interface within the LMD Atmospheric General Circulation Model. *Journal of Climate*, 6(2):248–273.

- Dufresne, J.-L., Foujols, M.-A., Denvil, S., Caubel, A., Marti, O., Aumont, O., Balkanski, Y., Bekki, S., Bellenger, H., Benshila, R., Bony, S., Bopp, L., Braconnot, P., Brockmann, P., Cadule, P., Cheruy, F., Codron, F., Cozic, A., Cugnet, D., de Noblet, N., Duvel, J.-P., Ethé, C., Fairhead, L., Fichefet, T., Flavoni, S., Friedlingstein, P., Grandpeix, J.-Y., Guez, L., Guilyardi, E., Hauglustaine, D., Hourdin, F., Idelkadi, A., Ghattas, J., Joussaume, S., Kageyama, M., Krinner, G., Labetoulle, S., Lahellec, A., Lefebvre, M.-P., Lefevre, F., Levy, C., Li, Z. X., Lloyd, J., Lott, F., Madec, G., Mancip, M., Marchand, M., Masson, S., Meurdesoif, Y., Mignot, J., Musat, I., Parouty, S., Polcher, J., Rio, C., Schulz, M., Swingedouw, D., Szopa, S., Talandier, C., Terray, P., Viovy, N., and Vuichard, N. (2013). Climate change projections using the IPSL-CM5 Earth System Model: from CMIP3 to CMIP5. *Climate Dynamics*, 40(9-10):2123–2165.
- Emberson, L., Ashmore, M., Cambridge, H., Simpson, D., and Tuovinen, J. (2000a). Modelling stomatal ozone flux across Europe. *Environmental Pollution*, 109(3):403–413.
- Emberson, L., Ashmore, M., Simpson, D., Tuovinen, J.-P., and Cambridge, H. (2001). Modelling and Mapping Ozone Deposition in Europe. *Water, Air and Soil Pollution*, 130:577–582.
- Emberson, L., Simpson, D., Tuovinen, J., Ashmore, M., and Cambridge, H. (2000b). Towards a model of ozone deposition and stomatal uptake over Europe. *EMEP MSC-W Note*, 6(2000):1–57.
- Engardt, M., Simpson, D., and Granat, L. (2017). Historical and projected (1900 to 2050) deposition of sulphur and nitrogen in europe. *submitted*.
- Falkowski, P., Scholes, R. J., Boyle, E., Canadell, J., Canfield, D., Elser, J., Gruber, N., Hibbard, K., Högberg, P., Linder, S., Mackenzie, F. T., Moore III, B., Pedersen, T., Rosenthal, Y., Seitzinger, S., Smetacek, V., and Steffen, W. (2000). The Global Carbon Cycle: A Test of Our Knowledge of Earth as a System. *Science*, 290(5490):291–296.
- Farage, P., Long, S., Lechner, E., and Baker, N. (1991). The Sequence of Change within the Photosynthetic Apparatus of Wheat following Short-Term Exposure to Ozone. *Plant Physiology*, 95(2):529.
- Fares, S., Goldstein, A., and Loreto, F. (2010). Determinants of ozone fluxes and metrics for ozone risk assessment in plants. *Journal of Experimental Botany*, 61(3):629–633.
- Fatichi, S., Leuzinger, S., and Koerner, C. (2014). Moving beyond photosynthesis: from carbon source to sink-driven vegetation modeling. *New Phytologist*, 201(4):1086–1095.
- Felzer, B., Kicklighter, D., Melillo, J., Wang, C., Zhuang, Q., and Prinn, R. (2004). Effects of ozone on net primary production and carbon sequestration in the conterminous United States using a biogeochemistry model. *Tellus B*, 56(3):230–248.

- Felzer, B., Reilly, J., Melillo, J., Kicklighter, D., Sarofim, M., Wang, C., Prinn, R., and Zhuang, Q. (2005). Future Effects of Ozone on Carbon Sequestration and Climate Change Policy Using a Global Biogeochemical Model. *Climatic Change*, 73(3):345–373.
- Feng, Z., Büker, P., Pleijel, H., Emberson, L., Karlsson, P. E., and Uddling, J. (2018). A unifying explanation for variation in ozone sensitivity among woody plants. *Global Change Biology*, 24(1):78–84.
- Feng, Z. and Kobayashi, K. (2009). Assessing the impacts of current and future concentrations of surface ozone on crop yield with meta-analysis. *Atmospheric Environment*, 43(8):1510–1519.
- Field, C., Jackson, R., and Mooney, H. (1995). Stomatal responses to increased  $CO_2$ : implications from the plant to the global scale. *Plant, Cell & Environment*, 18(10):1214–1225.
- Fiscus, E., Booker, F., and Burkey, K. (2005). Crop responses to ozone: uptake, modes of action, carbon assimilation and partitioning. *Plant, Cell & Environment*, 28(8):997–1011.
- Forkel, M., Carvalhais, N., Rödenbeck, C., Keeling, R., Heimann, M., Thonicke, K., Zaehle, S., and Reichstein, M. (2016). Enhanced seasonal  $CO_2$  exchange caused by amplified plant productivity in northern ecosystems. *Science*, 351(6274):696–699.
- Fowler, D., Coyle, M., Skiba, U., Sutton, M. A., Cape, J. N., Reis, S., Sheppard, L. J., Jenkins, A., Grizzetti, B., Galloway, J. N., Vitousek, P., Leach, A., Bouwman, A. F., Butterbach-Bahl, K., Dentener, F., Stevenson, D., Amann, M., and Voss, M. (2013). The global nitrogen cycle in the twenty-first century. *Philosophical Transactions of the Royal Society of London B: Biological Sciences*, 368(1621).
- Fowler, D., Pilegaard, K., Sutton, M., Ambus, P., Raivonen, M., Duyzer, J., Simpson, D., Fagerli, H., Fuzzi, S., Schjoerring, J., Granier, C., Neftel, A., Isaksen, I., Laj, P., Maione, M., Monks, P., Burkhardt, J., Daemmgen, U., Neiryneck, J., Personne, E., Wichink-Kruit, R., Butterbach-Bahl, K., Flechard, C., Tuovinen, J., Coyle, M., Gerosa, G., Loubet, B., Altimir, N., Gruenhage, N., Ammann, C., Cieslik, S., Paoletti, E., Mikkelsen, T., Ro-Poulsen, H., Cellier, P., Cape, J., Horváth, L., Loreto, F., Niinemets, Ü., Palmer, P., Rinne, J., Misztal, P., Nemitz, E., Nilsson, D., Pryor, S., Gallagher, M., Vesala, T., Skiba, U., Brüggemann, N., Zechmeister-Boltenstern, S., Williams, J., O’Dowd, C., Facchini, M., de Leeuw, G., Flossman, A., Chaumerliac, N., and Erisman, J. (2009). Atmospheric composition change: Ecosystems–atmosphere interactions. *Atmospheric Environment*, 43(33):5193–5267.
- Franz, M., Alonso, R., Arneth, A., Büker, P., Elvira, S., Gerosa, G., Emberson, L., Feng, Z., Le Thiec, D., Marzuoli, R., Oksanen, E., Uddling, J., Wilkinson, M., and Zaehle, S. (2018). Evaluation of simulated ozone effects in forest ecosystems against biomass damage estimates from fumigation experiments. *Biogeosciences*, 15(22):6941–6957.

- Franz, M., Simpson, D., Arneth, A., and Zaehle, S. (2017). Development and evaluation of an ozone deposition scheme for coupling to a terrestrial biosphere model. *Biogeosciences*, 14(1):45–71.
- Friedlingstein, P., Cox, P., Betts, R., Bopp, L., von Bloh, W., Brovkin, V., Cadule, P., Doney, S., Eby, M., Fung, I., Bala, G., John, J., Jones, C., Joos, F., Kato, T., Kawamiya, M., Knorr, W., Lindsay, K., Matthews, H. D., Raddatz, T., Rayner, P., Reick, C., Roeckner, E., Schnitzler, K.-G., Schnur, R., Strassmann, K., Weaver, A. J., Yoshikawa, C., and Zeng, N. (2006). Climate–Carbon Cycle Feedback Analysis: Results from the C<sup>4</sup>MIP Model Intercomparison. *Journal of Climate*, 19(14):3337–3353.
- Friend, A. (2001). Modelling canopy CO<sub>2</sub> fluxes: are ‘big-leaf’ simplifications justified? *Global Ecology and Biogeography*, 10(6):603–619.
- Friend, A. and Kiang, N. (2005). Land surface model development for the giss gcm: Effects of improved canopy physiology on simulated climate. *Journal of Climate*, 18(15):2883–2902.
- Fuhrer, J. (1994). Effects of ozone on managed pasture: I. Effects of open-top chambers on microclimate, ozone flux, and plant growth. *Environmental pollution*, 86(3):297–305.
- Fuhrer, J. and Booker, F. (2003). Ecological issues related to ozone: agricultural issues. *Environment International*, 29(2-3):141–154.
- Fusco, A. and Logan, J. (2003). Analysis of 1970–1995 trends in tropospheric ozone at Northern Hemisphere midlatitudes with the GEOS-CHEM model. *J. Geophys. Res.*, 108(4449):1988–1997.
- Galloway, J. N., Dentener, F. J., Capone, D. G., Boyer, E. W., Howarth, R. W., Seitzinger, S. P., Asner, G. P., Cleveland, C. C., Green, P., Holland, E. A., Karl, D., Michaels, A., Porter, J., Townsend, A., and Vöösmary, C. (2004). Nitrogen Cycles: Past, Present, and Future. *Biogeochemistry*, 70(2):153–226.
- Galloway, J. N., Schlesinger, W. H., Levy II, H., Michaels, A., and Schnoor, J. L. (1995). Nitrogen fixation: Anthropogenic enhancement–environmental response. *Global Biogeochemical Cycles*, 9(2):235–252.
- Gedney, N., Cox, P., Betts, R., Boucher, O., Huntingford, C., and Stott, P. (2006). Detection of a direct carbon dioxide effect in continental river runoff records. *Nature*, 439(7078):835–838.
- Gerosa, G., Cieslik, S., and Ballarin-Denti, A. (2003). Micrometeorological determination of time-integrated stomatal ozone fluxes over wheat: a case study in Northern Italy. *Atmospheric Environment*, 37(6):777–788.

- Gerosa, G., Marzuoli, R., Cieslik, S., and Ballarin-Denti, A. (2004). Stomatal ozone fluxes over a barley field in Italy. "Effective exposure" as a possible link between exposure-and flux-based approaches. *Atmospheric Environment*, 38(15):2421–2432.
- Gerosa, G., Vitale, M., Finco, A., Manes, F., Denti, A. B., and Cieslik, S. (2005). Ozone uptake by an evergreen Mediterranean forest (*Quercus ilex*) in Italy. Part I: Micrometeorological flux measurements and flux partitioning. *Atmospheric Environment*, 39(18):3255–3266.
- Gielen, B., Löw, M., Deckmyn, G., Metzger, U., Franck, F., Heerdt, C., Matyssek, R., Valcke, R., and Ceulemans, R. (2007). Chronic ozone exposure affects leaf senescence of adult beech trees: a chlorophyll fluorescence approach. *Journal of Experimental Botany*, 58(4):785–795.
- Gilmanov, T., Soussana, J., Aires, L., Allard, V., Ammann, C., Balzarolo, M., Barcza, Z., Bernhofer, C., Campbell, C., Cernusca, A., Cescatti, A., Clifton-Brown, J., Dirks, B., Dore, S., Eugster, W., Fuhrer, J., Gimeno, C., Gruenwald, T., Haszpra, L., Hensen, A., Ibrom, A., Jacobs, A., Jones, M., Lanigan, G., Laurila, T., Lohila, A., Manca, G., Marcolla, B., Nagy, Z., Pilegaard, K., Pinter, K., Pio, C Raschi, A., Rogiers, N., Sanz, M., Stefani, P., Sutton, M., Tuba, Z., Valentini, R., Williams, M., and Wohlfahrt, G. (2007). Partitioning European grassland net ecosystem  $CO_2$  exchange into gross primary productivity and ecosystem respiration using light response function analysis. *Agriculture, Ecosystems & Environment*, 121(1–2):93–120.
- Grace, J. (2004). Understanding and managing the global carbon cycle. *Journal of Ecology*, 92(2):189–202.
- Granier, A., Ceschia, E., Damesin, C., Dufrêne, E., Epron, D., Gross, P., Lebaube, S., Le Dantec, V., Le Goff, N., Lemoine, D., Lucot, E., Ottorini, J., Pontailler, J., and Saugier, B. (2000). The carbon balance of a young Beech forest. *Functional ecology*, 14(3):312–325.
- Grantz, D., Gunn, S., and VU, H. (2006).  $O_3$  impacts on plant development: a meta-analysis of root/shoot allocation and growth. *Plant, Cell & Environment*, 29(7):1193–1209.
- Grünwald, T. and Bernhofer, C. (2007). A decade of carbon, water and energy flux measurements of an old spruce forest at the Anchor Station Tharandt. *Tellus B*, 59(3):387–396.
- Grünzweig, J., Lin, T., Rotenberg, E., Schwartz, A., and Yakir, D. (2003). Carbon sequestration in arid-land forest. *Global Change Biology*, 9(5):791–799.
- Guderian, R. (1977). *Air Pollution. Phytotoxicity of Acidic Gases and Its Significance in Air Pollution Control*. Springer-Verlag, New York.

- Gurney, K. R., Baker, D., Rayner, P., and Denning, S. (2008). Interannual variations in continental-scale net carbon exchange and sensitivity to observing networks estimated from atmospheric  $CO_2$  inversions for the period 1980 to 2005. *Global Biogeochemical Cycles*, 22(3).
- Hanson, P., Samuelson, L., Wullschleger, S., Tabberer, T., and Edwards, G. (1994). Seasonal patterns of light-saturated photosynthesis and leaf conductance for mature and seedling *Quercus rubra* L. foliage: differential sensitivity to ozone exposure. *Tree Physiology*, 14(12):1351–1366.
- Hardacre, C., Wild, O., and Emberson, L. (2015). An evaluation of ozone dry deposition in global scale chemistry climate models. *Atmospheric Chemistry and Physics*, 15(11):6419–6436.
- Hayes, F., Jones, M., Mills, G., and Ashmore, M. (2007). Meta-analysis of the relative sensitivity of semi-natural vegetation species to ozone. *Environmental Pollution*, 146(3):754–762.
- Hayes, F., Wagg, S., Mills, G., Wilkinson, S., and Davies, W. (2012). Ozone effects in a drier climate: implications for stomatal fluxes of reduced stomatal sensitivity to soil drying in a typical grassland species. *Global Change Biology*, 18(3):948–959.
- Heagle, A., Body, D., and Heck, W. (1973). An Open-Top Field Chamber to Assess the Impact of Air Pollution on Plants. *Journal of Environmental Quality*, 2(3):365–368.
- Heath, R. (1994). Possible mechanisms for the inhibition of photosynthesis by ozone. *Photosynthesis Research*, 39(3):439–451.
- Heath, R., Lefohn, A., and Musselman, R. (2009). Temporal processes that contribute to nonlinearity in vegetation responses to ozone exposure and dose. *Atmospheric Environment*, 43(18):2919–2928.
- Heinsch, F. A., Running, S. W., Kimball, J. S., Nemani, R. R., Davis, K. J., Bolstad, P. V., Cook, B. D., Desai, A. R., Ricciuto, D. M., Law, B. E., Oechel, W. C., Wofsy, S. C., Dunn, A. L., Munger, J. W., Baldocchi, D. D., Hollinger, D. Y., Richardson, A. D., Stoy, P. C., Siqueira, M. B. S., Monson, R. K., Burns, S. P., and Flanagan, L. B. (2006). Evaluation of remote sensing based terrestrial productivity from modis using regional tower eddy flux network observations. *IEEE Transactions on Geoscience and Remote Sensing*, 44(7):1908–1925.
- Helton, J. and Davis, F. (2002). Illustration of Sampling-Based Methods for Uncertainty and Sensitivity Analysis. *Risk Analysis*, 22(3):591–622.
- Hempel, S., Frieler, K., Warszawski, L., Schewe, J., and Piontek, F. (2013). A trend-preserving bias correction—the ISI-MIP approach. *Earth System Dynamics*, 4(2):219–236.

- Hurttt, G. C., Chini, L. P., Frohking, S., Betts, R. A., Feddema, J., Fischer, G., Fisk, J. P., Hibbard, K., Houghton, R. A., Janetos, A., Jones, C. D., Kindermann, G., Kinoshita, T., Klein Goldewijk, K., Riahi, K., Shevliakova, E., Smith, S., Stehfest, E., Thomson, A., Thornton, P., van Vuuren, D. P., and Wang, Y. P. (2011). Harmonization of land-use scenarios for the period 1500–2100: 600 years of global gridded annual land-use transitions, wood harvest, and resulting secondary lands. *Climatic Change*, 109(1):117.
- Hyvönen, R., Ågren, G., Linder, S., Persson, T., Cotrufo, M., Ekblad, A., Freeman, M., Grelle, A., Janssens, I., Jarvis, P., Kellomäki, S., Lindroth, A., Loustau, D., Lundmark, T., Norby, R. J., Oren, R., Pilegaard, K., Ryan, M. G., Sigurdsson, B. D., Strömgren, M., van Oijen, M., and Wallin, G. (2007). The likely impact of elevated [CO<sub>2</sub>], nitrogen deposition, increased temperature and management on carbon sequestration in temperate and boreal forest ecosystems: a literature review. *New Phytologist*, 173(3):463–480.
- Isebrands, J., McDonald, E., Kruger, E., Hendrey, G., Percy, K., Pregitzer, K., Sober, J., and Karnosky, D. (2001). Growth responses of *Populus tremuloides* clones to interacting elevated carbon dioxide and tropospheric ozone. *Environmental Pollution*, 115(3):359–371.
- Jenkin, M. (2008). Trends in ozone concentration distributions in the UK since 1990: Local, regional and global influences. *Atmospheric Environment*, 42(21):5434–5445.
- Joos, F. and Spahni, R. (2008). Rates of change in natural and anthropogenic radiative forcing over the past 20,000 years. *Proceedings of the National Academy of Sciences*, 105(5):1425–1430.
- Jung, M., Reichstein, M., Margolis, H., Cescatti, A., Richardson, A., Arain, M., Arneth, A., Bernhofer, C., Bonal, D., Chen, J., Gianelle, D., Gobron, N., Kiely, G., Kutsch, W., Lasslop, G., Law, B., Lindroth, A., Merbold, L., Montagnani, L., Moors, E., Papale, D., Sottocornola, M., Vaccari, F., and Williams, C. (2011). Global patterns of land-atmosphere fluxes of carbon dioxide, latent heat, and sensible heat derived from eddy covariance, satellite, and meteorological observations. *Journal of Geophysical Research: Biogeosciences (2005–2012)*, 116(G3). G00J07.
- Jung, M., Reichstein, M., Schwalm, C. R., Huntingford, C., Sitch, S., Ahlström, A., Arneth, A., Camps-Valls, G., Ciais, P., Friedlingstein, P., Gans, F., Ichii, K., Jain, A. K., Kato, E., Papale, D., Poulter, B., Raduly, B., Rödenbeck, C., Tramontana, G., Viovy, N., Ping Wang, Y., Weber, U., Zaehle, S., and Zeng, N. (2017). Compensatory water effects link yearly global land CO<sub>2</sub> sink changes to temperature. *Nature*, 541(7638):516–520.
- Kangasjärvi, J., Talvinen, J., Utriainen, M., and Karjalainen, R. (1994). Plant defence systems induced by ozone. *Plant, Cell & Environment*, 17(7):783–794.
- Karlsson, P. E., Uddling, J., Braun, S., Broadmeadow, M., Elvira, S., Gimeno, B., Le Thiec, D., Oksanen, E., Vandermeiren, K., Wilkinson, M., and Emberson, L.

- (2004). New critical levels for ozone effects on young trees based on AOT40 and simulated cumulative leaf uptake of ozone. *Atmospheric Environment*, 38(15):2283–2294.
- Karnosky, D. F., Zak, D. R., Pregitzer, K. S., Awmack, C. S., Bockheim, J. G., Dickson, R. E., Hendrey, G. R., Host, G. E., King, J. S., Kopper, B. J., Kruger, E. L., Kubiske, M. E., Lindroth, R. L., Mattson, W. J., Mcdonald, E. P., Noormets, A., Oksanen, E., Parsons, W. F. J., Percy, K. E., Podila, G. K., Riemenschneider, D. E., Sharma, P., Thakur, R., Söber, A., Söber, J., Jones, W. S., Anttonen, S., Vapaavuori, E., Mankovska, B., Heilman, W., and Isebrands, J. G. (2003). Tropospheric  $O_3$  moderates responses of temperate hardwood forests to elevated  $CO_2$ : a synthesis of molecular to ecosystem results from the Aspen FACE project. *Functional Ecology*, 17(3):289–304.
- Keenan, T., Sabate, S., and Gracia, C. (2010). Soil water stress and coupled photosynthesis–conductance models: Bridging the gap between conflicting reports on the relative roles of stomatal, mesophyll conductance and biochemical limitations to photosynthesis. *Agricultural and Forest Meteorology*, 150(3):443–453.
- Keronen, P., Reissell, A., Rannik, U., Pohja, T., Siivola, E., Hiltunen, V., Hari, P., Kulmala, M., and Vesala, T. (2003). Ozone flux measurements over a Scots pine forest using eddy covariance method: performance evaluation and comparison with flux-profile method. *Boreal Environment Research*, 8(4):425–444.
- King, J., Kubiske, M., Pregitzer, K., Hendrey, G., McDonald, E., Giardina, C., Quinn, V., and Karnosky, D. (2005). Tropospheric  $O_3$  compromises net primary production in young stands of trembling aspen, paper birch and sugar maple in response to elevated atmospheric  $CO_2$ . *New Phytologist*, 168(3):623–636.
- Kjellstrom, E., Nikulin, G., Hansson, U., Strandberg, G., and Ullerstig, A. (2011). 21st century changes in the European climate: uncertainties derived from an ensemble of regional climate model simulations. *Tellus Series A-Dynamic Meteorology and Oceanography*, 63(1):24–40.
- Klingberg, J., Danielsson, H., Simpson, D., and Pleijel, H. (2008). Comparison of modelled and measured ozone concentrations and meteorology for a site in south-west Sweden: Implications for ozone uptake calculations. *Environmental Pollution*, 115(1):99–111.
- Klingberg, J., Engardt, M., Karlsson, P., Langner, J., and Pleijel, H. (2014). Declining risk of ozone impacts on vegetation in europe 1990–2050 due to reduced precursor emissions in a changed climate. *Biogeosciences Discussions*, 11(1):625–655.
- Knauer, J., Werner, C., and Zaehle, S. (2015). Evaluating stomatal models and their atmospheric drought response in a land surface scheme: A multibiome analysis. *Journal of Geophysical Research: Biogeosciences*, 120(10):1894–1911.

- Knauer, J., Zaehle, S., Medlyn, B. E., Reichstein, M., Williams, C. A., Migliavacca, M., De Kauwe, M. G., Werner, C., Keitel, C., Kolari, P., Limousin, J.-M., and Linderson, M.-L. (2018). Towards physiologically meaningful water-use efficiency estimates from eddy covariance data. *Global Change Biology*, 24(2):694–710.
- Knauer, J., Zaehle, S., Reichstein, M., Medlyn, B. E., Forkel, M., Hagemann, S., and Werner, C. (2017). The response of ecosystem water-use efficiency to rising atmospheric  $CO_2$  concentrations: sensitivity and large-scale biogeochemical implications. *New Phytologist*, 213(4):1654–1666.
- Kolb, T. and Matyssek, R. (2001). Limitations and perspectives about scaling ozone impacts in trees. *Environmental Pollution*, 115(3):373–393.
- Kozovits, A. R., Matyssek, R., Blaschke, H., Göttelein, A., and Grams, T. E. (2005). Competition increasingly dominates the responsiveness of juvenile beech and spruce to elevated  $CO_2$  and/or  $O_3$  concentrations throughout two subsequent growing seasons. *Global Change Biology*, 11(9):1387–1401.
- Krinner, G., Viovy, N., de Noblet-Ducoudré, N., Ogée, J., Polcher, J., Friedlingstein, P., Ciais, P., Sitch, S., and Prentice, I. (2005). A dynamic global vegetation model for studies of the coupled atmosphere-biosphere system. *Global Biogeochemical Cycles*, 19(1):GB1015.
- Kronfuß, G., Polle, A., Tausz, M., Havranek, W., and Wieser, G. (1998). Effects of ozone and mild drought stress on gas exchange, antioxidants and chloroplast pigments in current-year needles of young Norway spruce [*Picea abies* (L.) Karst.]. *Trees-Structure and Function*, 12(8):482–489.
- Krupa, S., Grünhage, L., Jäger, H., Nosal, M., Manning, W., Legge, A., and Hanewald, K. (1995). Ambient ozone ( $O_3$ ) and adverse crop response: A unified view of cause and effect. *Environmental Pollution*, 87(1):119–126.
- Kubiske, M., Quinn, V., Marquardt, P., and Karnosky, D. (2007). Effects of Elevated Atmospheric  $CO_2$  and/or  $O_3$  on Intra-and Interspecific Competitive Ability of Aspen. *Plant Biology*, 9(2):342–355.
- Kuenen, J., Denier van der Gon, H., Visschedijk, A., van der Brugh, H., and van Gijlswijk, R. (2011). Macc european emission inventory for the years 2003-2007. TNO Report TNO-060-UT-2011-00588, TNO, Utrecht, The Netherlands, www.tno.nl.
- Kutsch, W. L., Kolle, O., Rebmann, C., Knohl, A., Ziegler, W., and Schulze, E.-D. (2008). Advection and resulting  $CO_2$  exchange uncertainty in a tall forest in central Germany. *Ecological Applications*, 18(6):1391–1405.
- Lagergren, F., Lindroth, A., Dellwik, E., Ibrom, A., Lankreijer, H., Launiainen, S., Mölder, M., Kolari, P., Pilegaard, K., and Vesala, T. (2008). Biophysical controls on  $CO_2$  fluxes of three Northern forests based on long-term eddy covariance data. *Tellus B*, 60(2):143–152.

- Laisk, A., Kull, O., and Moldau, H. (1989). Ozone Concentration in Leaf Intercellular Air Spaces is Close to Zero. *Plant Physiology*, 90(3):1163–1167.
- Lamarque, J. F., Bond, T. C., Eyring, V., Granier, C., Heil, A., Klimont, Z., Lee, D., Lioussé, C., Mieville, A., Owen, B., Schultz, M. G., Shindell, D., Smith, S. J., Stehfest, E., Van Aardenne, J., Cooper, O. R., Kainuma, M., Mahowald, N., McConnell, J. R., Naik, V., Riahi, K., and van Vuuren, D. P. (2010). Historical (1850-2000) gridded anthropogenic and biomass burning emissions of reactive gases and aerosols: methodology and application. *Atmos. Chem. Physics*, 10(15):7017–7039.
- Langebartels, C., Kerner, K., Leonardi, S., Schraudner, M., Trost, M., Heller, W., and Sandermann Jr, H. (1991). Biochemical Plant Responses to Ozone: I. Differential Induction of Polyamine and Ethylene Biosynthesis in Tobacco. *Plant Physiology*, 95(3):882.
- Le Quéré, C., Andrew, R. M., Canadell, J. G., Sitch, S., Korsbakken, J. I., Peters, G. P., Manning, A. C., Boden, T. A., Tans, P. P., Houghton, R. A., Keeling, R. F., Alin, S., Andrews, O. D., Anthoni, P., Barbero, L., Bopp, L., Chevallier, F., Chini, L. P., Ciais, P., Currie, K., Delire, C., Doney, S. C., Friedlingstein, P., Gkritzalis, T., Harris, I., Hauck, J., Haverd, V., Hoppema, M., Klein Goldewijk, K., Jain, A. K., Kato, E., Körtzinger, A., Landschützer, P., Lefèvre, N., Lenton, A., Lienert, S., Lombardozzi, D., Melton, J. R., Metzl, N., Millero, F., Monteiro, P. M. S., Munro, D. R., Nabel, J. E. M. S., Nakaoka, S.-i., O'Brien, K., Olsen, A., Omar, A. M., Ono, T., Pierrot, D., Poulter, B., Rödenbeck, C., Salisbury, J., Schuster, U., Schwinger, J., Séférian, R., Skjelvan, I., Stocker, B. D., Sutton, A. J., Takahashi, T., Tian, H., Tilbrook, B., van der Laan-Luijkx, I. T., van der Werf, G. R., Viovy, N., Walker, A. P., Wiltshire, A. J., and Zaehle, S. (2016). Global carbon budget 2016. *Earth System Science Data*, 8(2):605–649.
- Leakey, A., Ainsworth, E., Bernacchi, C., Rogers, A., Long, S., and Ort, D. (2009). Elevated CO<sub>2</sub> effects on plant carbon, nitrogen, and water relations: six important lessons from FACE. *Journal of Experimental Botany*, 60(10):2859–2876.
- LeBauer, D. and Treseder, K. (2008). Nitrogen limitation of net primary productivity in terrestrial ecosystems is globally distributed. *Ecology*, 89(2):371–379.
- Leisner, C. and Ainsworth, E. (2012). Quantifying the effects of ozone on plant reproductive growth and development. *Global Change Biology*, 18(2):606–616.
- Li, P., Feng, Z., Catalayud, V., Yuan, X., Xu, Y., and Paoletti, E. (2017). A meta-analysis on growth, physiological and biochemical responses of woody species to ground-level ozone highlights the role of plant functional types. *Plant, Cell & Environment*, 40(10):2369–2380.
- Lindroth, A., Klemetsson, L., Grelle, A., Weslien, P., and Langvall, O. (2008). Measurement of net ecosystem exchange, productivity and respiration in three spruce forests in Sweden shows unexpectedly large soil carbon losses. *Biogeochemistry*, 89(1):43–60.

- Lombardozzi, D., Levis, S., Bonan, G., Hess, P., and Sparks, J. (2015). The Influence of Chronic Ozone Exposure on Global Carbon and Water Cycles. *Journal of Climate*, 28(1):292–305.
- Lombardozzi, D., Levis, S., Bonan, G., and Sparks, J. (2012a). Predicting photosynthesis and transpiration responses to ozone: decoupling modeled photosynthesis and stomatal conductance. *Biogeosciences*, 9:3113–3130.
- Lombardozzi, D., Sparks, J., Bonan, G., and Levis, S. (2012b). Ozone exposure causes a decoupling of conductance and photosynthesis: implications for the Ball-Berry stomatal conductance model. *Oecologia*, 169(3):651–659.
- Lombardozzi, D., Sparks, J. P., and Bonan, G. (2013). Integrating O<sub>3</sub> influences on terrestrial processes: photosynthetic and stomatal response data available for regional and global modeling. *Biogeosciences*, 10(11):6815–6831.
- LRTAP-Convention (2017). *Manual on Methodologies and Criteria for Modelling and Mapping Critical Loads and Levels; and Air Pollution Effects, Risks and Trends*. <https://icpvegetation.ceh.ac.uk/>.
- Luo, Y., Hui, D., and Zhang, D. (2006). Elevated CO<sub>2</sub> stimulates net accumulations of carbon and nitrogen in land ecosystems: a meta-analysis. *Ecology*, 87(1):53–63.
- Luyssaert, S., Inglima, I., Jung, M., Richardson, A. D., Reichstein, M., Papale, D., Piao, S., SCHULZE, E.-D., Wingate, L., Matteucci, G., Aragao, L., Aubinet, M., Beer, C., Bernhofer, C., Black, K. G., Bonal, D., Bonnefond, J. M., Chambers, J., Ciais, P., Cook, B., Davis, K. J., Dolman, A. J., Gielen, B., Goulden, M., Grace, J., Granier, A., Grelle, A., Griffis, T., Grünwald, T., Guidolotti, G., Hanson, P. J., Harding, R., Hollinger, D. Y., Hutyyra, L. R., Kolari, P., Kruijt, B., Kutsch, W., Lagergren, F., Laurila, T., Law, B. E., Le Maire, G., Lindroth, A., Loustau, D., Malhi, Y., Mateus, J., Migliavacca, M., Misson, L., Montagnani, L., Moncrieff, J., Moors, E., Munger, J. W., Nikinmaa, E., Ollinger, S. V., Pita, G., Rebmann, C., Roupsard, O., Saigusa, N., Sanz, M. J., Seufert, G., Sierra, C., Smith, M. L., Tang, J., Valentini, R., Vesala, T., and Janssens, I. A. (2007). CO<sub>2</sub> balance of boreal, temperate, and tropical forests derived from a global database. *Global Change Biology*, 13(12):2509–2537.
- Marcolla, B., Pitacco, A., and Cescatti, A. (2003). Canopy Architecture and Turbulence Structure in a Coniferous Forest. *Boundary-Layer Meteorology*, 108(1):39–59.
- Mareckova, K., Wankmüller, R., Pinterits, M., and Moosman, L. (2013). Inventory Review 2013. Stage 1 and 2 and review of gridded data. EMEP/CEIP Technical Report 1/2013, EEA/CEIP Vienna.
- Marenco, A., Gouget, H., Nédélec, P., Pagés, J., and Karcher, F. (1994). Evidence of a long-term increase in tropospheric ozone from Pic du Midi data series: Consequences: Positive radiative forcing. *Journal of Geophysical Research: Atmospheres* (1984–2012), 99(D8):16617–16632.

- Marzuoli, R., Gerosa, G., Desotgiu, R., Bussotti, F., and Denti, A. B. (2009). Ozone fluxes and foliar injury development in the ozone-sensitive poplar clone Oxford (*Populus maximowiczii* x *Populus berolinensis*): a dose-response analysis. *Tree physiology*, 29(1):67–76.
- Marzuoli, R., Monga, R., Finco, A., and Gerosa, G. (2016). Biomass and physiological responses of *Quercus robur* (L.) young trees during 2 years of treatments with different levels of ozone and nitrogen wet deposition. *Trees*, 30(6):1995–2010.
- Massman, W. (1998). A review of the molecular diffusivities of  $H_2O$ ,  $CO_2$ ,  $CH_4$ ,  $CO$ ,  $O_3$ ,  $SO_2$ ,  $NH_3$ ,  $N_2O$ ,  $NO$ , and  $NO_2$  in air,  $O_2$  and  $N_2$  near STP. *Atmospheric Environment*, 32(6):1111–1127.
- Matyssek, R., Karnosky, D. F., Wieser, G., Percy, K., Oksanen, E., Grams, T. E. E., Kubiske, M., Hanke, D., and Pretzsch, H. (2010). Advances in understanding ozone impact on forest trees: Messages from novel phytotron and free-air fumigation studies. *Environmental Pollution*, 158(6, SI):1990–2006.
- McAinsh, M., Evans, N., Montgomery, L., and North, K. (2002). Calcium signalling in stomatal responses to pollutants. *New Phytologist*, 153(3):441–447.
- McKay, M. D., Beckman, R. J., and Conover, W. J. (1979). Comparison of Three Methods for Selecting Values of Input Variables in the Analysis of Output from a Computer Code. *Technometrics*, 21(2):239–245.
- McManus, M. (2012). *Annual Plant Reviews, the Plant Hormone Ethylene*, volume 44. Wiley-Blackwell.
- Medlyn, B., Barton, C., Broadmeadow, M., Ceulemans, R., De Angelis, P., Forstreuter, M., Freeman, M., Jackson, S., Kellomäki, S., Laitat, E., et al. (2001). Stomatal conductance of forest species after long-term exposure to elevated  $CO_2$  concentration: A synthesis. *New Phytologist*, 149(2):247–264.
- Medlyn, B. E., Badeck, F. W., De Pury, D. G. G., Barton, C. V. M., Broadmeadow, M., Ceulemans, R., De Angelis, P., Forstreuter, M., Jach, M. E., Kellomäki, S., Laitat, E., Marek, M., Philippot, S., Rey, A., Strassmeyer, J., Laitinen, K., Liozon, R., Portier, B., Roberntz, P., Wang, K., and Jstbid, P. G. (1999). Effects of elevated [ $CO_2$ ] on photosynthesis in European forest species: a meta-analysis of model parameters. *Plant, Cell & Environment*, 22(12):1475–1495.
- Meinshausen, M., Smith, S. J., Calvin, K., Daniel, J. S., Kainuma, M., Lamarque, J.-F., Matsumoto, K., Montzka, S., Raper, S., Riahi, K., Thomson, A., Velders, G. J. M., and van Vuuren, D. P. (2011). The RCP greenhouse gas concentrations and their extensions from 1765 to 2300. *Climatic Change*, 109(1-2):213.
- Meleux, F., Solmon, F., and Giorgi, F. (2007). Increase in summer European ozone amounts due to climate change. *Atmospheric Environment*, 41(35):7577–7587.

- Melillo, J., Steudler, P., Aber, J., Newkirk, K., Lux, H., Bowles, F., Catricala, C., Magill, A., Ahrens, T., and Morrisseau, S. (2002). Soil Warming and Carbon-Cycle Feedbacks to the Climate System. *Science*, 298(5601):2173–2176.
- Melillo, J. M., Butler, S., Johnson, J., Mohan, J., Steudler, P., Lux, H., Burrows, E., Bowles, F., Smith, R., Scott, L., Vario, C., Hill, T., Burton, A., Zhou, Y.-M., and Tang, J. (2011). Soil warming, carbon–nitrogen interactions, and forest carbon budgets. *Proceedings of the National Academy of Sciences*, 108(23):9508–9512.
- Migliavacca, M., Meroni, M., Manca, G., Matteucci, G., Montagnani, L., Grassi, G., Zenone, T., Teobaldelli, M., Godeed, I., Colombo, R., and Seufert, G. (2009). Seasonal and interannual patterns of carbon and water fluxes of a poplar plantation under peculiar eco-climatic conditions. *Agricultural and Forest Meteorology*, 149(9):1460–1476.
- Mikkelsen, T. N., Ro-Poulsen, H., Hovmand, M. F., Jensen, N. O., Pilegaard, K., and Egeløv, A. H. (2004). Five-year measurements of ozone fluxes to a Danish Norway spruce canopy. *Atmospheric Environment*, 38(15):2361–2371.
- Mills, G., Hayes, F., Simpson, D., Emberson, L., Norris, D., Harmens, H., and Büker, P. (2011a). Evidence of widespread effects of ozone on crops and (semi-) natural vegetation in Europe (1990–2006) in relation to AOT40-and flux-based risk maps. *Global Change Biology*, 17(1):592–613.
- Mills, G., Hayes, F., Wilkinson, S., and Davies, W. (2009). Chronic exposure to increasing background ozone impairs stomatal functioning in grassland species. *Global Change Biology*, 15(6):1522–1533.
- Mills, G., Pleijel, H., Braun, S., Büker, P., Bermejo, V., Calvo, E., Danielsson, H., Emberson, L., Fernández, I., Grünhage, L., Harmens, H., Hayes, F., Karlsson, P., and Simpson, D. (2011b). New stomatal flux-based critical levels for ozone effects on vegetation. *Atmospheric Environment*, 45(28):5064–5068.
- Monteith, J. and Unsworth, M. (2007). *Principles of environmental physics*. Academic Press.
- Morison, J. (1998). Stomatal response to increased  $CO_2$  concentration. *Journal of Experimental Botany*, 49(Special Issue):443–452.
- Moss, R. H., Edmonds, J. A., Hibbard, K. A., Manning, M. R., Rose, S. K., Van Vuuren, D. P., Carter, T. R., Emori, S., Kainuma, M., Kram, T., Meehl, G. A., Mitchell, J. F. B., Nakicenovic, N., Riahi, K., Smith, S. J., Stouffer, R. J., Thomson, A. M., Weyant, J. P., and Wilbanks, T. J. (2010). The next generation of scenarios for climate change research and assessment. *Nature*, 463(7282):747.
- Mott, K. (1988). Do Stomata Respond to  $CO_2$  Concentrations Other than Intercellular? *Plant Physiology*, 86(1):200–203.

- Musselman, R., Lefohn, A., Massman, W., and Heath, R. (2006). A critical review and analysis of the use of exposure-and flux-based ozone indices for predicting vegetation effects. *Atmospheric Environment*, 40(10):1869–1888.
- Musselman, R. and Minnick, T. (2000). Nocturnal stomatal conductance and ambient air quality standards for ozone. *Atmospheric Environment*, 34(5):719–733.
- Musselman, R., Younglove, T., and McCool, P. (1994). Response of *Phaseolus vulgaris* L. to differing ozone regimes having identical total exposure. *Atmospheric Environment*, 28(16):2727–2731.
- Nakicenovic, N., Alcamo, J., Grubler, A., Riahi, K., Roehrl, R., Rogner, H.-H., and Victor, N. (2000). *Special report on emissions scenarios (SRES), a special report of Working Group III of the intergovernmental panel on climate change*. Cambridge University Press.
- New, M., Hulme, M., and Jones, P. (1999). Representing Twentieth-Century Space-Time Climate Variability. Part I: Development of a 1961-90 Mean Monthly Terrestrial Climatology. *Journal of climate*, 12(3):829–856.
- Niinemets, Ü., Keenan, T. F., and Hallik, L. (2015). A worldwide analysis of within-canopy variations in leaf structural, chemical and physiological traits across plant functional types. *New Phytologist*, 205(3):973–993.
- Noormets, A., Kull, O., Sôber, A., Kubiske, M., and Karnosky, D. (2010). Elevated  $CO_2$  response of photosynthesis depends on ozone concentration in aspen. *Environmental Pollution*, 158(4):992–999.
- Noormets, A., Sober, A., Pell, E., Dickson, R., Podila, G., Sober, J., Isebrands, J., and Karnosky, D. (2001). Stomatal and non-stomatal limitation to photosynthesis in two trembling aspen (*Populus tremuloides* Michx.) clones exposed to elevated  $CO_2$  and/or  $O_3$ . *Plant, Cell & Environment*, 24(3):327–336.
- Norby, R. (1998). Nitrogen deposition: a component of global change analyses. *New Phytologist*, 139(1):189–200.
- Norby, R., Cotrufo, M., Ineson, P., O'Neill, E., and Canadell, J. (2001). Elevated  $CO_2$ , litter chemistry, and decomposition: a synthesis. *Oecologia*, 127(2):153–165.
- Nunn, A., Weiser, G., Reiter, I., Häberle, K., Grote, R., Havranek, W., and Matyssek, R. (2006). Testing the unifying theory of ozone sensitivity with mature trees of *Fagus sylvatica* and *Picea abies*. *Tree Physiology*, 26(11):1391–1403.
- Oliver, R. J., Mercado, L. M., Sitch, S., Simpson, D., Medlyn, B. E., Lin, Y.-S., and Folberth, G. A. (2018). Large but decreasing effect of ozone on the European carbon sink. *Biogeosciences*, 15(13):4245–4269.

- Overmyer, K., Tuominen, H., Kettunen, R., Betz, C., Langebartels, C., Sandermann, H., and Kangasjärvi, J. (2000). Ozone-sensitive arabidopsis rcd1 mutant reveals opposite roles for ethylene and jasmonate signaling pathways in regulating superoxide-dependent cell death. *The Plant Cell Online*, 12(10):1849–1862.
- Padro, J. (1996). Summary of ozone dry deposition velocity measurements and model estimates over vineyard, cotton, grass and deciduous forest in summer. *Atmospheric Environment*, 30(13):2363–2369.
- Paoletti, E., Contran, N., Bernasconi, P., Günthardt-Goerg, M. S., and Vollenweider, P. (2010). Erratum to” Structural and physiological responses to ozone in Manna ash (*Fraxinus ornus* L.) leaves of seedlings and mature trees under controlled and ambient conditions”. *Science of the Total Environment*, 408(8):2014–2024.
- Paoletti, E. and Grulke, N. (2005). Does living in elevated  $CO_2$  ameliorate tree response to ozone? A review on stomatal responses. *Environmental Pollution*, 137(3):483–493.
- Paoletti, E. and Grulke, N. (2010). Ozone exposure and stomatal sluggishness in different plant physiognomic classes. *Environmental Pollution*, 158(8):2664–2671.
- Parrish, D. D., Law, K. S., Staehelin, J., Derwent, R., Cooper, O. R., Tanimoto, H., Volz-Thomas, A., Gilge, S., Scheel, H.-E., Steinbacher, M., and Chan, E. (2012). Long-term changes in lower tropospheric baseline ozone concentrations at northern mid-latitudes. *Atmospheric Chemistry and Physics*, 12(23):11485–11504.
- Pathre, U., Sinha, A., Shirke, P., and Sane, P. (1998). Factors determining the midday depression of photosynthesis in trees under monsoon climate. *Trees-Structure and Function*, 12(8):472–481.
- Pell, E., Schlaghaufer, C., and Arteca, R. (1997). Ozone-induced oxidative stress: Mechanisms of action and reaction. *Physiologia Plantarum*, 100(2):264–273.
- Percy, K., Nosal, M., Heilman, W., Dann, T., Sober, J., Legge, A., and Karnosky, D. (2007). New exposure-based metric approach for evaluating  $O_3$  risk to North American aspen forests. *Environmental Pollution*, 147(3):554–566.
- Pereira, J. S., Mateus, J. A., Aires, L. M., Pita, G., Pio, C., David, J. S., Andrade, V., Banza, J., David, T. S., Paço, T. A., and Rodrigues, A. (2007). Net ecosystem carbon exchange in three contrasting Mediterranean ecosystems? The effect of drought. *Biogeosciences*, 4(5):791–802.
- Pleijel, H., Danielsson, H., Emberson, L., Ashmore, M., and Mills, G. (2007). Ozone risk assessment for agricultural crops in Europe: further development of stomatal flux and flux–response relationships for European wheat and potato. *Atmospheric Environment*, 41(14):3022–3040.

- Pleijel, H., Danielsson, H., Ojanperä, K., Temmerman, L. D., Högy, P., Badiani, M., and Karlsson, P. (2004). Relationships between ozone exposure and yield loss in European wheat and potato—a comparison of concentration-and flux-based exposure indices. *Atmospheric Environment*, 38(15):2259–2269.
- Rebmann, C., Anthoni, P., Falge, E., Göckede, M., Mangold, A., Subke, J.-A., Thomas, C., Wichura, B., Schulze, E.-D., Tenhunen, J., and Foken, T. (2004). Carbon budget of a spruce forest ecosystem. In *Biogeochemistry of Forested Catchments in a Changing Environment*, pages 143–159. Springer.
- Reich, P. (1987). Quantifying plant response to ozone: a unifying theory. *Tree Physiology*, 3(1):63–91.
- Reich, P. B., Hobbie, S. E., and Lee, T. D. (2014). Plant growth enhancement by elevated  $CO_2$  eliminated by joint water and nitrogen limitation. *Nature Geoscience*, 7(12):920–924.
- Reichstein, M., Falge, E., Baldocchi, D., Papale, D., Aubinet, M., Berbigier, P., Bernhofer, C., Buchmann, N., Gilmanov, T., Granier, A., Grünwald, T., Havránková, K., Ilvesniemi, H., Janous, D., Knohl, A., Laurila, T., Lohila, A., Loustau, D., Matteucci, G., Meyers, T., Miglietta, F., Ourcival, J., Pumpanen, J., Rambal, S., Rotenberg, E., Sanz, M., Tenhunen, J., Seufert, G., Vaccari, F., Vesala, T., Yakir, D., and Valentini, R. (2005). On the separation of net ecosystem exchange into assimilation and ecosystem respiration: review and improved algorithm. *Global Change Biology*, 11(9):1424–1439.
- Ren, W., Tian, H., Liu, M., Zhang, C., Chen, G., Pan, S., Felzer, B., and Xu, X. (2007). Effects of tropospheric ozone pollution on net primary productivity and carbon storage in terrestrial ecosystems of China. *Journal of Geophysical Research: Atmospheres*, 112(D22).
- Ren, W., Tian, H., Tao, B., Chappelka, A., Sun, G., Lu, C., Liu, M., Chen, G., and Xu, X. (2011). Impacts of tropospheric ozone and climate change on net primary productivity and net carbon exchange of China’s forest ecosystems. *Global Ecology and Biogeography*, 20(3):391–406.
- Rey, A., Pegoraro, E., Tedeschi, V., De Parri, I., Jarvis, P. G., and Valentini, R. (2002). Annual variation in soil respiration and its components in a coppice oak forest in Central Italy. *Global Change Biology*, 8(9):851–866.
- Richardson, A. D., Aubinet, M., Barr, A. G., Hollinger, D. Y., Ibrom, A., Lasslop, G., and Reichstein, M. (2012). Uncertainty quantification. In *Eddy Covariance*, pages 173–209. Springer.
- Riikonen, J., Lindsberg, M.-M., Holopainen, T., Oksanen, E., Lappi, J., Peltonen, P., and Vapaavuori, E. (2004). Silver birch and climate change: variable growth and

- carbon allocation responses to elevated concentrations of carbon dioxide and ozone. *Tree Physiology*, 24(11):1227–1237.
- Roeckner, E., Brokopf, R., Esch, M., Giorgetta, M., Hagemann, S., Kornbluh, L., Manzini, E., Schlese, U., and Schulzweida, U. (2006). Sensitivity of Simulated Climate to Horizontal and Vertical Resolution in the ECHAM5 Atmosphere Model. *Journal of Climate*, 19(16):3771–3791.
- Samuelson, L. and Kelly, J. (1996). Carbon partitioning and allocation in northern red oak seedlings and mature trees in response to ozone. *Tree Physiology*, 16(10):853–858.
- Samuelson, L., Kelly, J., Mays, P., and Edwards, G. (1996). Growth and nutrition of *Quercus rubra* l. seedlings and mature trees after three seasons of ozone exposure. *Environmental Pollution*, 91(3):317–323.
- Samuelsson, P., Jones, C. G., Willen, U., Ullerstig, A., Gollvik, S., Hansson, U., Jansson, C., Kjellstrom, E., Nikulin, G., and Wyser, K. (2011). The Rossby Centre Regional Climate model RCA3: model description and performance. *Tellus Series A: Dynamic Meteorology and Oceanography*, 63(1):4–23.
- Sanz, M., Calatayud, V., and Sánchez-Peña, G. (2007). Measures of ozone concentrations using passive sampling in forests of South Western Europe. *Environmental Pollution*, 145(3):620–628.
- Sanz, M., Carrara, A., Gimeno, C., Bucher, A., and Lopez, R. (2004). Effects of a dry and warm summer conditions on  $CO_2$  and Energy fluxes from three Mediterranean ecosystems. In *Geophysical Research Abstracts*, volume 6, page 3239.
- Schaub, M., Skelly, J., Zhang, J., Ferdinand, J., Savage, J., Stevenson, R., Davis, D., and Steiner, K. (2005). Physiological and foliar symptom response in the crowns of *Prunus serotina*, *Fraxinus americana* and *Acer rubrum* canopy trees to ambient ozone under forest conditions. *Environmental Pollution*, 133(3):553–567.
- Scherer-Lorenzen, M., Schulze, E.-D., Don, A., Schumacher, J., and Weller, E. (2007). Exploring the functional significance of forest diversity: A new long-term experiment with temperate tree species (BIOTREE). *Perspectives in Plant Ecology, Evolution and Systematics*, 9(2):53–70.
- Schimel, D. S. (1995). Terrestrial ecosystems and the carbon cycle. *Global Change Biology*, 1(1):77–91.
- Sicard, P., Anav, A., Marco, A. D., and Paoletti, E. (2017). Projected global ground-level ozone impacts on vegetation under different emission and climate scenarios. *Atmospheric Chemistry and Physics*, 17(19):12177–12196.
- Simpson, D., Arneth, A., Mills, G., Solberg, S., and Uddling, J. (2014a). Ozone - the persistent menace: interactions with the n cycle and climate change. *Current Opinion in Environmental Sustainability*, 9-10:9–19.

- Simpson, D., Ashmore, M., Emberson, L., and Tuovinen, J.-P. (2007). A comparison of two different approaches for mapping potential ozone damage to vegetation. A model study. *Environmental Pollution*, 146(3):715–725.
- Simpson, D., Benedictow, A., Berge, H., Bergström, R., Emberson, L., Fagerli, H., Flechard, C., Hayman, G., Gauss, M., Jonson, J., Jenkin, M. E., Nyíri, A., Richter, C., Semeena, V. S., Tsyro, S., Tuovinen, J.-P., Valdebenito, A., and Wind, P. (2012). The EMEP MSC-W chemical transport model—technical description. *Atmospheric Chemistry and Physics*, 12:7825–7865.
- Simpson, D., Christensen, J., Engardt, M., Geels, C., Nyiri, A., Soares, J., Sofiev, M., Wind, P., , and Langner, J. (2014b). Impacts of climate and emission changes on nitrogen deposition in europe: a multi-model study. *Atmospheric Chemistry and Physics*, 14:6995–7017.
- Simpson, D., Tuovinen, J.-P., Emberson, L., and Ashmore, M. (2003). Characteristics of an ozone deposition module II: sensitivity analysis. *Water, Air and Soil Pollution*, 143:123–137.
- Simpson, D., Winiwarter, W., Börjesson, G., Cinderby, S., Ferreira, A., Guenther, A., Hewitt, C. N., Janson, R., Khalil, M. A. K., Owen, S., Pierce, T. E., Puxbaum, H., Shearer, M., Skiba, U., Steinbrecher, R., Tarrasón, L., and Öquist, M. G. (1999). Inventorying emissions from nature in Europe. *Journal of Geophysical Research: Atmospheres*, 104(D7):8113–8152.
- Sitch, S., Cox, P., Collins, W., and Huntingford, C. (2007). Indirect radiative forcing of climate change through ozone effects on the land-carbon sink. *Nature*, 448(7155):791–794.
- Sitch, S., Friedlingstein, P., Gruber, N., Jones, S. D., Murray-Tortarolo, G., Ahlström, A., Doney, S. C., Graven, H., Heinze, C., Huntingford, C., Levis, S., Levy, P. E., Lomas, M., Poulter, B., Viovy, N., Zaehle, S., Zeng, N., Arneeth, A., Bonan, G., Bopp, L., Canadell, J. G., Chevallier, F., Ciais, P., Ellis, R., Gloor, M., Peylin, P., Piao, S. L., Le Quéré, C., Smith, B., Zhu, Z., and Myneni, R. (2015). Recent trends and drivers of regional sources and sinks of carbon dioxide. *Biogeosciences*, 12(3):653–679.
- Smirnoff, N. (1996). Botanical briefing: The function and metabolism of ascorbic acid in plants. *Annals of Botany*, 78(6):661–669.
- Staehelin, J., Thudium, J., Buehler, R., Volz-Thomas, A., and Graber, W. (1994). Trends in surface ozone concentrations at Arosa (Switzerland). *Atmospheric Environment*, 28(1):75–87.
- Stan, H. and Schicker, S. (1982). Effect of repetitive ozone treatment on bean plants—stress ethylene production and leaf necrosis. *Atmospheric Environment (1967)*, 16(9):2267–2270.

- Stevenson, D. S., Dentener, F. J., Schultz, M. G., Ellingsen, K., van Noije, T. P. C., Wild, O., Zeng, G., Amann, M., Atherton, C. S., Bell, N., Bergmann, D. J., Bey, I., Butler, T., Cofala, J., Collins, W. J., Derwent, R. G., Doherty, R. M., Drevet, J., Eskes, H. J., Fiore, A. M., Gauss, M., Hauglustaine, D. A., Horowitz, L. W., Isaksen, I. S. A., Krol, M. C., Lamarque, J.-F., Lawrence, M. G., Montanaro, V., Müller, J.-F., Pitari, G., Prather, M. J., Pyle, J. A., Rast, S., Rodriguez, J. M., Sanderson, M. G., Savage, N. H., Shindell, D. T., Strahan, S. E., Sudo, K., and Szopa, S. (2006). Multimodel ensemble simulations of present-day and near-future tropospheric ozone. *Journal of Geophysical Research*, 111(D8):D08301.
- Stocker, T. (2014). *Climate change 2013: the physical science basis: Working Group I contribution to the Fifth assessment report of the Intergovernmental Panel on Climate Change*. Cambridge University Press.
- Stohl, A., Aamaas, B., Amann, M., Baker, L. H., Bellouin, N., Berntsen, T. K., Boucher, O., Cherian, R., Collins, W., Daskalakis, N., Dusinska, M., Eckhardt, S., Fuglestvedt, J. S., Harju, M., Heyes, C., Hodnebrog, Ø., Hao, J., Im, U., Kanakidou, M., Klimont, Z., Kupiainen, K., Law, K. S., Lund, M. T., Maas, R., MacIntosh, C. R., Myhre, G., Myriokefalitakis, S., Oľivié, D., Quaas, J., Quennehen, B., Raut, J.-C., Rumbold, S. T., Samset, B. H., Schulz, M., Seland, Ø., Shine, K. P., Skeie, R. B., Wang, S., Yttri, K. E., and Zhu, T. (2015). Evaluating the climate and air quality impacts of short-lived pollutants. *Atmospheric Chemistry and Physics*, 15(18):10529–10566.
- Sun, G., McLaughlin, S. B., Porter, J. H., Uddling, J., Mulholland, P. J., Adams, M. B., and Pederson, N. (2012). Interactive influences of ozone and climate on streamflow of forested watersheds. *Global Change Biology*, 18(11):3395–3409.
- Suni, T., Rinne, J., Reissell, A., Altimir, N., Keronen, P., Rannik, U., Maso, M., Kulmala, M., and Vesala, T. (2003). Long-term measurements of surface fluxes above a Scots pine forest in Hyytiälä, southern Finland, 1996-2001. *Boreal Environment Research*, 8(4):287–302.
- Talhelm, A. F., Pregitzer, K. S., Kubiske, M. E., Zak, D. R., Company, C. E., Burton, A. J., Dickson, R. E., Hendrey, G. R., Isebrands, J. G., Lewin, K. F., Nagy, J., and Karnosky, D. F. (2014). Elevated carbon dioxide and ozone alter productivity and ecosystem carbon content in northern temperate forests. *Global Change Biology*, 20(8):2492–2504.
- Tausz, M., Grulke, N., and Wieser, G. (2007). Defense and avoidance of ozone under global change. *Environmental Pollution*, 147(3):525–531.
- Tedeschi, V., Rey, A., Manca, G., Valentini, R., Jarvis, P. G., and Borghetti, M. (2006). Soil respiration in a Mediterranean oak forest at different developmental stages after coppicing. *Global Change Biology*, 12(1):110–121.
- Tingey, D., Standley, C., and Field, R. (1976). Stress ethylene evolution: A measure of ozone effects on plants. *Atmospheric Environment (1967)*, 10(11):969–974.

- Tirone, G., Dore, S., Matteucci, G., Greco, S., and Valentini, R. (2003). Evergreen mediterranean forests. carbon and water fluxes, balances, ecological and ecophysiological determinants. In *Fluxes of carbon, water and energy of European forests*, pages 125–149. Springer.
- Tjoelker, M., Volin, J., Oleksyn, J., and Reich, P. (1995). Interaction of ozone pollution and light effects on photosynthesis in a forest canopy experiment. *Plant, Cell & Environment*, 18(8):895–905.
- Tuovinen, J.-P., Ashmore, M., Emberson, L., and Simpson, D. (2004). Testing and improving the EMEP ozone deposition module. *Atmospheric Environment*, 38(15):2373–2385.
- Tuovinen, J.-P., Emberson, L., and Simpson, D. (2009). Modelling ozone fluxes to forests for risk assessment: status and prospects. *Annals of Forest Science*, 66(4):1–14.
- Tuovinen, J.-P., Simpson, D., Emberson, L., Ashmore, M., and Gerosa, G. (2007). Robustness of modelled ozone exposures and doses. *Environmental Pollution*, 146(3):578–586.
- Tuovinen, J.-P., Simpson, D., Mikkelsen, T., Emberson, L., Ashmore, M., Aurela, M., Cambridge, H., Hovmand, M., Jensen, N., Laurila, T., Pilegaard, K., and Ro-Poulsen, H. (2001). Comparisons of measured and modelled ozone deposition to forests in Northern Europe. *Water, Air and Soil Pollution: Focus*, 1(5-6):263–274.
- Uddling, J., Hogg, A., Teclaw, R., Carroll, M., and Ellsworth, D. (2010). Stomatal uptake of  $O_3$  in aspen and aspen-birch forests under free-air  $CO_2$  and  $O_3$  enrichment. *Environmental Pollution*, 158(6):2023–2031.
- Utriainen, J. and Holopainen, T. (2001). Nitrogen availability modifies the ozone responses of Scots pine seedlings exposed in an open-field system. *Tree Physiology*, 21(16):1205–1213.
- van Aardenne, J. A., Dentener, F. J., Olivier, J. G. J., Goldewijk, C. G. M. K., and Lelieveld, J. (2001). A  $1^\circ \times 1^\circ$  resolution data set of historical anthropogenic trace gas emissions for the period 1890–1990. *Global Biogeochemical Cycles*, 15(4):909–928.
- van Vuuren, D. P., Edmonds, J., Kainuma, M., Riahi, K., Thomson, A., Hibbard, K., Hurtt, G. C., Kram, T., Krey, V., Lamarque, J.-F., Masui, T., Meinshausen, M., Nakicenovic, N., Smith, S. J., and Rose, S. K. (2011). The representative concentration pathways: an overview. *Climatic Change*, 109(1):5.
- Vickers, C. E., Gershenson, J., Lerdau, M. T., and Loreto, F. (2009). A unified mechanism of action for volatile isoprenoids in plant abiotic stress. *Nature Chemical Biology*, 5(5):283–291.
- Vingarzan, R. (2004). A review of surface ozone background levels and trends. *Atmospheric Environment*, 38(21):3431–3442.

- Vitale, M., Gerosa, G., Ballarin-Denti, A., Manes, F., Denti, A. B., and Cieslik, S. (2005). Ozone uptake by an evergreen mediterranean forest (*Quercus ilex* L.) in Italy—Part II: flux modelling. Upscaling leaf to canopy ozone uptake by a process-based model. *Atmospheric Environment*, 39(18):3267–3278.
- Wang, B., Shugart, H. H., Shuman, J. K., and Lerdau, M. T. (2016). Forests and ozone: productivity, carbon storage, and feedbacks. *Scientific Reports*, 6:22133.
- Wieser, G. and Havranek, W. (1995). Environmental control of ozone uptake in *Larix decidua* Mill.: a comparison between different altitudes. *Tree Physiology*, 15(4):253–258.
- Wieser, G., Hecke, K., Tausz, M., Haberle, K., Grams, T., and Matyssek, R. (2002). The role of antioxidative defense in determining ozone sensitivity of Norway spruce (*Picea abies* (L.) Karst.) across tree age: Implications for the sun-and shade-crown. *PHYTON-HORN*, 42(3):245–254.
- Wieser, G. and Matyssek, R. (2007). Linking ozone uptake and defense towards a mechanistic risk assessment for forest trees. *New Phytologist*, 174(1):7–9.
- Wieser, G., Matyssek, R., Kostner, B., Oberhuber, W., and Köstner, B. (2003). Quantifying ozone uptake at the canopy level of spruce, pine and larch trees at the alpine timberline: an approach based on sap flow measurement. *Environmental Pollution*, 126(1):5–8.
- Wild, O., Fiore, A. M., Shindell, D., Doherty, R., Collins, W., Dentener, F., Schultz, M., Gong, S., MacKenzie, I., Zeng, G., Hess, P., Duncan, B. N., Bergmann, D. J., Szopa, S., Jonson, J. E., Keating, T. J., and Zuber, A. (2012). Modelling future changes in surface ozone: a parameterized approach. *Atmospheric Chemistry and Physics*, 12(4):2037–2054.
- Wilkinson, S. and Davies, W. (2009). Ozone suppresses soil drying-and abscisic acid (ABA)-induced stomatal closure via an ethylene-dependent mechanism. *Plant, Cell & Environment*, 32(8):949–959.
- Wilson, K., Goldstein, A., Falge, E., Aubinet, M., Baldocchi, D., Berbigier, P., Bernhofer, C., Ceulemans, R., Dolman, H., Field, C., Grelle, A., Ibrom, A., Law, B., Kowalski, A., Meyers, T., Moncrieff, J., Monson, R., Oechel, W., Tenhunen, J., Valentini, R., and Verma, S. (2002). Energy balance closure at FLUXNET sites. *Agricultural and Forest Meteorology*, 113(1–4):223–243.
- Wittig, V., Ainsworth, E., and Long, S. (2007). To what extent do current and projected increases in surface ozone affect photosynthesis and stomatal conductance of trees? A meta-analytic review of the last 3 decades of experiments. *Plant, Cell & Environment*, 30(9):1150–1162.

- Wittig, V., Ainsworth, E., Naidu, S., Karnosky, D., and Long, S. (2009). Quantifying the impact of current and future tropospheric ozone on tree biomass, growth, physiology and biochemistry: a quantitative meta-analysis. *Global Change Biology*, 15(2):396–424.
- Wohlfahrt, G., Anderson-Dunn, M., Bahn, M., Balzarolo, M., Berninger, F., Campbell, C., Carrara, A., Cescatti, A., Christensen, T., Dore, S., Eugster, W., Friborg, T., Furger, M., Gianelle, D., Gimeno, C., Hargreaves, K., Hari, P., Haslwanter, A., Johansson, T., Marcolla, B., Milford, C., Nagy, Z., Nemitz, E., Rogiers, N., Sanz, M., Siegwolf, R., Susiluoto, S., Sutton, M., Tuba, Z., Ugolini, F., Valentini, R., Zorer, R., and Cernusca, A. (2008a). Biotic, Abiotic, and Management Controls on the Net Ecosystem  $CO_2$  Exchange of European Mountain Grassland Ecosystems. *Ecosystems*, 11(8):1338–1351.
- Wohlfahrt, G., Hammerle, A., Haslwanter, A., Bahn, M., Tappeiner, U., and Cernusca, A. (2008b). Seasonal and inter-annual variability of the net ecosystem  $CO_2$  exchange of a temperate mountain grassland: Effects of weather and management. *Journal of Geophysical Research: Atmospheres*, 113(D8). D08110.
- Wohlgenuth, H., Mittelstrass, K., Kschieschan, S., Bender, J., Weigel, H., Overmyer, K., Kangasjärvi, J., Sandermann, H., and Langebartels, C. (2002). Activation of an oxidative burst is a general feature of sensitive plants exposed to the air pollutant ozone. *Plant, Cell & Environment*, 25(6):717–726.
- Wustman, B., Oksanen, E., Karnosky, D., Noormets, A., Isebrands, J., Pregitzer, K., Hendrey, G., Sober, J., and Podila, G. (2001). Effects of elevated  $CO_2$  and  $O_3$  on aspen clones varying in  $O_3$  sensitivity: can  $CO_2$  ameliorate the harmful effects of  $O_3$ ? *Environmental Pollution*, 115(3):473–481.
- Yendrek, C. R., Leisner, C. P., and Ainsworth, E. A. (2013). Chronic ozone exacerbates the reduction in photosynthesis and acceleration of senescence caused by limited N availability in *Nicotiana sylvestris*. *Global Change Biology*, 19(10):3155–3166.
- Zaehle, S., Ciais, P., Friend, A. D., and Prieur, V. (2011). Carbon benefits of anthropogenic reactive nitrogen offset by nitrous oxide emissions. *Nature Geoscience*, 4(9):601–605.
- Zaehle, S. and Friend, A. (2010). Carbon and nitrogen cycle dynamics in the O-CN land surface model: 1. Model description, site-scale evaluation, and sensitivity to parameter estimates. *Global Biogeochemical Cycles*, 24(1):GB1005.
- Zak, D. R., Pregitzer, K. S., Kubiske, M. E., and Burton, A. J. (2011). Forest productivity under elevated  $CO_2$  and  $O_3$ : positive feedbacks to soil N cycling sustain decade-long net primary productivity enhancement by  $CO_2$ . *Ecology Letters*, 14(12):1220–1226.
- Zhang, L., Brook, J., and Vet, R. (2003). A revised parameterization for gaseous dry deposition in air-quality models. *Atmospheric Chemistry and Physics*, 3(6):2067–2082.

Zhang, R., Lei, W., Tie, X., and Hess, P. (2004). Industrial emissions cause extreme urban ozone diurnal variability. *Proceedings of the National Academy of Sciences of the United States of America*, 101(17):6346–6350.

# Appendix

The papers on which chapter 2 and 3 of this thesis build have been published in an open access journal and are attached in the following.



# Development and evaluation of an ozone deposition scheme for coupling to a terrestrial biosphere model

Martina Franz<sup>1,2</sup>, David Simpson<sup>4,5</sup>, Almut Arneth<sup>6</sup>, and Sönke Zaehle<sup>1,3</sup>

<sup>1</sup>Biogeochemical Integration Department, Max Planck Institute for Biogeochemistry, Jena, Germany

<sup>2</sup>International Max Planck Research School (IMPRS) for Global Biogeochemical Cycles, Jena, Germany

<sup>3</sup>Michael Stifel Center Jena for Data-driven and Simulation Science, Jena, Germany

<sup>4</sup>EMEP MSC-W, Norwegian Meteorological Institute, Oslo, Norway

<sup>5</sup>Department of Earth & Space Sciences, Chalmers University of Technology, Gothenburg, Sweden

<sup>6</sup>Karlsruhe Institute of Technology (KIT), Department of Atmospheric Environmental Research (IMK-IFU), Garmisch-Partenkirchen, Germany

*Correspondence to:* Martina Franz (mfranz@bgc-jena.mpg.de)

Received: 18 July 2016 – Published in Biogeosciences Discuss.: 28 July 2016

Revised: 11 November 2016 – Accepted: 12 December 2016 – Published: 6 January 2017

**Abstract.** Ozone ( $O_3$ ) is a toxic air pollutant that can damage plant leaves and substantially affect the plant's gross primary production (GPP) and health. Realistic estimates of the effects of tropospheric anthropogenic  $O_3$  on GPP are thus potentially important to assess the strength of the terrestrial biosphere as a carbon sink. To better understand the impact of ozone damage on the terrestrial carbon cycle, we developed a module to estimate  $O_3$  uptake and damage of plants for a state-of-the-art global terrestrial biosphere model called OCN. Our approach accounts for ozone damage by calculating (a)  $O_3$  transport from 45 m height to leaf level, (b)  $O_3$  flux into the leaf, and (c) ozone damage of photosynthesis as a function of the accumulated  $O_3$  uptake over the lifetime of a leaf.

A comparison of modelled canopy conductance, GPP, and latent heat to FLUXNET data across European forest and grassland sites shows a general good performance of OCN including ozone damage. This comparison provides a good baseline on top of which ozone damage can be evaluated. In comparison to literature values, we demonstrate that the new model version produces realistic  $O_3$  surface resistances,  $O_3$  deposition velocities, and stomatal to total  $O_3$  flux ratios. A sensitivity study reveals that key metrics of the air-to-leaf  $O_3$  transport and  $O_3$  deposition, in particular the stomatal  $O_3$  uptake, are reasonably robust against uncertainty in the underlying parameterisation of the deposition scheme. Nevertheless, correctly estimating canopy conductance plays a

pivotal role in the estimate of cumulative  $O_3$  uptake. We further find that accounting for stomatal and non-stomatal uptake processes substantially affects simulated plant  $O_3$  uptake and accumulation, because aerodynamic resistance and non-stomatal  $O_3$  destruction reduce the predicted leaf-level  $O_3$  concentrations. Ozone impacts on GPP and transpiration in a Europe-wide simulation indicate that tropospheric  $O_3$  impacts the regional carbon and water cycling less than expected from previous studies. This study presents a first step towards the integration of atmospheric chemistry and ecosystem dynamics modelling, which would allow for assessing the wider feedbacks between vegetation ozone uptake and tropospheric ozone burden.

## 1 Introduction

Tropospheric ozone ( $O_3$ ) is a highly reactive and toxic gas. It enters the plants mainly through the stomata of the leaf, where it forms reactive oxygen species (ROs), which have the potential to damage the leaf. While leaves possess physiological pathways to produce compounds like ascorbate and polyamines, which help to neutralise the oxidising power of ROs (Kronfuß et al., 1998; Kangasjärvi et al., 1994; Tausz et al., 2007), ozone injury may occur when the leaf's antioxidant system becomes overwhelmed (Wieser and Matyssek, 2007).

In western Europe, tropospheric O<sub>3</sub> levels increased approximately by a factor 2 to 5 from pre-industrial values to the 1990s (Cooper et al., 2014; Marenco et al., 1994; Staehelin et al., 1994) (although the low values at the start of this period are very uncertain) and approximately doubled between 1950 and 1990s in the Northern Hemisphere (Parrish et al., 2012; Cooper et al., 2014). The major causes for this increased O<sub>3</sub> formation are the increased emission of O<sub>3</sub> precursor trace gases such as NO<sub>x</sub> and CO, primarily from combustion sources, non-methane volatile organic compounds from anthropogenic sources (combustion, solvents), and methane emissions from agriculture and industry (Fusco and Logan, 2003; Vingarzan, 2004). For instance, in western Europe, NO<sub>x</sub> emissions rose by a factor of 4.5 between 1955 and 1985 (Staehelin et al., 1994). In addition, downward transport of O<sub>3</sub> from the stratosphere to the troposphere (Vingarzan, 2004; Young et al., 2013) and intercontinental transport (Vingarzan, 2004; Jenkin, 2008; Fiore et al., 2009) can increase local and regional O<sub>3</sub> concentrations.

A commonly observed consequence of elevated levels of O<sub>3</sub> exposure is a decline in net photosynthesis (Morgan et al., 2003; Wittig et al., 2007), which may result from the damage of the photosynthetic apparatus or increased respiration due to the production of defence compounds and investments in injury repair (Wieser and Matyssek, 2007; Ainsworth et al., 2012). The reduction in net photosynthesis results in reduced growth and hence a reduced leaf area and plant biomass (Morgan et al., 2003; Lombardozzi et al., 2013; Wittig et al., 2009). The tight coupling between photosynthesis and stomatal conductance further affects canopy conductance, and thereby transpiration rates (Morgan et al., 2003; Wittig et al., 2009; Lombardozzi et al., 2013), likely affecting the ecosystem water balance.

Due to its phytotoxic effect, elevated O<sub>3</sub> levels as a consequence of anthropogenic air pollution may affect the land carbon cycle and potentially reduce the net land carbon uptake capacity (Sitch et al., 2007; Arneth et al., 2010; Simpson et al., 2014a), which currently corresponds to about a quarter of the anthropogenic fossil fuel emissions as a result of a sustained imbalance between photosynthetic carbon uptake and carbon loss through respiration and disturbance processes (Le Quéré et al., 2015). However, the extent to which O<sub>3</sub> affects plant health regionally and thereby alters terrestrial biogeochemistry and the terrestrial water balance is still subject of large uncertainty (Simpson et al., 2014a).

A number of O<sub>3</sub> exposure indices have been proposed to assess the potential detrimental effect of tropospheric O<sub>3</sub> on the plants (LRTAP Convention, 2010; Mills et al., 2011b). In Europe, the standard method of these indices is the concentration-based AOTX (ppb h) (accumulated O<sub>3</sub> concentration over a threshold of  $X$  ppb), which relates the free-air O<sub>3</sub> concentration to observed plant damage. Models assessing ozone damage to gross or net primary production based on AOTX have been used for many years and indicate that substantial reduction in plant growth and carbon

sequestration occurs globally and may reach reductions of more than 40% at O<sub>3</sub> hotspots (Felzer et al., 2004, 2005; Ren et al., 2011; Anav et al., 2011).

A significant caveat of concentration-based assessments of ozone toxicity effects is that species differ vastly in their canopy conductance as well as regional provenances of species. Stomatal control of the leaf gas exchange regulates photosynthesis and varies, inter alia, with plant-specific photosynthetic capacity and intrinsic water-use efficiency of photosynthesis; phenology; and environmental factors such as incident light, atmospheric vapour pressure deficit (VPD), and air temperature. The consequent differences in stomatal conductance implies that the actual O<sub>3</sub> dose, and thus the level of ozone-related damage, differs between species exposed to similar atmospheric O<sub>3</sub> concentrations (Wieser and Havranek, 1995). The O<sub>3</sub> dose, which is the integral of the instantaneous O<sub>3</sub> stomatal flux over a given period of time, has been observed to strongly correlate with the amount of injury of a plant suggesting that plants with higher stomatal conductance are subject to higher doses and hence more susceptible to injury (Reich, 1987; Wittig et al., 2009).

Accounting for the O<sub>3</sub> dose rather than the O<sub>3</sub> exposure in assessments of ozone damage results in diverging regional patterns of ozone damage, as regions with the highest exposure (O<sub>3</sub> concentrations) do not always coincide with regions of high uptake (Emberson et al., 2000; Mills et al., 2011a; Simpson et al., 2007). Regions with low AOT40 (AOTX above a threshold of 40 ppb) values might show moderate to high values of O<sub>3</sub> uptake because the flux approach accounts for climatic conditions that enable high stomatal conductances and hence high values of O<sub>3</sub> uptake (Mills et al., 2011a). Observed ozone damage in the field seems to be better correlated with flux-based risk assessment compared to concentration-based methods (Mills et al., 2011a). Following this the LRTAP Convention recommends flux-based methods as the preferred tool for risk assessment (LRTAP Convention, 2010).

When calculating the O<sub>3</sub> uptake into the plants, it is important to consider that stomatal uptake is not the only surface sink of O<sub>3</sub>. O<sub>3</sub> destruction also occurs at non-stomatal surfaces such as the leaves' cuticle and soil surface. The stomatal flux represents approximately half of the total O<sub>3</sub> flux to the surface (Gerosa et al., 2004; Fowler et al., 2009; Cieslik, 2004; Simpson et al., 2003). Accounting for this non-stomatal O<sub>3</sub> deposition reduces the amount of O<sub>3</sub> uptake into the plants by reducing the surface O<sub>3</sub> concentration (Tuovinen et al., 2009) and thus has the potential to affect flux-based ozone damage estimates.

A further challenge in estimating plant damage related to O<sub>3</sub> uptake is that plants differ in their ability to remove any ROS from the leaf before damage of leaf cellular organs is incurred (Luwe and Heber, 1995). Conceptually, one can describe the capacity as a plant-specific O<sub>3</sub> dose with which the antioxidant system of the leaves can cope such that no damage is observed (Musselman et al., 2006). The produc-

tion of defence compounds increases respiration costs and following this reduces net primary production what may result in reduced growth and biomass (Ainsworth et al., 2012). Ozone damage is only incurred once the  $O_3$  flux into the leaf exceeds this dose. A commonly used index to assess flux-based damage to plants is the  $POD_y$  (phytotoxic ozone dose,  $nmol\ m^{-2}\ s^{-1}$ ), which gives the accumulated  $O_3$  flux above a threshold of  $Y\ nmol\ m^{-2}\ s^{-1}$  for all daylight hours and a given time period. Common threshold values for  $POD_y$  range from 1 to  $6\ nmol\ m^{-2}\ s^{-1}$  (Pleijel et al., 2007; LRTAP Convention, 2010; Mills et al., 2011b), depending on the specific species sensitivity to  $O_3$ .

Only a few terrestrial biosphere models have adopted the flux approach to relate  $O_3$  exposure to plant damage and thus estimate  $O_3$ -induced reductions in terrestrial carbon sequestration in a process-based manner. Sitch et al. (2007) developed a version of the JULES model in which stomatal  $O_3$  uptake directly affects net primary production (NPP), thereby ignoring the effect of reduced photosynthesis under elevated levels of  $O_3$  on water fluxes. Lombardozzi et al. (2015) proposed a revised version of the Community Land Model (CLM), in which  $O_3$  imposes fixed reductions to net photosynthesis for two out of three modelled plant types. Atmospheric  $O_3$  concentrations and the amount of cumulated  $O_3$  uptake directly affect net photosynthesis only for one plant type.

In this paper, we present a new, globally applicable model to calculate  $O_3$  uptake and damage in a process-oriented manner, coupled to the terrestrial energy, water, carbon, and nitrogen budget of the OCN terrestrial biosphere model (Zaehle and Friend, 2010).

In this model, the canopy  $O_3$  abundance is calculated using aerodynamic resistance and surface resistances to soil surface, vegetation surfaces, and stomatal cavities to take account of non-stomatal  $O_3$  destruction. Canopy  $O_3$  abundance is used to simulate stomatal  $O_3$  uptake given instantaneous values of net photosynthesis and stomatal conductance.  $O_3$  uptake and its effect on net photosynthesis is then calculated based on an extensive meta-analysis across 28 tree species by Wittig et al. (2007) considering the ability of plants to detoxify a proportion of the  $O_3$  dose (Sitch et al., 2007).

We first give a detailed overview of the ozone scheme (Sect. 2.1); evaluate modelled gross primary production (GPP), canopy conductance, latent heat fluxes, and leaf area index (LAI) against data from the FLUXNET database (Baldocchi et al., 2001) to test the ability of the model to simulate observed values of key components affecting calculate  $O_3$  uptake (Sect. 3.1); evaluate the simulated  $O_3$  metrics against reported values in the literature (Sect. 3.2); provide a sensitivity analysis of critical variables and parameters of the deposition model to evaluate the reliability of simulated values of  $O_3$  uptake (Sect. 3.3); give an estimate of the effect of the present-day  $O_3$  burden on European GPP and transpiration (Sect. 3.4); and estimate the impact of using the  $O_3$  deposition scheme on  $O_3$  uptake and cumulated uptake (Sect. 3.5).

## 2 Methods

We developed an ozone deposition and leaf-uptake module for the terrestrial biosphere model OCN (Zaehle and Friend, 2010). OCN is a further development of the land-surface scheme ORCHIDEE (O) (Krinner et al., 2005), and simulates the terrestrial coupled carbon (C), nitrogen (N), and water cycles for 12 plant functional types (PFTs) driven by climate data, atmospheric composition (N deposition, as well as atmospheric  $CO_2$  and  $O_3$  burden), and land-use information (land cover and fertiliser application).

In OCN net photosynthesis is calculated for shaded and sunlit leaves in a multi-layer canopy with up to 20 layers (each with a thickness of up to 0.5 leaf area index) following a modified Farquhar scheme and considering the light profiles of diffuse and direct radiation (Zaehle and Friend, 2010). Photosynthetic capacity depends on leaf nitrogen concentration and leaf area, which are both affected by ecosystem available N. Increases in leaf nitrogen content enable higher net photosynthesis and higher stomatal conductance per unit leaf area. This in turn affects transpiration as well as  $O_3$  uptake and ozone damage estimates. Leaf N is highest in the top canopy and monotonically decreases with increasing canopy depth. Following this, stomatal conductance and  $O_3$  uptake is generally highest in the upper canopy and lowest in the bottom of the canopy.

The  $O_3$  and N-deposition data used for this study are provided by the EMEP MSC-W (European Monitoring and Evaluation Programme Meteorological Synthesizing Centre – West) chemical transport model (CTM) (Simpson et al., 2012). The  $O_3$  flux and deposition modules used in the EMEP model are advanced compared to most CTMs, and have been documented in a number of papers (Emberson et al., 2001; Tuovinen et al., 2004, 2009; Simpson et al., 2007, 2012; Klingberg et al., 2008). The ozone deposition scheme for OCN is adapted from the model used by EMEP MSC-W (Simpson et al., 2012) to fit the land-surface characteristics and process descriptions of the ORCHIDEE model. The leaf-level ozone concentrations computed by EMEP can not directly be used by OCN, since EMEP and OCN differ in a number of properties, as for instance in the number of simulated PFTs, and importantly their ecophysiological process representation. Both models differ in the simulation of various ecosystem processes (e.g. phenology, canopy processes, biogeochemical cycles, and vegetation dynamics, which are more explicitly represented in OCN), which in sum impact stomatal and non-stomatal ozone deposition and through this the leaf-level ozone concentration. A possible further development of the new OCN is the coupling to a CTM to allow for a consistent simulation of tropospheric  $O_3$  burden and vegetation  $O_3$  uptake.

## 2.1 Ozone module

The ozone deposition scheme calculates O<sub>3</sub> deposition to the leaf surface from the free atmosphere, represented by the O<sub>3</sub> concentration at the lowest level of the atmospheric CTM, taken to be at 45 m above the surface. The total O<sub>3</sub> dry deposition flux ( $F_g$ ) to the ground surface is calculated as

$$F_g = V_g \chi_{\text{atm}}^{\text{O}_3}, \quad (1)$$

where  $\chi_{\text{atm}}^{\text{O}_3}$  is the O<sub>3</sub> concentration at 45 m and  $V_g$  is the deposition velocity at that height. In OCN  $V_g$  is taken to be dependent on the aerodynamic resistance ( $R_a$ ), canopy-scale quasi-laminar layer resistance ( $R_b$ ) and the compound surface resistance ( $R_c$ ) to O<sub>3</sub> deposition.

$$V_g = \frac{1}{R_a + R_b + R_c} \quad (2)$$

$R_b$  is calculated from the friction velocity ( $u_*$ ) as

$$R_b = \frac{6}{u_*}. \quad (3)$$

The  $R_a$  between 45 m height and the canopy is not computed by OCN and is inferred from the logarithmic wind profile (for more details see Appendix A).  $R_c$  is calculated as the sum of the parallel resistances to stomatal/canopy ( $1/G_c^{\text{O}_3}$ ) and non-stomatal O<sub>3</sub> uptake ( $1/G_{\text{ns}}$ ) (Simpson et al., 2012, Eq. 55):

$$R_c = \frac{1}{G_c^{\text{O}_3} + G_{\text{ns}}}. \quad (4)$$

The stomatal conductance to O<sub>3</sub>  $G_{\text{st}}^{\text{O}_3}$  ( $\text{m s}^{-1}$ ) is computed by OCN (Zaehle and Friend, 2010) as

$$G_{\text{st}}^{\text{O}_3} = g_1 \frac{f(\Theta) f(q_{\text{air}}) f(C_i) f(\text{height}) A_{n,\text{sat}}}{1.51}, \quad (5)$$

where  $G_{\text{st}}^{\text{O}_3}$  is calculated as a function of net photosynthesis at saturating  $C_i$  ( $A_{n,\text{sat}}$ ), where  $g_1$  is the intrinsic slope between  $A_n$  and  $G_{\text{st}}$ . It further depends on a number of scalars to account for the effect of soil moisture ( $f(\Theta)$ ), water transport limitation with canopy height ( $f(\text{height})$ ), and atmospheric drought ( $f(q_{\text{air}})$ ), as well as an empirical non-linear sensitivity to the internal leaf CO<sub>2</sub> concentration ( $f(C_i)$ ), all as described in Friend and Kiang (2005). The factor 1.51 accounts for the different diffusivity of O<sub>3</sub> from water vapour (Massman, 1998). The canopy conductance to O<sub>3</sub>  $G_c^{\text{O}_3}$  is calculated by summing the  $G_{\text{st}}^{\text{O}_3}$  of all canopy layers. To yield reasonable conductance values in OCN compared to FLUXNET data (see Sect. 3.1), the original intrinsic slope between  $A_n$  and  $G_c$  called  $\alpha$  in Friend and Kiang (2005) is adapted such that  $g_1 = 0.7\alpha$ .

The non-stomatal conductance  $G_{\text{ns}}$  follows the EMEP approach (Simpson et al., 2012, Eq. 60) and represents the O<sub>3</sub> fluxes between canopy-air space and surfaces other than the stomatal cavities. The model accounts for O<sub>3</sub> destruction on the leaf surface ( $r_{\text{ext}}$ ), within-canopy resistance to O<sub>3</sub> transport ( $R_{\text{inc}}$ ), and ground surface resistance ( $R_{\text{gs}}$ ):

$$G_{\text{ns}} = \frac{\text{SAI}}{r_{\text{ext}}} + \frac{1}{R_{\text{inc}} + R_{\text{gs}}}, \quad (6)$$

where the surface area index (SAI) is equal to the LAI for herbaceous PFTs (grasses and crops) and  $\text{SAI} = \text{LAI} + 1$  for tree PFTs according to Simpson et al. (2012) in order to account for O<sub>3</sub> destruction on branches and stems. Unlike EMEP, we do not apply a day of the growing season constraint for crop exposure to O<sub>3</sub>, which in OCN is accounted for by the simulated phenology and seasonality of photosynthesis. The external leaf resistance ( $r_{\text{ext}}$ ) per unit surface area is calculated as

$$r_{\text{ext}} = r_{\text{ext},b} F_T, \quad (7)$$

where the base external leaf resistance ( $r_{\text{ext},b}$ ) of  $2500 \text{ m s}^{-1}$  is scaled by a low-temperature correction factor  $F_T$  and

$$F_T = e^{-0.2(1+T_s)}, \quad (8)$$

with  $1 \leq F_T \leq 2$  and  $T_s$  the 2 m air temperature ( $^{\circ}\text{C}$  Simpson et al., 2012, Eq. 60). For temperatures below  $-1^{\circ}\text{C}$  non-stomatal resistances are increased up to two times (Simpson et al., 2012; Zhang et al., 2003). The within-canopy resistance ( $R_{\text{inc}}$ ) is calculated as

$$R_{\text{inc}} = b \text{SAI} \frac{h}{u_*}, \quad (9)$$

where  $b$  is an empirical constant (set to  $14 \text{ s}^{-1}$ ) and  $h$  is the canopy height in m. The ground-surface resistance  $R_{\text{gs}}$  is calculated as

$$R_{\text{gs}} = \frac{1 - 2f_{\text{snow}}}{F_T \hat{R}_{\text{gs}}} + \frac{2f_{\text{snow}}}{R_{\text{snow}}} \quad (10)$$

(Simpson et al., 2012, Eq. 59).  $\hat{R}_{\text{gs}}$  represents base values of  $R_{\text{gs}}$  and takes values of  $2000 \text{ s m}^{-1}$  for bare soil,  $200 \text{ s m}^{-1}$  for forests and crops, and  $1000 \text{ s m}^{-1}$  for non-crop grasses (Simpson et al., 2012, Suppl.). As in EMEP, the ground-surface resistance of O<sub>3</sub> to snow ( $R_{\text{snow}}$ ) is set to a value of  $2000 \text{ s m}^{-1}$  according to Zhang et al. (2003).  $f_{\text{snow}}$  is calculated from the actual snow depth ( $s_d$ ) simulated by OCN, and the maximum possible snow depth ( $s_{d,\text{max}}$ ):

$$f_{\text{snow}} = \frac{s_d}{s_{d,\text{max}}} \quad (11)$$

with the constraint of  $0 \leq f_{\text{snow}} \leq 0.5$  to prevent negative values in the first fraction of Eq. (10).  $s_{d,\text{max}}$  is taken to be  $10 \text{ kg m}^{-2}$  (Ducoudré et al., 1993).

Given these resistances, the canopy  $O_3$  concentration ( $\chi_c^{O_3}$ ,  $\text{nmol m}^{-3}$ ) is then calculated based on a constant flux assumption:

$$\chi_c^{O_3} = \chi_{\text{atm}}^{O_3} \left(1 - \frac{R_a}{R_a + R_b + R_c}\right). \quad (12)$$

$\chi_c^{O_3}$  and the stomatal conductance to  $O_3$  ( $G_{\text{st}}^{O_3}$  in  $\text{m s}^{-1}$ ) are used to calculate the  $O_3$  flux into the leaf cavities ( $F_{\text{st}}$ ,  $\text{nmol m}^{-2} \text{s}^{-1}$ ):

$$F_{\text{st}} = (\chi_c^{O_3} - \chi_i^{O_3}) G_{\text{st}}^{O_3}. \quad (13)$$

According to Laisk et al. (1989) the leaf internal  $O_3$  concentration ( $\chi_i^{O_3}$ ) is assumed to be zero.

The OCN implementation of deposition and flux described above is a simplification of the deposition system used by EMEP in order to fit the process representation of ORCHIDEE, from which OCN has inherited its biophysical modules. The external leaf resistance is not included in the calculation of  $F_{\text{st}}$  (Tuovinen et al., 2007, 2009), which results in an overestimation of stomatal  $O_3$  uptake. Further, OCN's calculation of  $R_a$  is based upon neutral stability conditions (see Appendix), whereas the EMEP model makes use of rather detailed stability correction factors. However, a series of calculations with the full EMEP model have shown that the uncertainties associated with these simplifications are small, typically 0.5–5  $\text{mmol m}^{-2}$ . As base-case values of POD0 are typically ca. 30–50  $\text{mmol m}^{-2}$  in EU regions, these approximations do not seem to be a major cause of error, at least in regions with substantial ozone (and carbon) uptake. The full coupling of OCN to a CTM would be desirable to eliminate this bias and allow for a consistent calculation of tropospheric and surface near  $O_3$  burdens.

## 2.2 Relating stomatal uptake to leaf damage

An accumulation of  $F_{\text{st}}$  over time gives the accumulated uptake of  $O_3$  for a particular canopy layer ( $\text{CUO}_l$ ,  $\text{mmol m}^{-2}$ ), or for  $l = 1$  (top canopy layer) the phytotoxic  $O_3$  dose (POD,  $\text{mmol m}^{-2}$ ):

$$\frac{d\text{CUO}_l}{dt} = (1 - f_{\text{new}})\text{CUO}_l + c F_{\text{st},l}, \quad (14)$$

where  $c = 10^{-6}$  converts from  $\text{nmol}$  to  $\text{mmol}$  and the integration time step is 1800 s.

The phenology of leaves is accounted for by assuming that emerging leaves are undamaged and by reducing the  $\text{CUO}_l$  by the fraction of newly developed leaves per time step and layer ( $f_{\text{new}}$ ). Furthermore, deciduous PFTs shed all  $\text{CUO}$  at the end of the growing season and grow undamaged leaves the next spring. Evergreen PFTs shed proportionate amounts of  $\text{CUO}$  during the entire year whenever new leaves are grown.

The full canopy cumulative uptake of  $O_3$  is calculated by summing  $\text{CUO}_l$  over all present canopy layers ( $n$ ):

$$\text{CUO} = \sum_{l=1}^n \text{CUO}_l. \quad (15)$$

The  $\text{CUO}_l$  is used to approximate the damage to net photosynthesis ( $A_n$ ) by using the damage relationship of Wittig et al. (2007):

$$d_1^{O_3} = \frac{0.22\text{CUO}_l + 6.16}{100}, \quad (16)$$

where the factor 100 scales the percentage values of damage to fractions. Net photosynthesis accounting for ozone damage ( $A_n^{O_3}$ ) is then calculated by subtracting the damage fraction from the undamaged value of  $A_n$ :

$$A_{n,1}^{O_3} = A_{n,1}(1 - d_1^{O_3}). \quad (17)$$

Since  $G_{\text{st}}$  and  $A_n$  are tightly coupled (see Eq. 5), a damage of  $A_n$  results in a simultaneous reduction in  $G_{\text{st}}$ . The canopy-scale  $O_3$  flux into the leaf cavities ( $F_{\text{stC}}$ ) is calculated by summing  $F_{\text{st}}$  of all canopy layers, similar to the aggregation of  $A_{n,1}$  and  $G_{\text{st}}$  and  $\text{CUO}_l$ . Canopy  $O_3$  concentration,  $O_3$  uptake, canopy cumulative  $O_3$  uptake ( $\text{CUO}$ ), and damage to net photosynthesis are solved iteratively to account for the feedbacks between ozone damage, canopy conductance and canopy-air  $O_3$  concentrations.

Note that  $\text{CUO}$  and  $\text{POD}$  can be directly compared to estimates according to the LRTAP Convention (2010) notation when analysing only the top canopy layer (Mills et al., 2011b).

## 2.3 Sensitivity analysis

A sensitivity analysis is conducted to estimate the sensitivity of the modelled plant  $O_3$  uptake to the parameterisation of the model, to establish the robustness of the model, and to identify the most influential parameters. Three parameters (ground-surface resistance ( $R_{\text{gs}}$ ), external leaf resistance ( $r_{\text{ext}}$ ), and empirical constant ( $b$ ); see Eqs. 10, 6, and 9 respectively) and three modelled quantities (canopy conductance ( $G_c$ ), aerodynamic resistance ( $R_a$ ), and canopy-scale quasi-laminar layer resistance ( $R_b$ ); see Eqs. 5, 2), with considerable uncertainty due to the underlying parameters used to calculate these quantities, are perturbed within  $\pm 20\%$  of their central estimate.

A set of 100 parameter combinations is created with a Latin hypercube sampling method (McKay et al., 1979), simultaneously perturbing all six parameter values (R package: FME; function: Latinhyper). For each parameter combination, a transient run (see Sect. 2.4) is performed creating an ensemble of estimates for the key prognostic variables  $F_{\text{stC}}$  (Eq. 13),  $R_c$  (Eq. 4),  $V_g$  (Eq. 2) and the  $O_3$  flux ratio ( $F_R$ ) calculated as the ratio of  $F_{\text{stC}}$  and the total  $O_3$  flux to the surface ( $F_g$ , Eq. 1).

The summer months June, July, and August (JJA) are selected from the simulation output and used for further analysis. For each prognostic variable ( $F_{\text{stC}}$ ,  $R_c$ ,  $V_g$ ,  $F_R$ ), the sensitivity to changes in all six perturbed parameters/variables is estimated by calculating partial correlation coefficients (PCCs) and partial ranked correlation coefficients (PRCCs) (Helton and Davis, 2002). PCCs record the linear relationship between two variables where the linear effects of all other variables in the analysis are removed (Helton and Davis, 2002). In the case of nonlinear relationships, PRCCs can be used, which implies a rank transformation to linearise any monotonic relationship, such that the regression and correlation procedures as in the PCCs can follow (Helton and Davis, 2002). We estimate the magnitude of the parameter effect by creating mean summer values of the four prognostic variables for each sensitivity run, and regressing these values against the corresponding parameter/variable scaling values of the respective model run.

#### 2.4 Modelling protocol and data for site-level simulations

The site-level simulations (single-point simulations) at the FLUXNET sites are run using observed meteorological forcing, soil properties, and land cover from the La Thuile Dataset (<http://fluxnet.fluxdata.org/data/la-thuille-dataset/>) of the FLUXNET project (Baldocchi et al., 2001). Data on atmospheric  $\text{CO}_2$  concentrations are obtained from Sitch et al. (2015). Reduced and oxidised nitrogen deposition in wet and dry forms and hourly  $\text{O}_3$  concentrations at 45 m height are provided by the EMEP model (see Sect. 2.5).

OCN is brought into equilibrium in terms of the terrestrial vegetation and soil carbon and nitrogen pools in a first step with the forcing of the year 1900. In the next step, the model is run with a progressive simulation of the period 1900 up until the start year of the respective site. For this period atmospheric  $\text{O}_3$  and  $\text{CO}_2$  concentrations as well as N deposition of the respective simulated years are used. Due to lack of observed climate for the sites for this period, the site-specific observed meteorology from recent years is iterated for these first two steps. The observation years (see Table A1) are simulated with the climate and atmospheric conditions (N deposition,  $\text{CO}_2$  and  $\text{O}_3$  concentrations) of the respective years.

For the evaluation of the model output, net ecosystem exchange (NEE), and latent heat flux (LE), as well as meteorological observations, are obtained for 11 evergreen needle-leaved forest sites, 10 deciduous broadleaved forest sites, and 5  $\text{C}_3$  grassland sites in Europe (see Table A1) from the La Thuile Dataset of the FLUXNET project (Baldocchi et al., 2001). Leaf area indices (LAIs) based on discrete point measurements are obtained from the La Thuile ancillary database.

NEE measurements are used to estimate gross primary production (GPP) by the flux-partitioning method according to (Reichstein et al., 2005). Canopy conductance ( $G_c$ )

is derived by inverting the Penman–Monteith equation given the observed LE and atmospheric conditions as described in Knauer et al. (2015).

The half-hourly FLUXNET and model fluxes are filtered prior to deriving average growing-season fluxes (bud break to litter fall) to reduce the effect of model biases on the model-data comparison. Night-time and morning/evening hours are excluded by removing data with lower than 20 % of the daily maximum shortwave downward radiation. To avoid any biases associated with the soil moisture or atmospheric drought response of OCN, we further exclude data points with a modelled soil moisture constraint factor (range between 0 and 1) below 0.8 and an atmospheric vapour pressure deficit larger than 0.5 kPa.

Daily mean values are calculated from the remaining time steps only where both modelled and observed values are present. The derived daily values are furthermore constrained to the main growing season by excluding days where the daily GPP is less than 20 % of the yearly maximum daily GPP.

To derive representative diurnal cycles, data for the month July are filtered for daylight hours (taken as incoming shortwave radiation  $\geq 100 \text{ W m}^{-2}$ ), with periods of soil or atmospheric drought stress excluded as above. This is done for modelled  $F_{\text{stC}}$ ,  $R_c$ ,  $V_g$ , and  $F_R$  and for both modelled and FLUXNET observed GPP and  $G_c$ .

#### 2.5 Modelling protocol and data for regional simulations

For the regional simulations, OCN is run at a spatial resolution of  $0.5^\circ \times 0.5^\circ$  on a spatial domain focused on Europe. Daily meteorological forcing (temperature, precipitation, shortwave and longwave downward radiation, atmospheric specific humidity, and wind speed) for the years 1961 to 2010 is obtained from RCA3 regional climate model (Samuelsson et al., 2011; Kjellstrom et al., 2011), nested in the ECHAM5 model (Roeckner et al., 2006), and has been bias-corrected for temperatures and precipitation using the CRU climatology (New et al., 1999). Reduced and oxidised nitrogen deposition in wet and dry forms and  $\text{O}_3$  concentrations at 45 m height for the same years are obtained from the EMEP model, which is also run with RCA3 meteorology (as in Simpson et al., 2014b). Emissions for the EMEP runs in current years are as described in Simpson et al. (2014b), and are scaled back to 1900 using data from UNECE and van Aardenne et al. (2001) – see Appendix B. Further details of the EMEP model setup for this grid and meteorology can be found in Simpson et al. (2014b) and Engardt et al. (2017). For OCN, land cover, soil, and N fertiliser application are used as in Zaehle et al. (2011) and kept at 2005 values throughout the simulation. Data on atmospheric  $\text{CO}_2$  concentrations are obtained from Sitch et al. (2015).

OCN is brought into equilibrium in terms of the terrestrial vegetation and soil carbon and nitrogen pools by randomly

iterating the forcing from the period 1961–1970. This is followed by a simulation for the years 1961–2011 with time-varying climate and atmospheric conditions (N deposition, CO<sub>2</sub>, and O<sub>3</sub> concentrations) but with static land cover and land-use information (kept at year 2005 levels). An upscaled FLUXNET-MTE product of GPP (Jung et al., 2011), using the model tree ensembles (MTE) machine learning technique, is used to evaluate modelled GPP.

## 2.6 Impacts of using the ozone deposition scheme

In contrast to other terrestrial biosphere models, the OCN ozone module accounts for the effects of aerodynamic, stomatal and non-stomatal resistance to O<sub>3</sub> deposition. Due to these resistances, the deposition of O<sub>3</sub> to leaf level is reduced, and the canopy O<sub>3</sub> concentration is lower than the atmospheric O<sub>3</sub> concentration. Thus, using such a deposition scheme reduces modelled O<sub>3</sub> uptake into plants and accumulation. To get an estimate of the magnitude of this impact we compare simulations with the standard deposition scheme as described above (D) with a simulation where O<sub>3</sub> surface resistance is only determined by stomatal resistance and the non-stomatal depletion of O<sub>3</sub> is zero (D-STO), as well as a further simulation where no deposition scheme is used and the canopy O<sub>3</sub> concentration is equal to the atmospheric concentration (ATM).

## 3 Results

### 3.1 Evaluation against daily eddy-covariance data

Figure 1 a shows that, for most sites, modelled and observation-based GPP agree well (see Table A2 for  $R^2$  and RMSE values). The standard deviation is larger for the observation-based estimates because of the high level of noise in the eddy-covariance data. For sites dominated by needle-leaved trees, the modelled and observation-based GPP values are very close, with only slight under- and over-estimates by the model at some sites. At sites dominated by broadleaved trees, modelled GPP deviates more strongly from the observation-based GPP, underestimating the observations in 7 out of 10 cases. However, the results are within the range of standard deviation except for the drought-prone PT-Mi1 site (see Fig. A1a for an explicit site comparison). At C<sub>3</sub> grassland sites, modelled GPP is in good agreement with the observation-based GPP except for AT-Neu, which has the highest mean GPP of all sites observed by FLUXNET with a large standard deviation, which may reflect the effect of site management (e.g. mowing and fertilisation), for which no data were readily available as model forcing.

When comparing modelled and observed latent heat flux (LE), the model fits the observations best at the needle-leaved forest sites (Fig. 1c). However, LE is overestimated at 9 out of 10 broadleaved forest sites but remains within the range of the large observational standard deviation. At sites dom-

inated by C<sub>3</sub> grasses the modelled LE differs considerably from the observed value, at two sites overestimating and two underestimating the fluxes, again within the observational standard deviation.

In agreement with the comparison of GPP and LE, the comparison of modelled to observation-based canopy conductance ( $G_c$ ) shows the best agreement for sites dominated by needle-leaved trees (Fig. 1b). At sites dominated by broadleaved trees, the modelled  $G_c$  varies more widely from the FLUXNET  $G_c$ . The modelled  $G_c$  at sites dominated by C<sub>3</sub> grasses is in very good agreement with FLUXNET  $G_c$ , with slight overestimation of  $G_c$  at two out of three sites, except for the DE-Meh site, where means differ outside the standard deviation (see Fig. A1b).

The comparison of the average modelled summertime LAI and point measurements at the FLUXNET illustrates that the variability in the measured LAI is much greater than that of OCN (Fig. 1d). The modelled LAI values approach light-saturating, maximum LAI values and are not able to reproduce between-site differences in, for example, the growth stage, site history, or maximum possible LAI values. Furthermore, it should be borne in mind that the observed LAI values are averages of point measurements, which are not necessarily representative of the modelled time period, and that the model had not been parameterised specifically for the sites. Modelled GPP depends not only on LAI but also on light availability, temperature, and soil moisture. The much better represented values of GPP,  $G_c$ , and LE compared to FLUXNET data (Fig. 1a–c) indicate that OCN is able to adequately transform available energy into carbon uptake and water loss and thus simulate key variables impacting ozone uptake within a reasonable range.

### 3.2 Mean diurnal cycles of key O<sub>3</sub> parameters.

For further evaluation of the modelled O<sub>3</sub> uptake, we analysed the diurnal cycles of O<sub>3</sub> uptake ( $F_{stC}$ ), O<sub>3</sub> surface resistance ( $R_c$ ), O<sub>3</sub> deposition velocity ( $V_g$ ), and flux ratio ( $F_R$ ) as well as GPP and  $G_c$ . We selected three sites (a broadleaved, a needle-leaved, and a C<sub>3</sub> grass site) based on the selection criteria that modelled and FLUXNET GPP and LAI agree well and a minimum of five observation years is available to reduce possible biases from the inability of the model to simulate short-term variations from the mean. The selected sites are a temperate broadleaved summer green forest (IT-Ro1), a boreal needle-leaved evergreen forest (FI-Hyy), and a temperate C<sub>3</sub> grass land (CH-Oe1). We evaluate modelled GPP and  $G_c$  against observations from the FLUXNET sites. The modelled mean diurnal cycles of O<sub>3</sub> related variables ( $F_{stC}$ ,  $R_c$ ,  $V_g$ ,  $F_R$ ) are compared to reported values in the literature since we did not have access to site-specific observations.

Modelled and observed mean diurnal cycles of GPP and  $G_c$  are in general agreement at the three selected FLUXNET sites (see Fig. 2a, g, m and b, h, n) with particularly good

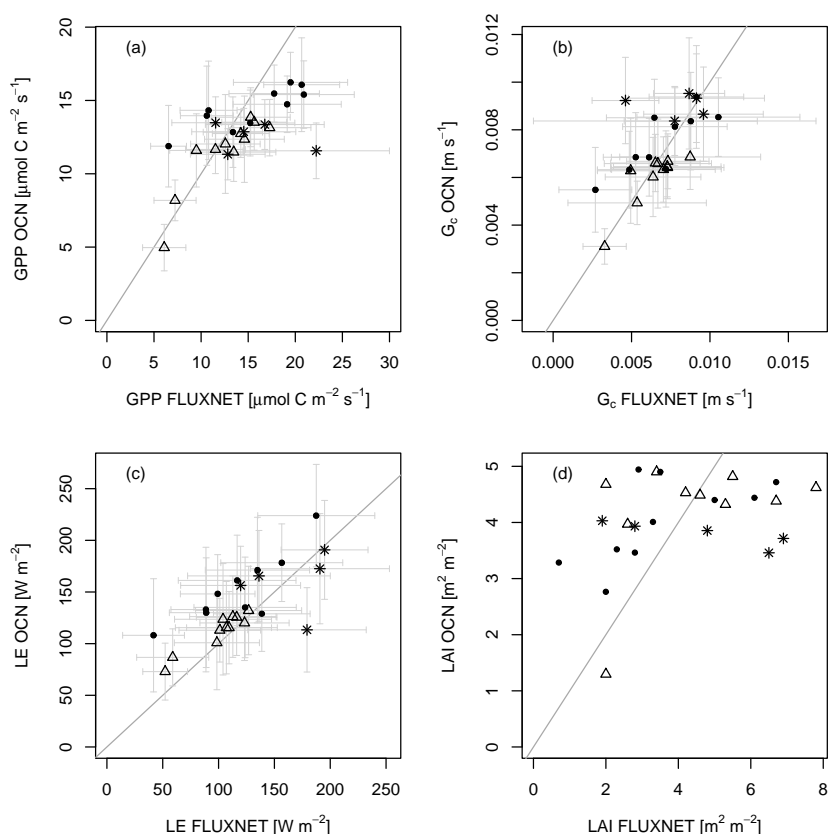


**Figure 1.** Comparison of measured (a) GPP, (b) canopy conductance ( $G_c$ ), (c) latent heat flux (LE), and (d) LAI at 26 European FLUXNET sites and simulations by OCN. Displayed are means and standard deviations of daily means of the measuring/simulation period, with the exception of FLUXNET-derived LAI, which is based on point measurements. Dots symbolise sites dominated by broadleaved trees, triangles sites dominated by needle-leaved trees, and asterisks sites dominated by  $C_3$  grasses. The grey line constitutes the 1 : 1 line.

agreement for the mean diurnal cycle of GPP at the needle-leaved site FI-Hyy, where the hourly means are very close and the observational standard deviation is narrow (see Fig. 2g). At the grassland site IT-Ro1 the overall daytime magnitude of the fluxes is reproduced in general except for the observed afternoon reduction in GPP (see Fig. 2a). The modelled hourly values fall in the range of the observed values. Modelled and observation-based hourly means of GPP at the site CH-Oe1 agree well except for the evening hours, where the observed values increase again. The mean diurnal cycles of  $G_c$  derived from the FLUXNET data are again best matched at the site FI-Hyy, whereas the model generally overestimates the diurnal cycle of  $G_c$  slightly at the site IT-Ro1, and overestimates peak  $G_c$  at the CH-Oe1 site. The fact that OCN does not always simulate the observed midday depression of  $G_c$ , suggests that the response of stomata to atmospheric and soil drought in OCN requires further evaluation and improvement. Similar to the daily mean values (see Fig. 1a, b), the mean hourly values show the best match of GPP and  $G_c$  for the needle-leaved tree site and stronger deviations for the sites covered by broadleaved trees and  $C_3$  grasses.

The stomatal  $O_3$  uptake  $F_{stC}$  (Fig. 2c, i, o) is close to zero during night-time, when the stomata are assumed to be closed, because gross photosynthesis is zero. At FI-Hyy and CH-Oe1, peak uptake occurred at noon, when photosynthesis (Fig. 2g, m) and stomatal conductance (Fig. 2h, n) are highest, at values between 8 and 9  $\text{nmol m}^{-2} \text{s}^{-1}$ . At the Italian site IT-Ro1, maximum uptake occurs in the afternoon hours around 15 h, with much larger standard deviation compared to the other two sites (Fig. 2c). The magnitude of stomatal  $O_3$  uptake corresponds well to some values reported, for example, for crops (Gerosa et al., 2003, 2004; daily maxima of 4–9  $\text{nmol m}^{-2} \text{s}^{-1}$ ) and holm oak (Vitale et al., 2005; approx. 7–8  $\text{nmol m}^{-2} \text{s}^{-1}$ ). Lower daily maximum values have been reported for an evergreen Mediterranean forest dominated by Holm Oak of 4  $\text{nmol m}^{-2} \text{s}^{-1}$  under dry weather conditions (Gerosa et al., 2005) and 1–6  $\text{nmol m}^{-2} \text{s}^{-1}$  for diverse southern European vegetation types (Cieslik, 2004). Much higher values are reported for *Picea abies* (50–90  $\text{nmol m}^{-2} \text{s}^{-1}$ ), *Pinus cembra* (10–50  $\text{nmol m}^{-2} \text{s}^{-1}$ ), and *Larix decidua* (10–40  $\text{nmol m}^{-2} \text{s}^{-1}$ ) at a site near Innsbruck, Austria (Wieser et al., 2003), where canopy  $O_3$  uptake was estimated by sap-flow measurements in contrast to the studies mentioned be-

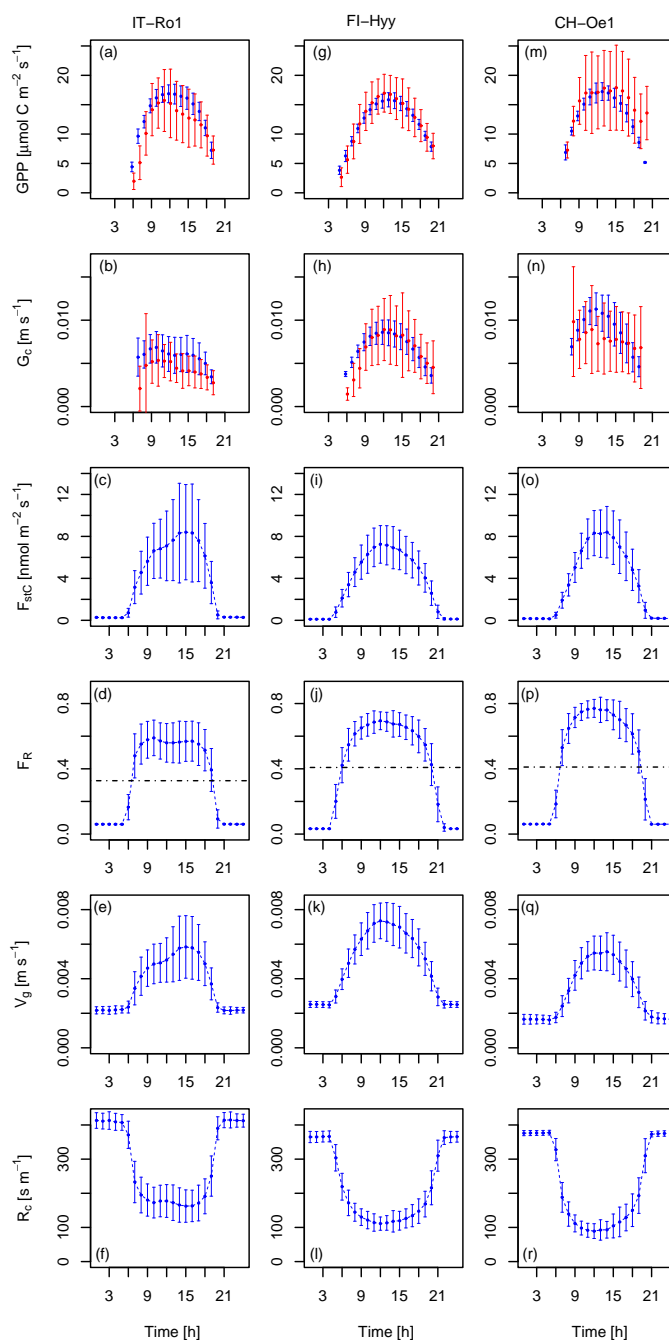


**Figure 2.** Simulated and observed hourly means over all days of the months of July of 2002–2006 for CH-Oe1 and IT-Ro1, as well as for 2001–2006 for FI-Hyy. Plotted are mean hourly values (local time) of **(a, g, m)** GPP (blue: OCN; red: FLUXNET), **(b, h, n)** canopy conductance ( $G_c$ ) (blue: OCN; red: FLUXNET), **(c, i, o)**  $O_3$  uptake ( $F_{stC}$ ), **(d, j, p)** the flux ratio ( $F_R$ ), **(e, k, q)**  $O_3$  deposition velocity ( $V_g$ ), and **(f, l, r)**  $O_3$  surface resistance ( $R_c$ ). The error bars indicate the standard deviation from the hourly mean. The dotted line in panels **(d, j)**, and **(p)** indicates the daily mean value.

fore where the eddy-covariance technique was applied. The much higher  $F_{stC}$  values in that study result from much higher canopy conductances to  $O_3$  ( $G_c^{O_3}$ ), which are up to 12 times higher than the modelled  $G_c^{O_3}$  values in our study (see Fig. 2,  $G_c^{O_3} = \frac{G_c}{1.51}$ ).

The ratio between the stomatal  $O_3$  uptake and the total surface uptake ( $F_R$ ) is close to zero during night-time hours and increases steeply in the morning hours (Fig. 2d, j, p). The 24 h average is approximately 0.3 for IT-Ro1 and 0.4 for FI-Hyy and CH-Oe1 (Fig. 2d, j, p). Peak hourly mean values

are close to 0.6 at IT-Ro1, around 0.7 at FI-Hyy, and close to 0.8 at CH-Oe1. These values are comparable to the ratios reported for crops (Gerosa et al., 2004; Fowler et al., 2009; 0.5–0.6), Norway spruce (Mikkelsen et al., 2004; 0.3–0.33), and various southern European vegetation types (Cieslik, 2004; 0.12–0.69). The modelled flux ratios here show slightly higher daily maximum flux ratios than reported in the listed studies. Daily mean flux ratios are well within the reported range.

The modelled deposition velocities  $V_g$  are lowest during night-time, with values of approximately  $0.002 \text{ m s}^{-1}$  (Fig. 2e, k, q). These values increase to maximum hourly means of  $0.006$ – $0.007 \text{ m s}^{-1}$  during daytime. These values compare well with reported values of deposition velocities, which range from  $0.003$  to  $0.009 \text{ m s}^{-1}$  at noon (Gerosa et al., 2004) for a barley field and are approximately  $0.006 \text{ m s}^{-1}$  at noon for a wheat field (Tuovinen et al., 2004) and approximately  $0.009 \text{ m s}^{-1}$  at noon at a potato field (Coyle et al., 2009). The estimates for FI-Hyy also agree well with maximum deposition velocities reported for Scots pine site of  $0.006 \text{ m s}^{-1}$  (Keronen et al., 2003; Tuovinen et al., 2004) and noon values from Danish Norway spruce sites of  $0.006$ – $0.010 \text{ m s}^{-1}$  (Mikkelsen et al., 2004; Tuovinen et al., 2001). Mean daytime deposition velocities of  $0.006 \text{ m s}^{-1}$  (range  $0.003$ – $0.008 \text{ m s}^{-1}$ ) are reported at a Finnish mountain birch site (Tuovinen et al., 2001). Simulated monthly mean values of  $V_g$  differ substantially between the sites (see Fig. A2). When comparing the monthly means over all sites (Fig. A2 dashed line) of a functional group (broadleaved, needle-leaved,  $C_3$  grasses) to the ensemble mean of 15 CTMs (Hardacre et al., 2015), the values simulated here are higher for needle-leaved tree sites. For broadleaved tree sites and grassland sites, higher values, but which are still within the observed ensemble range, are found for the summer months.

The modelled hourly mean  $\text{O}_3$  surface resistance  $R_c$  is highest during night-time, at approximately  $400 \text{ s m}^{-1}$ , and decreases during daytime to values of  $100$ – $180 \text{ s m}^{-1}$ , where the lowest surface resistance of approximately  $100 \text{ s m}^{-1}$  is modelled at the grassland site CH-Oe1 (Fig. 2f, l, r). These values are slightly higher than independent estimates (for grasses and crops obtained for other sites) of noon surface resistances ranging from  $50$  to  $100 \text{ s m}^{-1}$  (Padro, 1996; Coyle et al., 2009; Gerosa et al., 2004; Tuovinen et al., 2004). Tuovinen et al. (2004) reported noon values of approximately  $140 \text{ s m}^{-1}$  for a Scots pine forest and  $70$ – $140 \text{ s m}^{-1}$  for a Norway spruce forest site (Tuovinen et al., 2001), which compares well with the modelled  $R_c$  values at the needle-leaved forest site (FI-Hyy; Fig. 2l). Higher noon values of approximately  $250 \text{ s m}^{-1}$  are reported at a Danish Norway spruce site (Mikkelsen et al., 2004). For a mountain birch forest, noon values of  $110$ – $140 \text{ s m}^{-1}$  (Tuovinen et al., 2001) are observed which is slightly lower than the modelled value at the IT-Ro1 site (dominated by broadleaved tree PFT).

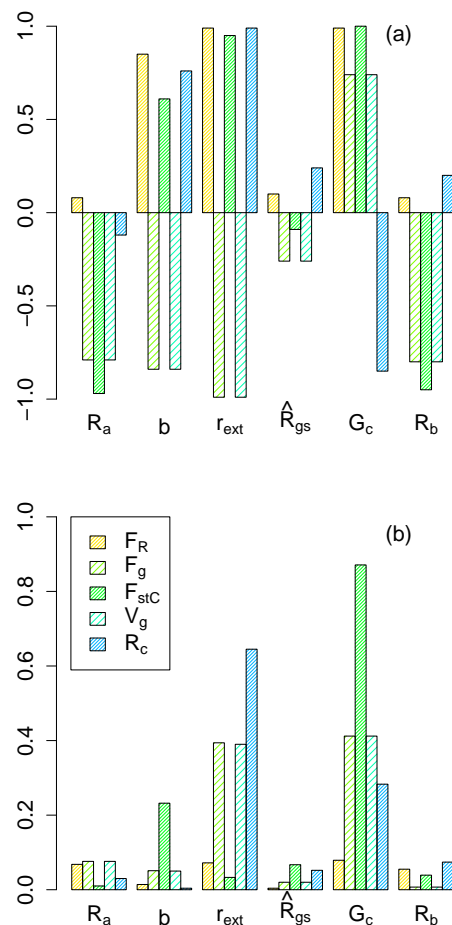


**Figure 3.** (a) Mean partial correlation coefficients and (b) strength of the correlation in % per %.  $R_a$ ,  $b$ ,  $r_{\text{ext}}$ ,  $\hat{R}_{\text{gs}}$ , and  $G_c$  are perturbed within  $\pm 20\%$  of their central estimate. Results from simulations at the FLUXNET site FI-Hyy for the simulation period 2001–2006.

### 3.3 Sensitivity analysis

We assess the sensitivity of the modelled  $\text{O}_3$  uptake and deposition, represented by  $F_g$ ,  $F_{\text{stC}}$ ,  $V_g$ , and  $R_c$ , to uncertainty in six weakly constrained variables and parameters of the  $\text{O}_3$  deposition scheme ( $R_a$ ,  $b$ ,  $r_{\text{ext}}$ ,  $\hat{R}_{\text{gs}}$ ,  $G_c$ , and  $R_b$ ). Figure 3a shows, for example, the results for the boreal needle-leaved forest FI-Hyy. As expected, all uptake/deposition variables, except for the flux ratio ( $F_R$ ) are negatively correlated with the aerodynamic resistance  $R_a$ , which describes the level of decoupling of the atmosphere and land surface. Increasing  $R_a$  decreases the canopy internal  $\text{O}_3$  concentration and hence stomatal ( $F_{\text{stC}}$ ) and total ( $F_g$ ) deposition as well as the deposition velocity ( $V_g$ ). The flux ratio  $F_R$  is slightly positively correlated with changes in  $R_a$  due to the stronger negative correlation of  $F_{\text{stC}}$  relative to  $F_g$ .

In decreasing order, but as expected, the level of external leaf resistance ( $r_{\text{ext}}$ ), the scaling factor  $b$  (Eq. 9), the soil resistance ( $\hat{R}_{\text{gs}}$ ), and the canopy-scale quasi-laminar layer re-

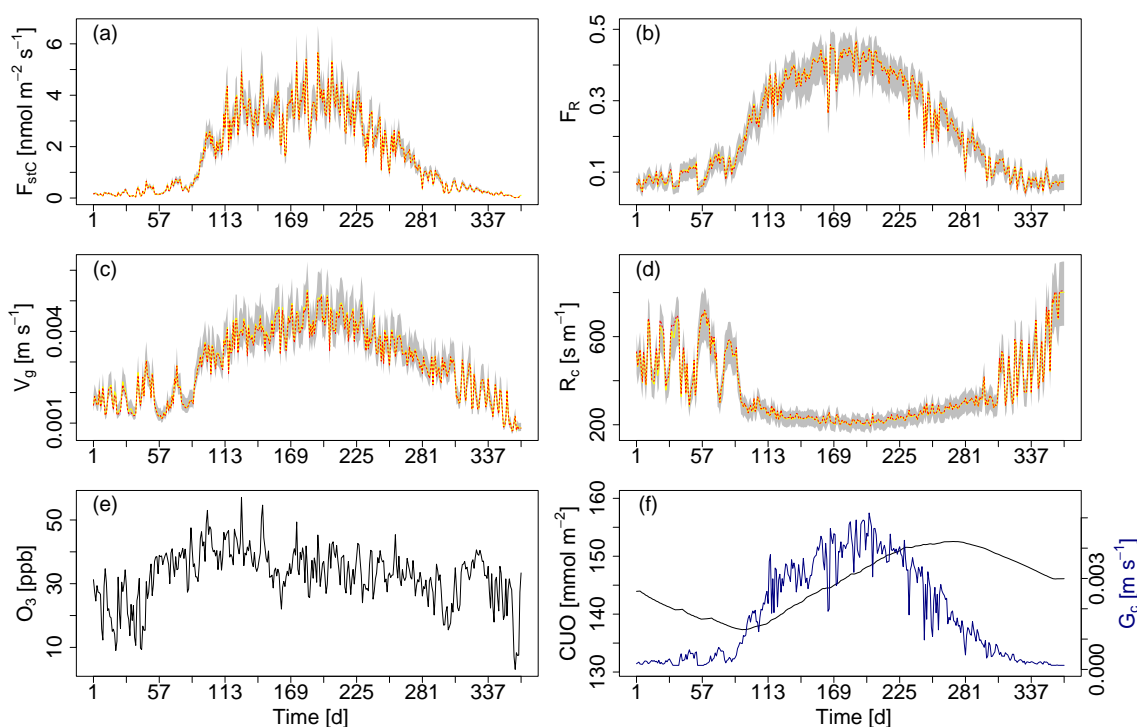


**Figure 4.** Ensemble range of key O<sub>3</sub> uptake/deposition variables resulting from the perturbation of  $R_a$ ,  $b$ ,  $r_{\text{ext}}$ ,  $\hat{R}_{\text{gs}}$ , and  $G_c$  within  $\pm 20\%$  of their central estimate. Shown are simulated daily mean values of (a) O<sub>3</sub> uptake ( $F_{\text{stC}}$ ), (b) the O<sub>3</sub> flux ratio ( $F_R$ ), (c) O<sub>3</sub> deposition velocity ( $v_g$ ) and (d) O<sub>3</sub> surface resistance ( $R_c$ ) for the boreal needle-leaved evergreen forest at the finish FLUXNET site FI-Hyy for the year 2001. Red dashed: unperturbed model; yellow: median of all sensitivity runs; light-grey area: min–max range of all sensitivity runs. Simulated daily mean values for the respective site and year of (e) atmospheric O<sub>3</sub> concentrations O<sub>3</sub> and (f) cumulative uptake of O<sub>3</sub> (CUO) and canopy conductance  $G_c$ .

sistance ( $R_b$ ) increase  $R_c$  and consequently reduce  $F_g$  and  $V_g$ . Reducing the non-stomatal deposition by increasing  $r_{\text{ext}}$ ,  $b$ ,  $\hat{R}_{\text{gs}}$ , and  $R_b$  increases the canopy internal O<sub>3</sub> concentration and thus stomatal O<sub>3</sub> uptake ( $F_{\text{stC}}$ ). The combined effects of a reduction in total deposition  $F_g$  and an increase in  $F_{\text{stC}}$  cause a positive correlation of  $F_R$  to  $r_{\text{ext}}$ ,  $b$ ,  $\hat{R}_{\text{gs}}$ , and  $R_b$ .

Increasing canopy conductance ( $G_c$ ) increases stomatal O<sub>3</sub> uptake ( $F_{\text{stC}}$ ) and thereby also increases  $V_g$  and  $F_g$ . The increased total O<sub>3</sub> uptake ( $F_g$ ) decreases the surface resistance to O<sub>3</sub> uptake  $R_c$ , resulting in a negative correlation of  $R_c$  with  $G_c$ . The stronger increase in  $F_{\text{stC}}$  relative to  $F_g$  results in a positive correlation of  $F_R$ .

Despite these partial correlations, only changed values for  $r_{\text{ext}}$  and  $G_c$  have a notable effect on the predicted fluxes (Fig. 3b), whereas for the other factors ( $R_a$ ,  $b$ , and  $\hat{R}_{\text{gs}}$ ) the impact on the simulated fluxes is less than 0.1 % due to a 1 % change in the variables/parameters of the deposition scheme.

The flux ratio  $F_R$  is very little affected by varying  $r_{\text{ext}}$  and  $G_c$ .

Notwithstanding the perturbations, all four O<sub>3</sub> related flux variables show a fairly narrow range of simulated values (Fig. 4). For all four variables the unperturbed model and the ensemble mean lie on top of each other (see dashed red and

yellow line in Fig. 4a–d). The seasonal course of the surface resistances and fluxes is maintained. The simulations show a strong day-to-day variability in  $F_{\text{stC}}$ , which is conserved with different parameter combinations and which is largely driven by the day-to-day variations in  $G_c$  and the atmospheric O<sub>3</sub> concentration (see Fig. 4f and e respectively). Ozone uptake by the leaves reduces the O<sub>3</sub> surface resistance during the growing season such that  $R_c$  becomes lowest. The cumulative uptake of O<sub>3</sub> (CUO) is lowest at the beginning of the growing season but not zero because the evergreen pine at the Hyytiälä site accumulates O<sub>3</sub> over several years (Fig. 4f). The CUO increases during the growing season and declines in autumn, when a larger fraction of old needles are shed.

The minor impact of the perturbations on the simulated O<sub>3</sub> uptake and deposition variables suggests that the calculated O<sub>3</sub> uptake is relatively robust against uncertainties in the parameterisation of some of the lesser known surface properties.

### 3.4 Regional simulations

We used the model to simulate the vegetation productivity, O<sub>3</sub> uptake, and associated ozone damage of plant produc-

tion over Europe for the period 2001–2010 (see Sect. 2.5 for modelling protocol).

Simulated mean annual GPP for the years 1982–2011 shows in general good agreement with an independent estimate of GPP based on upscaled eddy-covariance measurements (MTE; see Sect. 2.5), with OCN on average underestimating GPP by 16 % (European mean). A significant exception are cropland dominated areas (Fig. 5) in parts of eastern Europe, southern Russia, Turkey, and northern Spain, which show consistent overestimation of GPP by OCN of 400–900  $\text{g C m}^{-2} \text{yr}^{-1}$  (58 % overestimation on average). Regions with a strong disagreement coincide with high simulated LAI values by OCN and a higher simulated GPP in summer compared to the summer GPP by MTE. In addition, OCN simulates a longer growing season for croplands since sowing and harvest dates are not considered. It is worth noting, nevertheless, that there are no FLUXNET stations present in the regions of disagreement hotspots, making it difficult to assess the reliability of the MTE product in this region.

North of 60° N, OCN has the tendency to produce lower estimates of GPP than inferred from the observation-based product, which is particularly pronounced in low-productivity mountain regions of Norway and Sweden. It is unclear whether this bias is indicative of a N limitation that is too strong in the OCN model.

Average decadal  $\text{O}_3$  concentrations generally increase from northern to southern Europe (Fig. 6a) and with increasing altitude, with local deviations from this pattern in centres of substantial air pollution. The pattern of foliar  $\text{O}_3$  uptake differs distinctly from that of the  $\text{O}_3$  concentrations, showing highest uptake rates in central and eastern Europe and parts of southern Europe (Fig. 6b), associated with centres of high rates of simulated gross primary production (Fig. 5a) and thus canopy conductance. The cumulative  $\text{O}_3$  uptake reaches values of 40–60  $\text{mmol m}^{-2}$  in large parts of central Europe (Fig. 6c). The highest accumulation rates of 80–110  $\text{mmol m}^{-2}$  are found in eastern Europe and parts of Scandinavia as well as in Italy, the Alps, and the Bordeaux region. The concentration-based exposure index AOT40 (Fig. 6d) shows a strong north–south gradient similar to the  $\text{O}_3$  concentration (Fig. 6a) and is distinctly different to the flux-based CUO pattern (Fig. 6c).

Simulated reduction in mean decadal GPP due to  $\text{O}_3$  range from 80 to 160  $\text{g C m}^{-2} \text{yr}^{-1}$  over large areas of central, eastern, and south-eastern Europe (Fig. 7a) and is generally largest in regions of high productivity. The relative reduction in GPP is fairly consistent across large areas in Europe and averages 6–10 % (Fig. 7b). Higher reductions in relative terms are found in regions with high cover of  $\text{C}_4$  PFTs, e.g. the Black Sea area. Lower relative reductions are found in northern Europe and parts of southern Europe, where productivity is low and stomatal  $\text{O}_3$  uptake is reduced by, for example, low  $\text{O}_3$  concentrations or drought control on stomatal fluxes respectively. Slight increases or strong decreases in relative terms are found in regions with very small produc-

tivity like in northern Africa and the mountainous regions of Scandinavia. A slight increase in GPP might be caused by feedbacks of GPP damage on LAI, canopy conductance, and soil moisture content such that water savings, for example, enable a prolonged growing season and thus a slightly higher GPP. Overall, simulated European productivity has been reduced from 10.6 to 9.8  $\text{Pg C yr}^{-1}$  corresponding to a 7.6 % reduction.

The  $\text{O}_3$ -induced reductions in GPP are associated with a reduction in mean decadal transpiration rates of 8–15  $\text{mm yr}^{-1}$  over large parts of central and eastern Europe (Fig. 7c). These reductions correspond to 3–6 % of transpiration in central Europe and 6–10 % in northern Europe. As expected, the relative reductions in transpiration rates are therefore slightly less than for GPP due to the role of aerodynamic resistance in controlling water fluxes in addition to canopy conductance. Very high reductions in transpiration are found in the eastern Black Sea area associated with strong reductions in GPP and in the mountainous regions of Scandinavia, where absolute changes in transpiration are very small. Regionally (in particular in eastern Spain, northern Africa, and around the Black Sea) lower reductions in transpiration or even slight increases are found (Fig. 7d). These are related to  $\text{O}_3$ -induced soil moisture savings during the wet growing season, leading to lower water stress rates during the drier season. The very strong reduction in transpiration west of the Crimean Peninsula are related to the strong reductions in GPP mentioned above. Overall, simulated European mean transpiration has been reduced from 170.4 to 163.3  $\text{mm}$  corresponding to a 4.2 % reduction.

### 3.5 Impacts of using the ozone deposition scheme

At the FI-Hyy site the canopy  $\text{O}_3$  concentration, uptake and accumulated uptake (CUO) increases approximately 10–15 % for the D-STO model (non-stomatal depletion of  $\text{O}_3$  is zero) and 20–25 % for the ATM model version (canopy  $\text{O}_3$  concentration is equal to the atmospheric concentration) compared to the standard deposition scheme (D) used here (Figs. 8a–c and A3). The exact values however are site- and PFT-specific (see Fig. A3 for the CH-Oe1 and IT-Ro1 site).

The regional impact of using the ozone deposition scheme on CUO is shown in Fig. 9. CUO substantially decreases for the D-STO (Fig. 9b) compared to the ATM model (Fig. 9a). Using the standard deposition model D (Fig. 9c) further reduces the CUO compared to the ATM version where the stomata respond directly to the atmospheric  $\text{O}_3$  concentration.

Calculating the canopy  $\text{O}_3$  concentration with the help of a deposition scheme that accounts for stomatal and non-stomatal  $\text{O}_3$  deposition thus reduces  $\text{O}_3$  accumulation in the vegetation.

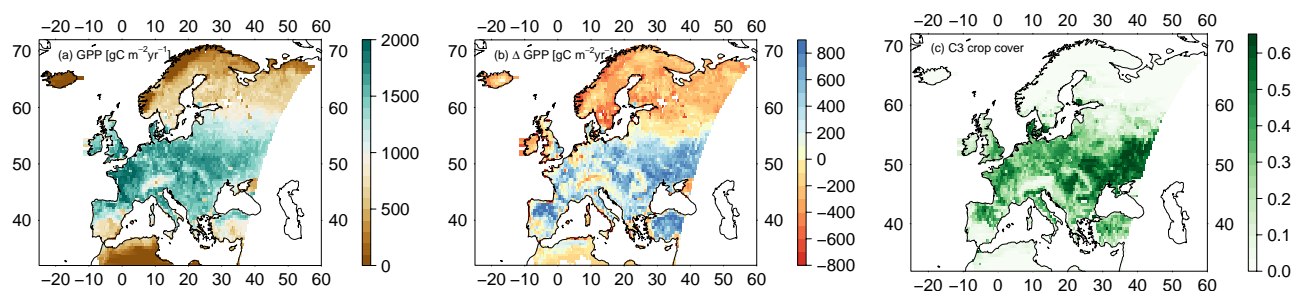


**Figure 5.** Europe-wide simulated GPP and difference between modelled GPP by OCN and a GPP estimate by a FLUXNET-MTE product. Plotted, for the years 1982–2011, are (a) the simulated mean GPP accounting for ozone damage in  $\text{gC m}^{-2} \text{yr}^{-1}$ , (b) the mean differences for OCN minus MTE GPP in  $\text{gC m}^{-2} \text{yr}^{-1}$ , and (c) the mean simulated grid cell cover of the  $\text{C}_3$ -crop PFT in OCN, given as fractions of the total grid cell area.

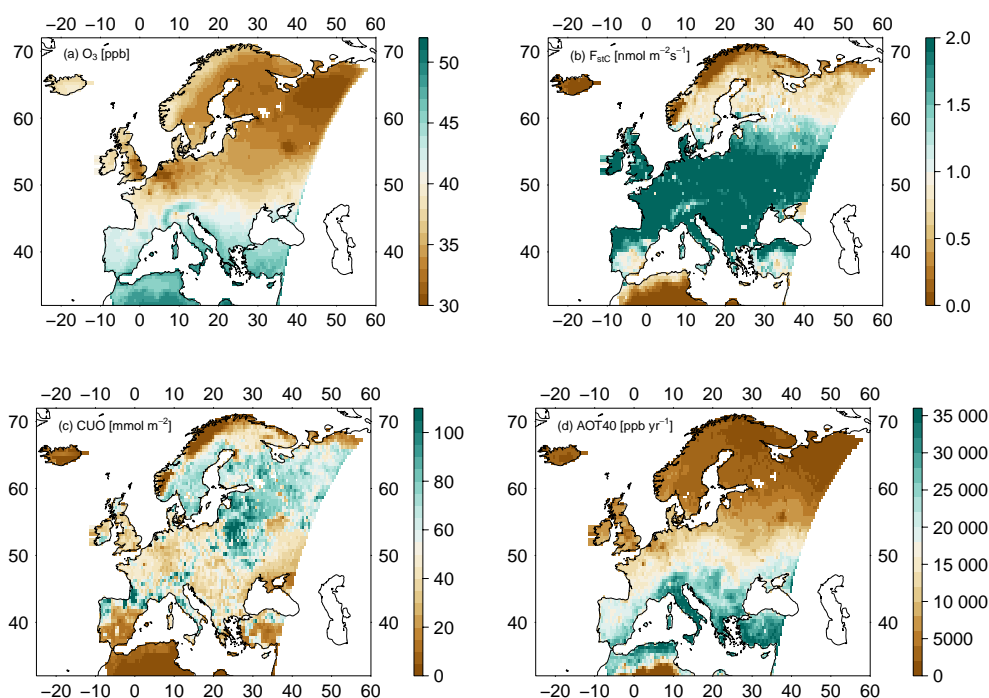


**Figure 6.** Mean decadal (a)  $\text{O}_3$  concentration (ppb), (b) canopy-integrated  $\text{O}_3$  uptake into the leaves ( $\text{nmol m}^{-2} \text{s}^{-1}$ ), (c) canopy-integrated cumulative uptake of  $\text{O}_3$  (CUO) ( $\text{mmol m}^{-2}$ ), and (d) AOT40 ( $\text{ppm yr}^{-1}$ ), for Europe of the years 2001–2010.

#### 4 Discussion

We extended the terrestrial biosphere model OCN by a scheme to account for the atmosphere–leaf transfer of  $\text{O}_3$  in order to better account for air pollution effects on net photosynthesis and hence regional to global water, carbon, and nitrogen cycling. This ozone deposition scheme calculates canopy  $\text{O}_3$  concentrations and uptake into the leaves depending on surface conditions and vegetation carbon uptake

Estimates of the regional damage to annual average GPP ( $-7.6\%$ ) and transpiration ( $-4.2\%$ ) simulated by OCN for 2001–2010 are lower than previously reported estimates. Meta-analyses suggest on average a 11% (Wittig et al., 2007)

and a 21% (Lombardozzi et al., 2013) reduction in instantaneous photosynthetic rates. However, because of carry-over effects, this does not necessarily translate directly into reductions in annual GPP. Damage estimates using the CLM suggest GPP reductions of 10–25% in Europe and 10.8% globally (Lombardozzi et al., 2015). Reductions in transpiration have been estimated as 5–20% for Europe and 2.2% globally (Lombardozzi et al., 2015). Lombardozzi et al. (2015), however, used fixed reductions of photosynthesis (12–20%) independent of cumulative  $\text{O}_3$  uptake for two out of three simulated plant types. Damage was only related to cumulative  $\text{O}_3$  uptake for one plant type with a very small slope and hence little increase in damage due to increases in cu-

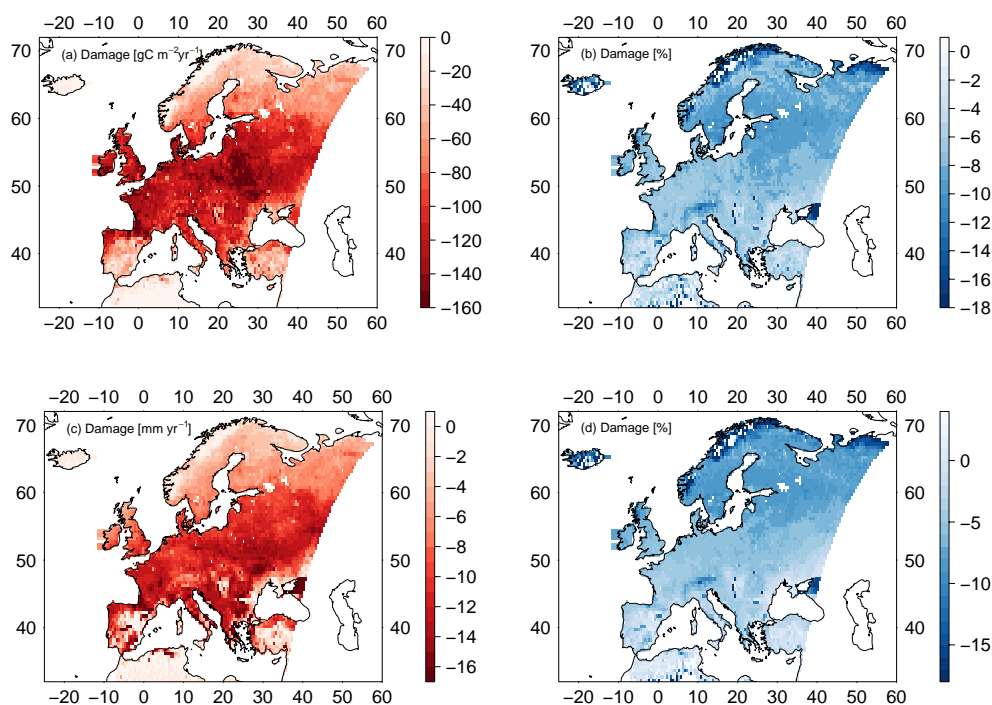


**Figure 7.** Mean decadal (a) reduction in GPP ( $\text{gC m}^{-2} \text{yr}^{-1}$ ), (b) percent reduction in GPP, (c) reduction in transpiration ( $\text{mm yr}^{-1}$ ), and (d) percent reduction in transpiration due to ozone damage averaged for the years 2001–2010.

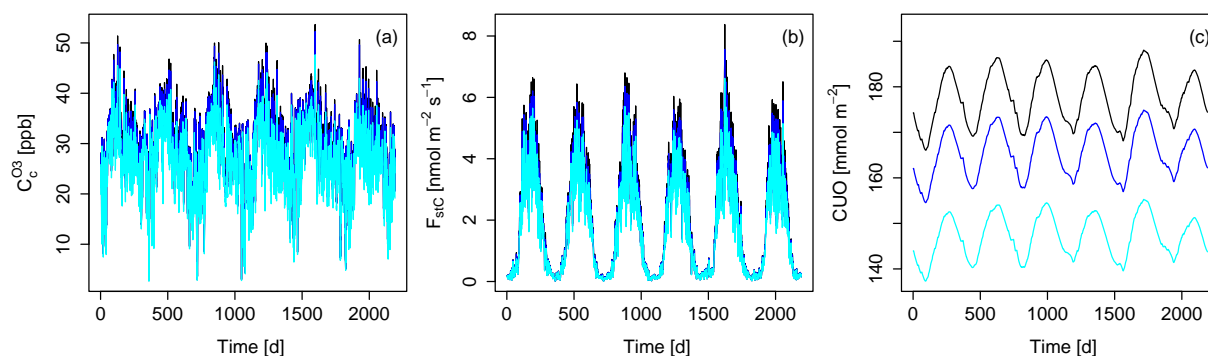


**Figure 8.** Mean daily values of the (a)  $\text{O}_3$  surface concentration (ppb), (b) canopy-integrated  $\text{O}_3$  uptake into the leaves ( $\text{nmol m}^{-2} \text{s}^{-1}$ ), and (c) canopy-integrated cumulative uptake of  $\text{O}_3$  (CUO) ( $\text{mmol m}^{-2}$ ) at the FLUXNET site FI-Hyy. Black: ATM model; dark blue: D-STO model; light blue: standard deposition model (D).

mulative  $\text{O}_3$  uptake. Sitch et al. (2007) simulated global GPP reductions of 8–14 % (under elevated and fixed  $\text{CO}_2$  respectively) for low plant ozone sensitivity and 15–23 % (under elevated and fixed  $\text{CO}_2$  respectively) for high plant ozone sensitivity for the year 2100 compared to 1901. For the Euro-Mediterranean region an average GPP reduction of 22 % was estimated by the ORCHIDEE model for the year 2002 using an AOT40-based approach (Anav et al., 2011).

Possible causes for the discrepancies are differences in dose–response relationships, flux thresholds accounting for the detoxification ability of the plants, atmospheric  $\text{O}_3$  concentrations, simulation periods, and simulation of climate

change (elevated  $\text{CO}_2$ ) and air pollution (nitrogen deposition). We discuss the most important aspects below. To elucidate the reasons for the substantial differences in the damage estimates, further studies are necessary to disentangle the combined effects of differing flux thresholds, damage relationships, climate change, and deposition of nitrogen.

#### 4.1 Atmosphere–leaf transport of ozone

The sensitivity analysis in Sect. 3.3 demonstrates that the estimate of canopy conductance ( $G_c$ ) is crucial for calculating plant ozone uptake; therefore, reliable observations to

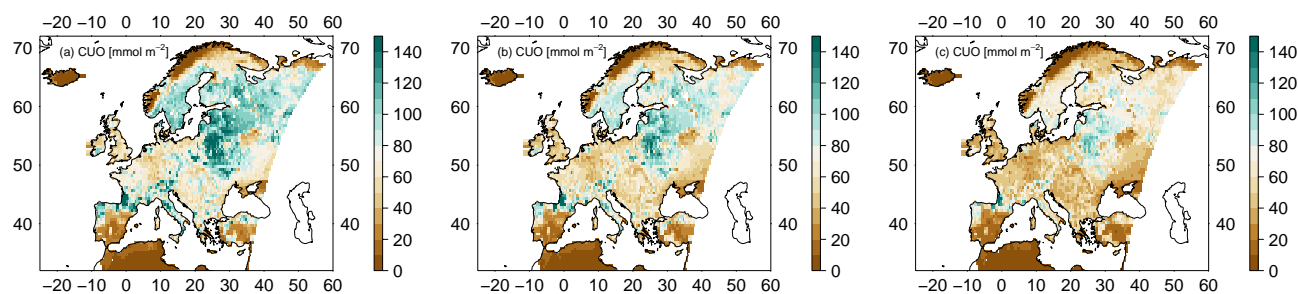


**Figure 9.** Mean decadal canopy-integrated cumulative uptake of  $O_3$  (CUO) ( $\text{mmol m}^{-2}$ ) for Europe of the years 2001–2010. (a) Canopy  $O_3$  concentration is equal to the atmospheric concentration (ATM) and (b)  $O_3$  surface resistance is only determined by stomatal resistance (D-STO). (c) Standard ozone deposition scheme (D).

constrain modelled canopy conductance are highly important. The site-level evaluation shows that OCN produces reasonable estimates of simulated gross primary productivity (GPP), canopy conductance, and latent heat flux (LE) compared to FLUXNET observations. This agreement has to be seen in the light of the diverse set of random and systematic errors in the eddy-covariance measurements as well as derived flux and conductance estimates (Richardson et al., 2012; Knauer et al., 2016). Next to uncertainties about the strength of the aerodynamic coupling between atmosphere and canopy, problems exist at many sites with respect to the energy balance closure (Wilson et al., 2002). Failure to close the energy balance can cause underestimation of sensible and latent heat, as well as an overestimation of available energy, with mean bias of 20 % where the imbalance is greatest during nocturnal periods (Wilson et al., 2002). This imbalance propagates to estimates of canopy conductance, which is inferred from latent and sensible heat fluxes. The energy imbalance furthermore appears to affect estimates of  $CO_2$  uptake and respiration (Wilson et al., 2002). Flux partitioning algorithms which extrapolate night-time ecosystem respiration estimates to daytime introduce an additional potential for bias in the estimation of GPP (Reichstein et al., 2005). Nevertheless, the general good agreement of  $G_c$  compared to FLUXNET estimates, together with the finding that modelled values of key ozone variables are within observed ranges, supports the use of the extended OCN model for determining the effect of air pollution on terrestrial carbon, nitrogen, and water cycling.

A key difference from previous studies is our use of the use of the ozone deposition scheme, which reduces  $O_3$  surface concentrations and hence also the estimated  $O_3$  uptake and accumulation (see Fig. 9). Accounting for stomatal and non-stomatal deposition in the calculation of the surface  $O_3$  concentrations considerably impacts the estimated plant uptake of  $O_3$ .  $O_3$  uptake and cumulated uptake are considerably overestimated when atmospheric ozone concentrations are used to calculate  $O_3$  uptake or when in the calculation of leaf-level  $O_3$  concentrations only stomatal destruction of  $O_3$  is regarded (see Sect. 3.5). Compared to the values that

would have been obtained if the CTM  $O_3$  concentrations of the atmosphere (from ca. 45 m height) had been used directly at the leaf surface, our simulations yield a decrease in CUO by 31 % (European means for the years 2001–2010). A significant fraction of the decreases is associated with non-stomatal  $O_3$  uptake and destruction at the surface, which decreased the simulated cumulative  $O_3$  uptake by 16 %. To obtain an estimate of CUO that is as accurate as possible, stomatal and non-stomatal destruction of  $O_3$  and their impacts on canopy  $O_3$  concentrations should be accounted for in terrestrial biosphere models (Tuovinen et al., 2009). Flux-based ozone damage assessment models may overestimate ozone-related damage unless they properly account for non-stomatal  $O_3$  uptake at the surface.

We note that vegetation type and dynamics also impact the stomatal and non-stomatal deposition of  $O_3$ , and hence the calculation of the leaf-level  $O_3$  concentrations. This impedes the use of CTM-derived leaf-level  $O_3$  concentration, as CTM and vegetation specifications may differ strongly. Using the  $O_3$  from the lowest level of the atmosphere reduces this problem, but running a terrestrial biosphere with a fixed atmospheric boundary condition (and not coupled to a atmospheric CTM) is still a simplification that prevents biosphere–atmosphere feedbacks and therefore to potential discrepancies between vegetation and CTM. Not accounting for this feedback and stomatal and non-stomatal  $O_3$  deposition might result in an overestimation of  $O_3$  uptake and hence potential damage in the vegetation model. The deposition scheme in OCN offers the potential to couple vegetation and chemical transport modelling and is thus a step forward towards coupled atmosphere–vegetation simulations.

#### 4.2 Estimating vegetation damage from ozone uptake

A key aspect of ozone damage estimates are the assumed dose–response relationships, which relate  $O_3$  uptake to plant damage. The use of flux-based relationships is generally thought to improve damage estimates compared to concentration-based metrics (e.g. AOT40), since stomatal constraints on  $O_3$  uptake are taken into account, yielding

very different spatial patterns of exposure hotspots (Simpson et al., 2007). Similar to Simpson et al. (2007), we find strongly differing patterns between cumulative O<sub>3</sub> uptake (CUO) and AOT40 in our simulations here (see Fig. 6), where highest exposure is found not only in southern Europe, where the O<sub>3</sub> concentration is highest, but also in eastern Europe.

Several dose–response relationships exist for biomass or yield damage (see LRTAP Convention, 2010, for an overview), there are few estimates of the likely cause of this damage, i.e. the reduction in net photosynthesis. In this study, the damage relationship to net photosynthesis proposed by Wittig et al. (2007) is used. The major advantage of this relationship is that it has been obtained by meta-analysis of many different tree species and thus might indicate an average response. This relationship is therefore used for all modelled PFTs. However, a substantial disadvantage is that the meta-analysis implies a damage of 6.16 % at zero accumulated O<sub>3</sub> uptake with a rather minor increase in damage with increasing O<sub>3</sub> uptake. This might be an important factor explaining the lower ozone damage estimates of OCN compared to other terrestrial biosphere models. In Lombardozzi et al. (2015) also a damage relationship derived from a meta-analysis is used; however, the disadvantage of predicted ozone damage at zero accumulated O<sub>3</sub> uptake there is even greater compared to Wittig et al. (2007). Two out of three modelled PFTs assume –12.5 and –16.1 % ozone damage at zero accumulated O<sub>3</sub> uptake (broadleaved and needle-leaved species respectively) and the third PFT (grass and crop) assumes 19.8 % at zero accumulated O<sub>3</sub> uptake together with a small increase in damage with increasing O<sub>3</sub> uptake (Lombardozzi et al., 2015). An evaluation of the different proposed damage functions implemented in terrestrial biosphere models (e.g. Wittig et al., 2007; Lombardozzi et al., 2015; Sitch et al., 2007) is necessary to elucidate which are able to reproduce, for example, observed patterns of biomass damage and hence might be suitable to predict regional or global damage estimates. Furthermore, new damage relationships for different plant groups would be desirable for use in dynamic vegetation models to improve the ozone damage estimates, for example by ensuring an intercept close to one (zero damage at zero accumulated O<sub>3</sub>).

The use of a (possibly PFT-specific) flux threshold and its magnitude naturally also impacts the CUOY (canopy cumulative O<sub>3</sub> uptake above a threshold of  $Y \text{ nmol m}^{-2} \text{ s}^{-1}$ ) and possible damage estimates (Tuovinen et al., 2007). The included damage function (Wittig et al., 2007) is designed for the CUO without a flux threshold ( $Y = 0$ ). The impacts of using different flux thresholds on regional estimates of O<sub>3</sub> uptake, accumulation, and damage are still poorly understood and need further research.

It should be noted that using plant O<sub>3</sub> uptake based on leaf-level O<sub>3</sub> concentrations, as done here, together with empirical ozone damage functions, where O<sub>3</sub> uptake is calculated from atmospheric O<sub>3</sub> concentrations, introduces a dis-

crepancy. The O<sub>3</sub> uptake rates of the experiments forming the damage relationship however are calculated from mean ozone concentrations, for example, over the exposure period and the respective average stomatal conductances (Wittig et al., 2007) such that the estimated O<sub>3</sub> uptake and cumulated uptake used to derive the damage relationship are coarse approximations and underlie considerable uncertainty. The error introduced in OCN by using leaf-level O<sub>3</sub> concentrations instead of atmospheric concentrations seems small, especially since the use of the leaf-level O<sub>3</sub> concentration is the physiologically more appropriate approach.

In the current version of OCN only ozone damage to net photosynthesis is accounted for. Other processes like detoxification of O<sub>3</sub> and injury repair (Wieser and Matyssek, 2007; Ainsworth et al., 2012), stomatal sluggishness (Paoletti and Grulke, 2010), and early senescence (Gielen et al., 2007; Ainsworth et al., 2012) are not accounted for. Decoupling of photosynthesis and stomatal conductance (e.g. through stomatal sluggishness) might impact GPP and transpiration damage estimates and requires further analysis. Accounting for direct impairment of the stomata might reduce the reported reductions in transpiration or even cause an increase compared to simulations with no ozone damage. Reduced carbon gain due to early senescence might impact the growth and biomass accumulation of plants (Gielen et al., 2007; Ainsworth et al., 2012) and ought to also be included in terrestrial biosphere models.

## 5 Conclusions

Estimates of O<sub>3</sub> impacts on plant gross primary productivity vary substantially. This uncertainty in the magnitude of damage and hence the potential impact on the global carbon budget is related to different approaches to model ozone damage. The use of a comparatively detailed ozone deposition scheme that accounts for non-stomatal as well as stomatal deposition when calculating surface O<sub>3</sub> concentrations substantially affects O<sub>3</sub> uptake in our model. We therefore recommend that non-stomatal O<sub>3</sub> uptake be routinely included in model assessments of ozone damage to obtain a better estimate of ozone uptake and accumulation. We show that O<sub>3</sub> uptake into the stomata is mainly determined by the canopy conductance in the ozone deposition scheme used here. This highlights the importance of reliable modelling of canopy conductances as well as realistic surface O<sub>3</sub> concentrations to obtain as accurate as possible estimates of O<sub>3</sub> uptake, which are the basis for plant damage estimates. Suitable ozone damage relationships to net photosynthesis for different plant groups are essential to relate the accumulated O<sub>3</sub> uptake to plant damage in a model. Mean responses of plant groups similar to commonly modelled PFTs are also desirable. Only a few damage relationships exist, which indicate mean responses of several species (e.g. Wittig et al., 2007; Lombardozzi et al., 2013, which, however, propose very different relationships).

Furthermore, the impact of the plants ability to detoxify  $O_3$  should be considered by using, for example, flux thresholds, as well as the combined effects of  $O_3$  with air pollution (nitrogen deposition) and climate change (elevated  $CO_2$ ) on the plants' carbon uptake.

## 6 Data availability

No original measurements were used. The FLUXNET measurements can be accessed from the La Thuile Dataset (<http://fluxnet.fluxdata.org/data/la-thuille-dataset/>).

### Appendix A: Aerodynamic resistance

To calculate the O<sub>3</sub> deposition of the free atmosphere at the lowest level of the CTM (approximately 45 m) to the vegetation canopy, it is necessary to know the aerodynamic resistance between these heights ( $R_{a,45}$ ). These data are model- and land-cover-specific, and thus not provided by the CTM. Instead, we approximate  $R_{a,45}$  from the wind speed at 45 m height ( $u_{45}$ ) and the friction velocity  $u_*$  according to

$$R_{a,45} = \frac{u_{45}}{u_*^2}, \quad (\text{A1})$$

where  $u_*$  is calculated from the wind speed at 10 m height ( $u_{10}$ ) using the atmospheric resistance calculations of the ORCHIDEE model (Krinner et al., 2005). The wind at 45 m ( $u_{45}$ ) is approximated by assuming the logarithmic wind profile for neutral atmospheric conditions (Monteith and Unsworth, 2007) due to the lack of information on any other relevant atmospheric properties at 45 m height:

$$u_{45} = u_{10} \frac{\log\left(\frac{45}{z_0}\right)}{\log\left(\frac{10}{z_0}\right)}, \quad (\text{A2})$$

where  $z_0$  is the roughness length.

It varies depending on surface conditions and vegetation carbon uptake.

### Appendix B: Emissions inventory

Emissions for the EMEP model were derived by merging data from three main sources. Firstly, emissions for 2005 and 2010 were taken from the ECLIPSE database produced by IIASA for various EU Projects and the Task Force on Hemispheric Transport of Air Pollution (Amann et al., 2013; Stohl et al., 2015), although with improved spatial resolution over Europe by making use of the 7 km resolution MACC-2 emissions produced by TNO (Kuenen et al., 2014). For 1990, emissions from land-based sources were taken directly from the EMEP database for that year, since 1990 had been the subject of recent review and quality control (e.g. Mareckova et al., 2013). Emissions between 1990 and 2005 were estimated via linear interpolation between these 2005 and EMEP 1990 values. Emissions prior to 1990 were derived by scaling the EMEP 1990 emissions by the emissions ratios found in the historical data series of Lamarque et al. (2010).

Emissions of the biogenic hydrocarbon isoprene from vegetation are calculated using the model's land cover and meteorological data (Simpson et al., 2012, 1999). Emissions of NO from biogenic sources (soils, forest fires, etc.) were set to zero given both their uncertainty and sporadic occurrence. Tests have shown that this approximation has only a small impact on annual deposition totals to the EU area, even for simulations at the start of the 20th century. Volcanic emissions of sulfur dioxide (SO<sub>2</sub>) were set to a constant value from the year 2010.

**Table A1.** Characteristics of the FLUXNET sites used in this study.

Sites	Latitude	Longitude	Climate <sup>a</sup>	PFT <sup>b</sup>	Years	Reference
AT-Neu	47.12	11.32	Cfb	TeH	2002–2005	Wohlfahrt et al. (2008b)
CH-Oe1	47.29	7.73	Cfb	TeH	2002–2006	Ammann et al. (2007)
DE-Bay	50.14	11.87	Cfb	CEF	1997–1998	Rebmann et al. (2004)
DE-Hai	51.08	10.45	Cfb	TeBDF	2000–2006	Kutsch et al. (2008)
DE-Meh	51.28	10.66	Cfb	TeH	2004–2006	Scherer-Lorenzen et al. (2007)
DE-Tha	50.96	13.57	Cfb	CEF	2004–2006	Grünwald and Bernhofer (2007)
DK-Lva	55.68	12.08	Cfb	TeH	2005–2006	Gilmanov et al. (2007)
DK-Sor	55.49	11.65	Cfb	TeBDF	1997–2006	Lagergren et al. (2008)
ES-ES1	39.35	−0.32	Csa	CEF	1999–2004	Sanz et al. (2004)
FI-Hyy	61.85	24.29	Dfc	CEF	2001–2006	Suni et al. (2003)
FR-Hes	48.67	7.06	Cfb	TeBDF	2001–2006	Granier et al. (2000)
FR-LBr	44.72	−0.77	Cfb	CEF	2003–2006	Berbigier et al. (2001)
FR-Pue	43.74	3.60	Csa	TeBEF	2001–2006	Keenan et al. (2010)
IL-Yat	31.34	35.05	BSh	CEF	2001–2002	Grünzweig et al. (2003)
IT-Cpz	41.71	12.38	Csa	TeBEF	2001–2006	Tirone et al. (2003)
IT-Lav	45.96	11.28	Cfb	CEF	2006–2006	Marcolla et al. (2003)
IT-MBo	46.02	11.05	Cfb	TeH	2003–2006	Wohlfahrt et al. (2008a)
IT-PT1	45.20	9.06	Cfa	TeBDF	2003–2004	Migliavacca et al. (2009)
IT-Ro1	42.41	11.93	Csa	TeBDF	2002–2006	Rey et al. (2002)
IT-Ro2	42.39	11.92	Csa	TeBDF	2002–2006	Tedeschi et al. (2006)
IT-SRo	43.73	10.28	Csa	CEF	2003–2006	Chiesi et al. (2005)
NL-Loo	52.17	5.74	Cfb	CEF	1997–2006	Dolman et al. (2002)
PT-Esp	38.64	−8.60	Csa	TeBEF	2002–2006	Pereira et al. (2007)
PT-Mi1	38.54	−8.00	Csa	TeS	2003–2005	Pereira et al. (2007)
SE-Fla	64.11	19.46	Dfc	CEF	2000–2002	Lindroth et al. (2008)
SE-Nor	60.09	17.48	Dfb	CEF	1996–1997	Lagergren et al. (2008)

<sup>a</sup> Köppen–Geiger climate zone (BSh: hot arid steppe; Cfa: humid, warm temperate, hot summer; Cfb: humid, warm temperate, warm summer; Csa: summer dry, warm temperate, hot summer; Dfb: cold, humid, warm summer; Dfc: cold, humid, cold summer). <sup>b</sup> Plant functional type (TeBEF: temperate broadleaf evergreen forest; TeBDF: temperate broadleaf deciduous forest; CEF: coniferous evergreen forest; TeS: temperate open woodland with C<sub>3</sub> grass; TeH: C<sub>3</sub> grassland).

**Table A2.** Coefficient of determination ( $R^2$ ) and root mean square error (RMSE) for GPP, canopy conductance ( $G_c$ ), and latent heat flux (LE) for all sites and for sites dominated by broadleaved trees, needle-leaved trees, C<sub>3</sub> grass, and C<sub>3</sub> grass excluding the AT-Neu site (outlier).

	All sites	Broadleaved	Needle-leaved	C <sub>3</sub> grass	C <sub>3</sub> grass (excluding AT-Neu)
$R^2$ : GPP	0.465	0.714	0.8	0.139	0.058
RMSE: GPP	3.495	3.771	1.944	5.175	2.257
$R^2$ : $G_c$	0.458	0.69	0.722	0.013	0.01
RMSE: $G_c$	0.001	0.002	0.001	0.002	0.002
$R^2$ : LE	0.566	0.725	0.9	0.022	0.002
RMSE: LE	30.897	39.725	13.977	37.124	40.493

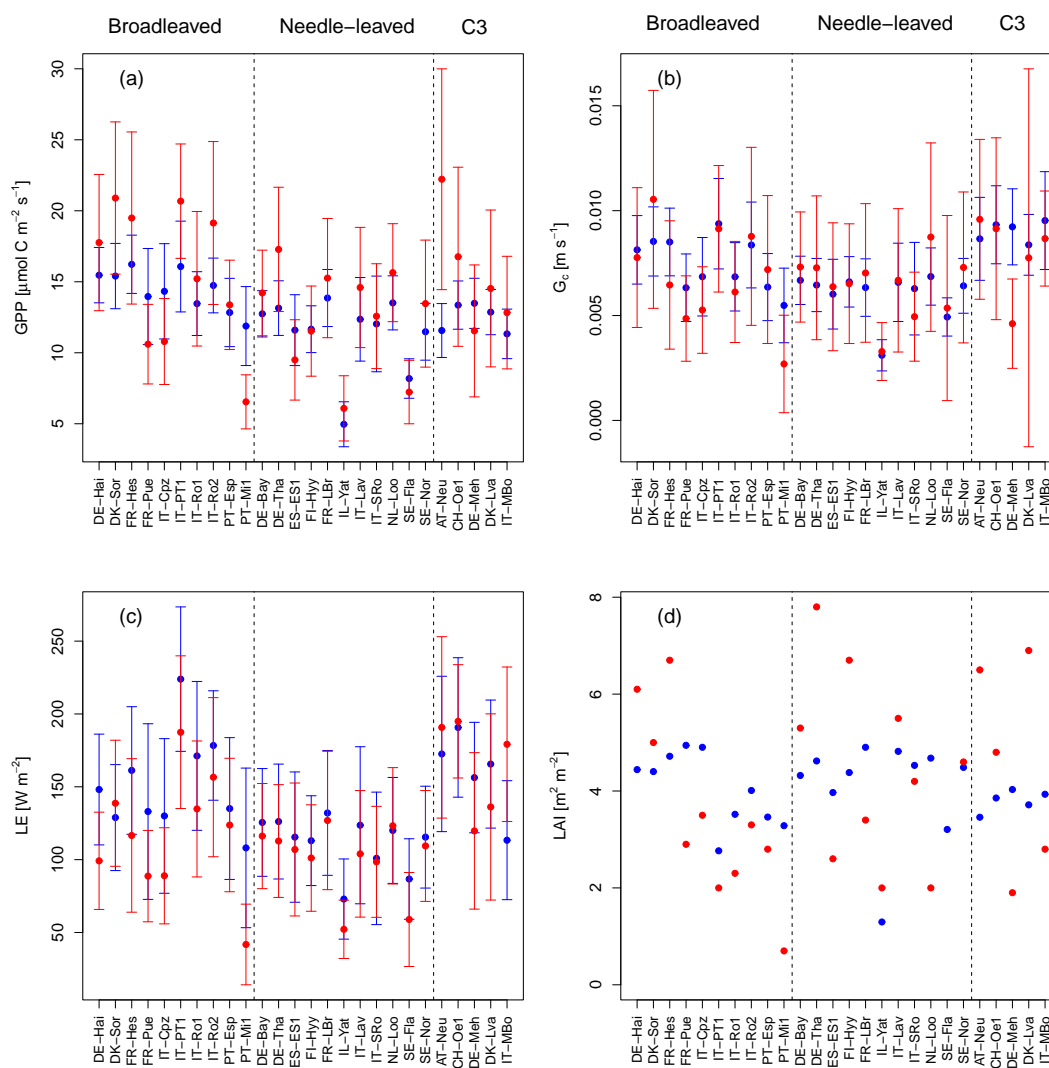


**Figure A1.** Comparison of measured (a) GPP, (b)  $G_c$ , (c) latent heat flux (LE), and (d) LAI at 26 European FLUXNET sites (red) and simulations by OCN (blue). Displayed are means and standard deviation of daily means of the measuring/simulation period, with the exceptions of FLUXNET-derived LAI, which is based on point measurements.

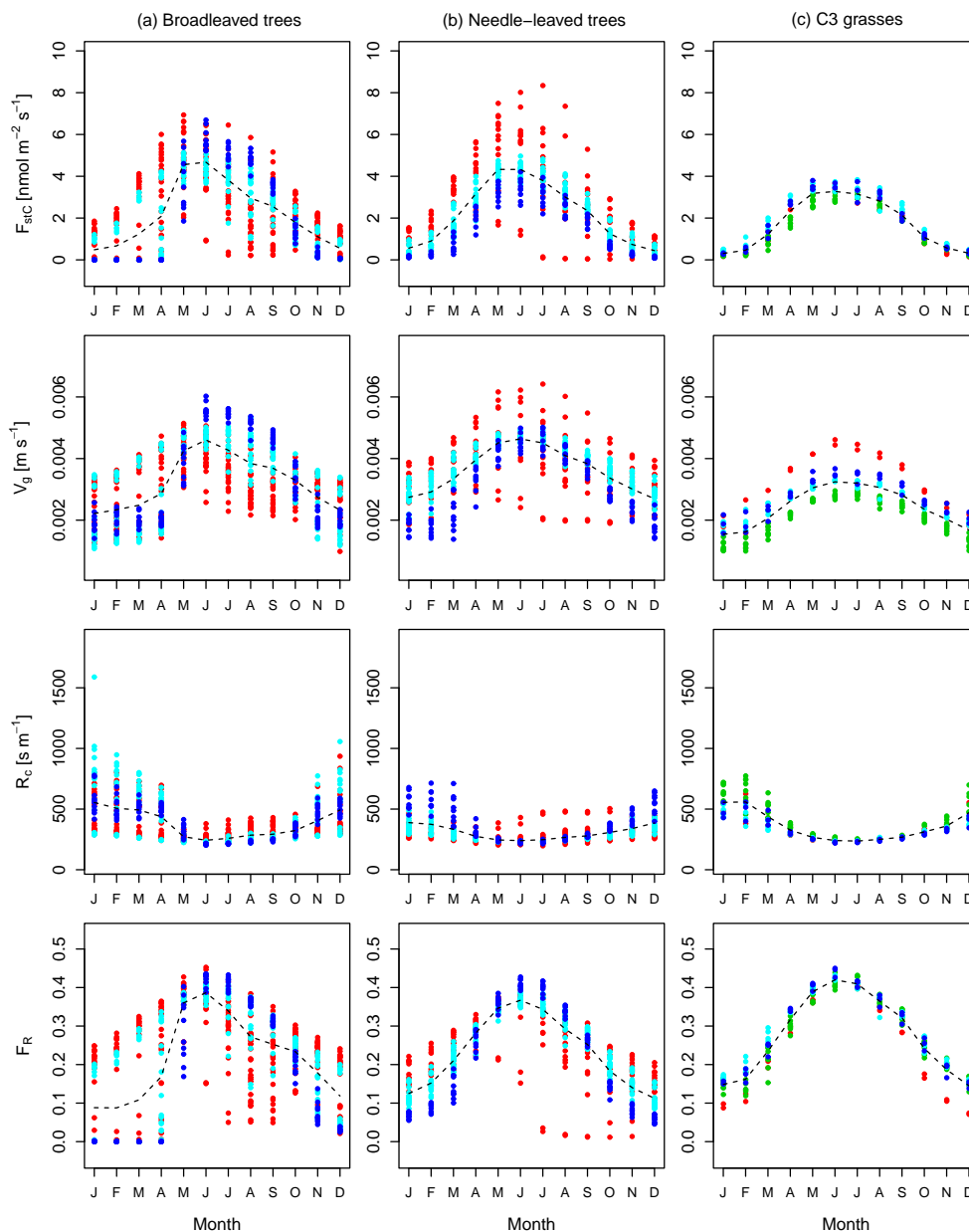


**Figure A2.** Simulated monthly mean values of  $\text{O}_3$  uptake ( $F_{stc}$ ),  $\text{O}_3$  deposition velocity ( $V_g$ ),  $\text{O}_3$  surface resistance ( $R_c$ ), and the flux ratio ( $F_R$ ) for sites dominated by broadleaved trees (left column), needle-leaved trees (central column), and  $\text{C}_3$  grasses (right column). The colour indicates the location of the site. Dark blue: Denmark, Sweden, and Finland; light blue: Germany, France, and Netherlands; green: Austria and Switzerland; red: Italy, Portugal, Spain, and Israel. Broken line: mean of all sites and years of the 12 months.

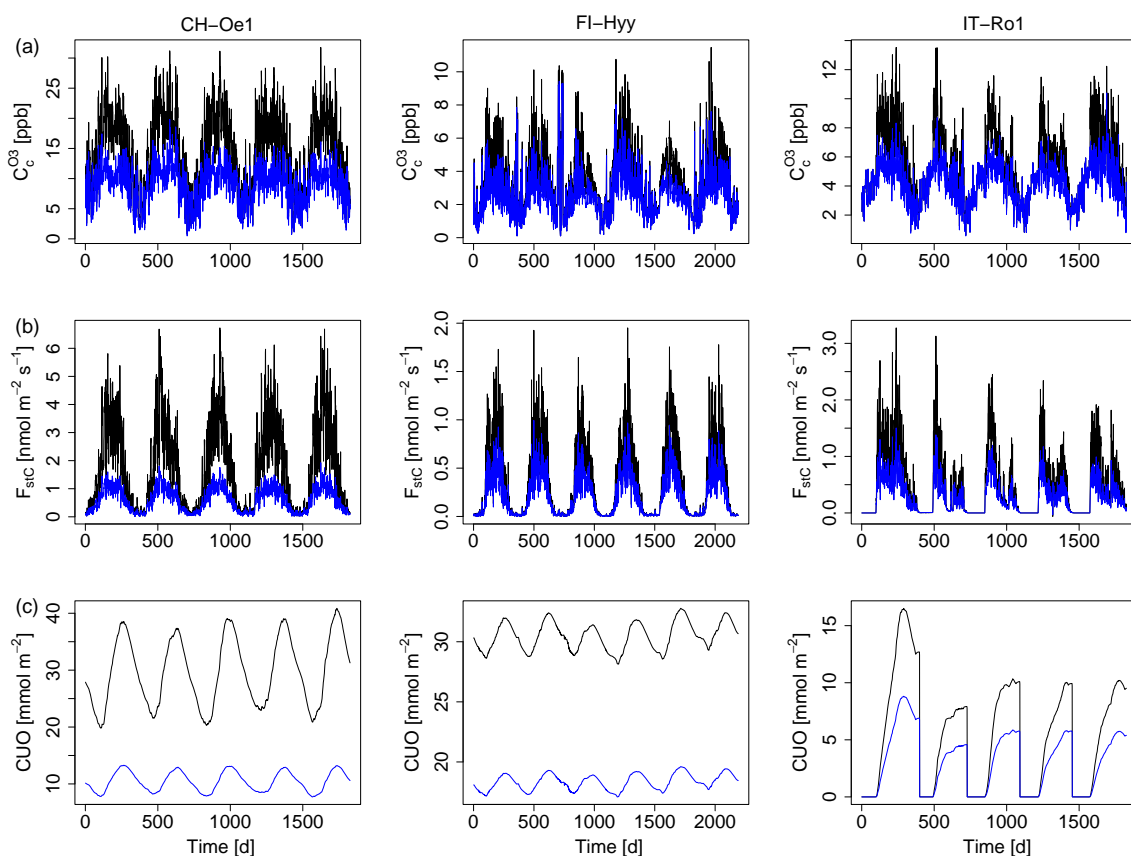


**Figure A3.** Differences in mean daily values of the (a) O<sub>3</sub> surface concentration (ppb), (b) canopy-integrated O<sub>3</sub> uptake into the leaves ( $\text{nmol m}^{-2} \text{s}^{-1}$ ), and (c) canopy-integrated cumulative uptake of O<sub>3</sub> (CUO) ( $\text{mmol m}^{-2}$ ) for the three FLUXNET sites CH-Oe1, FI-Hyy and IT-Ro1. Blue: difference between the D-STO model and the standard model (D); black: difference between the ATM model and the standard model (D).

**Acknowledgements.** We would like to thank Magnus Engardt of the Swedish Meteorological and Hydrological Institute for providing the RCA3 climate dataset. The research leading to this publication was supported by the EU Framework Programme through grant no. 282910 (ECLAIRE), as well as the Max Planck Society for the Advancement of Science e.V. through the ENIGMA project. This project received funding from the European Research Council (ERC) under the European Union's Horizon 2020 research and innovation programme (grant agreement no. 647204; QUINCY). Computer time for EMEP model runs was supported by the Research Council of Norway (Programme for Supercomputing).

Edited by: A. V. Eliseev

Reviewed by: F. Dentener and one anonymous referee

## References

- Ainsworth, E. A., Yendrek, C. R., Sitch, S., Collins, W. J., and Emberson, L. D.: The Effects of Tropospheric Ozone on Net Primary Productivity and Implications for Climate Change, *Ann. Rev. Plant Biol.*, 63, 637–661, 2012.
- Amann, M., Klimont, Z., and Wagner, F.: Regional and Global Emissions of Air Pollutants: Recent Trends and Future Scenarios, *Ann. Rev. Env. Res.*, 38, 31–55, doi:10.1146/annurev-environ-052912-173303, 2013.
- Ammann, C., Flechard, C., Leifeld, J., Neftel, A., and Fuhrer, J.: The carbon budget of newly established temperate grassland depends on management intensity, *Agr. Ecosys. Environ.*, 121, 5–20, 2007.
- Anav, A., Menut, L., Khvorostyanov, D., and Viovy, N.: Impact of tropospheric ozone on the Euro-Mediterranean vegetation, *Glob. Change Biol.*, 17, 2342–2359, 2011.
- Arnth, A., Harrison, S. P., Zaehle, S., Tsigaridis, K., Menon, S., Bartlein, P. J., Feichter, J., Korhola, A., Kulmala, M., O'Donnell, D., Schurgers, G., Sorvari, S., and Vesala, T.: Terrestrial biogeochemical feedbacks in the climate system, *Nat. Geosci.*, 3, 525–532, doi:10.1038/ngeo905, 2010.
- Baldocchi, D., Falge, E., Gu, L., Olson, R., Hollinger, D., Running, S., Anthoni, P., Bernhofer, C., Davis, K., Evans, R., Fuentes, J., Goldstein, A., Katul, G., Law, B., Lee, X., Malhi, Y., Meyers, T., Munger, W., Oechel, W., and Paw, U. K.: FLUXNET: A new tool to study the temporal and spatial variability of ecosystem-scale carbon dioxide, water vapor, and energy flux densities, *Bull. Am. Meteorol. Soc.*, 82, 2415–2434, 2001.
- Berbigier, P., Bonnefond, J.-M., and Mellmann, P.: CO<sub>2</sub> and water vapour fluxes for 2 years above Euroflux forest site, *Agr. Forest Meteorol.*, 108, 183–197, 2001.
- Chiesi, M., Maselli, F., Bindi, M., Fibbi, L., Cherubini, P., Arlotta, E., Tirone, G., Matteucci, G., and Seufert, G.: Modelling carbon budget of Mediterranean forests using ground and remote sensing measurements, *Agr. Forest Meteorol.*, 135, 22–34, 2005.
- Cieslik, S. A.: Ozone uptake by various surface types: a comparison between dose and exposure, *Atmos. Environ.*, 38, 2409–2420, 2004.
- Cooper, O. R., Parrish, D., Ziemke, J., Balashov, N., Cupeiro, M., Galbally, I., Gilge, S., Horowitz, L., Jensen, N., Lamarque, J.-F., Naik, V., Oltmans, S., Schwab, J., Shindell, D., Thompson, A., Thouret, V., Wang, Y., and Zbinden, R.: Global distribution and trends of tropospheric ozone: An observation-based review, *Elementa*, 2, 000029, doi:10.12952/journal.elementa.000029, 2014.
- Coyle, M., Nemitz, E., Storeton-West, R., Fowler, D., and Cape, J. N.: Measurements of ozone deposition to a potato canopy, *Agr. Forest Meteorol.*, 149, 655–666, 2009.
- Dolman, A., Moors, E., and Elbers, J.: The carbon uptake of a mid latitude pine forest growing on sandy soil, *Agr. Forest Meteorol.*, 111, 157–170, 2002.
- Ducoudré, N. I., Laval, K., and Perrier, A.: SECHIBA, a new set of parameterizations of the hydrologic exchanges at the land-atmosphere interface within the LMD atmospheric general circulation model, *J. Clim.*, 6, 248–273, 1993.
- Emberson, L., Ashmore, M., Cambridge, H., Simpson, D., and Tuovinen, J.: Modelling stomatal ozone flux across Europe, *Environ. Pollut.*, 109, 403–413, 2000.
- Emberson, L., Ashmore, M., Simpson, D., Tuovinen, J.-P., and Cambridge, H.: Modelling and mapping ozone deposition in Europe, *Water Air Soil Pollut.*, 130, 577–582, 2001.
- Engardt, M., Simpson, D., and Granat, L.: Historical and projected (1900 to 2050) deposition of sulphur and nitrogen in Europe, submitted, 2017.
- Felzer, B., Kicklighter, D., Melillo, J., Wang, C., Zhuang, Q., and Prinn, R.: Effects of ozone on net primary production and carbon sequestration in the conterminous United States using a biogeochemistry model, *Tellus B*, 56, 230–248, 2004.
- Felzer, B., Reilly, J., Melillo, J., Kicklighter, D., Sarofim, M., Wang, C., Prinn, R., and Zhuang, Q.: Future effects of ozone on carbon sequestration and climate change policy using a global biogeochemical model, *Climatic Change*, 73, 345–373, 2005.
- Fiore, A., Dentener, F., Wild, O., Cuvelier, C., Schultz, M., Textor, C., Schulz, M., Atherton, C., Bergmann, D., Bey, I., Carmichael, G., Doherty, R., Duncan, B., Faluvegi, G., Folberth, G., Garcia Vivanco, M., Gauss, M., Gong, S., Hauglustaine, D., Hess, P., Holloway, T., Horowitz, L., Isaksen, I., Jacob, D., Jonson, J., Kaminski, J., Keating, T., Lupu, A., MacKenzie, I., Marmer, E., Montanaro, V., Park, R., Pringle, K., Pyle, J., Sander, M., Schroeder, S., Shindell, D., Stevenson, D., Szopa, S., Van Dingenen, R., Wind, P., Wojcik, G., Wu, S., Zeng, G., and Zuber, A.: Multi-model estimates of intercontinental source-receptor relationships for ozone pollution, *J. Geophys. Res.*, 114, doi:10.1029/2008JD010816, doi:10.1029/2008JD010816, 2009.
- Fowler, D., Pilegaard, K., Sutton, M., Ambus, P., Raivonen, M., Duyzer, J., Simpson, D., Fagerli, H., Fuzzi, S., Schjørring, J., Granieri, C., Neftel, A., Isaksen, I., Laj, P., Maione, M., Monks, P., Burkhardt, J., Daemmgen, U., Neiryneck, J., Personne, E., Wichink-Kruit, R., Butterbach-Bahl, K., Flechard, C., Tuovinen, J., Coyle, M., Gerosa, G., Loubet, B., Altimir, N., Gruenhage, N., Ammann, C., Cieslik, S., Paoletti, E., Mikkelsen, T., Røpoulsen, H., Cellier, P., Cape, J., Horvath, L., Loreto, F., Ninnemets, Ü., Palmer, P., Rinne, J., Misztal, P., Nemitz, E., Nilsson, D., Pryor, S., Gallagher, M., Vesala, T., Skiba, U., Brüggemann, N., and Zechmeister-Boltenstern, S.: Atmospheric composition change: ecosystems–atmosphere interactions, *Atmos. Environ.*, 43, 5193–5267, 2009.
- Friend, A. and Kiang, N.: Land surface model development for the GISS GCM: Effects of improved canopy physiology on simulated climate, *J. Clim.*, 18, 2883–2902, 2005.

- Fusco, A. and Logan, J.: Analysis of 1970–1995 trends in tropospheric ozone at Northern Hemisphere midlatitudes with the GEOS-CHEM model, *J. Geophys. Res.*, 108, 1988–1997, 2003.
- Gerosa, G., Cieslik, S., and Ballarin-Denti, A.: Micrometeorological determination of time-integrated stomatal ozone fluxes over wheat: a case study in Northern Italy, *Atmos. Environ.*, 37, 777–788, 2003.
- Gerosa, G., Marzuoli, R., Cieslik, S., and Ballarin-Denti, A.: Stomatal ozone fluxes over a barley field in Italy, “Effective exposure” as a possible link between exposure-and flux-based approaches, *Atmos. Environ.*, 38, 2421–2432, 2004.
- Gerosa, G., Vitale, M., Finco, A., Manes, F., Denti, A. B., and Cieslik, S.: Ozone uptake by an evergreen Mediterranean forest (*Quercus ilex*) in Italy. Part I: Micrometeorological flux measurements and flux partitioning, *Atmos. Environ.*, 39, 3255–3266, 2005.
- Gielen, B., Löw, M., Deckmyn, G., Metzger, U., Franck, F., Heerdt, C., Matyssek, R., Valcke, R., and Ceulemans, R.: Chronic ozone exposure affects leaf senescence of adult beech trees: a chlorophyll fluorescence approach, *J. Experim. Bot.*, 58, 785–795, doi:10.1093/jxb/erl222, 2007.
- Gilmanov, T., Soussana, J., Aires, L., Allard, V., Ammann, C., Balzarolo, M., Barcza, Z., Bernhofer, C., Campbell, C., Cernusca, A., Cescatti, A., Clifton-Brown, J., Dirks, B., Dore, S., Eugster, W., Fuhrer, J., Gimeno, C., Gruenwald, T., Haszpra, L., Hensen, A., Ibrom, A., Jacobs, A., Jones, M., Lanigan, G., Laurila, T., Lohila, A., Manca, G., Marcolla, B., Nagy, Z., Pilegaard, K., Pinter, K., Pio, C Raschi, A., Rogiers, N., Sanz, M., Stefani, P., Sutton, M., Tuba, Z., Valentini, R., Williams, M., and Wohlfahrt, G.: Partitioning European grassland net ecosystem CO<sub>2</sub> exchange into gross primary productivity and ecosystem respiration using light response function analysis, *Agr. Ecosys. Environ.*, 121, 93–120, 2007.
- Granier, A., Ceschia, E., Damesin, C., Dufrière, E., Epron, D., Gross, P., Lebaube, S., Le Dantec, V., Le Goff, N., Lemoine, D., Lucot, E., Ottorini, J., Pontailler, J., and Saugier, B.: The carbon balance of a young beech forest, *Funct. Ecol.*, 14, 312–325, 2000.
- Grünwald, T. and Bernhofer, C.: A decade of carbon, water and energy flux measurements of an old spruce forest at the Anchor Station Tharandt, *Tellus B*, 59, 387–396, 2007.
- Grünzweig, J., Lin, T., Rotenberg, E., Schwartz, A., and Yakir, D.: Carbon sequestration in arid-land forest, *Glob. Change Biol.*, 9, 791–799, 2003.
- Hardacre, C., Wild, O., and Emberson, L.: An evaluation of ozone dry deposition in global scale chemistry climate models, *Atmos. Chem. Phys.*, 15, 6419–6436, doi:10.5194/acp-15-6419-2015, 2015.
- Helton, J. and Davis, F.: Illustration of sampling-based methods for uncertainty and sensitivity analysis, *Risk Anal.*, 22, 591–622, 2002.
- Jenkin, M.: Trends in ozone concentration distributions in the UK since 1990: Local, regional and global influences, *Atmos. Environ.*, 42, 5434–5445, 2008.
- Jung, M., Reichstein, M., Margolis, H., Cescatti, A., Richardson, A., Arain, M., Arneth, A., Bernhofer, C., Bonal, D., Chen, J., Gianelle, D., Gobron, N., Kiely, G., Kutsch, W., Lasslop, G., Law, B., Lindroth, A., Merbold, L., Montagnani, L., Moors, E., Papale, D., Sottocornola, M., Vaccari, F., and Williams, C.: Global patterns of land-atmosphere fluxes of carbon dioxide, latent heat, and sensible heat derived from eddy covariance, satellite, and meteorological observations, *J. Geophys. Res.-Biogeol.*, 116, g00J07, doi:10.1029/2010JG001566, 2011.
- Kangasjärvi, J., Talvinen, J., Utrianen, M., and Karjalainen, R.: Plant defence systems induced by ozone, *Plant Cell Environ.*, 17, 783–794, 1994.
- Keenan, T., Sabate, S., and Gracia, C.: Soil water stress and coupled photosynthesis–conductance models: Bridging the gap between conflicting reports on the relative roles of stomatal, mesophyll conductance and biochemical limitations to photosynthesis, *Agr. Forest Meteorol.*, 150, 443–453, 2010.
- Keronen, P., Reissell, A., Rannik, U., Pohja, T., Siivola, E., Hiltunen, V., Hari, P., Kulmala, M., and Vesala, T.: Ozone flux measurements over a Scots pine forest using eddy covariance method: performance evaluation and comparison with flux-profile method, *Boreal Environ. Res.*, 8, 425–444, 2003.
- Kjellstrom, E., Nikulin, G., Hansson, U., Strandberg, G., and Ullerstig, A.: 21st century changes in the European climate: uncertainties derived from an ensemble of regional climate model simulations, *Tellus A*, 63, 24–40, doi:10.1111/j.1600-0870.2010.00475.x, 2011.
- Klingberg, J., Danielsson, H., Simpson, D., and Pleijel, H.: Comparison of modelled and measured ozone concentrations and meteorology for a site in south-west Sweden: Implications for ozone uptake calculations, *Environ. Poll.*, 115, 99–111, 2008.
- Knauer, J., Werner, C., and Zaehle, S.: Evaluating stomatal models and their atmospheric drought response in a land surface scheme: A multibiome analysis, *J. Geophys. Res.-Biogeol.*, 120, 1894–1911, 2015.
- Knauer, J., Zaehle, S., Reichstein, M., Medlyn, B. E., Forkel, M., Hagemann, S., and Werner, C.: The response of ecosystem water-use efficiency to rising atmospheric CO<sub>2</sub> concentrations: sensitivity and large-scale biogeochemical implications, *New Phytol.*, 2016–22438, doi:10.1111/nph.14288, 2016.
- Krinner, G., Viovy, N., de Noblet-Ducoudré, N., Ogée, J., Polcher, J., Friedlingstein, P., Ciais, P., Sitch, S., and Prentice, I.: A dynamic global vegetation model for studies of the coupled atmosphere-biosphere system, *Global Biogeochem. Cy.*, 19, GB1015, doi:10.1029/2003GB002199, 2005.
- Kronfuß, G., Polle, A., Tausz, M., Havranek, W., and Wieser, G.: Effects of ozone and mild drought stress on gas exchange, antioxidants and chloroplast pigments in current-year needles of young Norway spruce (*Picea abies* (L.) Karst.), *Trees-Struct. Funct.*, 12, 482–489, 1998.
- Kuenen, J., Denier van der Gon, H., Visschedijk, A., van der Brugh, H., and van Gijlswijk, R.: MACC European emission inventory for the years 2003–2007, TNO Report TNO-060-UT-2011-00588, TNO, Utrecht, the Netherlands, www.tno.nl, 2011.
- Kuenen, J., Visschedijk, A., Jozwicka, M., and Denier van der Gon, H.: TNO-MACC\_II emission inventory; a multi-year (2003–2009) consistent high-resolution European emission inventory for air quality modelling, *Atmos. Chem. Phys.*, 14, 10963, doi:10.5194/acp-14-10963-2014, 2014.
- Kutsch, W. L., Kolle, O., Rebmann, C., Knohl, A., Ziegler, W., and Schulze, E.-D.: Advection and resulting CO<sub>2</sub> exchange uncertainty in a tall forest in central Germany, *Ecol. Appl.*, 18, 1391–1405, 2008.
- Lagergren, F., Lindroth, A., Dellwik, E., Ibrom, A., Lankreijer, H., Launiainen, S., Mölder, M., Kolari, P., Pilegaard, K., and Vesala,

- T.: Biophysical controls on CO<sub>2</sub> fluxes of three northern forests based on long-term eddy covariance data, *Tellus B*, 60, 143–152, 2008.
- Laisk, A., Kull, O., and Moldau, H.: Ozone concentration in leaf intercellular air spaces is close to zero, *Plant Physiol.*, 90, 1163–1167, 1989.
- Lamarque, J. F., Bond, T. C., Eyring, V., Granier, C., Heil, A., Klimont, Z., Lee, D., Liousse, C., Mieville, A., Owen, B., Schultz, M. G., Shindell, D., Smith, S. J., Stehfest, E., Van Aardenne, J., Cooper, O. R., Kainuma, M., Mahowald, N., McConnell, J. R., Naik, V., Riahi, K., and van Vuuren, D. P.: Historical (1850–2000) gridded anthropogenic and biomass burning emissions of reactive gases and aerosols: methodology and application, *Atmos. Chem. Physics*, 10, 7017–7039, doi:10.5194/acp-10-7017-2010, 2010.
- Le Quéré, C., Moriarty, R., Andrew, R. M., Peters, G. P., Ciais, P., Friedlingstein, P., Jones, S. D., Sitch, S., Tans, P., Arneeth, A., Boden, T. A., Bopp, L., Bozec, Y., Canadell, J. G., Chini, L. P., Chevallier, F., Cosca, C. E., Harris, I., Hoppema, M., Houghton, R. A., House, J. I., Jain, A. K., Johannessen, T., Kato, E., Keeling, R. F., Kitidis, V., Klein Goldewijk, K., Koven, C., Landa, C. S., Landschützer, P., Lenton, A., Lima, I. D., Marland, G., Mathis, J. T., Metzl, N., Nojiri, Y., Olsen, A., Ono, T., Peng, S., Peters, W., Pfeil, B., Poulter, B., Raupach, M. R., Regnier, P., Rödenbeck, C., Saito, S., Salisbury, J. E., Schuster, U., Schwinger, J., Séférian, R., Segsneider, J., Steinhoff, T., Stocker, B. D., Sutton, A. J., Takahashi, T., Tilbrook, B., van der Werf, G. R., Viovy, N., Wang, Y.-P., Wanninkhof, R., Wiltshire, A., and Zeng, N.: Global carbon budget 2014, *Earth Syst. Sci. Data*, 7, 47–85, doi:10.5194/essd-7-47-2015, 2015.
- Lindroth, A., Klemetsson, L., Grelle, A., Weslien, P., and Langvall, O.: Measurement of net ecosystem exchange, productivity and respiration in three spruce forests in Sweden shows unexpectedly large soil carbon losses, *Biogeochemistry*, 89, 43–60, 2008.
- Lombardozi, D., Sparks, J. P., and Bonan, G.: Integrating O<sub>3</sub> influences on terrestrial processes: photosynthetic and stomatal response data available for regional and global modeling, *Biogeosciences*, 10, 6815–6831, doi:10.5194/bg-10-6815-2013, 2013.
- Lombardozi, D., Levis, S., Bonan, G., Hess, P., and Sparks, J.: The Influence of Chronic Ozone Exposure on Global Carbon and Water Cycles, *J. Clim.*, 28, 292–305, 2015.
- LRTAP Convention: Manual on Methodologies and Criteria for Modelling and Mapping Critical Loads and Levels; and Air Pollution Effects, Risks and Trends, <http://www.rivm.nl/en/themasites/icpmm/index.html>, 2010.
- Luwe, M. and Heber, U.: Ozone detoxification in the apoplast and symplast of spinach, broad bean and beech leaves at ambient and elevated concentrations of ozone in air, *Planta*, 197, 448–455, 1995.
- Marcolla, B., Pitacco, A., and Cescatti, A.: Canopy architecture and turbulence structure in a coniferous forest, *Bound.-Layer Meteorol.*, 108, 39–59, 2003.
- Mareckova, K., Wankmüller, R., Pinterits, M., and Moosman, L.: Inventory Review 2013. Stage 1 and 2 and review of gridded data, EMEP/CEIP Technical Report 1/2013, EEA/CEIP Vienna, 2013.
- Marengo, A., Gouget, H., Nédélec, P., Pagés, J., and Karcher, F.: Evidence of a long-term increase in tropospheric ozone from Pic du Midi data series: Consequences: Positive radiative forcing, *J. Geophys. Res.-Atmos.*, 99, 16617–16632, 1994.
- Massman, W.: A review of the molecular diffusivities of H<sub>2</sub>O, CO<sub>2</sub>, CH<sub>4</sub>, CO, O<sub>3</sub>, SO<sub>2</sub>, NH<sub>3</sub>, N<sub>2</sub>O, NO, AND NO<sub>2</sub> in air, O<sub>2</sub> AND N<sub>2</sub> near STP, *Atmo. Environ.*, 32, 1111–1127, doi:10.1016/S1352-2310(97)00391-9, 1998.
- McKay, M. D., Beckman, R. J., and Conover, W. J.: Comparison of three methods for selecting values of input variables in the analysis of output from a computer code, *Technometrics*, 21, 239–245, 1979.
- Migliavacca, M., Meroni, M., Manca, G., Matteucci, G., Montagnani, L., Grassi, G., Zenone, T., Teobaldelli, M., Goded, I., Colombo, R., and Seufert, G.: Seasonal and interannual patterns of carbon and water fluxes of a poplar plantation under peculiar eco-climatic conditions, *Agr. Forest Meteorol.*, 149, 1460–1476, 2009.
- Mikkelsen, T. N., Ro-Poulsen, H., Hovmand, M. F., Jensen, N. O., Pilegaard, K., and Egeløv, A. H.: Five-year measurements of ozone fluxes to a Danish Norway spruce canopy, *Atmos. Environ.*, 38, 2361–2371, 2004.
- Mills, G., Hayes, F., Simpson, D., Emberson, L., Norris, D., Harmens, H., and Büker, P.: Evidence of widespread effects of ozone on crops and (semi-) natural vegetation in Europe (1990–2006) in relation to AOT40-and flux-based risk maps, *Glob. Change Biol.*, 17, 592–613, 2011a.
- Mills, G., Pleijel, H., Braun, S., Büker, P., Bermejo, V., Calvo, E., Danielsson, H., Emberson, L., Fernández, I., Grünhage, L., Harmens, H., Hayes, F., Karlsson, P., and Simpson, D.: New stomatal flux-based critical levels for ozone effects on vegetation, *Atmos. Environ.*, 45, 5064–5068, 2011b.
- Monteith, J. and Unsworth, M.: Principles of environmental physics, Academic Press, 2007.
- Morgan, P., Ainsworth, E., and Long, S.: How does elevated ozone impact soybean? A meta-analysis of photosynthesis, growth and yield, *Plant Cell Environ.*, 26, 1317–1328, 2003.
- Musselman, R., Lefohn, A., Massman, W., and Heath, R.: A critical review and analysis of the use of exposure-and flux-based ozone indices for predicting vegetation effects, *Atmos. Environ.*, 40, 1869–1888, 2006.
- New, M., Hulme, M., and Jones, P.: Representing twentieth-century space-time climate variability, Part I: Development of a 1961–1990 mean monthly terrestrial climatology, *J. Clim.*, 12, 829–856, 1999.
- Padro, J.: Summary of ozone dry deposition velocity measurements and model estimates over vineyard, cotton, grass and deciduous forest in summer, *Atmos. Environ.*, 30, 2363–2369, 1996.
- Paoletti, E. and Grulke, N.: Ozone exposure and stomatal sluggishness in different plant physiognomic classes, *Environ. Pollut.*, 158, 2664–2671, 2010.
- Parrish, D. D., Law, K. S., Staehelin, J., Derwent, R., Cooper, O. R., Tanimoto, H., Volz-Thomas, A., Gilge, S., Scheel, H.-E., Steinbacher, M., and Chan, E.: Long-term changes in lower tropospheric baseline ozone concentrations at northern mid-latitudes, *Atmos. Chem. Phys.*, 12, 11485–11504, doi:10.5194/acp-12-11485-2012, 2012.
- Pereira, J. S., Mateus, J. A., Aires, L. M., Pita, G., Pio, C., David, J. S., Andrade, V., Banza, J., David, T. S., Paço, T. A., and Rodrigues, A.: Net ecosystem carbon exchange in three contrast-

- ing Mediterranean ecosystems – the effect of drought, *Biogeosciences*, 4, 791–802, doi:10.5194/bg-4-791-2007, 2007.
- Pleijel, H., Danielsson, H., Emberson, L., Ashmore, M., and Mills, G.: Ozone risk assessment for agricultural crops in Europe: further development of stomatal flux and flux–response relationships for European wheat and potato, *Atmos. Environ.*, 41, 3022–3040, 2007.
- Rebmann, C., Anthoni, P., Falge, E., Göckede, M., Mangold, A., Subke, J.-A., Thomas, C., Wichura, B., Schulze, E.-D., Tenhunen, J., and Foken, T.: Carbon budget of a spruce forest ecosystem, Springer, 2004.
- Reich, P.: Quantifying plant response to ozone: a unifying theory, *Tree Physiol.*, 3, 63–91, 1987.
- Reichstein, M., Falge, E., Baldocchi, D., Papale, D., Aubinet, M., Berbigier, P., Bernhofer, C., Buchmann, N., Gilmanov, T., Granier, A., Grünwald, T., Havránková, K., Ilvesniemi, H., Janous, D., Knohl, A., Laurila, T., Lohila, A., Loustau, D., Matteucci, G., Meyers, T., Miglietta, F., Ourcival, J., Pumpanen, J., Rambal, S., Rotenberg, E., Sanz, M., Tenhunen, J., Seufert, G., Vaccari, F., Vesala, T., Yakir, D., and Valentini, R.: On the separation of net ecosystem exchange into assimilation and ecosystem respiration: review and improved algorithm, *Glob. Change Biol.*, 11, 1424–1439, 2005.
- Ren, W., Tian, H., Tao, B., Chappelka, A., Sun, G., Lu, C., Liu, M., Chen, G., and Xu, X.: Impacts of tropospheric ozone and climate change on net primary productivity and net carbon exchange of China's forest ecosystems, *Glob. Ecol. Biogeogr.*, 20, 391–406, 2011.
- Rey, A., Pegoraro, E., Tedeschi, V., De Parri, I., Jarvis, P. G., and Valentini, R.: Annual variation in soil respiration and its components in a coppice oak forest in Central Italy, *Glob. Change Biol.*, 8, 851–866, 2002.
- Richardson, A. D., Aubinet, M., Barr, A. G., Hollinger, D. Y., Ibrom, A., Lasslop, G., and Reichstein, M.: Uncertainty quantification, Springer, 2012.
- Roeckner, E., Brokopf, R., Esch, M., Giorgetta, M., Hagemann, S., Kornbluh, L., Manzini, E., Schlese, U., and Schulzweida, U.: Sensitivity of simulated climate to horizontal and vertical resolution in the ECHAM5 atmosphere model, *J. Clim.*, 19, 3771–3791, doi:10.1175/JCLI3824.1, 2006.
- Samuelsson, P., Jones, C. G., Willen, U., Ullerstig, A., Gollvik, S., Hansson, U., Jansson, C., Kjellstrom, E., Nikulin, G., and Wyser, K.: The Rossby Centre Regional Climate model RCA3: model description and performance, *Tellus A*, 63, 4–23, doi:10.1111/j.1600-0870.2010.00478.x, 2011.
- Sanz, M., Carrara, A., Gimeno, C., Bucher, A., and Lopez, R.: Effects of a dry and warm summer conditions on CO<sub>2</sub> and Energy fluxes from three Mediterranean ecosystems, vol. 6, 2004.
- Scherer-Lorenzen, M., Schulze, E.-D., Don, A., Schumacher, J., and Weller, E.: Exploring the functional significance of forest diversity: a new long-term experiment with temperate tree species (BIOTREE), *Perspect. Plant Ecol.*, 9, 53–70, 2007.
- Simpson, D., Winiwarter, W., Börjesson, G., Cinderby, S., Ferreiro, A., Guenther, A., Hewitt, C. N., Janson, R., Khalil, M. A. K., Owen, S., Pierce, T. E., Puxbaum, H., Shearer, M., Skiba, U., Steinbrecher, R., Tarrasón, L., and Öquist, M. G.: Inventorying emissions from Nature in Europe, *J. Geophys. Res.*, 104, 8113–8152, 1999.
- Simpson, D., Tuovinen, J.-P., Emberson, L., and Ashmore, M.: Characteristics of an ozone deposition module II: sensitivity analysis, *Water Air Soil Pollut.*, 143, 123–137, 2003.
- Simpson, D., Ashmore, M., Emberson, L., and Tuovinen, J.-P.: A comparison of two different approaches for mapping potential ozone damage to vegetation. A model study, *Environ. Pollut.*, 146, 715–725, 2007.
- Simpson, D., Benedictow, A., Berge, H., Bergström, R., Emberson, L. D., Fagerli, H., Flechard, C. R., Hayman, G. D., Gauss, M., Jonson, J. E., Jenkin, M. E., Nyíri, A., Richter, C., Semeena, V. S., Tsyro, S., Tuovinen, J.-P., Valdebenito, Á., and Wind, P.: The EMEP MSC-W chemical transport model – technical description, *Atmos. Chem. Phys.*, 12, 7825–7865, doi:10.5194/acp-12-7825-2012, 2012.
- Simpson, D., Arneth, A., Mills, G., Solberg, S., and Uddling, J.: Ozone – the persistent menace: interactions with the N cycle and climate change, *Current Opinion in Environmental Sustainability*, 9/10, 9–19, doi:10.1016/j.cosust.2014.07.008, 2014a.
- Simpson, D., Christensen, J., Engardt, M., Geels, C., Nyíri, A., Soares, J., Sofiev, M., Wind, P., and Langner, J.: Impacts of climate and emission changes on nitrogen deposition in Europe: a multi-model study, *Atmos. Chem. Physics*, 14, 6995–7017, doi:10.5194/acp-14-6995-2014, 2014b.
- Sitch, S., Cox, P., Collins, W., and Huntingford, C.: Indirect radiative forcing of climate change through ozone effects on the land-carbon sink, *Nature*, 448, 791–794, 2007.
- Sitch, S., Friedlingstein, P., Gruber, N., Jones, S. D., Murray-Tortarolo, G., Ahlström, A., Doney, S. C., Graven, H., Heinze, C., Huntingford, C., Levis, S., Levy, P. E., Lomas, M., Poulter, B., Viovy, N., Zaehle, S., Zeng, N., Arneth, A., Bonan, G., Bopp, L., Canadell, J. G., Chevallier, F., Ciais, P., Ellis, R., Gloor, M., Peylin, P., Piao, S. L., Le Quéré, C., Smith, B., Zhu, Z., and Myneni, R.: Recent trends and drivers of regional sources and sinks of carbon dioxide, *Biogeosciences*, 12, 653–679, doi:10.5194/bg-12-653-2015, 2015.
- Staehelin, J., Thudium, J., Buehler, R., Volz-Thomas, A., and Graber, W.: Trends in surface ozone concentrations at Arosa (Switzerland), *Atmos. Environ.*, 28, 75–87, 1994.
- Stohl, A., Aamaas, B., Amann, M., Baker, L. H., Bellouin, N., Berntsen, T. K., Boucher, O., Cherian, R., Collins, W., Daskalakis, N., Dusinska, M., Eckhardt, S., Fuglestedt, J. S., Harju, M., Heyes, C., Hodnebrog, Ø., Hao, J., Im, U., Kanakidou, M., Klimont, Z., Kupiainen, K., Law, K. S., Lund, M. T., Maas, R., MacIntosh, C. R., Myhre, G., Myriokefalitakis, S., Olivíé, D., Quaas, J., Quennehen, B., Raut, J.-C., Rumbold, S. T., Samset, B. H., Schulz, M., Seland, Ø., Shine, K. P., Skeie, R. B., Wang, S., Yttri, K. E., and Zhu, T.: Evaluating the climate and air quality impacts of short-lived pollutants, *Atmos. Chem. Phys.*, 15, 10529–10566, doi:10.5194/acp-15-10529-2015, 2015.
- Suni, T., Rinne, J., Reissell, A., Altimir, N., Keronen, P., Rannik, U., Maso, M., Kulmala, M., and Vesala, T.: Long-term measurements of surface fluxes above a Scots pine forest in Hyytiälä, southern Finland, 1996–2001, *Boreal Environ. Res.*, 8, 287–302, 2003.
- Tausz, M., Grulke, N., and Wieser, G.: Defense and avoidance of ozone under global change, *Environ. Pollut.*, 147, 525–531, 2007.
- Tedeschi, V., Rey, A., Manca, G., Valentini, R., Jarvis, P. G., and Borghetti, M.: Soil respiration in a Mediterranean oak forest

- at different developmental stages after coppicing, *Glob. Change Biol.*, 12, 110–121, 2006.
- Tirone, G., Dore, S., Matteucci, G., Greco, S., and Valentini, R.: Evergreen Mediterranean forests. carbon and water fluxes, balances, Ecological and ecophysiological determinants, Springer, 2003.
- Tuovinen, J.-P., Simpson, D., Mikkelsen, T., Emberson, L., Ashmore, M., Aurela, M., Cambridge, H., Hovmand, M., Jensen, N., Laurila, T., Pilegaard, K., and Ro-Poulsen, H.: Comparisons of measured and modelled ozone deposition to forests in Northern Europe, *Water Air Soil Pollut.*, 1, 263–274, 2001.
- Tuovinen, J.-P., Ashmore, M., Emberson, L., and Simpson, D.: Testing and improving the EMEP ozone deposition module, *Atmos. Environ.*, 38, 2373–2385, 2004.
- Tuovinen, J.-P., Simpson, D., Emberson, L., Ashmore, M., and Gerosa, G.: Robustness of modelled ozone exposures and doses, *Environ. Pollut.*, 146, 578–586, 2007.
- Tuovinen, J.-P., Emberson, L., and Simpson, D.: Modelling ozone fluxes to forests for risk assessment: status and prospects, *Ann. Forest Sci.*, 66, 1–14, 2009.
- van Aardenne, J. A., Dentener, F. J., Olivier, J. G. J., Goldewijk, C. G. M. K., and Lelieveld, J.: A  $1^\circ \times 1^\circ$  resolution data set of historical anthropogenic trace gas emissions for the period 1890–1990, *Global Biogeochem. Cy.*, 15, 909–928, doi:10.1029/2000GB001265, 2001.
- Vingarzan, R.: A review of surface ozone background levels and trends, *Atmos. Environ.*, 38, 3431–3442, 2004.
- Vitale, M., Gerosa, G., Ballarin-Denti, A., and Manes, F.: Ozone uptake by an evergreen mediterranean forest (*Quercus ilex* L.) in Italy – Part II: flux modelling. Upscaling leaf to canopy ozone uptake by a process-based model, *Atmos. Environ.*, 39, 3267–3278, 2005.
- Wieser, G. and Havranek, W.: Environmental control of ozone uptake in *Larix decidua* Mill.: a comparison between different altitudes, *Tree Physiol.*, 15, 253–258, 1995.
- Wieser, G. and Matyssek, R.: Linking ozone uptake and defense towards a mechanistic risk assessment for forest trees, *New Phytol.*, 174, 7–9, 2007.
- Wieser, G., Matyssek, R., Kostner, B., Oberhuber, W., and Kötnner, B.: Quantifying ozone uptake at the canopy level of spruce, pine and larch trees at the alpine timberline: an approach based on sap flow measurement, *Environ. Pollut.*, 126, 5–8, doi:10.1016/S0269-7491(03)00184-2, 2003.
- Wilson, K., Goldstein, A., Falge, E., Aubinet, M., Baldocchi, D., Berbigier, P., Bernhofer, C., Ceulemans, R., Dolman, H., Field, C., Grelle, A., Ibrom, A., Law, B., Kowalski, A., Meyers, T., Moncrieff, J., Monson, R., Oechel, W., Tenhunen, J., Valentini, R., and Verma, S.: Energy balance closure at FLUXNET sites, *Agr. Forest Meteorol.*, 113, 223–243, 2002.
- Wittig, V., Ainsworth, E., and Long, S.: To what extent do current and projected increases in surface ozone affect photosynthesis and stomatal conductance of trees? A meta-analytic review of the last 3 decades of experiments, *Plant Cell Environ.*, 30, 1150–1162, 2007.
- Wittig, V., Ainsworth, E., Naidu, S., Karnosky, D., and Long, S.: Quantifying the impact of current and future tropospheric ozone on tree biomass, growth, physiology and biochemistry: a quantitative meta-analysis, *Glob. Change Biol.*, 15, 396–424, 2009.
- Wohlfahrt, G., Anderson-Dunn, M., Bahn, M., Balzarolo, M., Berninger, F., Campbell, C., Carrara, A., Cescatti, A., Christensen, T., Dore, S., Eugster, W., Friborg, T., Furger, M., Gianelle, D., Gimeno, C., Hargreaves, K., Hari, P., Haslwanter, A., Johansson, T., Marcolla, B., Milford, C., Nagy, Z., Nemitz, E., Rogiers, N., Sanz, M., Siegwolf, R., Susiluoto, S., Sutton, M., Tuba, Z., Ugolini, F., Valentini, R., Zorer, R., and Cernusca, A.: Biotic, abiotic, and management controls on the net ecosystem  $\text{CO}_2$  exchange of European mountain grassland ecosystems, *Ecosystems*, 11, 1338–1351, 2008a.
- Wohlfahrt, G., Hammerle, A., Haslwanter, A., Bahn, M., Tappeiner, U., and Cernusca, A.: Seasonal and inter-annual variability of the net ecosystem  $\text{CO}_2$  exchange of a temperate mountain grassland: Effects of weather and management, *J. Geophys. Res.-Atmos.*, 113, d08110, doi:10.1029/2007JD009286, 2008b.
- Young, P. J., Archibald, A. T., Bowman, K. W., Lamarque, J.-F., Naik, V., Stevenson, D. S., Tilmes, S., Voulgarakis, A., Wild, O., Bergmann, D., Cameron-Smith, P., Cionni, I., Collins, W. J., Dalsson, S. B., Doherty, R. M., Eyring, V., Faluvegi, G., Horowitz, L. W., Josse, B., Lee, Y. H., MacKenzie, I. A., Nagashima, T., Plummer, D. A., Righi, M., Rumbold, S. T., Skeie, R. B., Shindell, D. T., Strode, S. A., Sudo, K., Szopa, S., and Zeng, G.: Pre-industrial to end 21st century projections of tropospheric ozone from the Atmospheric Chemistry and Climate Model Intercomparison Project (ACCMIP), *Atmos. Chem. Physics*, 13, 2063–2090, doi:10.5194/acp-13-2063-2013, 2013.
- Zaehle, S. and Friend, A.: Carbon and nitrogen cycle dynamics in the O-CN land surface model: 1. Model description, site-scale evaluation, and sensitivity to parameter estimates, *Global Biogeochem. Cy.*, 24, GB1005, doi:10.1029/2009GB003521, 2010.
- Zhang, L., Brook, J. R., and Vet, R.: A revised parameterization for gaseous dry deposition in air-quality models, *Atmos. Chem. Phys.*, 3, 2067–2082, doi:10.5194/acp-3-2067-2003, 2003.
- Zaehle, S., Ciais, P., Friend, A. D., and Prieur, V.: Carbon benefits of anthropogenic reactive nitrogen offset by nitrous oxide emissions, *Nat. Geosci.*, 4, 601–605, 2011.



## Evaluation of simulated ozone effects in forest ecosystems against biomass damage estimates from fumigation experiments

Martina Franz<sup>1,2</sup>, Rocío Alonso<sup>4</sup>, Almut Arneth<sup>5</sup>, Patrick Büker<sup>6</sup>, Susana Elvira<sup>4</sup>, Giacomo Gerosa<sup>7</sup>, Lisa Emberson<sup>6</sup>, Zhaozhong Feng<sup>8</sup>, Didier Le Thiec<sup>9</sup>, Riccardo Marzuoli<sup>7</sup>, Elina Oksanen<sup>10</sup>, Johan Uddling<sup>11</sup>, Matthew Wilkinson<sup>12</sup>, and Sönke Zaehle<sup>1,3</sup>

<sup>1</sup>Biogeochemical Integration Department, Max Planck Institute for Biogeochemistry, Jena, Germany

<sup>2</sup>International Max Planck Research School (IMPRS) for Global Biogeochemical Cycles, Jena, Germany

<sup>3</sup>Michael Stifel Center Jena for Data-driven and Simulation Science, Jena, Germany

<sup>4</sup>Ecotoxicology of Air Pollution, CIEMAT – Research Center for Energy, Environment and Technology, Avda. Complutense 40, edif.70, Madrid 28040, Spain

<sup>5</sup>Karlsruhe Institute of Technology (KIT), Department of Atmospheric Environmental Research (IMK-IFU), Garmisch-Partenkirchen, Germany

<sup>6</sup>Stockholm Environment Institute at York, Environment Dept., University of York, York, YO10 5NG, UK

<sup>7</sup>Department of Mathematics and Physics, Catholic University of Brescia, via Musei 41, Brescia, Italy

<sup>8</sup>State Key Laboratory of Urban and Regional Ecology, Research Center for Eco-Environmental Sciences, Chinese Academy of Sciences, Shuangqing Road 18, Haidian District, Beijing, 100085, China

<sup>9</sup>Inra, Université de Lorraine, AgroParisTech, Silva, 54280 Champenoux, France

<sup>10</sup>Department of Environmental and Biological Sciences, University of Eastern Finland, 80101 Joensuu, Finland

<sup>11</sup>Department of Biological and Environmental Sciences, University of Gothenburg, Gothenburg, Sweden

<sup>12</sup>Centre for Sustainable Forestry and Climate Change, Forest Research, Farnham, UK

**Correspondence:** Martina Franz (mfranz@bgc-jena.mpg.de)

Received: 25 July 2018 – Discussion started: 27 July 2018

Revised: 4 November 2018 – Accepted: 5 November 2018 – Published: 21 November 2018

**Abstract.** Regional estimates of the effects of ozone pollution on forest growth depend on the availability of reliable injury functions that estimate a representative ecosystem response to ozone exposure. A number of such injury functions for forest tree species and forest functional types have recently been published and subsequently applied in terrestrial biosphere models to estimate regional or global effects of ozone on forest tree productivity and carbon storage in the living plant biomass. The resulting impacts estimated by these biosphere models show large uncertainty in the magnitude of ozone effects predicted. To understand the role that these injury functions play in determining the variability in estimated ozone impacts, we use the O-CN biosphere model to provide a standardised modelling framework. We test four published injury functions describing the leaf-level, photosynthetic response to ozone exposure (targeting the maximum carboxylation capacity of Rubisco ( $V_{\text{cmax}}$ ) or net pho-

tosynthesis) in terms of their simulated whole-tree biomass responses against data from 23 ozone filtration/fumigation experiments conducted with young trees from European tree species at sites across Europe with a range of climatic conditions. Our results show that none of these previously published injury functions lead to simulated whole-tree biomass reductions in agreement with the observed dose–response relationships derived from these field experiments and instead lead to significant over- or underestimations of the ozone effect. By re-parameterising these photosynthetically based injury functions, we develop linear, plant-functional-type-specific dose–response relationships, which provide accurate simulations of the observed whole-tree biomass response across these 23 experiments.

## 1 Introduction

Ozone is a phytotoxic air pollutant which enters plants mainly through the leaf stomata, where reactive oxygen species (ROs) are formed that can injure essential leaf functioning (Ainsworth et al., 2012). Ozone-induced declines in net photosynthesis (Morgan et al., 2003; Wittig et al., 2007) have been observed as the result of injury of the photosynthetic apparatus and increased respiration rates caused by investments in the repair of injury, as well as the production of defence compounds (Wieser and Matyssek, 2007; Ainsworth et al., 2012). At the leaf-scale, ozone injury occurs and accumulates when the instantaneous stomatal ozone uptake of leaves surpasses the ability of the leaf to detoxify ozone (Wieser and Matyssek, 2007). These effects are likely the primary cause for reduced rates of net photosynthesis and a decreased supply of carbon and energy for growth and net primary production (NPP), which contributes to the commonly observed ozone-induced reductions in leaf area and plant biomass (Morgan et al., 2003; Lombardozzi et al., 2013; Wittig et al., 2009). Changes in tropospheric ozone abundance and associated changes in ozone-induced injury thus have the potential to affect the ability of the terrestrial biosphere to sequester carbon (Harmens and Mills, 2012; Oliver et al., 2018). However, a quantitative understanding of the effect of ozone pollution on forest growth and carbon sequestration at the regional scale is still lacking. Terrestrial biosphere models can be used to obtain regional or global estimates of ozone damage based on an understanding of how ozone affects plant processes leading to C assimilation and growth. Modelling algorithms to estimate regional or global impacts of ozone on gross primary production (GPP) have been developed for several of these terrestrial biosphere models (Sitch et al., 2007; Lombardozzi et al., 2012a, 2015; Franz et al., 2017; Oliver et al., 2018). However, simulated reductions in GPP due to ozone-induced injury vary substantially between models and model versions (Lombardozzi et al., 2012a, 2015; Franz et al., 2017; Sitch et al., 2007).

This uncertainty is predominantly due to the different approaches that these models use to relate ozone uptake (or ozone exposure) to reductions in whole-tree biomass and in the exact parameterisation of the injury functions and dose–response relationships applied (Karlsson et al., 2004; Pleijel et al., 2004; Wittig et al., 2007; Lombardozzi et al., 2012a, 2013). The injury functions employed by current terrestrial biosphere models differ decidedly in their slope (i.e. the change in injury per unit of time-integrated ozone uptake), intercept (ozone injury at zero time-integrated ozone uptake) and their assumed threshold, below which the ozone uptake rate is considered sufficiently low that ozone will be detoxified before any injury occurs (Karlsson et al., 2004; Pleijel et al., 2004; Lombardozzi et al., 2012a). For example, Sitch et al. (2007) relates the instantaneous ozone uptake exceeding a flux threshold to net photosynthetic injury via an empirically derived factor. An alternative approach has been

to relate ozone injury to net photosynthesis in response to the accumulated ozone uptake rather than to the instantaneous ozone uptake as in Sitch et al. (2007), e.g. by using the CUOY, which refers to the cumulative canopy O<sub>3</sub> uptake above a flux threshold of  $Y \text{ nmol m}^{-2} \text{ s}^{-1}$  (Wittig et al., 2007; Lombardozzi et al., 2012a, 2013; Cailleret et al., 2018).

The effect of ozone on plant growth has been investigated by ozone filtration/fumigation experiments either at the individual experimental level or by pooling data from multiple experiments that have been conducted according to a standardised experimental method. These experiments typically rely on young trees because of their small size. A challenge in developing and testing process-based models of ozone damage from these ozone fumigation experiments is that often only the difference in biomass accumulation between plants grown in an ozone treatment and in ambient or charcoal-filtered air at the end of the experiment are reported. Data from these studies provide evidence for a linear, species-specific relationship between accumulated ozone uptake and reductions in plant biomass (Pleijel et al., 2004; Mills et al., 2011; Nunn et al., 2006, e.g.). Sitch et al. (2007) for instance calibrated their instantaneous leaf-level injury function between ozone uptake and photosynthesis by relating simulated annual net primary production and accumulated ozone uptake to observed biomass dose–response relationships developed by Karlsson et al. (2004) and Pleijel et al. (2004), where biomass/yield damage is related to the phytotoxic ozone dose (POD<sub>y</sub>). The POD<sub>y</sub> refers to the accumulated ozone uptake above a flux threshold of  $y \text{ nmol m}^{-2} \text{ s}^{-1}$  by the leaves representative of the upper-canopy leaves of the plant. Such an approach applies biomass dose–response relationships of young trees to mature trees. However, the effects of ozone on leaf physiology (e.g. net photosynthesis and stomatal conductance) or plant carbon allocation may differ between juvenile and adult trees (Hanson et al., 1994; Samuelson and Kelly, 1996; Kolb and Matyssek, 2001; Paoletti et al., 2010). Whether or not biomass dose–response relationships can be used to calibrate injury functions for mature trees is uncertain.

An alternative approach is to directly simulate ozone injury to photosynthesis, which may have been a major cause for the observed decline in plant biomass production (Ainsworth et al., 2012). Possible injury targets in the simulations can be, for example, the net photosynthesis or leaf-specific photosynthetic activity (such as represented by the maximum carboxylation capacity of Rubisco,  $V_{c\text{max}}$ ). For instance, Lombardozzi et al. (2012a) based their injury function on an experimental study involving a single forest tree species, whereas more recent publications (e.g. Lombardozzi et al., 2015 and Franz et al., 2017) have used injury functions from meta-analyses of a far larger set of filtration/fumigation studies. Meta-analyses have attempted to summarise the responses of plant performance to ozone exposure across a wider range of experiments and vegetation types (Wittig et al., 2007; Lombardozzi et al., 2013; Feng and Kobayashi,

2009; Li et al., 2017; Wittig et al., 2009) and to develop injury functions for plant groups that might provide an estimate of mean plant group responses to ozone. However, these meta-analyses suffer from a lack of consistency in the derivation of either plant injury or ozone exposure and generally report a large amount of unexplained variance. A further complication in the meta-analyses of ozone injury (e.g. Wittig et al., 2007; Lombardozi et al., 2013) is that they have to indirectly estimate the cumulative ozone uptake underlying the observed ozone injury based on a restricted amount of data, which causes uncertainty in the derived injury functions.

Büker et al. (2015) provides an independent data set of whole-tree biomass plant responses to ozone uptake which is independent of data sets that were used to describe injury functions by Wittig et al. (2007) and Lombardozi et al. (2013). This data set has been collected from experiments that follow a more standardised methodology to assess dose–responses and has associated meteorological and ozone data at a high time resolution that allow more accurate estimates of modelled ozone uptake to be made. These dose–response relationships describe whole-tree biomass reductions in young trees derived from standardised ozone filtration/fumigation methods for eight European tree species at 10 locations across Europe (see Table A2 for details; Büker et al., 2015). These data thus provide an opportunity to evaluate simulations of biosphere models that use leaf-level injury functions (describing the effect of ozone uptake on photosynthetic variables) to estimate C assimilation, growth and ultimately whole-tree biomass against these robust empirical dose–response relationships that relate ozone exposure directly to whole-tree biomass response.

Here we test four alternative, previously published ozone injury functions that target either net photosynthesis or the leaf carboxylation capacity ( $V_{\text{cmax}}$ ), which have been included in state-of-the-art terrestrial biosphere models (Lombardozi et al., 2012a, 2015; Franz et al., 2017) against these new biomass dose–response relationships by Büker et al. (2015). We incorporate these injury functions into a single modelling framework, the O-CN model (Zaehle and Friend, 2010; Franz et al., 2017). To reduce model–data mismatch, we test the functions in simulations that mimic to the extent possible the conditions of each of the experiments in the Büker et al. (2015) data set, in particular the young age, such that we can directly compare the simulated to the observed whole-tree biomass reductions in the empirically derived dose–response relationships. This allows us to identify the contribution of these alternative injury function formulations on the simulated whole-tree biomass response. The simulated biomass dose–response relationships are then compared to the data from the experiments to evaluate the capability of the different model versions to reproduce observed dose–response relationships. Based on these comparisons we use a similar approach to that of Sitch et al. (2007) and develop alternative parameterisations of the injury functions to improve the capability of the O-CN model to simu-

late the whole-tree biomass responses observed in the fumigation experiments, with the notable exception that we explicitly simulate in-fumigation experiments and the approximate age of the trees. Finally, we explore whether or not there is a substantial difference in the biomass response to ozone of young or mature trees by using a sequence of model simulations and comparing the response both in terms of whole-tree biomass as well as net primary production.

## 2 Methods

We use the O-CN terrestrial biosphere model (Zaehle and Friend, 2010; Franz and Zaehle, 2018), which is an extension of the ORCHIDEE model (Krinner et al., 2005) to simulate conditions of the ozone fumigation experiments described in Büker et al. (2015). The O-CN model, an average–individual dynamic vegetation model, simulates the terrestrial coupled carbon (C), nitrogen (N) and water cycles for up to 12 plant functional types and is driven by climate data and atmospheric composition.

O-CN simulates a multilayer canopy with up to 20 layers with a thickness of up to 0.5 leaf area index each. Net photosynthesis is calculated according to a modified Farquhar scheme for shaded and sunlit leaves considering the light profiles of diffuse and direct radiation (Zaehle and Friend, 2010). Leaf nitrogen concentration and leaf area determine the photosynthetic capacity. Increases in the leaf nitrogen content increase  $V_{\text{cmax}}$  and  $J_{\text{max}}$  (nitrogen-specific rates of maximum light harvesting, electron transport) and hence maximum net photosynthesis and stomatal conductance per leaf area. The leaf N content is highest at the top of the canopy and exponentially decreases with increasing canopy depth (Friend, 2001; Niinemets et al., 2015). Following this net photosynthesis, stomatal conductance and ozone uptake are generally highest in the top canopy and decrease with increasing canopy depth.

Canopy-integrated assimilated carbon enters a labile non-structural carbon pool, which can either be used to fuel maintenance respiration (a function of tissue nitrogen), storage (for seasonal leaf and fine-root replacement and buffer of inter-annual variability in assimilation) or biomass growth. The labile pool responds within days to changes in GPP; the long-term reserve has a response time of several months, depending on its use to support seasonal foliage and fine-root development or sustain growth in periods of reduced photosynthesis. After accounting for reproductive production (flowers and fruits), biomass growth is partitioned into leaves, fine roots and sapwood according to a modified pipe model (Zaehle and Friend, 2010), accounting for the costs of biomass formation (growth respiration). In other words, changes in leaf-level productivity affect the build-up of plant pools and storage and thereby feed back on the ability of plants to acquire C through photosynthesis or nutrients through fine-root uptake.

## 2.1 Ozone injury calculation in O-CN

Throughout the paper we refer to the biological response to  $O_3$  uptake at the leaf level as “injury” and to responses of plant production, growth and biomass at the ecosystem level as “damage” following Guderian (1977). The relationship between ozone uptake and injury is called “injury function”; the relationship between ozone uptake and damage is called “dose–response relationship”.

Leaf-level ozone uptake is determined by stomatal conductance and atmospheric  $O_3$  concentrations, as described in Franz et al. (2017). To mimic the conditions of the fumigation experiments with plot-level controlled atmospheric  $O_3$  concentrations, simulations are conducted with a model version of O-CN, in which atmospheric  $O_3$  concentrations are directly used to calculate ozone uptake into the leaves, and the transfer and destruction of ozone between the atmosphere and the surface is ignored (ATM model version in Franz et al., 2017). Deviating from Franz et al. (2017), stomatal conductance  $g_{st}$  here is calculated based on the Ball and Berry formulation (Ball et al., 1987) as

$$g_{st,l} = g_0 + g_1 \times \frac{A_{n,l} \times RH \times f(\text{height}_l)}{C_a}, \quad (1)$$

where net photosynthesis ( $A_{n,l}$ ) is calculated as described in Zaehle and Friend (2010) as a function of the leaf-internal partial pressure of  $CO_2$ , absorbed photosynthetic photon flux density on shaded and sunlit leaves, leaf temperature, the nitrogen-specific rates of maximum light harvesting, electron transport ( $J_{max}$ ) and carboxylation rates ( $V_{cmax}$ ). RH is the atmospheric relative humidity,  $f(\text{height}_l)$  the water-transport limitation with canopy height,  $C_a$  the atmospheric  $CO_2$  concentration,  $g_0$  the residual conductance when  $A_n$  approaches zero, and  $g_1$  the stomatal-slope parameter as in Krinner et al. (2005). The index  $l$  indicates that  $g_{st}$  is calculated separately for each canopy layer.

The stomatal conductance to ozone  $g_{st,l}^{O_3}$  is calculated as

$$g_{st,l}^{O_3} = \frac{g_{st,l}}{1.51}, \quad (2)$$

where the factor 1.51 accounts for the different diffusivity of  $O_3$  from water vapour (Massman, 1998).

For each canopy layer, the  $O_3$  stomatal flux ( $f_{st,l}$ ,  $\text{nmol m}^{-2}$  (leaf area)  $\text{s}^{-1}$ ) is calculated from the atmospheric  $O_3$  concentration the plants in the field experiments were fumigated with ( $\chi_{atm}^{O_3}$ ), and  $g_{st,l}$  is calculated as

$$f_{st,l} = (\chi_{atm}^{O_3} - \chi_i^{O_3}) g_{st,l}^{O_3}, \quad (3)$$

where the leaf-internal  $O_3$  concentration ( $\chi_i^{O_3}$ ) is assumed to be zero (Laisk et al., 1989).

The accumulation of ozone fluxes above a threshold of  $Y$   $\text{nmol m}^{-2}$  (leaf area)  $\text{s}^{-1}$  ( $f_{st,l,Y}$ ,  $\text{nmol m}^{-2}$  (leaf area)  $\text{s}^{-1}$ ) with

$$f_{st,l,Y} = \text{MAX}(0, f_{st,l} - Y) \quad (4)$$

gives the  $CUOY_l$ . The canopy value of  $CUOY$  is calculated by summing  $CUOY_l$  over all canopy layers (Franz et al., 2017).

For comparison to observations, the POD ( $\text{mmol m}^{-2}$ ) can be diagnosed by the accumulation of  $f_{st,l}$  for the top canopy layer ( $l = 1$ ), in accordance with LRTAP-Convention (2017) and B ker et al. (2015). The accumulation of ozone fluxes of the top canopy layer above a threshold of  $y$   $\text{nmol m}^{-2}$  (leaf area)  $\text{s}^{-1}$  gives the  $POD_y$ . The estimates of  $POD_y$  (both  $POD_2$  and  $POD_3$ ) can be used offline to re-construct dose–response relationships equivalent to those described in B ker et al. (2015). These modelled dose–response relationships can then be compared with the empirically derived dose–response relationships to assess the ability of the model to estimate injury. As such, the  $POD_2$  and  $POD_3$  used for the formation of these modelled dose–response relationships are purely diagnostic variables and not involved in the injury calculation of the model. The flux thresholds (2 and 3  $\text{nmol m}^{-2}$  (leaf area)  $\text{s}^{-1}$ ) are not the flux thresholds that are used to estimate biomass response in the O-CN model simulations.

Ozone injury, i.e. the fractional loss of carbon uptake associated with ozone uptake  $d_l^{O_3}$ , is calculated as a linear function of the cumulative leaf-level uptake of ozone above a threshold of  $Y$   $\text{nmol m}^{-2}$  (leaf area)  $\text{s}^{-1}$  ( $CUOY_l$ )

$$d_l^{O_3} = a - b \times CUOY_l, \quad (5)$$

where  $a$  is the intercept and  $b$  is the slope of the injury function. The injury fraction ( $d_l^{O_3}$ ) is calculated separately for each canopy layer  $l$  based on the specific accumulated ozone uptake of the respective canopy layer ( $CUOY_l$ ) and takes values between 0 and 1. The magnitude of  $d_l^{O_3}$  in Eq. (5) varies between the canopy layers because  $CUOY_l$  varies driven by within-canopy gradients in stomatal conductance and photosynthetic capacity.

The effect of ozone injury on plant carbon uptake is calculated by

$$x_l^{O_3} = x_l(1 - d_l^{O_3}), \quad (6)$$

where  $x_l$  is either leaf-level net photosynthesis  $A_{n,l}$  or the maximum photosynthetic capacity ( $J_{max,l}$  and  $V_{cmax,l}$ ), which is used in the calculation of  $A_{n,l}$ .  $J_{max,l}$  and  $V_{cmax,l}$  are reduced in proportion such that the ratio between the two is not altered. While there is some evidence that ozone can affect the ratio between  $J_{max}$  and  $V_{cmax}$ , we believe that for the purpose of this paper, it is justifiable to assume a fixed ratio between them.

Reductions in  $A_{n,l}$  cause a decline in stomatal conductance ( $g_{st,l}$ ) due to the tight coupling between both. Other stress factors that impact  $g_{st,l}$  are accounted for in the preceding calculation of the  $g_{st,l}$  uninjured by ozone (see Eq. 1). Reductions in  $g_{st,l}$  decrease the  $O_3$  uptake into the plant ( $f_{st,l}$ ) and slow the increase in  $CUOY_l$  and thus ozone injury.

## 2.2 Model set-up

Four published injury functions were applied within the O-CN model (see Table 1 for the respective slopes, intercepts and flux thresholds). As shown below in Fig. 1 and explained in the results section, these did not match well with the observed biomass dose–response relationships by B ker et al. (2015). Following this we manually calibrated two additional injury relationships – one each for  $A_n$  or  $V_{cmax}$  – based on the data presented in B ker et al. (2015) (see Table 1 for slopes and intercepts). For these calibrated injury functions, we chose a flux threshold value of  $1 \text{ nmol m}^{-2} (\text{leaf area}) \text{ s}^{-1}$ , as suggested by LRTAP-Convention (2017). We forced the intercept ( $a$ ) of these relationships to 1 to simulate zero ozone injury at zero accumulated  $\text{O}_3$  (for ozone levels that cause less than  $1 \text{ nmol m}^{-2} (\text{leaf area}) \text{ s}^{-1}$  instantaneous ozone uptake). As described above, in all model versions, ozone injury is calculated independently for each canopy layer based on the accumulated  $\text{O}_3$  uptake ( $\text{CUOY}_l$ ) in that layer, above a specific flux threshold of  $Y \text{ nmol m}^{-2} (\text{leaf area}) \text{ s}^{-1}$  for the respective injury function (see Table 1).

## 2.3 Model and protocol for young trees

Single-point simulations were run for each fumigation experiment using meteorological input from the daily CRU-NCEP climate data set (CRU-NCEP version 5; LSCE ([https://vesg.ipsl.upmc.fr/thredds/catalog/store/p529viov/cruncep/V5\\_1901\\_2013/catalog.html](https://vesg.ipsl.upmc.fr/thredds/catalog/store/p529viov/cruncep/V5_1901_2013/catalog.html), last access: 15 November 2018) at the nearest grid cell to the coordinates of the experiment sites. The meteorological data provided by the experiments incompletely described the atmospheric boundary conditions required to drive the O-CN model. Atmospheric  $\text{CO}_2$  concentrations were taken from Sitch et al. (2015), and reduced as well as oxidised nitrogen deposition in wet and dry forms was provided by the EMEP model (Simpson et al., 2014). Hourly  $\text{O}_3$  concentrations were obtained from the experiments, as in B ker et al. (2015).

B ker et al. (2015) report data for eight tree species at 11 sites across Europe (see Table A2 for experiment and simulation details). The O-CN model simulates 12 plant functional types (PFTs) rather than explicit species; therefore, the species from the experiments were assigned to the corresponding PFT: all broadleaved species except *Quercus ilex* were assigned to the temperate broadleaved summer-green PFT. *Quercus ilex* was classified as temperate broadleaved evergreen PFT. All needleleaf species were assigned to the temperate needleleaf evergreen PFT.

The fumigation experiments were conducted on young trees or cuttings. Prior to the simulation of the experiment, the model was run in an initialisation phase from bare ground until the simulated stand-scale tree age was stable and representative of 1–2 year old trees. During this initialisation, O-CN was run with the climate of the years preceding the

experiment and zero atmospheric  $\text{O}_3$  concentrations. Using ambient ozone concentrations during the initialisation phase would have resulted in different initial biomass values for the different response functions, which would have reduced the comparability of the different model runs. The impact of the ozone concentrations in the initialisation phase on our results here can be considered negligible since we only evaluate the simulated biomass from different treatments in relation to each other and do not evaluate it in absolute terms.

The duration of the initialisation phase depends on the site and PFT and averages 7.8 years (mean over all simulated experiments). Some of the published injury functions and/or parameterisations applied have intercepts unequal to 1 ( $a$  in Eq. 5; see Table 1), which induces reductions ( $a < 1$ ) or increases ( $a > 1$ ) in photosynthesis at zero ozone concentration and thus causes a bias in biomass and in particular foliage area at the end of the initialisation phase. To eliminate this bias, the nitrogen-specific photosynthetic capacity of a leaf was adjusted for each of the six parameterisations of the model to obtain comparable leaf area index (LAI) values at the beginning of the experiment (see Table A1). This adaptation of the nitrogen-specific photosynthetic capacity of a leaf only counterbalances the fixed increases or decreases in the calculation of photosynthesis implied by the intercepts unequal to 1 and has no further impact on ozone uptake and injury calculations.

The simulations of the experiments relied on the meteorological and atmospheric forcing of the experiment years. Simulations were made for all reported  $\text{O}_3$  treatments of the specific experiment, including the respective control treatments. B ker et al. (2015) obtained estimates of biomass reductions due to ozone by calculating the hypothetical biomass at zero ozone uptake for all experiments that reported ozone concentrations greater than zero for the control group (e.g. for charcoal-filtered or non-filtered air) and calculated the biomass damage from the treatments against a completely undamaged biomass. Our model allows us to run simulations with zero ozone concentrations and skip the calculation of the hypothetical biomass at zero ozone concentrations as done by B ker et al. (2015). Following this, we ran additional reference simulations with zero  $\text{O}_3$  and based our biomass damage calculations upon them.

## 2.4 Modelling protocol for mature trees

To test whether biomass dose–response relationships of mature forests will show a similar relationship as observed in the simulations of young trees, we ran additional simulations with mature trees. To allow the development of a mature forest where biomass accumulation reached a maximum, and high and medium turnover soil pools reached an equilibrium, the model was run for 300 years in the initialisation phase. The simulations were conducted with the respective climate previous to the experiment period and zero atmospheric  $\text{O}_3$  concentration. For the simulation years previous

**Table 1.** Slopes and intercepts, partly PFT specific, of all four published (W07<sub>PS</sub>, L12<sub>PS</sub>, L12<sub>VC</sub>, L13<sub>PS</sub>) and two tuned (tun<sub>PS</sub>, tun<sub>VC</sub>) injury functions included in O-CN. Targets of ozone injury are net photosynthesis (PS) or  $V_{\text{cmax}}$ . Injury calculations base on the CUOY with a specific flux threshold for each injury function.

ID	Target	Slope ( <i>b</i> )	Intercept ( <i>a</i> )	Plant group	Flux threshold ( $\text{nmol m}^{-2}$ (leaf area) $\text{s}^{-1}$ )	Reference
W07 <sub>PS</sub>	PS	0.0022	0.9384	All	0	Wittig et al. (2007)
L12 <sub>PS</sub>	PS	0.2399	1.0421	All	0.8	Lombardozzi et al. (2012a)
L12 <sub>VC</sub>	$V_{\text{cmax}}$	0.1976	0.9888	All	0.8	Lombardozzi et al. (2012a)
L13 <sub>PS</sub>	PS	0	0.8752	Broadleaf	0.8	Lombardozzi et al. (2013)
L13 <sub>PS</sub>	PS	0	0.839	Needleleaf	0.8	Lombardozzi et al. (2013)
tun <sub>PS</sub>	PS	0.065	1	Broadleaf	1	Tuned here
tun <sub>PS</sub>	PS	0.021	1	Needleleaf	1	Tuned here
tun <sub>VC</sub>	$V_{\text{cmax}}$	0.075	1	Broadleaf	1	Tuned here
tun <sub>VC</sub>	$V_{\text{cmax}}$	0.025	1	Needleleaf	1	Tuned here

to 1901, the yearly climate is randomly chosen from the years 1901–1930. Constant values of atmospheric  $\text{CO}_2$  concentrations are used in simulated years previous to 1750 followed by increasing concentrations up to the experiment years. The subsequent experiment years are simulated in the same way as the simulations with the young trees. The ozone injury for mature trees is calculated based on the same tun<sub>VC</sub> injury function (see Table 1) that is used in the simulation of young trees (see Sect. 2.5 for details on the development of tun<sub>VC</sub>).

## 2.5 Calculation of the biomass damage relationships

The ozone-induced biomass damage is calculated from the difference between a treatment and a control simulation. At each experiment site and for all treatments, the annual reduction in biomass due to ozone (RB) is calculated as in Bükler et al. (2015):

$$\text{RB} = \left( \frac{\text{BM}_{\text{treat}}}{\text{BM}_{\text{zero}}} \right)^{\frac{1}{n}}, \quad (7)$$

where  $\text{BM}_{\text{treat}}$  represents the biomass of a simulation which experienced an  $\text{O}_3$  treatment and  $\text{BM}_{\text{zero}}$  the biomass of the control simulation with zero atmospheric  $\text{O}_3$  concentration. The exponent imposes an equal fractional biomass reduction across all simulation years for experiments lasting longer than 1 year.

Bükler et al. (2015) report the dose–response relationships for biomass reduction with reference to  $\text{POD}_y$  with flux thresholds  $y$  of 2 and 3  $\text{nmol m}^{-2}$  (leaf area)  $\text{s}^{-1}$  ( $\text{POD}_2$  and  $\text{POD}_3$ ) for the needleleaf and broadleaf category, respectively, where the  $\text{POD}_y$  values were derived from simulations with the  $\text{DO}_3\text{SE}$  model (Emberson et al., 2000) given site-specific meteorology and ozone concentrations. To be able to compare the simulated biomass reduction by O-CN with these estimates, we also diagnosed these  $\text{POD}_y$  values for each simulation from the accumulated ozone uptake of

the top canopy layer ( $\text{POD}_{y\text{O-CN}} = \text{CUOY}_{l=1}$ ). Note that the  $\text{POD}_{y\text{O-CN}}$  is purely diagnostic and not used in the injury calculations, which are based on the  $\text{CUOY}_l$  (see Eq. 5). As O-CN computes continuous, half-hourly values of ozone uptake (see Franz et al., 2017, for details), the  $\text{POD}_{y\text{O-CN}}$  values have to be transformed to be comparable to the simulated mean annual  $\text{POD}_y$  values reported in Bükler et al. (2015). For deciduous species, the yearly maximum of  $\text{POD}_{y\text{O-CN}}$  was taken as a yearly increment  $\text{POD}_{y\text{O-CN},i}$ . The  $\text{POD}_{y\text{O-CN}}$  of evergreen species was continuously accumulated over several years. To obtain the yearly increment  $\text{POD}_{y\text{O-CN},i}$ , the  $\text{POD}_{y\text{O-CN}}$  at the beginning of the year  $i$  is subtracted from the  $\text{POD}_{y\text{O-CN}}$  at the end of the year  $i$ .

The selected yearly  $\text{POD}_{y\text{O-CN},i}$  was used to calculate mean annual values necessary for the formation of the dose–response relationships integrating all simulation years ( $\text{POD}_y^{\text{dr}}$ ) as

$$\text{POD}_{y\text{O-CN}}^{\text{dr}} = \frac{\sum_{k=1}^i \text{POD}_{y\text{O-CN},i}}{i}, \quad (8)$$

where  $\text{POD}_{y\text{O-CN},i}$  is the  $\text{POD}_y$  of the  $i$ th year calculated by O-CN. The  $\text{POD}_y^{\text{dr}}$  values are used to derive biomass dose–response relationships.

Separate biomass dose–response relationships were estimated by grouping site data for broadleaved and needleleaf species. The biomass dose–response relationships are obtained from the simulation output by fitting a linear model to the simulated values of RB and  $\text{POD}_y^{\text{dr}}$  (with flux thresholds of 2 and 3  $\text{nmol m}^{-2}$  (leaf area)  $\text{s}^{-1}$  for needleleaf and broadleaved species, respectively), where the regression line is forced through 1 at zero  $\text{POD}_y^{\text{dr}}$ . Bükler et al. (2015) report two alternative dose–response relationships for their data set: the simple and the standard model –  $B_{\text{SI}}$  and  $B_{\text{ST}}$ , respectively. We evaluate our different model versions regarding their ability to reach the area between those two functions (target area) with the biomass dose–response relationships

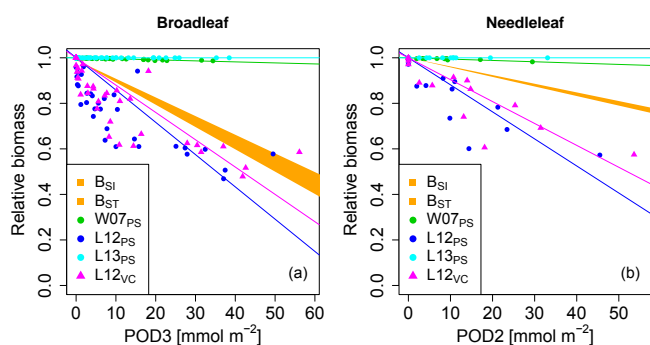


**Figure 1.** Biomass dose–response relationships for simulations based on published injury relationships, separate for (a) broadleaved species and (b) needleleaf species. The dose–response relationships by B<sub>Si</sub> and B<sub>ST</sub> (Büker et al., 2015) define the target area (orange). The displayed dose–response relationships are simulated by model versions which base injury calculations either on net photosynthesis W07<sub>PS</sub> (Wittig et al., 2007), L12<sub>PS</sub> (Lombardozzi et al., 2012a) and L13<sub>PS</sub> (Lombardozzi et al., 2013) or on  $V_{\text{cmax}}$  L12<sub>VC</sub> (Lombardozzi et al., 2012a) (see Table 1 for more details). See Tables A3 and A4 for slopes, intercepts,  $R^2$  and  $p$  values of the displayed regression lines. Injury calculation in the simulations is based on CUOY (see Table 1) and not on POD2 or POD3 (see Sec. 2.5 for more details).

computed from their output. The tuned injury relationships  $tun_{PS}$  and  $tun_{VC}$  were obtained by adjusting the slope  $b$  in Eq. (5) such that the corresponding biomass dose–response relationships fits the target area. The intercept of the injury relationships are forced to 1 to simulate zero ozone injury at ozone fluxes lower than  $1 \text{ nmol m}^{-2} (\text{leaf area}) \text{ s}^{-1}$ .

### 3 Results

#### 3.1 Testing published injury functions

None of the versions where ozone injury is calculated based on previously published injury functions fit the observations well. Some versions strongly overestimate the simulated biomass dose–response relationship and others strongly underestimate it (see Fig. 1) compared to the dose–response relationships developed by Büker et al. (2015).

In the W07<sub>PS</sub> simulations, where injury is calculated based on the injury function by Wittig et al. (2007), biomass damage is strongly underestimated compared to the estimates from Büker et al. (2015). Ozone injury estimates are mainly driven by the intercept of the relationship, which assumes a reduction in net photosynthesis by 6.16 % at zero ozone uptake. Little additional ozone damage occurs due to the accumulation of ozone uptake. As a consequence, the ozone treatments and reference simulations differ little in their simulated biomass. Similarly, the Lombardozzi et al. (2013) injury function (L13<sub>PS</sub>) calculates ozone injury as a fixed reduction in net photosynthesis independent of the actual accu-

mulated ozone uptake. The reference simulations with zero atmospheric ozone thus equal the simulations with ozone treatments and result in an identical simulated biomass. We tested accounting for effects of ozone on stomatal conductance besides net photosynthesis as suggested by Lombardozzi et al. (2013). However, this additional direct injury to stomatal conductance yielded a minimal decrease in simulated biomass accumulation in needleleaf trees, but did not qualitatively change the results (results not shown). These results indicate that injury functions, with a large intercept and a very shallow (or non-existing) slope cannot simulate the impact of spatially varying  $\text{O}_3$  concentrations or altered atmospheric  $\text{O}_3$  concentrations.

The simulations L12<sub>PS</sub> and L12<sub>VC</sub> (net photosynthesis and  $V_{\text{cmax}}$  injury according to Lombardozzi et al. (2012a), respectively) strongly overestimate biomass damage compared to Büker et al. (2015). Both injury functions assume an extensive injury to carbon fixation at low ozone accumulation values (CUOY) of about  $5 \text{ mmol O}_3$ . This results in a very steep decline in relative biomass at low values of POD3. Notably, despite a linear injury function, the very steep initial decline in biomass of broadleaved trees at low values of POD3 is not continued at higher exposure, resulting in a non-linear biomass dose–response relationships. Higher accumulation of ozone doses does not result in higher injury rates beyond a threshold of about  $5 \text{ mmol O}_3 \text{ m}^{-2}$  leaf area, and relative biomass declines remain at 50 % to 70 %. Whereas non-linear dose–response relationships are observed in experiments, e.g. for leaf injury (Marzuoli et al., 2009), such a non-linear relationship is not produced in the biomass dose–response relationship by Büker et al. (2015).

We investigated the cause for this using the example of the *Pinus halepensis* stand in the Ebro Delta with a high ozone treatment as shown in Fig. 2. The simulated CUOY quickly increases after the onset of fumigation (Fig. 2a) and is paralleled by a rapid decline in canopy-integrated net photosynthesis ( $A_n^{\text{can}}$ , see Fig. 2b). Once all canopy layers accumulated more than  $5 \text{ mmol O}_3 \text{ m}^{-2}$ , the canopy photosynthesis is fully reduced, and  $A_n^{\text{can}}$  becomes negative as a consequence of ongoing leaf maintenance respiration. Thereafter, leaf and total biomass steadily decline (Fig. 2c, d), and the plants are kept alive only by the consumption of stored non-structural carbon reserves. Despite the 100 % reduction in gross photosynthesis, the biomass compared to a control simulation (relative biomass, RB) reaches only values of approximately 0.7 (Fig. 2e) because of the remaining woody and root tissues (see Eq. 7 for the calculation of RB).

#### 3.2 Tuned injury relationships

We next tested whether a linear injury function is in principle able to reproduce the observed biomass dose–response relationships. Simulations conducted with our tuned injury relationships produce biomass dose–response relationships which fit the target area defined by the B<sub>Si</sub> and B<sub>ST</sub>

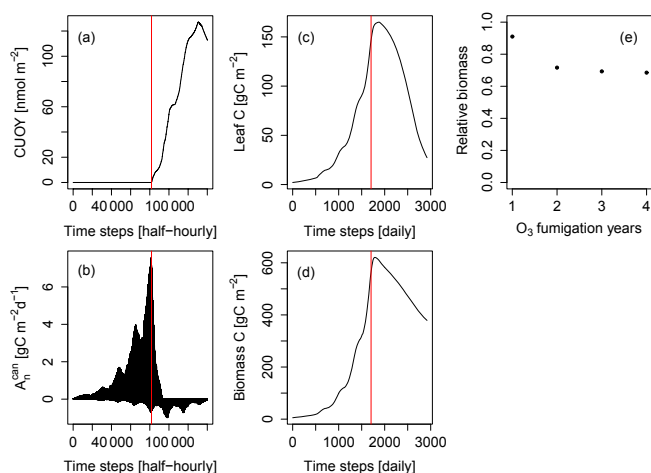


**Figure 2.** Simulated cumulative ozone uptake above a threshold of  $0.8 \text{ nmol m}^{-2}$  (leaf area)  $\text{s}^{-1}$  (CUOY), canopy-integrated net photosynthesis ( $A_n^{\text{can}}$ ), leaf carbon content (Leaf C), total carbon in biomass (biomass C) and relative biomass (RB) of *Pinus halepensis* at the Ebro Delta fumigated with the NF+ ozone treatment. Simulations are conducted with the L12PS model version. Panels (a–d) display the entire simulation period. The red line indicates the onset of  $\text{O}_3$  fumigation (NF+) in the fifth of eight simulations years. The relative biomass compared to a control simulation with zero  $\text{O}_3$  concentration (e) is displayed for the  $\text{O}_3$  fumigation years.

dose–response relationships by Büker et al. (2015) (see Fig. 3 and Tables A5, A6). For the calibrated relationships used in these simulations, we chose a flux threshold value of  $1 \text{ nmol m}^{-2}$  (leaf area)  $\text{s}^{-1}$ , as suggested by LRTAP-Convention (2017). We forced the intercept ( $a$ ) of these relationships through 1, to simulate zero ozone injury at ozone fluxes lower than  $1 \text{ nmol m}^{-2}$  (leaf area)  $\text{s}^{-1}$ . The resulting slope of the  $\text{tun}_{\text{PS}}$  function for broadleaved PFTs is approximately 30 times higher compared to the slope suggested by Wittig et al. (2007) and a fourth of the slope by Lombardozzi et al. (2012a). For the needleleaf PFT, the tuned slope ( $\text{tun}_{\text{PS}}$ ) is approximately 10 times higher (lower) than the slopes by Wittig et al. (2007) and Lombardozzi et al. (2012a), respectively. Notably, we did not observe any difference in the model performance irrespective of whether net photosynthesis or photosynthetic capacity ( $V_{\text{cmax}}$  and simultaneously  $J_{\text{max}}$ ) was reduced.

### 3.3 Ozone injury to mature trees

The simulation of young trees (simulated as in the previous section) compared to adult trees with the same model version reveals a distinct difference between the simulated-versus-observed dose–response relationship when expressed as reduction in biomass. Ozone injury causes a much shallower simulated biomass dose–response relationship for adult trees ( $\text{tun}_{\text{VC}}^{\text{mature}}$  in Fig. 4a, b) compared to young trees ( $\text{tun}_{\text{VC}}^{\text{young}}$  in Fig. 4a, b), both for broadleaved and needleleaf

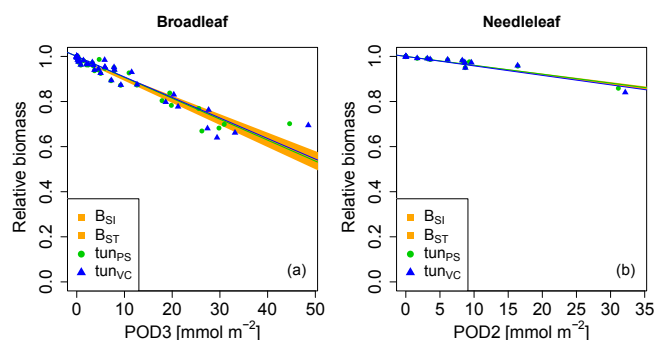


**Figure 3.** Biomass dose–response relationships for simulations based on tuned injury functions (see Table 1 for abbreviations), separate for (a) broadleaved species and (b) needleleaf species. The dose–response relationships by Büker et al. (2015) ( $B_{\text{SI}}$  and  $B_{\text{ST}}$ ) define the target area (orange). See Tables A5 and A6 for slopes, intercepts,  $R^2$  and  $p$  values of the displayed regression lines. Injury calculation in the simulations is based on CUO1 (see Table 1) and not on POD2 or POD3 (see Sect. 2.5 for more details).

**Table 2.** Slopes and intercepts of biomass (RB) and NPP (RN) dose–response relationships (DRRs) for broadleaved species simulated by the  $\text{tun}_{\text{VC}}^{\text{young}}$  model version (see Table 1). The fumigation of young trees ( $\text{tun}_{\text{VC}}^{\text{young}}$ ) with  $\text{O}_3$  is compared to the fumigation of mature trees ( $\text{tun}_{\text{VC}}^{\text{mature}}$ ).

DRR	ID	Intercept (a)	Slope (b)	$R^2$	$p$ value
RB	$\text{tun}_{\text{VC}}^{\text{young}}$	1	0.0091	0.93	$5 \times 10^{-25}$
RB	$\text{tun}_{\text{VC}}^{\text{mature}}$	1	0.00142	0.91	$9.8 \times 10^{-23}$
RN	$\text{tun}_{\text{VC}}^{\text{young}}$	1	0.0167	0.96	$6.2 \times 10^{-30}$
RN	$\text{tun}_{\text{VC}}^{\text{mature}}$	1	0.0144	0.93	$1.4 \times 10^{-24}$

species. It is worth noting that this is primarily the consequence of the higher initial biomass of the adult trees before ozone fumigation starts ( $\text{tun}_{\text{VC}}^{\text{mature}}$ ). Comparing the dose–response relationship of young and mature trees based on the annual NPP shows nearly identical slopes for needleleaf species (Fig. 4d and Table 3), whereas the slopes for broadleaved tree species (Fig. 4c and Table 2) suggest only a slightly lower reduction in NPP in mature compared to young trees, likely related to the larger amount of non-structural reserves that increases the resilience of mature versus young trees.

## 4 Discussion

Injury functions that relate accumulated ozone uptake to fundamental plant processes such as photosynthesis are a key component for models that aim to estimate the potential impacts of ozone pollution on forest productivity, growth and carbon sequestration. We tested four published injury functions for net photosynthesis and  $V_{\text{cmax}}$  within the frame-

**Table 3.** Slopes and intercepts of biomass (RB) and NPP (RN) dose–response relationships (DRRs) for needleleaf species simulated by the  $\text{tun}_{\text{VC}}$  model version (see Table 1). The fumigation of young trees ( $\text{tun}_{\text{VC}}^{\text{young}}$ ) with  $\text{O}_3$  is compared to the fumigation of mature trees ( $\text{tun}_{\text{VC}}^{\text{mature}}$ ).

DRR	ID	Intercept (a)	Slope (b)	$R^2$	$p$ value
RB	$\text{tun}_{\text{VC}}^{\text{young}}$	1	0.0042	0.93	$2.2 \times 10^{-09}$
RB	$\text{tun}_{\text{VC}}^{\text{mature}}$	1	0.000785	0.79	$4.2 \times 10^{-06}$
RN	$\text{tun}_{\text{VC}}^{\text{young}}$	1	0.00858	0.97	$2.3 \times 10^{-12}$
RN	$\text{tun}_{\text{VC}}^{\text{mature}}$	1	0.00808	0.99	$3.7 \times 10^{-16}$

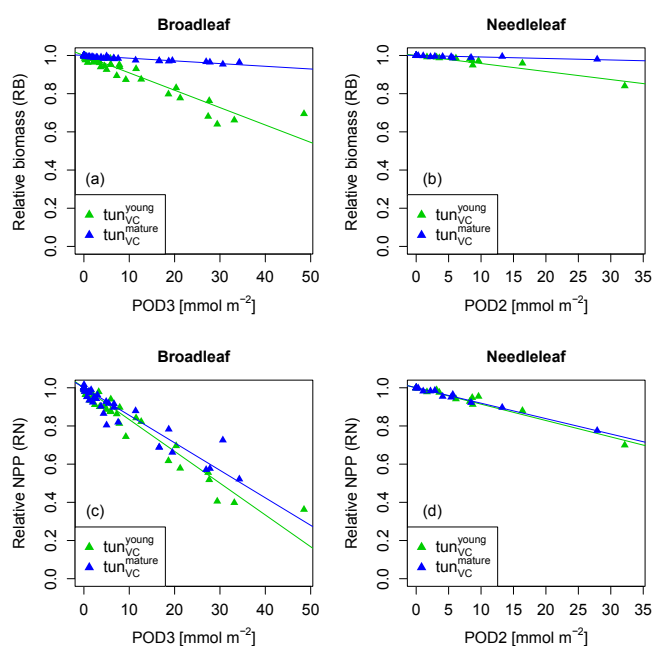


**Figure 4.** Biomass (RB) and NPP (RN) dose–response relationships of simulations with young ( $\text{tun}_{\text{VC}}^{\text{young}}$ ) and mature trees ( $\text{tun}_{\text{VC}}^{\text{mature}}$ ) separately for (a, c) broadleaf species and (b, d) needleleaf species.

work of the O-CN model to assess their ability to reproduce the empirical whole-tree biomass dose–response relationships derived by B ker et al. (2015). The biomass dose–response relationships calculated from the O-CN simulations show that the parameterisation of the injury functions included in the model has a large impact on the simulated whole-tree biomass: the published injury functions either substantially over- or substantially underestimated whole-tree biomass reduction compared to the data presented by B ker et al. (2015). Our results highlight the importance for improved evaluation of injury functions applied in the simulation of ozone damage for large-scale risk assessments, and we discuss a number of important considerations for an improved parameterisation below.

The simulation results from the O-CN version applying an injury function based on a single, ozone-sensitive species (Lombardozi et al., 2012a) to a range of European tree species leads to a strong overestimation of the simulated biomass damage compared to the observations used in this study. The problem of using such injury parameterisations based on short-term experiments of ozone-sensitive species is further highlighted when applying them in simulations of multiple season fumigation experiments and/or high ozone concentrations. Under such conditions, fumigation with high  $\text{O}_3$  concentrations can lead to lethal doses, which might not be observed in field experiments due to restricted experiment lengths. Previous studies have suggested that in large areas of Europe, the eastern US and southeast Asia average growing season values of  $\text{CUOY}$  for recent years range between 10 and  $100 \text{ mmol O}_3 \text{ m}^{-2}$  (Lombardozi et al., 2015; Franz et al., 2017). The injury relationships L12<sub>PS</sub> and L12<sub>VC</sub> by Lombardozi et al. (2012a) assume a 100 % injury to net photosynthesis or  $V_{\text{cmax}}$  at accumulation values of about  $5 \text{ mmol O}_3 \text{ m}^{-2}$ . This would imply that in these large geographic regions, photosynthesis would have been completely impaired by ozone, which is clearly not the case. This result highlights the need for a representative set of species for the development of injury functions for large-scale biosphere models. Overall, our results suggest that the estimates by Lombardozi et al. (2012a) of global GPP reduction as a result of ozone pollution are strongly overestimated.

Meta-analyses (Wittig et al., 2007; Lombardozi et al., 2013) are designed to minimise the effect of species-specific ozone sensitivities and provide estimates of the average species response. However, we found that the relationships derived by these meta-analyses substantially underestimate biomass damage. Technically, the reasons for this are a weak or non-existent increase in the ozone injury with increased ozone uptake (shallow or non-existent slopes) and/or high ozone injury at zero accumulated ozone uptake (intercept lower than 1). Apparently, the diversity of species responses and experimental settings that are assembled in the meta-analyses by Wittig et al. (2007) and Lombardozi et al. (2013), together with uncertainties in precisely estimating accumulated ozone uptake in these databases preclude the identification of injury functions that are consistent with the damage estimates by B ker et al. (2015). The high intercepts in the meta-analyses by Wittig et al. (2007) and Lombardozi et al. (2013), which assume a considerable injury fraction even when no ozone is taken up at all, seem to be ecologically illogical and suggest that an alternative approach is necessary to simulate ozone injury. As a consequence of these points, the Europe-wide GPP reduction estimates by Franz et al. (2017), which have been based on the injury function by Wittig et al. (2007), may substantially underestimate actual GPP reduction. Similarly, global GPP by Lombardozi et al. (2015), based on Lombardozi et al. (2013), are virtually independent of actual ozone concentrations or uptake for

all tree plant functional types and should be interpreted with caution.

A crucial aspect in forming dose–response relationships is the calculation of the accumulated ozone uptake (e.g.  $POD_y$  or  $CUOY$ ). The calculation of accumulated ozone uptake is realised in different ways in the meta-analyses and the study by B ker et al. (2015) as well as in our approach here. Experiments synthesised in the meta-analyses generally do not have access to stomatal conductance values at high resolution measured throughout the experiment, which impedes precise determination of  $O_3$  uptake. The uncertainty in the necessary approximations of accumulated ozone uptake can be assumed to be considerable, and it is thus highly recommendable to measure and report required observations in future ozone fumigation experiments. B ker et al. (2015) use the  $DO_3SE$  model to simulate ozone uptake and accumulation in a similar way as in our model here. These modelled values for ozone uptake and accumulation can be assumed to be more reliable since both models simulate processes that determine ozone uptake continuously for the entire experiment length at high temporal resolution. They account for diurnal changes in stomatal conductance as well as climate factors restricting stomatal conductance and hence ozone uptake. However, both models vary in their complexity of the simulated plants, carbon assimilation and growth processes, which will also impact the estimates of ozone accumulation ( $POD_y$ ) and hence their suggested biomass dose–response relationships.

The meta-analyses do not account for non-stomatal ozone deposition (e.g. to the leaf cuticle or soil), which imposes a bias towards overestimating ozone uptake and accumulation, contrary to the  $DO_3SE$  model used by B ker et al. (2015), which accounts for this. The O-CN model in principle can simulate non-stomatal ozone deposition from the free atmosphere to ground level (see Franz et al., 2017). The leaf boundary layer is implicitly included in the calculation of the aerodynamic resistance of O-CN and included in Franz et al. (2017). However, for the simulation of the chamber experiments we used the observed chamber  $O_3$  concentrations, rather than estimating the canopy-level  $O_3$  concentration based on the free atmosphere (approximately 45 m above the surface) and atmospheric turbulence. This required not accounting for aerodynamic resistance and therefore also the leaf-boundary layer resistance as it prevented the calculation of the non-stomatal deposition, which may lead to a slight overestimation of ozone uptake and accumulation in our simulations.

The calibration of injury functions to net photosynthesis and  $V_{cmax}$  shows that, in principle, the linear structure of Eq. (5) is sufficient to simulate biomass dose–response relationships comparable to B ker et al. (2015) in O-CN. An advantage of the injury functions derived here compared to previously published injury functions (Wittig et al., 2007; Lombardozzi et al., 2012a, 2013) is the intercept of 1, implying that simulated ozone injury is zero at zero ac-

cumulated  $O_3$  and steadily increases with increased ozone accumulation. The flux threshold used in the simulations is  $1 \text{ nmol m}^{-2} (\text{leaf area}) \text{ s}^{-1}$  as suggested by the LRTAP-Convention (2017). Since the tuned injury functions are structurally identical to previously published injury functions based on accumulated ozone uptake, they can be directly compared to them. Slopes of the tuned injury functions lie in between the values proposed by Wittig et al. (2007) and Lombardozzi et al. (2012a) and thus take values in an expected range. We did not find any significant difference in simulated biomass responses between the use of net photosynthesis or leaf-specific photosynthetic capacity ( $V_{cmax}$ ) as a target for the ozone injury function, although we do note that the slopes were slightly lower for the net photosynthesis-based functions. The simulation of ozone effects on leaf-specific photosynthetic capacity ( $V_{cmax}$ ) seems preferable over the adjustment of net photosynthesis because  $V_{cmax}$  and  $J_{max}$  are parameters in the calculation of net photosynthesis and thus are likely more easily transferable between models. Models with different approaches to simulate net photosynthesis might obtain better comparable results by using injury relationships that target  $V_{cmax}$  instead of net photosynthesis.

All injury functions included in the O-CN model base injury calculations on the injury index  $CUOY$  (canopy value) rather than  $POD_y$ , as used by some other models, e.g. the  $DO_3SE$  model (Emberson et al., 2000). We tested the effect of basing the injury calculation on  $POD1$  rather than  $CUO1$  and found that these produced comparable biomass dose–response relationships as the injury relationships based on  $CUO1$  presented in Fig. 3 (results not shown). The slopes of injury functions based on  $POD1$  are approximately two-thirds and half compared to the slopes based on  $CUO1$  for broadleaved and needleleaf species, respectively. The difference in the slope values associated with  $POD1$  and  $CUO1$  results from the different calculation and application of them.  $POD_y$  is calculated in the top canopy layer and the respective injury fraction is then applied uniformly to all canopy layers.  $CUOY$  and the associated injury fraction is calculated separately for each canopy layer and varies with the canopy profile of stomatal conductance and therefore the distribution of light and photosynthetic capacity (other factors such as vertical gradients of temperature or ozone are currently not represented in O-CN). More analysis of the gradients of ozone injury within deep canopies are required to evaluate whether the scaling of top-of-the-canopy injury to whole-canopy injury is appropriate or if alternative simulation approaches need to be developed. Higher-frequency data on the ozone injury incurred by plants are required to disentangle whether an ozone injury parameterisation based on instantaneous (e.g. similar to the approach by Sitch et al., 2007) or accumulated ozone uptake results in a more accurate simulation of the seasonal effects of ozone fumigation.

Further aspects that determine ozone sensitivity and damage to the carbon gain of plants, like leaf morphology (Ca-

latayud et al., 2011; Bussotti, 2008), different sensitivity of sunlit and shaded leaves (Tjoelker et al., 1995; Wieser et al., 2002), early senescence (Gielen et al., 2007; Ainsworth et al., 2012), and costs for the detoxification of ozone and/or the repair of ozone injury that likely increases the plant's respiration costs (Dizengremel, 2001; Wieser and Matyssek, 2007), are not considered by either approach. Marzuoli et al. (2016) observed an ozone-induced reduction in biomass but no significant reduction in physiological parameters like  $V_{\text{cmax}}$ . They suggest that the reduced growth is caused by higher energy investments and reducing power for the detoxification of ozone whereas the photosynthetic apparatus remained uninjured (Marzuoli et al., 2016).

Species within the same plant functional type are known to exhibit different sensitivities to ozone (Wittig et al., 2007, 2009; Mills et al., 2011; B ker et al., 2015). This suggests that the application of a single injury function for a large set of species and plant functional types may not be sufficient to yield reliable estimates of large-scale damage estimates. Species interaction and competition, differing genotypes, and individuals ontogeny may further alter ozone impacts on plants and ecosystems (Matyssek et al., 2010). For instance, a modelling study using an individual-based forest model showed that ozone may not reduce the carbon sequestration capacity in forests if at the ecosystem level the reduced carbon fixation of ozone-sensitive species is compensated for by an increased carbon fixation of less ozone-sensitive species (Wang et al., 2016). First-generation dynamic global vegetation models such as O-CN do not simulate separate species but are based on plant functional types, which combine a large set of species. This restricts per se the ability of global models to simulate ozone-induced community dynamics and may therefore lead to overestimates of the net ozone impact if the parameterisation of the damage functions is entirely based on ozone-sensitive species. In our study, we have presented an approach to use the existing experimental evidence to parameterise a globally applicable model in a simple design to generate injury functions which are based on a relevant range of species rather than relying on species-specific injury functions as a first step towards a more reliable parameterisation of large-scale ozone damage.

Some studies have found that ozone-affected stomata respond much more slowly to environmental stimuli than unaffected cells (Paoletti and Grulke, 2005), which can delay closure and trigger stomatal sluggishness, an uncoupling of stomatal conductance and photosynthesis (Reich, 1987; Tjoelker et al., 1995; Lombardozzi et al., 2012b) and thus impact transpiration rates (Mills et al., 2009; Paoletti and Grulke, 2010; Lombardozzi et al., 2012b) and the plant's water use efficiency (Wittig et al., 2007; Mills et al., 2009; Lombardozzi et al., 2012b). The O-CN model is able to directly impair stomatal conductance, by uncoupling injury to net photosynthesis from the subsequent injury to stomatal conductance. In this version of the O-CN model, both net photosynthesis and stomatal conductance can directly be in-

jured by individual injury functions. The simulation of this kind of direct injury to stomatal conductance additional to the injury of net photosynthesis, both according to the injury functions by Lombardozzi et al. (2013), have a negligible impact on biomass production compared to not accounting for direct injury to the stomata (results not shown). However, our above-mentioned concerns regarding the structure of the injury relationships by Lombardozzi et al. (2013) should be taken into account when considering this result.

A key challenge for the use of fumigation experiments to parameterise ozone injury in models is that trees (as opposed to grasses fumigated from seeds) typically possess a certain amount of biomass at the beginning of the fumigation experiment. Even at lethal ozone doses, the relative biomass thus cannot decline to zero, and tree death may occur at values of a relative biomass greater than zero. The relative biomass is positive even if carbon fixation is fully reduced and the plants survive due to the use of stored carbon. The higher the initial biomass and the slower the annual biomass growth rate of the tree is, the harder it is to obtain low values of RB. When comparing RB values obtained from trees with substantially different initial biomass and tree species with different growth rates, proportionate damage rates thus cannot be directly inferred. This indicates that the explanatory value of the relative biomass between a control and a treatment to estimate long-term plant damage at a given  $\text{O}_3$  concentration is limited. This is particularly the case when evaluating the damage of more mature forests. The simulated biomass dose–response relationships of adult trees are much more shallow than dose–response relationships of young trees (see Fig. 4) because of the high initial biomass prior to fumigation. This suggests that the use of biomass injury functions derived from experiments with young trees to parameterise the biomass loss of adult trees, as done in Sitch et al. (2007), will likely lead to an overestimation of plant damage and loss of carbon storage. Dose–response relationships based on biomass increments or growth rates might be better transferable between young and mature trees and hence better suitable for parameterising global terrestrial biosphere models.

Our approach to overcome this challenge was to alter the vegetation model to simulate the ozone damage of young trees, where we could directly compare simulated biomass reductions to observations. Since we used injury relationships that are based on the calculation of leaf-level photosynthesis, we are able to apply the calibrated model also for mature stands. Our simulations have demonstrated that despite the different sizes of young and mature trees and associated changes in the wood growth rate and the available amount of non-structural carbon reserves to repair incurred injury, the simulated effect of ozone on the net annual biomass production (NPP) was very similar when using an injury function associated with leaf-level photosynthesis. Overall our findings support the idea that the photosynthesis-based injury relationships developed here and evaluated against fumigation experiments of young trees might be useful to estimate effect

on forest production of older trees. Monitoring approaches of ozone damage that are either capable of measuring the actual increment of biomass or quantify at the leaf and canopy level the change in net photosynthesis over the growing season would allow us to develop injury/damage estimates that could be more readily translated into modelling frameworks.

The extrapolation of results from short-term experiments with young trees to estimate responses of adult trees grown under natural conditions is subject to several issues, e.g. due to the differing environmental conditions and changing ozone sensitivities with increasing tree size or age (Schaub et al., 2005; Cailleret et al., 2018). It is still uncertain whether the simulation of injury to photosynthesis based on experiments with young trees can indeed be transferred to adult trees to yield realistic biomass damage estimates. The sparse knowledge of ozone effects on the biomass of adult forest trees prevents an evaluation of simulated ozone damage of adult trees. Ozone fumigation is mostly found to reduce the biomass or diameter of adult trees (e.g. Matyssek et al., 2010 for an overview), but this is not always the case (Samuelson et al., 1996; Percy et al., 2007). Results from phytotron and free-air fumigation studies suggest that in natural forests, a multitude of abiotic and biotic factors exist that have the potential to impact the plants ozone effects (Matyssek et al., 2010). If more data become available, e.g. regarding the changes in ozone sensitivity between young and mature trees, a more realistic damage parameterisation of mature forests in terrestrial biosphere models might become possible.

Terrestrial biosphere models in general assume that plant growth is primarily determined by carbon uptake. However, an alternative concept proposes that plant growth is more limited by direct environmental controls (temperature, water and nutrient availability) than by carbon uptake and photosynthesis (Fatichi et al., 2014). The O-CN model provides a first step into this direction because it separates the step of carbon acquisition from biomass production, both in terms of a non-structural carbon buffer as well as a stoichiometric nutrient limitation on growth independent of the current photosynthetic rate. This would in principle allow us to account for ozone effects on the carbon sink dynamics within plants. However, it is not clear that data readily exist to parameterise such effects. Instead of targeting net photosynthesis as done in our approach here, ozone injury might be better simulated by targeting biomass growth rates or processes that limit these, e.g. stomatal conductance, which impacts the plants' water balance, assuming that suitable data to parameterise a large-scale model become available.

All in all, a multitude of aspects that impact ozone damage to plants has not yet been incorporated into global terrestrial biosphere models. The ongoing discussion of which processes are major drivers for observed damage, how they interact and impact different species and plant types, and the lack of suitable data needed to parameterise a global model are reasons why the simulation of ozone damage has up to

now focussed only on a few aspects where suitable data are available, as presented in our study.

## 5 Conclusion

The inclusion of previously published injury functions in the terrestrial biosphere model O-CN led to a strong over- or underestimation of simulated biomass damage compared to the biomass dose–response relationship by Büker et al. (2015). Injury functions included in terrestrial biosphere models are a key aspect in the simulation of ozone damage and have a great impact on the estimated damage in large-scale ozone risk assessments. The calibration of injury functions performed in this study provides the advantage of calculating ozone injury close to where the actual physiological injury might occur (photosynthetic apparatus) and simultaneously reproduces observed biomass damage relationships for a range of European forest species used by Büker et al. (2015). The calibration of ozone injury functions similar to our approach here in other ozone sub-models of terrestrial biosphere models might improve damage estimates compared to previously published injury functions and might lead to better estimates of terrestrial carbon sequestration. The comparison of simulated biomass dose–response relationships of young and mature trees shows strongly different slopes. This suggests that observed biomass damage relationships from young trees might not be suitable for estimating the biomass damage of mature trees. The comparison of simulated NPP dose–response relationships of young and mature trees shows similar slopes and suggests that they might more readily be transferred between trees differing in age.

*Data availability.* For data on the ozone fumigation/filtration experiments, please see Büker et al. (2015). The model source code can be found in Franz and Zaehle (2018).

## Appendix A

**Table A1.** Original and adapted values of the nitrogen-specific photosynthetic capacity of a leaf (npl) for three out of four different O-CN versions (ID) including published injury functions. The intercept of the fourth O-CN version (L12<sub>VC</sub>) is very close to 1 and simulations produce comparable LAI values without an adaption of npl.

ID	PFT	npl original	npl adapted
W07 <sub>PS</sub>	Broadleaf	1.50	1.60
W07 <sub>PS</sub>	Needleleaf	0.75	0.80
L12 <sub>PS</sub>	Broadleaf	1.50	1.45
L12 <sub>PS</sub>	Needleleaf	0.75	0.70
L13 <sub>PS</sub>	Broadleaf	1.50	1.75
L13 <sub>PS</sub>	Needleleaf	0.75	0.90

**Table A2.** List of fumigation experiments used by Büker et al. (2015) and simulated here.

Site	Longitude (° E)	Latitude (°N)	Species	O <sub>3</sub> treatment start year	Fumigation (yr)
Östad (S)	12.4	57.9	<i>Betula pendula</i>	1997	2
Birmensdorf (CH)	8.45	47.36	<i>Betula pendula</i>	1989	1
Birmensdorf (CH)	8.45	47.36	<i>Betula pendula</i>	1990	1
Birmensdorf (CH)	8.45	47.36	<i>Betula pendula</i>	1992	1
Birmensdorf (CH)	8.45	47.36	<i>Betula pendula</i>	1993	1
Kuopio (FIN)	27.58	62.21	<i>Betula pendula</i>	1994	2
Kuopio (FIN)	27.58	62.21	<i>Betula pendula</i>	1996	3
Kuopio (FIN)	27.58	62.21	<i>Betula pendula</i>	1994	5
Schönenbuch (CH)	7.5	47.54	<i>Fagus sylvatica</i>	1991	2
Zugerberg (CH)	8.54	47.15	<i>Fagus sylvatica</i>	1987	2
Zugerberg (CH)	8.54	47.15	<i>Fagus sylvatica</i>	1989	3
Zugerberg (CH)	8.54	47.15	<i>Fagus sylvatica</i>	1991	2
Curno (I)	9.03	46.17	<i>Populus spec.</i>	2005	1
Grignon (F)	1.95	48.83	<i>Populus spec.</i>	2008	1
Ebro Delta (SP)	0.5	40.75	<i>Quercus ilex</i>	1998	3
Col-du-Donon (F)	7.08	48.48	<i>Quercus robur or petraea</i>	1999	2
Headley (U.K.)	-0.75	52.13	<i>Quercus robur or petraea</i>	1997	2
Ebro Delta (SP)	0.5	40.75	<i>Pinus halepensis</i>	1993	4
Col-du-Donon (F)	7.08	48.48	<i>Pinus halepensis</i>	1997	2
Schönenbuch (CH)	7.5	47.54	<i>Picea abies</i>	1991	2
Zugerberg (CH)	8.54	47.15	<i>Picea abies</i>	1991	2
Östad (S)	12.4	57.9	<i>Picea abies</i>	1992	5
Headley (UK)	-0.75	52.13	<i>Pinus sylvestris</i>	1995	2

**Table A3.** Slopes and intercepts of biomass dose–response relationships for broadleaved species simulated by O-CN versions based on published injury functions to net photosynthesis or  $V_{\text{cmax}}$  (see Table 1).  $B_{\text{SI}}$  and  $B_{\text{ST}}$  represent the simple and standard model of Büker et al. (2015). A dash (“–”) indicates that no values were available.

ID	Intercept ( $a$ )	Slope ( $b$ )	$R^2$	$p$ value
$B_{\text{SI}}$	0.99	0.0082	0.34	<0.001
$B_{\text{ST}}$	0.99	0.0098	0.38	<0.001
W07PS	1	0.00045	0.93	$1 \times 10^{-24}$
L12PS	1	0.0142	0.77	$2 \times 10^{-14}$
L15PS	1	0.0000	–	–
L12VC	1	0.0120	0.80	$1.9 \times 10^{-15}$

**Table A4.** Slopes and intercepts of biomass dose–response relationships for needleleaf species simulated by O-CN versions based on published injury functions to net photosynthesis or  $V_{\text{cmax}}$  (see Table 1).  $B_{\text{SI}}$  and  $B_{\text{ST}}$  represent the simple and standard model by Büker et al. (2015). A dash (“–”) indicates that no values were available.

ID	Intercept ( $a$ )	Slope ( $b$ )	$R^2$	$p$ value
$B_{\text{SI}}$	1	0.0038	0.46	<0.001
$B_{\text{ST}}$	1	0.0042	0.52	<0.001
W07PS	1	0.00058	0.93	$1.5 \times 10^{-09}$
L12PS	1	0.0119	0.83	$9.4 \times 10^{-07}$
L15PS	1	0.0000	–	–
L12VC	1	0.0096	0.85	$3.5 \times 10^{-07}$

**Table A5.** Slopes and intercepts of biomass dose–response relationships for broadleaved species simulated by O-CN versions based on tuned injury functions to net photosynthesis or  $V_{\text{cmax}}$  (see Table 1).  $B_{\text{SI}}$  and  $B_{\text{ST}}$  represent the simple and standard model by Büker et al. (2015).

ID	Intercept ( $a$ )	Slope ( $b$ )	$R^2$	$p$ value
$B_{\text{SI}}$	0.99	0.0082	0.34	<0.001
$B_{\text{ST}}$	0.99	0.0098	0.38	<0.001
tunPS	1	0.0093	0.94	$1.4 \times 10^{-26}$
tunVC	1	0.0091	0.93	$5 \times 10^{-25}$

**Table A6.** Slopes and intercepts of biomass dose–response relationships for needleleaf species simulated by O-CN versions based on tuned injury functions to net photosynthesis or  $V_{\text{cmax}}$  (see Table 1).  $B_{\text{SI}}$  and  $B_{\text{ST}}$  represent the simple and standard model by Büker et al. (2015).

ID	Intercept ( $a$ )	Slope ( $b$ )	$R^2$	$p$ value
$B_{\text{SI}}$	1	0.0038	0.46	<0.001
$B_{\text{ST}}$	1	0.0042	0.52	<0.001
tunPS	1	0.0039	0.94	$4.8 \times 10^{-10}$
tunVC	1	0.0042	0.93	$2.2 \times 10^{-09}$

*Author contributions.* MF and SZ developed the experiment design. MF developed the model, performed the simulations and analyses, and led the writing of the paper. PB shared the data from Bükler et al. (2015). All co-authors contributed to writing of the paper.

*Competing interests.* The authors declare that they have no conflict of interest.

*Acknowledgements.* We would like to thank Per Erik Karlsson of the IVL Swedish Environmental Research Institute, Göteborg, Sweden, Sabine Braun of the Institute for Applied Plant Biology, Witterswil, Switzerland, and Gerhard Wieser of the Federal Research and Training Centre for Forests, Natural Hazards and Landscape (BFW), Innsbruck, Austria, for providing collected data from their ozone fumigation experiments. The research leading to this publication was supported by the EU Framework programme through grant no. 282910 (ECLAIRE) and the Max Planck Society for the Advancement of Science e.V. through the ENIGMA project. This project has received funding from the European Research Council (ERC) under the European Union's Horizon 2020 research and innovation programme (grant agreement no. 647204; QUINCY).

The article processing charges for this open-access publication were covered by the Max Planck Society.

Edited by: Martin De Kauwe

Reviewed by: Bin Wang and Marcus Schaub

## References

- Ainsworth, E. A., Yendrek, C. R., Sitch, S., Collins, W. J., and Emberson, L. D.: The Effects of Tropospheric Ozone on Net Primary Productivity and Implications for Climate Change, *Annu. Rev. Plant Biol.*, 63, 637–661, 2012.
- Ball, J. T., Woodrow, I. E., and Berry, J. A.: A model predicting stomatal conductance and its contribution to the control of photosynthesis under different environmental conditions, *Prog. Photosynthesis Res. Proc. Int. Congress 7th*, Providence, 10–15 August 1986, 221–224, 1987.
- Bükler, P., Feng, Z., Uddling, J., Briolat, A., Alonso, R., Braun, S., Elvira, S., Gerosa, G., Karlsson, P., Le Thiec, D., Marzuoli, R., Mills, G., Oksanen, E., Wieser, G., Wilkinson, M., and Emberson, L.: New flux based dose-response relationships for ozone for European forest tree species, *Environ. Pollut.*, 206, 163–174, <https://doi.org/10.1016/j.envpol.2015.06.033>, 2015.
- Bussotti, F.: Functional leaf traits, plant communities and acclimation processes in relation to oxidative stress in trees: a critical overview, *Glob. Change Biol.*, 14, 2727–2739, 2008.
- Cailleret, M., Ferretti, M., Gessler, A., Rigling, A., and Schaub, M.: Ozone effects on European forest growth – Towards an integrative approach, *J. Ecol.*, 106, 1377–1389, 2018.
- Calatayud, V., Cerveró, J., Calvo, E., García-Breijo, F.-J., Reig-Armiñana, J., and Sanz, M. J.: Responses of evergreen and deciduous *Quercus* species to enhanced ozone levels, *Environ. Pollut.*, 159, 55–63, 2011.
- Dizengremel, P.: Effects of ozone on the carbon metabolism of forest trees, *Plant Physiol. and Bioch.*, 39, 729–742, 2001.
- Emberson, L., Simpson, D., Tuovinen, J., Ashmore, M., and Cambridge, H.: Towards a model of ozone deposition and stomatal uptake over Europe, *EMEP MSC-W Note*, 6, 1–57, 2000.
- Faticchi, S., Leuzinger, S., and Koerner, C.: Moving beyond photosynthesis: from carbon source to sink-driven vegetation modeling, *New Phytol.*, 201, 1086–1095, <https://doi.org/10.1111/nph.12614>, 2014.
- Feng, Z. and Kobayashi, K.: Assessing the impacts of current and future concentrations of surface ozone on crop yield with meta-analysis, *Atmos. Environ.*, 43, 1510–1519, 2009.
- Franz, M. and Zaehle, S.: O-CN ozone version rev 298, available at: <https://projects.bgc-jena.mpg.de/OCN/browser/branches/ozone> (last access: 19 November 2018.), 2018.
- Franz, M., Simpson, D., Arneth, A., and Zaehle, S.: Development and evaluation of an ozone deposition scheme for coupling to a terrestrial biosphere model, *Biogeosciences*, 14, 45–71, <https://doi.org/10.5194/bg-14-45-2017>, 2017.
- Friend, A.: Modelling canopy CO<sub>2</sub> fluxes: are “big-leaf” simplifications justified?, *Global Ecol. Biogeogr.*, 10, 603–619, 2001.
- Gielen, B., Löw, M., Deckmyn, G., Metzger, U., Franck, F., Heerd, C., Matyssek, R., Valcke, R., and Ceulemans, R.: Chronic ozone exposure affects leaf senescence of adult beech trees: a chlorophyll fluorescence approach., *J. Exp. Bot.*, 58, 785–795, <https://doi.org/10.1093/jxb/erl222>, 2007.
- Guderian, R.: Air Pollution. Phytotoxicity of Acidic Gases and Its Significance in Air Pollution Control, Springer-Verlag, New York, 1977.
- Hanson, P., Samuelson, L., Wullschlegel, S., Tabberer, T., and Edwards, G.: Seasonal patterns of light-saturated photosynthesis and leaf conductance for mature and seedling *Quercus rubra* L. foliage: differential sensitivity to ozone exposure, *Tree Physiol.*, 14, 1351–1366, 1994.
- Harmens, H. and Mills, G.: Ozone Pollution: Impacts on carbon sequestration in Europe, *NERC/Centre for Ecology & Hydrology*, 2012.
- Karlsson, P. E., Uddling, J., Braun, S., Broadmeadow, M., Elvira, S., Gimeno, B. S., Le Thiec, D., Oksanen, E., Vandermeiren, K., Wilkinson, M., and Emberson, L.: New critical levels for ozone effects on young trees based on AOT40 and simulated cumulative leaf uptake of ozone, *Atmos. Environ.*, 38, 2283–2294, 2004.
- Kolb, T. and Matyssek, R.: Limitations and perspectives about scaling ozone impacts in trees, *Environ. Pollut.*, 115, 373–393, 2001.
- Krinner, G., Viovy, N., de Noblet-Ducoudré, N., Ogée, J., Polcher, J., Friedlingstein, P., Ciais, P., Sitch, S., and Prentice, I.: A dynamic global vegetation model for studies of the coupled atmosphere-biosphere system, *Global Biogeochem. Cy.*, 19, GB1015, <https://doi.org/10.1029/2003GB002199>, 2005.
- Laisk, A., Kull, O., and Moldau, H.: Ozone concentration in leaf intercellular air spaces is close to zero, *Plant Physiol.*, 90, 1163–1167, 1989.
- Li, P., Feng, Z., Catalayud, V., Yuan, X., Xu, Y., and Paoletti, E.: A meta-analysis on growth, physiological and biochemical responses of woody species to ground-level ozone highlights the role of plant functional types, *Plant Cell Environ.*, 40, 2369–2380, 2017.
- Lombardozzi, D., Levis, S., Bonan, G., and Sparks, J. P.: Predicting photosynthesis and transpiration responses to ozone: decou-

- pling modeled photosynthesis and stomatal conductance, *Biogeosciences*, 9, 3113–3130, <https://doi.org/10.5194/bg-9-3113-2012>, 2012a.
- Lombardozi, D., Sparks, J., Bonan, G., and Levis, S.: Ozone exposure causes a decoupling of conductance and photosynthesis: implications for the Ball-Berry stomatal conductance model, *Oecologia*, 169, 1–9, 2012b.
- Lombardozi, D., Sparks, J. P., and Bonan, G.: Integrating O<sub>3</sub> influences on terrestrial processes: photosynthetic and stomatal response data available for regional and global modeling, *Biogeosciences*, 10, 6815–6831, <https://doi.org/10.5194/bg-10-6815-2013>, 2013.
- Lombardozi, D., Levis, S., Bonan, G., Hess, P., and Sparks, J.: The Influence of Chronic Ozone Exposure on Global Carbon and Water Cycles, *J. Climate*, 28, 292–305, 2015.
- LRTAP-Convention: Manual on Methodologies and Criteria for Modelling and Mapping Critical Loads and Levels; and Air Pollution Effects, Risks and Trends, available at: <https://icpvegetation.ceh.ac.uk/sites/default/files/Chapter3-Mappingcriticallevelsforvegetation.pdf> (last access: 14 November 2018), 2017.
- Marzuoli, R., Gerosa, G., Desotgiu, R., Bussotti, F., and Denti, A. B.: Ozone fluxes and foliar injury development in the ozone-sensitive poplar clone Oxford (*Populus maximowiczii* × *Populus berolinensis*): a dose-response analysis, *Tree Physiol.*, 29, 67–76, <https://doi.org/10.1093/treephys/tpn012>, 2009.
- Marzuoli, R., Monga, R., Finco, A., and Gerosa, G.: Biomass and physiological responses of *Quercus robur* (L.) young trees during 2 years of treatments with different levels of ozone and nitrogen wet deposition, *Trees*, 30, 1995–2010, 2016.
- Massman, W.: A review of the molecular diffusivities of H<sub>2</sub>O, CO<sub>2</sub>, CH<sub>4</sub>, CO, O<sub>3</sub>, SO<sub>2</sub>, NH<sub>3</sub>, N<sub>2</sub>O, NO, AND NO<sub>2</sub> in air, O<sub>2</sub> AND N<sub>2</sub> near STP, *Atmos. Environ.*, 32, 1111–1127, [https://doi.org/10.1016/S1352-2310\(97\)00391-9](https://doi.org/10.1016/S1352-2310(97)00391-9), 1998.
- Matyssek, R., Karnosky, D. F., Wieser, G., Percy, K., Oksanen, E., Grams, T. E. E., Kubiske, M., Hanke, D., and Pretzsch, H.: Advances in understanding ozone impact on forest trees: Messages from novel phytotron and free-air fumigation studies, *Environ. Pollut.*, 158, 1990–2006, <https://doi.org/10.1016/j.envpol.2009.11.033>, 2010.
- Mills, G., Hayes, F., Wilkinson, S., and Davies, W.: Chronic exposure to increasing background ozone impairs stomatal functioning in grassland species, *Glob. Change Biol.*, 15, 1522–1533, 2009.
- Mills, G., Pleijel, H., Braun, S., Büker, P., Bermejo, V., Calvo, E., Danielsson, H., Emberson, L., Fernández, I., Grünhage, L., Harmens, H., Hayes, F., Karlsson, P., and Simpson, D.: New stomatal flux-based critical levels for ozone effects on vegetation, *Atmos. Environ.*, 45, 5064–5068, 2011.
- Morgan, P., Ainsworth, E., and Long, S.: How does elevated ozone impact soybean? A meta-analysis of photosynthesis, growth and yield, *Plant Cell Environ.*, 26, 1317–1328, 2003.
- Niinemets, Ü., Keenan, T. F., and Hallik, L.: A worldwide analysis of within-canopy variations in leaf structural, chemical and physiological traits across plant functional types, *New Phytol.*, 205, 973–993, 2015.
- Nunn, A., Weiser, G., Reiter, I., Häberle, K., Grote, R., Havranek, W., and Matyssek, R.: Testing the unifying theory of ozone sensitivity with mature trees of *Fagus sylvatica* and *Picea abies*, *Tree Physiol.*, 26, 1391–1403, 2006.
- Oliver, R. J., Mercado, L. M., Sitch, S., Simpson, D., Medlyn, B. E., Lin, Y.-S., and Folberth, G. A.: Large but decreasing effect of ozone on the European carbon sink, *Biogeosciences*, 15, 4245–4269, <https://doi.org/10.5194/bg-15-4245-2018>, 2018.
- Paoletti, E. and Grulke, N.: Does living in elevated CO<sub>2</sub> ameliorate tree response to ozone? A review on stomatal responses, *Environ. Pollut.*, 137, 483–493, 2005.
- Paoletti, E. and Grulke, N.: Ozone exposure and stomatal sluggishness in different plant physiognomic classes, *Environ. Pollut.*, 158, 2664–2671, 2010.
- Paoletti, E., Conran, N., Bernasconi, P., Günthardt-Goerg, M. S., and Vollenweider, P.: Erratum to “Structural and physiological responses to ozone in Manna ash (*Fraxinus ornus* L.) leaves of seedlings and mature trees under controlled and ambient conditions”, *Sci. Total Environ.*, 408, 2014–2024, 2010.
- Percy, K., Nosal, M., Heilman, W., Dann, T., Sober, J., Legge, A., and Karnosky, D.: New exposure-based metric approach for evaluating O<sub>3</sub> risk to North American aspen forests, *Environ. Pollut.*, 147, 554–566, 2007.
- Pleijel, H., Danielsson, H., Ojanperä, K., Temmerman, L. D., Högy, P., Badiani, M., and Karlsson, P.: Relationships between ozone exposure and yield loss in European wheat and potato – a comparison of concentration- and flux-based exposure indices, *Atmos. Environ.*, 38, 2259–2269, 2004.
- Reich, P.: Quantifying plant response to ozone: a unifying theory, *Tree Physiol.*, 3, 63–91, 1987.
- Samuelson, L. and Kelly, J.: Carbon partitioning and allocation in northern red oak seedlings and mature trees in response to ozone, *Tree Physiol.*, 16, 853–858, 1996.
- Samuelson, L., Kelly, J., Mays, P., and Edwards, G.: Growth and nutrition of *Quercus rubra* L. seedlings and mature trees after three seasons of ozone exposure, *Environ. Pollut.*, 91, 317–323, 1996.
- Schaub, M., Skelly, J., Zhang, J., Ferdinand, J., Savage, J., Stevenson, R., Davis, D., and Steiner, K.: Physiological and foliar symptom response in the crowns of *Prunus serotina*, *Fraxinus americana* and *Acer rubrum* canopy trees to ambient ozone under forest conditions, *Environ. Pollut.*, 133, 553–567, 2005.
- Simpson, D., Andersson, C., Christensen, J. H., Engardt, M., Geels, C., Nyiri, A., Posch, M., Soares, J., Sofiev, M., Wind, P., and Langner, J.: Impacts of climate and emission changes on nitrogen deposition in Europe: a multi-model study, *Atmos. Chem. Phys.*, 14, 6995–7017, <https://doi.org/10.5194/acp-14-6995-2014>, 2014.
- Sitch, S., Cox, P., Collins, W., and Huntingford, C.: Indirect radiative forcing of climate change through ozone effects on the land-carbon sink, *Nature*, 448, 791–794, 2007.
- Sitch, S., Friedlingstein, P., Gruber, N., Jones, S. D., Murray-Tortarolo, G., Ahlström, A., Doney, S. C., Graven, H., Heinze, C., Huntingford, C., Levis, S., Levy, P. E., Lomas, M., Poulter, B., Viovy, N., Zaehle, S., Zeng, N., Arneth, A., Bonan, G., Bopp, L., Canadell, J. G., Chevallier, F., Ciais, P., Ellis, R., Gloor, M., Peylin, P., Piao, S. L., Le Quéré, C., Smith, B., Zhu, Z., and Myneni, R.: Recent trends and drivers of regional sources and sinks of carbon dioxide, *Biogeosciences*, 12, 653–679, <https://doi.org/10.5194/bg-12-653-2015>, 2015.

- Tjoelker, M., Volin, J., Oleksyn, J., and Reich, P.: Interaction of ozone pollution and light effects on photosynthesis in a forest canopy experiment, *Plant Cell Environ.*, 18, 895–905, 1995.
- Wang, B., Shugart, H. H., Shuman, J. K., and Lerdau, M. T.: Forests and ozone: productivity, carbon storage, and feedbacks, *Sci. Rep.-UK*, 6, 22133, <https://doi.org/10.1038/srep22133>, 2016.
- Wieser, G. and Matyssek, R.: Linking ozone uptake and defense towards a mechanistic risk assessment for forest trees, *New Phytol.*, 174, 7–9, 2007.
- Wieser, G., Hecke, K., Tausz, M., Haberle, K., Grams, T., and Matyssek, R.: The role of antioxidative defense in determining ozone sensitivity of Norway spruce (*Picea abies* (L.) Karst.) across tree age: Implications for the sun-and shade-crown, *PHYTON-HORN-*, 42, 245–254, 2002.
- Wittig, V., Ainsworth, E., and Long, S.: To what extent do current and projected increases in surface ozone affect photosynthesis and stomatal conductance of trees? A meta-analytic review of the last 3 decades of experiments, *Plant Cell Environ.*, 30, 1150–1162, 2007.
- Wittig, V., Ainsworth, E., Naidu, S., Karnosky, D., and Long, S.: Quantifying the impact of current and future tropospheric ozone on tree biomass, growth, physiology and biochemistry: a quantitative meta-analysis, *Glob. Change Biol.*, 15, 396–424, 2009.
- Zaehle, S. and Friend, A.: Carbon and nitrogen cycle dynamics in the O-CN land surface model: 1. Model description, site-scale evaluation, and sensitivity to parameter estimates, *Global Biogeochem. Cy.*, 24, GB1005, <https://doi.org/10.1029/2009GB003521>, 2010.